

Aus dem Deutschen Zentrum für Neurodegenerative Erkrankungen  
und dem Adolf-Butenandt-Institut  
Lehrstuhl: Stoffwechselbiochemie  
im Biomedizinischen Zentrum der  
Ludwig-Maximilians-Universität München  
Vorstand: Prof. Dr. rer. nat. Dr. h.c. Christian Haass

# **Molecular mechanisms and biomarkers of familial FTD/ALS**

- Dissertation -

zum Erwerb des Doktorgrades der Naturwissenschaften (Dr. rer. nat.)  
an der Medizinischen Fakultät der Ludwig-Maximilians-Universität München



vorgelegt von  
Carina Petra Lehmer  
aus Burglengenfeld

2018

Gedruckt mit Genehmigung der Medizinischen Fakultät der Ludwig-Maximilians-Universität München

Betreuer: Prof. Dr. rer. nat. Dr. h.c. Christian Haass

Zweitgutachter: Prof. Dr. Christian Behrends

Dekan: Herr Prof. Dr. med. dent. Reinhard HICKEL

Tag der mündlichen Prüfung: 04.12.2018

## **Eidesstattliche Versicherung**

Ich erkläre hiermit an Eides statt, dass ich die vorliegende Dissertation mit dem Thema selbständig verfasst, mich außer der angegebenen keiner weiteren Hilfsmittel bedient und alle Erkenntnisse, die aus dem Schrifttum ganz oder annähernd übernommen sind, als solche kenntlich gemacht und nach ihrer Herkunft unter Bezeichnung der Fundstelle einzeln nachgewiesen habe.

Ich erkläre des Weiteren, dass die hier vorgelegte Dissertation nicht in gleicher oder in ähnlicher Form bei einer anderen Stelle zur Erlangung eines akademischen Grades eingereicht wurde.

München, 25.3.2019

---

Carina Petra Lehmer

*Das habe ich noch nie vorher versucht,  
also bin ich völlig sicher,  
dass ich es schaffe.  
-Pippi Langstrumpf*

*Vo nix kummt nix.  
-Ovid*

# Table of Contents

List of Abbreviations .....	6
Publications of this thesis .....	9
I. Introduction .....	10
1. Frontotemporal Dementia and Amyotrophic Lateral Sclerosis .....	10
1.1. Clinical, genetic and neuropathological features of FTD, ALS and FTD/ALS.....	10
1.1.1. <i>Clinical features of FTD</i> .....	10
1.1.2. <i>Clinical features of ALS</i> .....	11
1.1.3. <i>Clinical features of FTD/ALS</i> .....	11
1.1.4. <i>Genetic evidence and pathological inclusions in FTD/ALS</i> .....	12
1.2. Pathogenic mechanisms in FTD/ALS.....	13
1.2.1. <i>Protein homeostasis</i> .....	14
1.2.2. <i>Mitochondria</i> .....	18
2. <i>C9orf72</i> –mutations are the most common cause of familial FTD/ALS.....	20
2.1. Function and genetic link to FTD/ALS .....	20
2.2. Current hypothesis of <i>C9orf72</i> disease related pathomechanisms.....	20
3. <i>CHCHD10</i> - A mitochondrial link to FTD/ALS.....	23
3.1. Structural features and mitochondrial import .....	23
3.2. Function and genetic link to FTD/ALS .....	26
3.3. Current hypothesis of <i>CHCHD10</i> disease-related pathomechanisms.....	28
4. Clinical biomarkers and therapy approaches in FTD and ALS.....	29
4.1. Biomarkers for neurodegenerative diseases .....	29
4.2. Therapeutic approaches for FTD/ALS.....	30
II. Zusammenfassung .....	32
III. Summary .....	35
IV. Results.....	37
1. Publication I and contribution .....	37
2. Publication II and contribution .....	57
3. Publication III and contribution .....	82
4. Publication IV and contribution.....	95
References.....	115
Acknowledgements .....	130

## List of Abbreviations

aa	Amino acid
A $\beta$	$\beta$ -amyloid
AD	Alzheimer's disease
AICAR	AMPK activator 5-amino-1- $\beta$ -D-ribofuranosylimidazole-4-carboxamide
AIF	Apoptosis inducing factor
ALS	Amyotrophic lateral sclerosis
AMPK	AMP-activated protein kinase
ASO	Antisense oligonucleotide
Atg5	Autophagy related 5
Atg7	Autophagy related 7
ATP	Adenosin triphosphate
bvFTD	Behavioral variant frontotemporal dementia
C9orf72	Chromosome 9 open reading frame 72 gene (C9orf72)
CHCHD10	Coiled-coil-helix-coiled-coil-helix domain containing protein 10
CHMP2B	Charged multivesicular body protein 2b
CNS	Central nervous system
CSF	Cerebrospinal fluid
CytC	Cytochrome C
CPC	Cysteine-proline-cysteine
COX	Cytochrome C oxidase
CX <sub>9</sub> C	Cysteine-X <sub>9</sub> -Cysteine
DENN	After differentially expressed in neoplastic versus normal cells
DM2	Myotonic dystrophy type 2
DPR	Dipeptide repeat
E1	Ubiquitin-activating enzyme
E2	Ubiquitin-conjugating enzyme
E3	Ubiquitin-ligating enzyme
Erv1	Essential for respiration and vegetative growth
FDA	Food and drug administration
FTD	Frontotemporal dementia
FUS	Fused in sarcoma
G-Q	G-quadruplex
GA	Glycine-alanine
GEF	Guanine nucleotide exchange factor
GOF	Gain-of-function
GP	Glycine-proline
GR	Glycine-arginine
GRN	Progranulin
IMM	Inner mitochondrial membrane
IMS	Intermembrane space

iPSC	Induced pluripotent stem cells
KD	Knock down
KO	Knock out
LCD	Low complexity domain
LCL	Lymphoblastoid cell lines
LOF	Loss-of-function
MAPT	Microtubule-associated protein tau
Mia	Mitochondrial intermembrane space import and assembly
MICOS	Mitochondrial contact site and cristae organizing system
miRNA	MicroRNA
mito.	Mitochondrial
MM	Mitochondrial myopathy
MND	Motor neuron disease
MPP	Mitochondrial processing peptidase
MRI	Magnetic resonance imaging
MTS	Mitochondrial targeting signal
NMD	Nonsense-mediated mRNA decay
OMM	Outer mitochondrial membrane
OPTN	Optineurin
ORE	Oxygen responsive element
OXPPOS	Oxidative phosphorylation
PA	Proline-alanine
PAM	Presequence translocase associated import motor
PD	Parkinson's disease
PET	Positron emission tomography
PLS	Primary lateral sclerosis
PMA	Progressive muscular atrophy
PNFA	Progressive non-fluent aphasia
PGC-1 $\alpha$	PPAR $\gamma$ coactivator-1 $\alpha$
PPA	Primary progressive aphasia
PPAR $\gamma$	Peroxisome proliferator-activated receptor gamma
PR	Proline-arginine
PrP	Prion protein
Rab	Ras-related in brain
RAN	Repeat-associated non-ATG
RBP	RNA-binding protein
ROS	Reactive oxygen species
SAM	Sorting and assembly machinery
SCA8	Spinocerebellar ataxia type 8
SD	Semantic dementia
SMCR8	Smith-magenis syndrome chromosome region, candidate 8
SOD1	Superoxide dismutase 1

SQSTM1/p62	Sequestome 1
TBK1	TANK-binding kinase 1
TDP-43/TARDBP	TAR DNA-binding protein 43
TIA-1	T-cell intracellular antigen 1
TIM	Translocase of the inner mitochondrial membrane
TOM	Translocase in the outer membrane of mitochondria
TREM2	Triggering receptor expressed on myeloid cells 2
UBQLN2	Ubiquilin 2
UPS	Ubiquitin-proteasome system
VCP	Valosin-containing protein
WDR41	WD repeat domain 41

## Publications of this thesis

### I. A novel CHCHD10 mutation implicates a Mia40-dependent mitochondrial import deficit in ALS

Lehmer C, Schludi MH, Ransom L, Greiling J, Junghänel M, Exner N, Riemenschneider H, van der Zee J, Van Broeckhoven C, Weydt P, Heneka MT, Edbauer D.

EMBO Mol Med. 2018, doi: 10.15252/emmm.201708558

### II. In situ structure of neuronal C9orf72 poly-GA aggregates reveals proteasome recruitment

Guo Q, Lehmer C, Martínez-Sánchez A, Rudack T, Beck F, Hartmann H, Pérez-Berlanga M, Frottin F, Hipp MS, Hartl FU, Edbauer D, Baumeister W, Fernández-Busnadiego R.

Cell. 2018, doi: 10.1016/j.cell.2017.12.030

### III. Poly-GP in cerebrospinal fluid links C9orf72-associated dipeptide repeat expression to the asymptomatic phase of ALS/FTD

Lehmer C, Oeckl P, Weishaupt JH, Volk AE, Diehl-Schmid J, Schroeter ML, Lauer M, Kornhuber J, Levin J, Fassbender K, Landwehrmeyer B; German Consortium for Frontotemporal Lobar Degeneration, Schludi MH, Arzberger T, Kremmer E, Flatley A, Feederle R, Steinacker P, Weydt P, Ludolph AC, Edbauer D, Otto M.

EMBO Mol Med. 2017, doi: 10.15252/emmm.201607486

### IV. Antibodies inhibit transmission and aggregation of C9orf72 poly-GA dipeptide repeat proteins

Zhou Q, Lehmer C, Michaelsen M, Mori K, Alterauge D, Baumjohann D, Schludi MH, Greiling J, Farny D, Flatley A, Feederle R, May S, Schreiber F, Arzberger T, Kuhm C, Klopstock T, Hermann A, Haass C, Edbauer D.

EMBO Mol Med. 2017, doi: 10.15252/emmm.201607054

# I. Introduction

## 1. Frontotemporal Dementia and Amyotrophic Lateral Sclerosis

Frontotemporal dementia (FTD) and amyotrophic lateral sclerosis (ALS) are two severe neurodegenerative disorders without cure and with very limited treatment options (Tsai and Boxer, 2016). FTD is one of the major causes of early-onset dementia and the third most common form of dementia in all age groups worldwide (Bang et al., 2015; Vieira et al., 2013). ALS is the most common form of motor neuron diseases (MND). Both FTD and ALS have overlapping clinical, pathological and genetic features and therefore are often referred to as the extreme ends of a disease spectrum with multisystem degeneration (Ferrari et al., 2011).

### 1.1. Clinical, genetic and neuropathological features of FTD, ALS and FTD/ALS

#### 1.1.1. Clinical features of FTD

In 1892, FTD was described for the first time by the Czech neuropsychiatrist Arnold Pick in a 71-year-old man with cognitive defects and aggressive behavior, but normal motor function. Autopsy revealed severe brain atrophy in the left hemisphere (Berrios and Girling, 1994).

Approximately 5-15% of all dementia cases suffer from FTD. Predominantly, presenile individuals (< 65 years) are affected by FTD and the disease duration is typically 6-12 years (Kansal et al., 2016; Rademakers et al., 2012). The diagnosis of FTD is mainly done by clinical assessment and neuroimaging techniques. Atrophy of the frontal lobes can be visualized using magnetic resonance imaging (MRI) and computer tomography. Furthermore, changes in brain activity can be assessed by measuring glucose metabolism by positron emission tomography (PET) (Rascovsky et al., 2011).

Depending on symptoms, FTD is further classified into different clinical subgroups: Behavioral variant frontotemporal dementia (bvFTD) and primary progressive aphasia (PPA), which is subdivided into semantic dementia (SD) and progressive non-fluent aphasia (PNFA). Although, these syndromes often overlap, a particular feature is usually dominant (Bang et al., 2015; Ferrari et al., 2011). Among these variants, bvFTD is the most common form and is mainly characterized by cognitive impairment and behavior problems, e.g. changes in personal and social conduct, disinhibition, apathy, loss of sympathy or empathy. These symptoms originate from degeneration of the frontal lobe (Bang et al., 2015; Hogan et al., 2016; Rosen et al., 2002). PPA-patients often present progressive and insidious language impairment interfering with their daily life. The two main criteria for SD are anomia and single word comprehension deficits caused by degeneration of the anterior lobe. In contrast, atrophy in the left posterior frontal and

insular region is predominantly present in PNFA patients who suffer from agrammatism as well as hesitant and nonfluent speech (Bang et al., 2015; Gorno-Tempini et al., 2011).

In later stages, FTD symptoms of the three clinical syndromes often converge, affecting large regions in the frontal and temporal lobes and leading to globally impaired cognitive and motor deficits. Patients usually die due to pneumonia or other secondary infections (Bang et al., 2015).

### **1.1.2. Clinical features of ALS**

ALS was first reported by Jean-Martin Charcot in 1874. He identified ALS as a primary neuronal disease, by linking its symptoms to the loss of motor neurons in brain and spinal cord. Charcot and his colleague Joffrey observed that lesions in the anterior horn, but not in the lateral column of the spinal cord lead to muscle atrophy (Kumar et al., 2011; Rowland, 2001).

ALS is the most prevalent form of MND and has an average age of onset of 55 years. ALS is ruthlessly progressive with 50% of patients dying within 30 months after symptom onset (Chio et al., 2013; Ferrari et al., 2011; Kiernan et al., 2011). Diagnosis of ALS consists of a combination of physical examination and neurological testing such as nerve conduction studies and electromyography. To exclude alternative pathological changes in patients, additional MRI is often used (Brooks et al., 2000; Kiernan et al., 2011).

No biomarkers allow definitive distinction between the pure upper motor neuron disease, primary lateral sclerosis (PLS), and the pure lower motor neuron disease, progressive muscular atrophy (PMA), during the early stages (Al-Chalabi et al., 2016). Clinically, PLS usually leads to hyperreflexia accompanied by spasticity, while PMA is associated with progressive muscle weakness and wasting. The main cause for death in ALS patients is respiratory failure (Ferrari et al., 2011).

### **1.1.3. Clinical features of FTD/ALS**

In 1981, in-depth neuropathological analysis revealed that ALS pathology is often accompanied by degeneration of the frontal and frontotemporal regions of the brain, as well as atrophy of the substantia nigra and globus pallidus (Ferrari et al., 2011; Hudson, 1981).

In the following years, cognitive dysfunction and other signs of FTD have been detected in ALS patients (up to 50% of patients) and, vice versa, motor deficits have been documented in FTD patients suggesting shared pathomechanisms between the two diseases (Burrell et al., 2011; Ozel-Kizil et al., 2013; Strong et al., 2003).

### 1.1.4. Genetic evidence and pathological inclusions in FTD/ALS

Approximately 40% of all FTD patients and 10% of all ALS cases have a positive family history suggestive of autosomal dominant inheritance (Rademakers et al., 2012; Snowden et al., 2002; Van Damme and Robberecht, 2009).

In recent years, a number of genes causing pure FTD, ALS or mixed FTD/ALS have been identified. Mutations in the microtubule-associated protein Tau (*MAPT*), progranulin (*GRN*) or less frequently in charged multivesicular body protein 2b (*CHMP2B*) and triggering receptor expressed on myeloid cells 2 (*TREM2*) are connected to pure FTD (Baker et al., 2006; Borroni et al., 2014; Cruts et al., 2006; Hutton et al., 1998; Skibinski et al., 2005). In contrast, mutations in the superoxide dismutase 1 (*SOD1*), TAR DNA-binding protein 43 (*TARDBP*) and fused in sarcoma (*FUS*) are the most frequent genes associated with pure ALS (Kwiatkowski et al., 2009; Rosen et al., 1993; Sreedharan et al., 2008; Vance et al., 2009). In 2011, two groups independently identified a massive GGGGCC-repeat expansion mutation upstream of the coding region of the chromosome 9 open reading frame 72 gene (*C9orf72*) (DeJesus-Hernandez et al., 2011; Renton et al., 2011). These *C9orf72* repeat expansions are the most common cause of familial FTD/ALS (Majounie et al., 2012; van Blitterswijk et al., 2012). Less common mutations in the coiled-coil-helix-coiled-coil-helix domain containing protein 10 (*CHCHD10*), sequestome 1 (*SQSTM1/p62*), optineurin (*OPTN*), valosin-containing protein (*VCP*), TANK-binding kinase 1 (*TBK1*) and ubiquilin 2 (*UBQLN2*) are linked to FTD/ALS as well (Fig. 1A) (Bannwarth et al., 2014; Cirulli et al., 2015; Deng et al., 2011; Fecto et al., 2011; Maruyama et al., 2010; Pottier et al., 2015; Rubino et al., 2012; Watts et al., 2004).

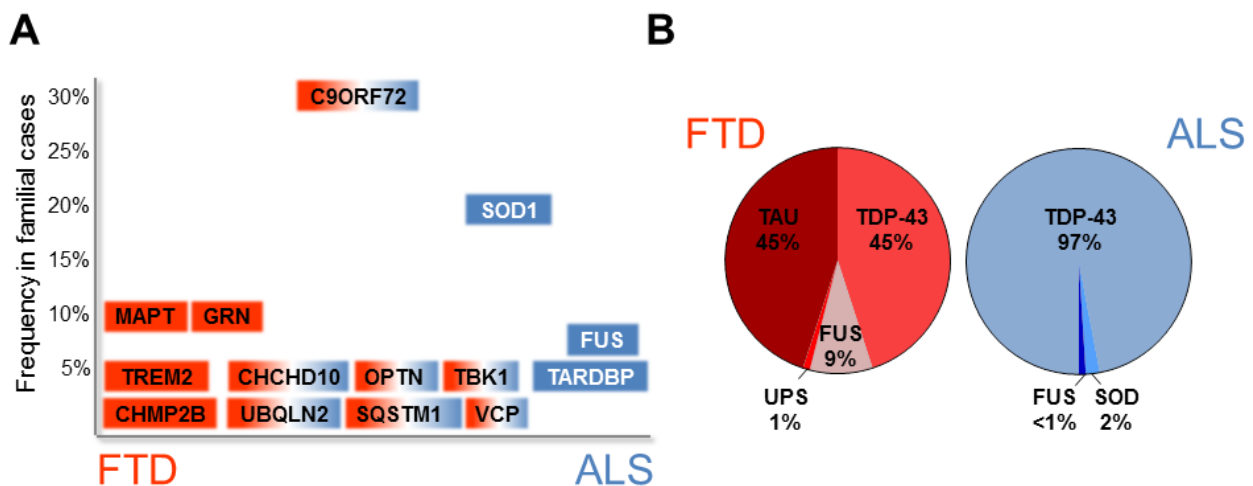


**Figure 1 Schematic illustration of most common genes and neuropathological inclusions linked to familial FTD and ALS.** (A) FTD (red) and ALS (blue) are thought as the extreme ends of a disease spectrum. Genes linked to FTD are illustrated in red, to ALS in blue and genes associated to both diseases are mixed colored. Genes are arranged based on their frequency in familial cases. Adapted from (Guerreiro et al., 2015). (B) Neuropathological protein inclusions in FTD and ALS are classified according to the main aggregating protein. TDP-43 and FUS inclusions depict the pathological overlap of these disorders. Adapted from (Ling et al., 2013).

In 2006, the RNA-binding protein (RBP) TDP-43 was identified as the major ubiquitinated protein that is present in inclusions of ~45% of FTD and nearly all ALS cases (97%) (Arai et al., 2006; Neumann et al., 2006). Subsequently, another RBP, FUS, was found in pathological inclusions of FTD patients without TDP-43 pathology resulting in a reclassification of FTD based on the main aggregated protein (Mackenzie et al., 2010). Thus, FTD is nowadays divided in FTLD-TAU (45%), FTLD-TDP-43 (45%), FTLD-FUS (9%) and FTLD-UPS (ubiquitin-proteasome system, 1%) (Fig. 1B). Inclusions in TDP-43 and FUS represent the pathological overlap in FTD and ALS.

Altogether, FTD and ALS share several clinical, genetic and pathological features implying common pathogenic pathways are involved in disease onset and progression.

## 1.2. Pathogenic mechanisms in FTD/ALS

Similar to other neurodegenerative diseases, multiple pathomechanisms related to protein aggregation, protein-homeostasis and mitochondrial functions as well as cell-to-cell transmission of protein aggregates that ultimately lead to neuron death, have been described in FTD/ALS (Fig. 2). Since two common aggregating proteins in FTD/ALS are RBPs, RNA metabolism plays a special role.

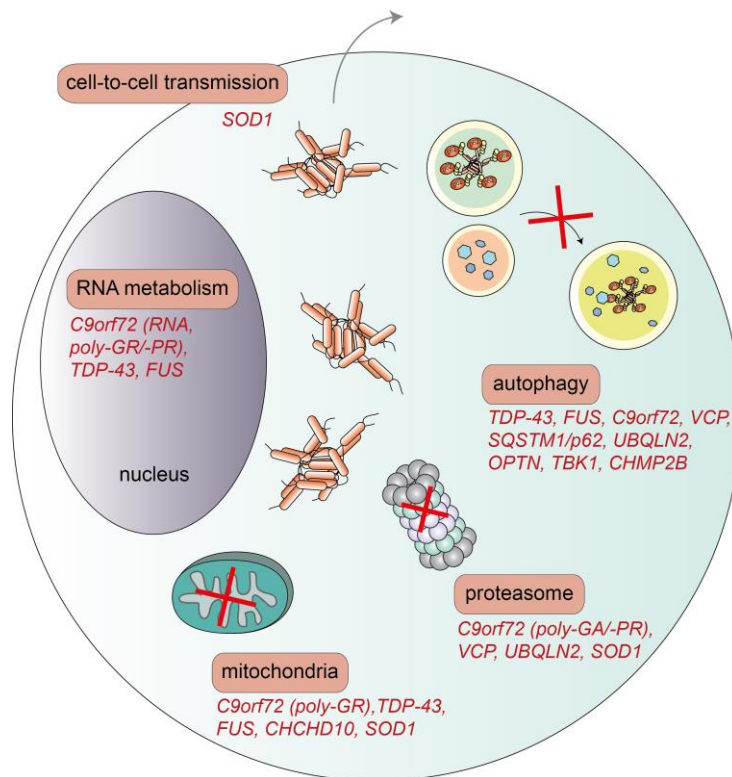


**Figure 2 Putative pathogenic mechanisms described in FTD/ALS.**

Pathogenic protein aggregates (orange) impair RNA metabolism, autophagy, proteasomal and mitochondrial functions. Moreover, cell-to-cell transmission has been described in several neurodegenerative diseases. FTD/ALS associated mutated and/or aggregated proteins disrupt these pathways by loss-of-function and/or gain-of-function mechanisms and are listed in red below the respective pathway.

The nuclear proteins TDP-43 and FUS are involved in multiple steps of RNA processing but both proteins form cytoplasmic aggregates in different subtypes of FTD and ALS (Fig. 1) (Neumann et al., 2006; Vance et al., 2009). Cells with cytoplasmic TDP-43 and FUS aggregates show pronounced nuclear clearance of the respective protein suggesting that nuclear loss-of-function (LOF) and cytoplasmic gain-of-function (GOF) mechanisms may contribute to disease (Ling et al., 2013; Vance et al., 2009). Rare mutations in the aggregation-prone low complexity domain (LCD) of TDP-43 and FUS lead to FTD and ALS and promote protein aggregation (King et al., 2012). LCDs mediate reversible liquid-liquid phase separation into liquid droplet and transition to more solid hydrogel states (Conicella et al., 2016; Murakami et al., 2015), which is crucial for the physiological formation of dynamic RNA containing compartments like stress granules (Alberti and Hyman, 2016; Courchaine et al., 2016). Since TDP-43 and FUS inclusions contain stress granule proteins, it has been suggested that liquid droplets/stress granules are precursors to pathological aggregates in FTD/ALS (Alberti and Hyman, 2016; King et al., 2012; Ling et al., 2013).

Moreover, the expanded repeat RNA in *C9orf72* FTD/ALS, forms nuclear RNA foci that are thought to sequester various RBPs and thereby impair their function (Cooper-Knock et al., 2014; Mori et al., 2013b). Unconventional translation of sense and antisense repeat transcripts results in five aggregating dipeptide repeat (DPR) proteins (poly-GA, -GP, -GR, -PA, -PR), unique to *C9orf72* patients (Mori et al., 2013a; Mori et al., 2013c). Of those DPR proteins, poly-GR and -PR interfere with many LCD-containing RBPs and thereby disrupt their phase separation ability (Lee et al., 2016).

Since the research focus of this thesis is on FTD/ALS-causing mutations in *C9orf72* and *CHCHD10*, with a focus on protein aggregation, impaired protein degradation, cell-to-cell transmission and mitochondrial impairment, I will describe these pathways in the following paragraphs in more detail.

### **1.2.1. Protein homeostasis**

The term protein homeostasis describes cellular processes that together maintain the proteome intact. Protein biogenesis, folding, trafficking and degradation are tightly controlled and coordinated by a complex network. Proteins are co-translationally folded with the help of chaperons that recognize misfolded proteins with hydrophobic residues on the protein surface and/or incorrect disulfide bond formation. However, some proteins remain misfolded or later aggregate due to mutations or cellular stressors such as oxygen radicals or heavy iron metals. Protein misfolding and aggregation may cause LOF and GOF mechanisms. Therefore, an intact protein quality control system with chaperons, which are constantly monitoring protein folding, is

crucial for cells. If misfolded proteins cannot be refolded in their correct conformation, they are normally targeted to and finally eliminated by the major protein clearance pathways: autophagy and the UPS (Fig. 3) (Ciechanover and Kwon, 2015; Shahheydari et al., 2017; Webster et al., 2017).

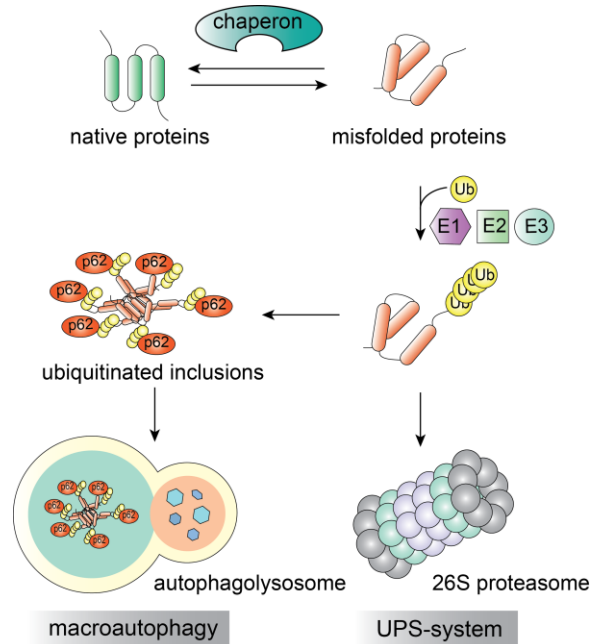


**Figure 3 Main degradation pathways of misfolded proteins.**

Cellular chaperons constantly facilitate refolding of misfolded proteins. Misfolded proteins are guided to the UPS by poly-ubiquitin (Ub) chains that are added by the three enzymes (E1, E2 and E3). After ubiquitination, those proteins are targeted to the 26S proteasome for proteolysis. Misfolded proteins that cannot be degraded via the UPS form poly-ubiquitinated cytoplasmic inclusions which are delivered to the autophagosome via the adaptor SQSTM1/p62. Subsequently, fusion of the autophagosome with the lysosome occurs forming the autophagolysosome and leading to aggregate digestion by lysosomal hydrolases. Adapted from (Ciechanover and Kwon, 2015).

### *The UPS and its dysfunction in FTD/ALS*

The UPS is a primary route for degradation of short-lived and misfolded proteins. First, lysine residues of misfolded proteins are marked by ubiquitin chains added through a specific cascade of three major enzymes: the ubiquitin activating (E1), the ubiquitin conjugating (E2) and the ubiquitin ligating (E3) enzyme (Shahheydari et al., 2017). Then, poly-ubiquitinated proteins are recognized and degraded by the 26S proteasome. The proteasome is a multimeric adenosine triphosphate (ATP)-dependent protease complex containing one or two 19S regulatory cap subunits and a proteolytic 20S core chamber. After poly-ubiquitinated substrates are bound and unfolded by the 19S subunit, they are guided into the 20S core particle. The latter has chymotrypsin-like, trypsin-like and caspase-like catalytic activities cleaving substrates into small peptides (Driscoll and Goldberg, 1989; Eytan et al., 1989; Heinemeyer et al., 1997; Voges et al., 1999).

Evidence from familial and sporadic cases of ALS supports proteasome dysfunction in disease. Pathogenic mutations inhibit substrate delivery to the proteasome (*VCP*, *UBQLN2*) and overall proteasome activity (*SOD1*, *VCP*) (Cheroni et al., 2009; Dai and Li, 2001; Deng et al., 2011; Ko et al., 2004; Webster et al., 2017). Additionally, sporadic ALS cases have decreased 20S proteasome subunit levels and impaired proteasomal activity in spinal cord (Kabashi et al., 2012). Conditional knock out (KO) of the proteasome subunit Rpt3 in mice results not only in motor neuron degeneration and locomotor defects but also in TDP-43 and FUS containing inclusions (Tashiro et al., 2012). In addition, the poly-GA and -PR DPR species in *C9orf72* FTD/ALS have been linked to UPS dysfunction. Poly-GA causes cellular toxicity and traps UPS components, however, the mechanistic link of protein aggregation to impaired UPS function is unclear (Gupta et al., 2017; May et al., 2014).

#### *The autophagy pathway and its dysfunction in FTD/ALS*

Autophagy is a cellular pathway for degrading cytoplasmic components like misfolded proteins or damaged organelles and is especially important in post-mitotic cells such as neurons. Misfolded proteins are recruited via autophagy receptors, like SQSTM1/p62 and OPTN, to the growing phagophore. The phagophore engulfs the cargo by forming a double membrane compartment, the so-called autophagosome. Fusion with lysosomes results to degradation of its content by hydrolases (Webster et al., 2017).

Several genes mutated in familial FTD/ALS are involved in distinct stages of autophagy, e.g. initiation (*C9orf72*), substrate delivery to the autophagosome (*UBQLN2*, *OPTN*, *SQSTM1/p62*, *TBK1*), maturation of the autophagosome (*VCP*) and autophagic degradation (*CHMP2B*) (Filimonenko et al., 2007; Goode et al., 2016; Ju et al., 2009; Maruyama et al., 2010; Osaka et al., 2015; Webster et al., 2016; Webster et al., 2017). Furthermore, mice lacking essential autophagy genes, like *Atg5* or *Atg7*, show poly-ubiquitinated inclusions, axonal dystrophy, neurodegenerative symptoms and impaired motor function (Hara et al., 2006; Komatsu et al., 2006). Since *C9orf72* is part of the autophagy initiation complex (Sellier et al., 2016; Webster et al., 2016) and decreased levels of the *C9orf72* protein have been described in patient brain (Waite et al., 2014), impaired autophagy may contribute to disease pathogenesis. Ubiquitin and SQSTM1/p62 are enriched in the cytoplasmic inclusions in FTD/ALS (Al-Sarraj et al., 2011; Mori et al., 2013a; Neumann et al., 2006; Vance et al., 2009). The cytoplasmic TDP-43, FUS and the DPR proteins are probably not sufficiently degraded by the impaired autophagic system and accumulate in insoluble inclusions in FTD/ALS (Webster et al., 2016). Taken together, these indicate that autophagy is crucial for neuronal health and has a primary role in the pathogenesis of FTD/ALS.

### Seeding and spreading mechanisms

Prion diseases are a group of rare fatal neurodegenerative disorders characterized by misfolded prion protein (PrP) that is orally transmissible. The first prion disease described in humans was Creutzfeldt-Jakob disease (Zabel and Reid, 2015). The infectious cycle starts with a conformational change of normal  $\alpha$ -helical PrP<sup>C</sup> to a  $\beta$ -sheet-rich conformation termed PrP<sup>Sc</sup> scrapie (PrP<sup>Sc</sup>). PrP<sup>Sc</sup> triggers conversion of further PrP<sup>C</sup> into the pathological PrP<sup>Sc</sup> conformation in a positive feedback loop that is associated with extremely fast clinical disease progression (Jucker and Walker, 2011).

Later, prion-like templated-aggregation was described as a characteristic feature in common non-infectious neurodegenerative diseases for extracellular and intracellular aggregating proteins:  $\beta$ -amyloid (A $\beta$ ) peptide and tau in Alzheimer's disease (AD),  $\alpha$ -synuclein in Parkinson's disease (PD) and huntingtin in Huntington's disease (Jucker and Walker, 2011; Luk et al., 2012; Sanders et al., 2014). Biophysical characterization and recently cryo-electron tomography analyses clearly show that these macromolecular aggregates form  $\beta$ -sheet-rich amyloid fibrils (Bauerlein et al., 2017; Fitzpatrick et al., 2017; Guerrero-Ferreira et al., 2018; Schmidt et al., 2015). For intracellular aggregates template directed aggregation is associated with cell-to-cell transmission possibly along synaptic connections. Here, misfolded proteins with amyloid-like conformation, serve as templates for further aggregation of native proteins in the receiver cell (Fig. 4). This is the molecular correlate of the spreading of Tau pathology through the brain during progression of Alzheimer's disease (Braak and Braak, 1991).

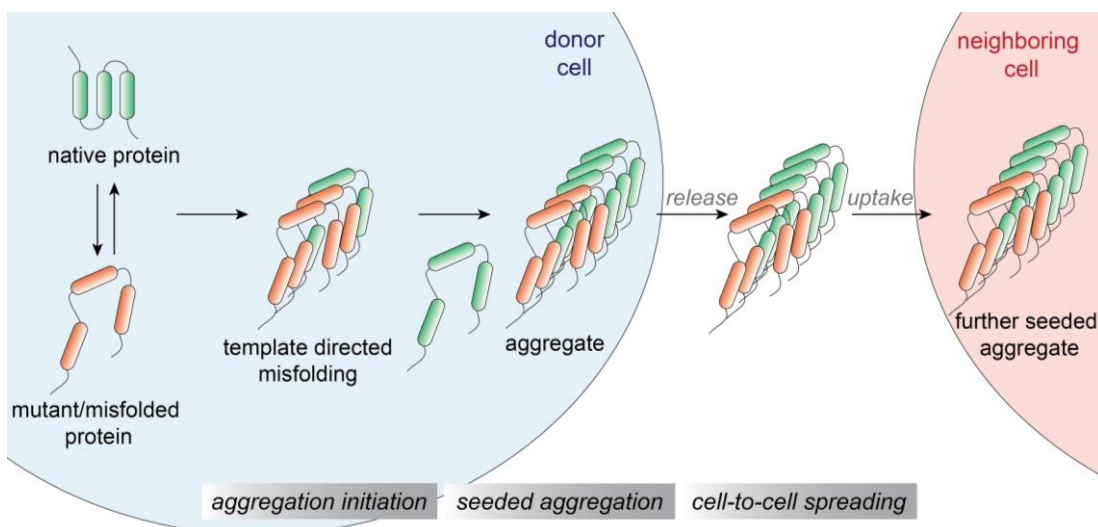


**Figure 4 Prion like cell-to-cell transmission of aggregates.**

Misfolded proteins form a seed of aggregation and thereby initiate misfolding of wildtype proteins leading to further seeded aggregation. Afterwards, aggregates are released to the extracellular space where they are uptaken by neighboring cells. Here, aggregates further induce misfolding and aggregation. Adapted from (Ling et al., 2013).

In familial ALS, this prion-like phenomenon was also reported for mutant SOD1, which forms fibrils, aggregates with misfolded wildtype protein and shows spreading abilities (Chattopadhyay et al., 2008; Grad et al., 2011; Munch et al., 2011). Furthermore, TDP-43 and FUS contain LCDs that might contribute to aggregation and seeding (Gitler and Shorter, 2011; Johnson et al., 2008) and several *in vitro* studies demonstrate amyloidogenic features of TDP-43 and FUS (Guo et al., 2018; Murray et al., 2017). Insoluble TDP-43, isolated from FTD or ALS patient brains with TDP-43 pathology, triggers aggregation of transfected TDP-43 in cultured cells (Nonaka et al., 2013). Additionally, neuropathological studies of FTLD-TDP-43 cases suggest propagation of phosphorylated TDP-43 aggregates in patient brain along anatomical connections (Brettschneider et al., 2014). Altogether, these findings suggest a prion-like spreading mechanism exists in FTD/ALS.

Although, short DPR peptides are taken up by cells (Chang et al., 2016; Kwon et al., 2014), release and uptake of larger aggregates has not been shown. Studying seeding and spreading of DPR proteins is crucial as the poor spatial correlation of all *C9orf72*-specific changes, including DPR inclusions with TDP-43 pathology and neurodegeneration, suggests the non-cell autonomous and/or synergistic effects are crucial for *C9orf72* pathogenesis.

### **1.2.2. Mitochondria**

Mitochondria are essential cellular organelles that regulate energy metabolism, calcium homeostasis and apoptosis. Neurons completely depend on an aerobic metabolism and mitochondrial calcium homeostasis, e.g. for regulating neurotransmitter release (Fig. 5). Moreover, mitochondria are also the main source of reactive oxygen species (ROS) leading to oxidative stress, e.g. damages of mitochondrial DNA, proteins and membranes (Fig. 5A). Oxidative stress can even induce Cytochrome C release resulting in apoptosis (Fig. 5C).

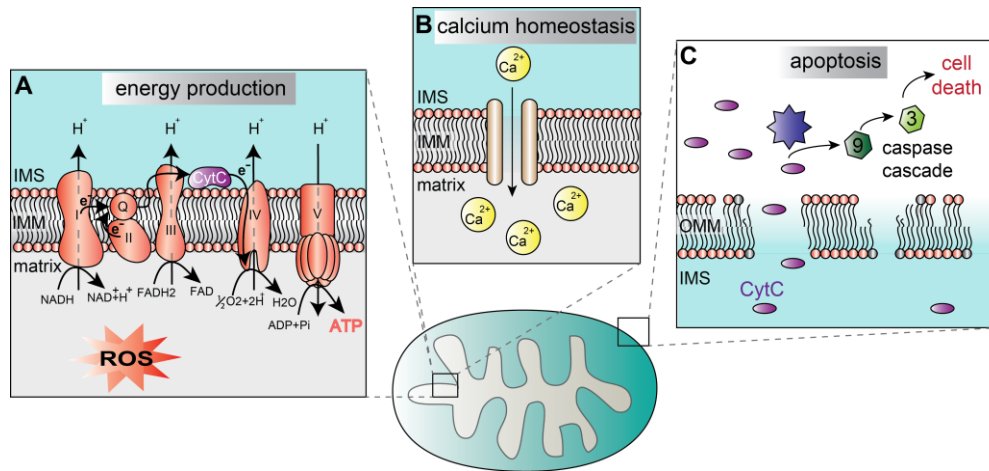


**Figure 5 Overview of three major mitochondrial features.**

Mitochondria are essential for many cellular processes. **(A)** Mitochondria produce most cellular ATP. At the inner mitochondrial membrane (IMM), electrons ( $e^-$ ) from NADH and FADH<sub>2</sub> pass through the electron transport chain complexes (I-IV) to oxygen (O<sub>2</sub>) reducing it to water (H<sub>2</sub>O). The released energy is used to generate a proton (H<sup>+</sup>) gradient across the IMM by actively pumping H<sup>+</sup> into the intermembrane space (IMS). Finally, ADP is phosphorylated to ATP by the ATP-synthase complex V with the energy of the H<sup>+</sup> gradient (Hatefi, 1985). Mitochondria are also the major reactive oxygen species (ROS) producers, which can lead to further oxidative damage in mitochondria. **(B)** Mitochondria are capable of storing calcium (Ca<sup>2+</sup>) and are therefore important for the cellular Ca<sup>2+</sup> homeostasis. Ca<sup>2+</sup> is taken up into the matrix by the mitochondrial Ca<sup>2+</sup> uniporter in the IMM (Contreras et al., 2010). **(C)** The intrinsic/mitochondrial apoptotic pathway is characterized by permeabilisation of the outer mitochondrial membrane (OMM) and release of Cytochrome C (CytC) into the cytoplasm. CytC is the major inducer of caspase activation downstream of mitochondria. First, CytC is involved in the formation of the apoptosome (purple star), a multi-protein complex initiating the activation of the caspase cascade through caspase 9. Caspase 9 activates caspase 3 leading to cell death (Elmore, 2007).

Post-mitotic neurons are vulnerable to accumulation of damage arising from impaired mitochondria (Smith et al., 2017). In PD, mitochondrial DNA damage, compromised mitophagy and dysfunctional respiratory chain complexes have been observed in patient brains providing a solid link between neurodegeneration and mitochondrial impairment (Dolle et al., 2016; Gao et al., 2017). In familial ALS, mutant SOD1 accumulates to mitochondria, whereby overexpression models show impaired electron transport, inefficient calcium buffering, altered mitochondrial morphology and aberrant import mechanism (Damiano et al., 2006; Li et al., 2010; Magrane et al., 2012). It is associated with cellular energy imbalance, apoptosis and impaired calcium homeostasis (Fig. 5) (Magrane et al., 2014). Additionally, mutations in SOD1 lead to misfolding on mitochondrial membranes resulting in a toxic GOF (Vande Velde et al., 2011). Similarly, translocation of mutant FUS to mitochondria seems to have an important role in disease progression (Deng et al., 2015). Colocalization of TDP-43 with mitochondria in motor neurons correlates with damage to mitochondria (Wang et al., 2013). Furthermore, the repeat expansions in *C9orf72* are linked to mitochondrial dysfunction via characteristic DPR aggregates with poly-GR, that induce oxidative stress and alterations of mitochondrial architecture (Lopez-Gonzalez et al., 2016). Moreover, mutations in mitochondrial CHCHD10 are linked to FTD/ALS, but some geneticists are concerned by the low penetrance. Since the precise molecular function of CHCHD10 and the molecular mechanism of *CHCHD10* mutations remain largely unknown, further functional analyses are required.

## **2. C9orf72 –mutations are the most common cause of familial FTD/ALS**

Five years after a locus on chromosome 9p21, associated with FTD and ALS, was identified, two groups finally pinpointed the mutation to a GGGGCC- repeat expansion located in a non-coding region of the *C9orf72* gene (DeJesus-Hernandez et al., 2011; Morita et al., 2006; Renton et al., 2011; Vance et al., 2006). This mutation is by far the most common known genetic cause of FTD and ALS with a prevalence of roughly 25% in familial FTD and 34% in familial ALS in Europe. An additional 5% of sporadic FTD and ALS are caused by the *C9orf72* mutation (Ng et al., 2015; Zou et al., 2017). Clinically, *C9orf72* patients have been reported to show a younger age of onset, a higher frequency of cognitive deficits and a faster disease progression compared to non-*C9orf72* FTD/ALS patients (Byrne et al., 2012; Chio et al., 2012).

### **2.1. Function and genetic link to FTD/ALS**

The first hint for the cellular functions of the *C9orf72* protein came from identification of a so-called differentially expressed in normal and neoplastic cells (DENN) domain within *C9orf72* suggesting it could act as a guanine nucleotide exchange factor (GEF) of small GTPases, e.g. the Rab protein family, comparable to other members of the DENN-like superfamily. Rab GTPases are molecular switches involved in several steps of cellular membrane trafficking (Levine et al., 2013). Indeed, *C9orf72* forms a complex with WDR41 and SMCR8, another DENN protein, and interacts with several Rab proteins suggesting *C9orf72* might play a role in endocytosis and autophagy (Fig. 6C) (Farg et al., 2014; Sellier et al., 2016).

Three broadly expressed *C9orf72* transcripts potentially result in two distinct isoforms of the protein. The longer protein product is by far most abundant and is localized to the cytoplasm (Saber et al., 2018). The FTD/ALS linked GGGGCC-repeat expansion is present between the two non-coding exons 1a and 1b. Depending on the transcript, the GGGGCC-repeat is either located in intron 1 (for V1 and V3) or in the promoter region (for V2) (Fig. 6) (DeJesus-Hernandez et al., 2011).

### **2.2. Current hypothesis of C9orf72 disease related pathomechanisms**

How the GGGGCC-repeat expansion in *C9orf72* causes FTD/ALS remains elusive. Both LOF and GOF mechanisms through three main mechanisms have been discussed. First, the GGGGCC-repeat expansion impairs expression of the longer isoform and may thus cause *C9orf72* haploinsufficiency. Second, the GGGGCC sense and antisense repeat transcripts accumulate in RNA foci that are thought to sequester RBPs (RNA toxicity). Third, repeat containing transcripts are unconventionally translated into DPR proteins, which form aggregates and trap important cellular proteins (protein toxicity) (Fig. 6) (Edbauer and Haass, 2016).

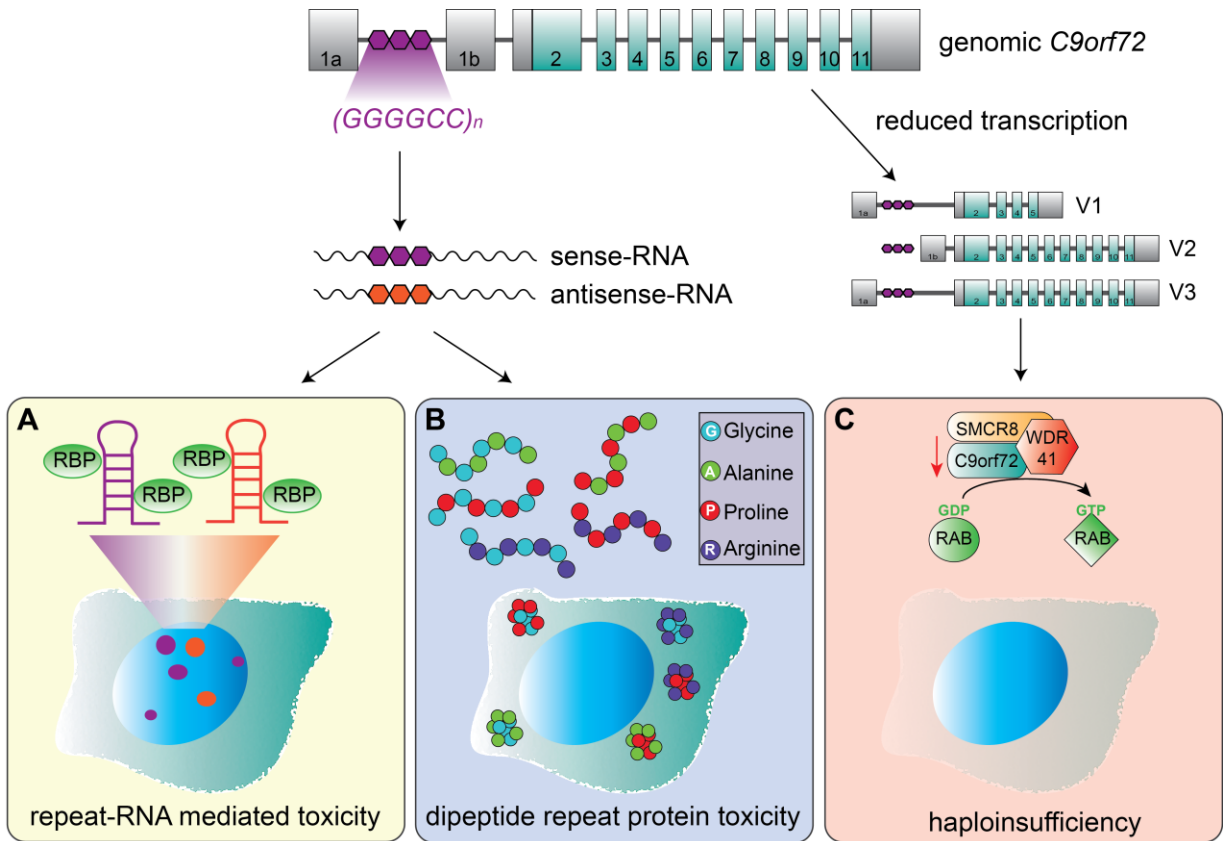


**Figure 6 Overview of current hypothesis of *C9orf72* repeat expansion mediated pathogenic mechanisms.**

The human *C9orf72* gene (grey: non-coding region; green: coding exons) harbors a hexanucleotide (GGGGCC)<sub>n</sub> repeat expansion (purple) between the alternative exons 1a and 1b. Three *C9orf72* transcripts are produced. Sense and antisense transcription of the repeat RNA also occurs. The three mutually non-exclude pathomechanisms are depicted (see text). Adapted from (Gitler and Tsuiji, 2016; Ling et al., 2013).

Based on these three hypothesized mechanisms, many research groups made huge efforts to decipher and verify the individual processes. Both, mRNA and protein levels have been reported to be reduced in *C9orf72* FTD/ALS cases suggesting haploinsufficiency as a possible disease cause (DeJesus-Hernandez et al., 2011; Waite et al., 2014). Although *C9orf72* knock down (KD) in zebrafish led to reduced axon length of motor neurons and locomotion impairment, *C9orf72* ablation in neuron specific KO mice did not show any FTD/ALS-like pathology, such as motor neuron degeneration, or motor defects (Ciura et al., 2013; Koppers et al., 2015). Complete KO of *C9orf72* causes systemic inflammation in mice (Sudria-Lopez et al., 2016). Therefore, *C9orf72* LOF is likely not the main driving mechanism of FTD/ALS but could contribute to disease by inhibiting autophagy or promoting inflammation (Fig. 6C) (Sellier et al., 2016; Webster et al., 2016; Yang et al., 2016).

Interestingly, it has been shown, that both sense and antisense repeat transcripts form stable inter- and intramolecular structures, such as G-quadruplexes (G-Q), R-loops or hairpins, in *C9orf72* patients. Nuclear RNA foci are found in many cell types and may sequester crucial

RBPs (e.g. hnRNPs), and thereby impair overall RNA metabolism (Fig. 6A) (Cooper-Knock et al., 2014; Gendron et al., 2013; Kumar et al., 2016; Mori et al., 2013b).

Repeat associated non-AUG translation was first discovered for CAG repeats in spinocerebellar ataxia type 8 (SCA8) and Myotonic dystrophy type 2 (DM2), and has since been reported in other repeat expansion disorders (Zu et al., 2011). Surprisingly, even the intronic GGGGCC-expansion in *C9orf72* is translated in all reading frames into coaggregating DPR proteins: poly-glycine-alanine (GA), poly-glycine-proline (GP), poly-glycine-arginine (GR), poly-proline-arginine (PR) and poly-proline-alanine (PA) (Fig. 6B). These DPR proteins form pathological inclusions in neurons of *C9orf72* patients. Poly-GA is most abundant in patients followed by poly-GP and poly-GR (Mori et al., 2013a; Mori et al., 2013c). DPR inclusions colocalize with SQSTM1/p62 in star-shaped cytoplasmic, nuclear, or neuritic inclusions, and only rarely colocalize with TDP-43 (Mori et al., 2013c). Several studies showed toxicity of the different DPR species in distinct cellular systems, primary neurons, and mice (Jovicic et al., 2015; May et al., 2014; Schludi et al., 2017; Yamakawa et al., 2015; Zhang et al., 2016). Poly-GA is highly aggregation prone *in vitro* and GA<sub>15</sub> peptides form  $\beta$ -sheet structures with cell-to-cell transmission properties (Chang et al., 2016). Poly-GA inclusions trap essential cellular proteins, including various components of the UPS, which leads to UPS impairment and thus to toxicity (May et al., 2014; Yamakawa et al., 2015; Zhang et al., 2016; Zhang et al., 2014). The arginine rich DPR species, poly-GR and poly-PR, trigger nucleolar stress, nuclear transport impairment, and RNA processing alterations. Furthermore, they interact with the translation complex and ribosomal proteins, thereby impairing overall protein translation and causing neurotoxicity (Kanekura et al., 2016; Mizielinska et al., 2014).

However, it still remains unknown how DPR aggregates exactly contribute to *C9orf72* FTD/ALS. A better resolution of DPR aggregate structure would provide relevant information, e.g. to unravel spreading properties of distinct DPR aggregates or to help to identify interacting cellular organelles or macromolecules.

Of note, in end-stage patient brains neither DPR pathology, RNA foci nor *C9orf72* mRNA/protein levels robustly correlate with neurodegeneration (Mackenzie et al., 2013). However, the temporal course of events cannot be deciphered via post-mortem studies for a rare disease such as FTD/ALS. Several neuropathology case reports suggest DPR accumulation starts early in disease, before TDP-43 pathology is present, but further cross-sectional and ideally longitudinal studies are required to clarify the role of DPR proteins in *C9orf72* FTD/ALS pathogenesis (Baborie et al., 2015; Proudfoot et al., 2014; Vatsavayai et al., 2016). For this purpose, poly-GP might be a suitable biomarker candidate not only because of its relatively high solubility but also due to its high expression throughout the central nervous system (CNS) (Peters et al., 2015;

Schludi et al., 2015). Furthermore, poly-GP has been detected in cerebrospinal fluid (CSF) in a small case series of *C9orf72* FTD/ALS (Su et al., 2014). It is unknown whether extracellular poly-GP reaches the CSF by unconventional secretion or by release from dead cells. Developing an *in vivo* biomarker for repeat translation will be important for preclinical studies, e.g. to monitor potential therapies.

### 3. *CHCHD10* - A mitochondrial link to FTD/ALS

Mitochondria have long been suspected to play a causative, primary role in ALS pathogenesis, which was supported by the identification of a *CHCHD10* missense mutation (S59L) in a family with late onset myopathy and motor and cognitive phenotypes, including MND- and FTD-like symptoms (Bannwarth et al., 2014).

#### 3.1. Structural features and mitochondrial import

*CHCHD10* encodes a soluble 142 amino acid (aa) protein, which is predominantly present in the IMS of mitochondria (Bannwarth et al., 2014). It consists of a positively charged N-terminus, a central hydrophobic helix and a CHCH domain located at the C-terminal region of the protein (Ajroud-Driss et al., 2015; Cozzolino et al., 2015; Perrone et al., 2017) (Fig. 7A). CHCH domains are mainly found in mitochondrial localized proteins and are involved in metal binding and in protein import in the IMS (Banci et al., 2009b). For other members of the CHCH protein family, disulfide bridge formation within two Cysteine-X<sub>9</sub>-Cysteine (CX<sub>9</sub>C) motifs stabilizes the protein and has been linked to mitochondrial import (Fig. 7B).

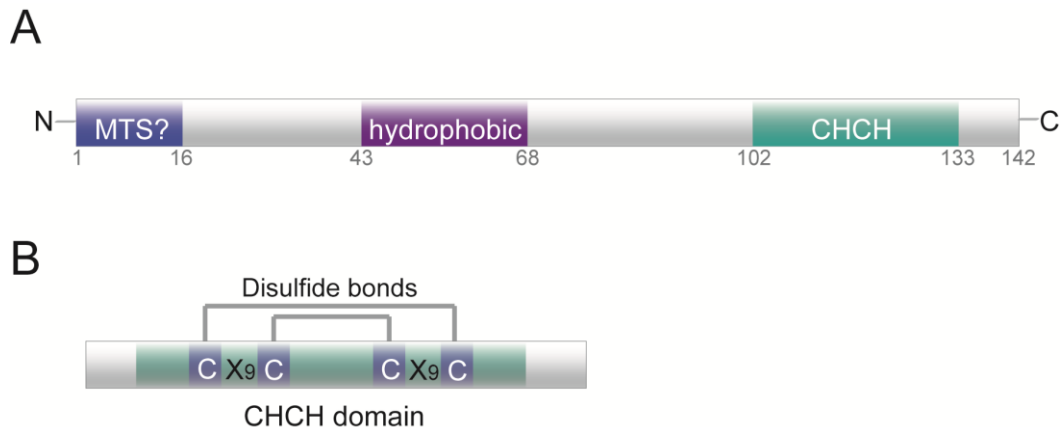


**Figure 7 Structure of *CHCHD10* and its CHCH domain.**

**(A)** The N-terminal end of *CHCHD10* is often referred to as a putative mitochondrial targeting signal (MTS?, blue) and is followed by a hydrophobic (purple) and a C-terminal CHCH domain (green). **(B)** Between two CX<sub>9</sub>C motifs, disulfide bonds are formed in the CHCH domain of *CHCHD10*.

Nearly all mitochondrial proteins are encoded in the nucleus, synthesized as cytosolic precursor proteins and transported into mitochondria via diverse import machineries (Harmey et al., 1977; Modjtahedi et al., 2016; Zhou et al., 2017). The translocase in the outer membrane of

mitochondria (TOM) complex is the first contact for proteins entering the mitochondria (Hase et al., 1983; Kang et al., 2017; Kiebler et al., 1990; MacPherson and Tokatlidis, 2017). Targeting signals within the immature precursor proteins guide them on different transport routes to their final mitochondrial localization.

$\beta$ -barrel proteins harbor a  $\beta$ -signal and are handed over to the small translocase of the inner mitochondrial membrane (TIM) chaperons in the IMS where they are subsequently delivered to the outer mitochondrial membrane (OMM) via the sorting and assembly machinery (SAM) complex (Kozjak et al., 2003; Lutz et al., 2003; Paschen et al., 2003). The import pathway of hydrophobic carrier proteins that are present in the IMM of mitochondria is also mediated by small TIM chaperons in conjunction with the translocase TIM22 complex (Dudek et al., 2013; Kerscher et al., 1997; MacPherson and Tokatlidis, 2017; Sirrenberg et al., 1996). Moreover, the TIM23 complex is the central junction of the mitochondria import pathway for presequence containing proteins. Such proteins are either inserted into the IMS or imported to the matrix. For matrix translocation an additional motor, named presequence translocase associated import motor (PAM), is required. After entering the matrix, presequences are proteolytically cleaved by mitochondrial processing peptidases (MPP) (Dudek et al., 2013; Frazier et al., 2004; Kozany et al., 2004). Proteins of the IMS, that harbor a cysteine-rich signal ( $CX_nC$ ), typically located in a CHCH domain, are imported via the mitochondrial intermembrane space import and assembly (Mia) pathway (Fig. 8) (Chacinska et al., 2004). Thus, the Mia pathway could also mediate import of CHCHD10, although it also has a predicted N-terminal presequence.

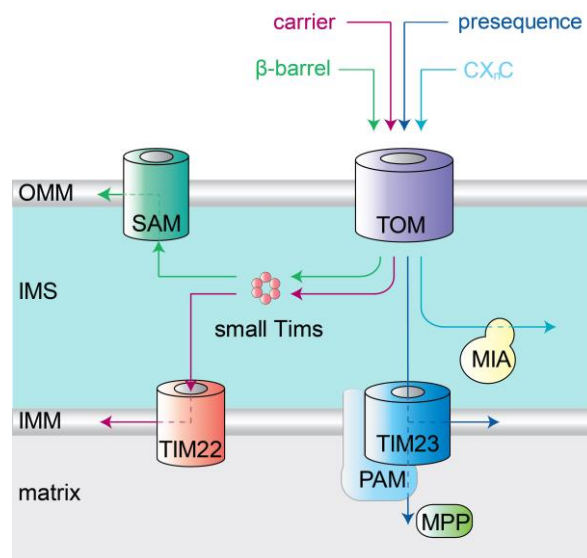


**Figure 8 Mitochondrial import pathways.**

Precursor proteins such as  $\beta$ -barrel proteins, carrier proteins, presequence containing proteins and proteins with cysteine-rich signals ( $CX_nC$ ) are imported in a post-translational manner via specific pathways (see text). The majority of mitochondrial proteins enter the mitochondria through the TOM complex. Adapted from (Dudek et al., 2013).

The oxidoreductase Mia40 contains two essential structural and functional elements: An N-terminal redox active cysteine-proline-cysteine (CPC) motif and a C-terminal hydrophobic substrate binding cleft (Kawano et al., 2009). Human Mia40 physically interacts with the membrane-bound apoptosis inducing factor (AIF) (Hangen et al., 2015; Hofmann et al., 2005; Kawano et al., 2009). Mia40 additionally plays a key role in the import of small IMS proteins by catalyzing their intact oxidative folding and maturation via covalent disulfide bridges formation (Banci et al., 2009a; Weckbecker et al., 2012). Precursor proteins enter the IMS via the TOM complex and first interact with the hydrophobic binding pocket of Mia40 (Peleh et al., 2016). Oxidized Mia40 then forms transient intermolecular disulfide bonds with free cysteine residues, located either in CX<sub>3</sub>C or CX<sub>9</sub>C motifs of substrate proteins (Kawano et al., 2009). After complete disulfide bond formation, oxidized proteins are released into the IMS and Mia40 remains in its reduced state. Re-oxidation of Mia40 is mediated by Erv1 (essential for respiration and vegetative growth), a FAD-linked sulfhydryl oxidase (Lee et al., 2000; Muller et al., 2008). Subsequently, reduced Erv1 shuttles its electrons to CytC, where they finally enter the respiratory chain via the CytC oxidase (COX) complex (Fig. 9) (Dabir et al., 2007).

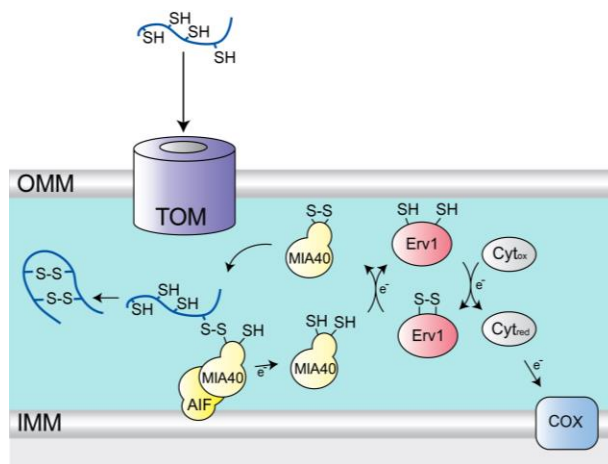


**Figure 9 The Mia40 mediated IMS import pathway.**

Cysteine-rich precursor proteins enter the IMS via the TOM complex. Mia40 forms intermediate disulfides with the emerging precursor proteins and catalyzes their oxidation and folding. After complete disulfide bond formation, the proteins are released into the IMS. Mia40 itself is reduced and requires oxidation by Erv1. Erv1 transfers electrons directly to CytC where they are finally transferred to the COX complex of the respiratory machinery. Adapted from (Dudek et al., 2013; Stojanovski et al., 2008).

Due to its interspaced conserved arginine residues, several bioinformatic prediction tools suggest a classical N-terminal mitochondrial targeting signal (MTS) for CHCHD10. Therefore, the N-terminus is often referred as putative MTS (aa 1-16) in literature (Cozzolino et al., 2015; Perrone et al., 2017). Since mutations in the N-terminal region (R15L, R15S) still localize to mitochondria and mutations in the CHCH domain (Q108\*) have not been functionally studied so far, it is not clear how CHCHD10 is imported to mitochondria (Ajroud-Driss et al., 2015; Woo et al., 2017).

### 3.2. Function and genetic link to FTD/ALS

Although the exact molecular function of CHCHD10 is still unknown, previous work suggests a role in mitochondrial morphology, cristae structure integrity, as well as stability of the mitochondrial genome (Bannwarth et al., 2014; Genin et al., 2016). Additionally, it has been reported that CHCHD10 is part of the mitochondrial contact site and cristae organizing system (MICOS) complex, which is crucial for the formation and integrity of mitochondrial cristae structure (Genin et al., 2016). Together, CHCHD10 and CHCHD2, another CHCH containing protein that is associated with PD, form complexes that play a key role in cellular respiration, especially under stress conditions (Burstein et al., 2018; Straub et al., 2018). Furthermore, it was found that CHCHD10 enables phosphorylation of CHCHD2 by recruiting Abl2 kinase and thereby stimulating COX activity in mitochondria (Purandare et al., 2018). Rapid protein turnover argues for a regulatory function of CHCHD10, i.e. for metal transport and respiratory chain complex assembly (Burstein et al., 2018). Some argue CHCHD10 may also enter the nucleus and repress genes harboring an oxygen responsive element (ORE) or help to retain TDP-43 in the nucleus (Purandare et al., 2018; Woo et al., 2017).

After the identification of the first missense mutations S59L in *CHCHD10*, other labs screened *CHCHD10* in several distinct cohorts of ALS, FTD or mitochondrial myopathy (MM) patients and identified many additional missense mutations (Fig. 10) (Ajroud-Driss et al., 2015; Auranen et al., 2015; Blauwendraat et al., 2018; Brockmann et al., 2018; Burstein et al., 2018; Chaussenot et al., 2014; Dols-Icardo et al., 2014; Genin et al., 2016; Jiao et al., 2016; Johnson et al., 2014; Kurzwelly et al., 2015; Muller et al., 2014; Penttila et al., 2017; Perrone et al., 2017; Rubino et al., 2018; Straub et al., 2018; Wong et al., 2015; Woo et al., 2017; Xiao et al., 2017).

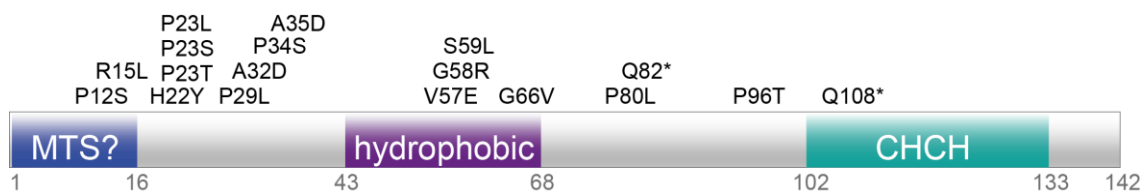


**Figure 10 Reported CHCHD10 variants in families with ALS, FTD, FTD/ALS or MM.**

CHCHD10 mutations and their localization in the respective regions: putative MTS (blue), hydrophobic (purple) and CHCH (green) domain.

CHCHD10 variants, identified in FTD/ALS families, cluster in the N-terminus suggesting a functional relevance. However, a clear pathogenic mechanism has not been shown for any of these variants (Table 1). Pathogenicity has essentially been ruled out for P34S based on genetic data.

**Table 1 Reported CHCHD10 variants linked to ALS, FTD, FTD/ALS or MM and their putative pathogenic phenotypes in patient material, cellular and *in vivo* models.**

variant	disease	pathogenic phenotypes		reference
		patient	cells/ <i>in vivo</i>	
P12S	ALS	-	-	Dols-Icardo et al.
R15L	ALS	<b>fibroblasts:</b> reduced protein level, mitochondrial hyperfusion, respiration deficiency, altered OXPHOS complexes <b>LCL:</b> reduced protein level, reduced mRNA	<b>HEK293:</b> increased protein degradation reduced mito. colocalization reduced ATP synthesis reduced mito. mRNA level <b>NIH3T3:</b> fragmented mitochondria reduced mito. colocalization TIA-1 granule induction cyto. TDP-43 accumulation <b>neurons:</b> cyto. TDP-43 accumulation reduced pre-/postsynaptic integrity <b>HT22:</b> increased TDP-43 ind. apoptosis <b>transduced mice:</b> synaptic damage	Brockmann et al., Burstein et al., Müller et al., Johnson et al., Kurzweily et al., Straub et al., Woo et al.
R15S	MM	-	-	Ajrroud-Driss et al.
H22Y	FTD	-	-	Jiao et al.
P23L/S	FTD	-	-	Jiao et al.
P23T	FTD	-	-	Zhang et al.
A32D	FTD	-	-	Jiao et al.
P34S	ALS, FTD	-	<b>HeLa:</b> reduced mito. nucleoids	Brockmann et al., Chaussenot et al., Dols-Icardo et al., Genin et al., Ronchi et al., Wong et al., Zhang et al.
A35D	FTD,AD	-	-	Xiao et al., Zhang et al.
V57E	FTD	-	-	Jiao et al.
G58R	MM	-	<b>HEK293:</b> fragmented mitochondria	Ajrroud-Driss et al.
S59L	FTD/ALS	<b>muscle:</b> ragged-red/COX-negative fibres, mtDNA deletions, respiration deficiency, altered OXPHOS complexes <b>fibroblasts:</b> fragmented mitochondria, ultrastructural alterations, respiration deficiency, altered OXPHOS complexes, reduced nucleoids, partial MICOS disassembly	<b>HeLa:</b> fragmented mitochondria, ultrastructure alterations, reduced nucleoids <b>Hek293:</b> punctate distribution reduced mito. colocalization reduced ATP synthesis reduced mito. mRNA level <b>NIH3T3:</b> fragmented mitochondria reduced mito. colocalization TIA-1 granule induction cyto. TDP-43 accumulation <b>neurons:</b> cyto. TDP-43 accumulation reduced pre-/postsynaptic integrity <b>HT22:</b> increased TDP-43 ind. apoptosis <b>transduced mice:</b> synaptic damage	Bannwarth et al., Blauwendraat et al., Burstein et al., Genin et al., Woo et al.
G66V	ALS	<b>fibroblasts:</b> reduced protein level	<b>HEK293:</b> increased protein degradation, respiration deficiency, increased ROS	Auranen et al., Brockmann et al., Müller et al., Penttilä et al., Purandare et al.
P80L	ALS	-	<b>HEK293:</b> respiration deficiency, increased ROS	Ronchi et al., Zhang et al., Purandare et al.
Q82*	FTD	-	-	Dols-Icardo et al.
P96T	MM, ALS, FTD	-	-	Dols-Icardo et al., Rubino et al., Teyssso et al.
Q108*	FTD	<b>LCL:</b> NMD of mutant transcript	-	Perrone et al.

Abbreviations: Lymphoblastoid cell lines (LCL), mitochondrial (mito.) nonsense-mediated mRNA decay (NMD), oxidative phosphorylation (OXPHOS), T-cell intracellular antigen 1 (TIA-1).

### 3.3. Current hypothesis of *CHCHD10* disease-related pathomechanisms

Since very little is known about the exact molecular pathomechanisms of *CHCHD10* variants, the debate about a LOF or a GOF mechanism is still ongoing.

Reduced steady state protein levels of *CHCHD10* mutants and decreased mRNA support a LOF mechanism (Brockmann et al., 2018; Straub et al., 2018). Additionally, respiration defects as well as decreased COX activity and ATP levels were reported upon *CHCHD10* KD, in patient fibroblasts and KO cells (Purandare et al., 2018; Straub et al., 2018). *In vivo* experiments in *C. elegans* revealed that KO of *har-1*, the orthologue of mammalian *CHCHD10*, lead to reduced life-span and significant locomotion deficits. Moreover, mutant proteins (R15L, S59L) fail to rescue the KO phenotype in *C. elegans* (Woo et al., 2017; Zubovych et al., 2010). *In vivo* experiments with *CHCHD10* KD zebrafish models further strengthened a LOF mechanism, since KD caused axonal motoneuron pathology, abnormalities in myofibrillar structure and motility deficits (Brockmann et al., 2018). However, recent *CHCHD10* KO mice showed neither any characteristic symptoms for neurodegenerative diseases nor mitochondrial abnormalities in brain, muscle and heart as shown in human patient fibroblasts with reduced *CHCHD10* (Burstein et al., 2018; Straub et al., 2018). Since impaired respiration could only be detected in muscle but not in brain of these mice, cell type specific effects might play an essential role in the *CHCHD10* underlying pathogenesis (Burstein et al., 2018).

Several studies with patient cells or transiently transfected cellular models reported DNA instability, mitochondrial fragmentation and cristae disorganization (Ajroud-Driss et al., 2015; Bannwarth et al., 2014; Genin et al., 2016). Moreover, S59L *CHCHD10* leads to impairment of the respiratory chain, shown in patient muscle as well as fibroblasts (Bannwarth et al., 2014). Other missense mutations, such as G66V and P80L, impaired both nuclear and mitochondrial function of *CHCHD10* (Purandare et al., 2018).

Since disease progression of *CHCHD10* associated FTD/ALS is rather slow (6-12 years), age of onset usually pretty late (50s) and penetrance incomplete, some geneticists raised doubts about the true pathogenicity of *CHCHD10* mutations. A clear underlying pathomechanism that could fully support *CHCHD10* as *bona fide* FTD/ALS gene is not known for any of the *CHCHD10* mutations. Furthermore, sequencing of *CHCHD10* in larger populations is needed to determine the mutation frequency. Functional analysis of several *CHCHD10* mutations is crucial to strengthen the link between *CHCHD10* to FTD/ALS (van Rheenen et al., 2014).

#### **4. Clinical biomarkers and therapy approaches in FTD and ALS**

There is no effective disease-modifying therapy for FTD and ALS so far. Although intensive efforts are devoted to developing new therapies, and several clinical trials have reached phase II/III, only two drugs, riluzole and edaravone, are approved by the Food and Drug Administration (FDA) for ALS patients. Unfortunately, these drugs are not very effective. Riluzole only extends survival by an average of 2-3 months (Bensimon et al., 1994; Miller et al., 2012). The underlying mechanism of edaravone is unknown, but it is presumed to reduce oxidative stress in ALS and thereby may slow down disease progression specifically in patients with very aggressive disease (Cruz, 2018). The tremendous progress in FTD and ALS genetics in recent years has led to better understanding of the underlying pathomechanisms and may improve therapeutic interventions in the future. It is likely that many of the pathways identified in familial FTD/ALS will be relevant for understanding sporadic FTD/ALS because the neuropathology and clinical presentation is often indistinguishable. A key factor to improve future therapeutic studies is to include pharmacodynamic biomarkers to document a biological response to therapeutic treatment during preclinical and clinical studies (Balendra et al., 2017).

##### **4.1. Biomarkers for neurodegenerative diseases**

Presymptomatic stages of neurodegenerative diseases offer an interesting window to study early disease stages and are usually the ideal time to start therapy before irreversible neuronal damage occur. Neuroimaging biomarkers enable visualization of pathological changes in the brain, and have already been established for AD and Huntington's disease. In AD, MRI is used to show atrophy, while PET is used to detect A $\beta$  and tau aggregates and metabolic abnormalities (e.g. glucose metabolism) (Schilling et al., 2016). As imaging technologies are expensive and expose brain and body to radioactive compounds, developing biomarkers from body fluid such as CSF, blood or urine is of high interest (Gozes, 2017). Immunoassays are the most sensitive and specific technology to validate and measure biomarkers to date. Monoclonal antibodies allow a standardized analysis of biomarker levels. Another big advantage is that they are not vulnerable to limited availability or batch-to-batch variability, which is critical for the use as a therapeutic biomarker.

Neurofilament light chain (NfL) is a powerful biomarker for axonal injury, reflecting disease severity and progression, as well as brain atrophy for FTD, ALS and other neurodegenerative disease including AD (Lu et al., 2015; Meeter et al., 2016; Scherling et al., 2014; Zetterberg et al., 2016). Currently A $\beta$ 42, tau, and phospho-tau are used as biomarkers to confirm AD via the CSF. Here, a decrease of CSF A $\beta$ 42 burden and an increase in tau correlates with amyloid plaque deposition, neuronal death, and accumulation of tangles (Gozes, 2017; Randall et al.,

2013). Interestingly, soluble TREM2 was shown to change dynamically during respective AD stages (Suarez-Calvet et al., 2016). In *C9orf72* FTD/ALS, poly-GP has been detected in CSF of a small cohort of ALS cases by an immunoassay using polyclonal antibodies (Su et al., 2014). Further studies in a large diverse cohort are required to potentially establish poly-GP as a pharmacodynamic biomarker. Detecting reduced levels of poly-GP may show target engagement in therapeutic trials, e.g. with antisense oligonucleotides (ASO).

## 4.2. Therapeutic approaches for FTD/ALS

TDP-43 is an attractive therapeutic target for FTD/ALS, since nearly all cases of ALS and 45% of FTD show TDP-43 positive protein inclusion. As misfolded TDP-43 leads to nuclear LOF and cytoplasmic toxic GOF, it would be interesting to promote refolding or degradation of misfolded TDP-43 via the UPS and/or autophagy (Scotter et al., 2015). In *C9orf72* FTD/ALS, repeat RNA and DPR proteins may stepwise trigger TDP-43 pathology resulting in a brain region-specific neurodegeneration (Edbauer and Haass, 2016).

In recent years, several interesting strategies to treat *C9orf72*-mediated disease have been suggested. *C9orf72* haploinsufficiency is suspected to contribute to *C9orf72* FTD/ALS and associated with impaired autophagy. Therefore, induction of *C9orf72* expression, e.g. by targeting chromatin modification, might be a reasonable treatment strategy to rescue normal autophagy, but could also promote repeat-mediated RNA and protein toxicity (DeJesus-Hernandez et al., 2011; Sellier et al., 2016).

Another promising approach is to interfere with GGGGCC-repeat containing RNA. Chemically modified single-stranded ASO allow long-lasting suppression of target genes through RNase H mediated cleavage (Miller and Harris, 2016). For infantile-onset spinal muscular atrophy, an ASO-based therapy has already successfully passed phase 3 clinical studies and is now approved in Europe (Wan and Dreyfuss, 2017). Specific degradation of the repeat-containing introns using ASOs may block both RNA and DPR toxicity in *C9orf72*. Interestingly, several publications demonstrated that ASOs, targeting the GGGGCC-containing intron, reduce RNA foci and toxic DPR proteins without affecting overall *C9orf72* mRNA levels in patient cells. Further ASO studies in *C9orf72* BAC-transgenic mice confirmed these observations and successfully alleviated behavioral deficits (Donnelly et al., 2013; Jiang et al., 2016; Lagier-Tourenne et al., 2013).

Since both RBP sequestration and RAN translation are potentially influenced by the structure of GGGGCC-repeat-containing RNAs, targeting the G-Q confirmation may be another exciting treatment option. Small molecules targeting G-Qs reduced both RNA foci and DPR proteins in neurons, transdifferentiated from fibroblasts, of *C9orf72* patients (Su et al., 2014). DPR proteins

were also reduced in GGGGCC-repeat-expressing flies and extended survival (Simone et al., 2018). Altogether, these findings suggest that targeting repeat RNA structure is an encouraging strategy to slow down or even prevent *C9orf72* mediated disease progression.

Spreading of toxic protein aggregates is another mechanism thought to contribute to propagation of disease pathology. Therefore, antibody-based immunotherapy may slow or stop the spreading of protein aggregation by increasing phagocytosis through microglia and/or interfering with neuronal uptake. Immunotherapy targeting intracellular tau aggregates has shown beneficial neurological effects in a mouse model (Yanamandra et al., 2013). A $\beta$  immunotherapy reduced A $\beta$  pathology in AD patients in early disease stages (Sevigny et al., 2016). Although antibodies only target extracellular proteins, they are thought to also act on intracellular aggregates during transmission between cells. If similar transmission occurs for DPR proteins, vaccination might be a promising therapeutic approach to target DPR aggregates in *C9orf72* FTD/ALS.

Another attempt for FTD/ALS treatment may be to restore mitochondrial activity. Several small molecules have been designed to act on respiration/ATP production, apoptosis, and ROS-induced DNA damage (Malty et al., 2015). Nicotinamide administration promotes mitophagy in cell culture, prevents cognitive defects, and selectively reduced phospho-tau (Thr 231) in an AD mouse model (Green et al., 2008; Jang et al., 2012). Interestingly, the synthetic AMP-activated protein kinase (AMPK) activator 5-amino-1- $\beta$ -D-ribofuranosylimidazole-4-carboxamide (AICAR), improved motor performance in mice, e.g. by correcting COX deficiency (Viscomi et al., 2011). Pramipexole is a neuroprotective dopamine analogue that prevents activation of the mitochondrial/intrinsic apoptotic pathway, and reduces free radical levels in ALS patients (Pattee et al., 2003). Another strategy is to induce transcription of genes involved in mitochondrial biogenesis or oxidative stress response, e.g. via PPAR $\gamma$  coactivator-1 $\alpha$  (PGC-1 $\alpha$ ). PGC-1 $\alpha$  mRNA levels in ALS patients are reduced, and activation of PGC-1 $\alpha$  shows protective effects in a SOD1 mouse model of ALS (Puigserver and Spiegelman, 2003; Thau et al., 2012).

Edaravone, which is known to reduce oxidative stress in neurons, showed promise in fast-progressing patients and in is the first mitochondrial therapy approved by the FDA for ALS (Mitsumoto et al., 2014; Poppe et al., 2014).

Neuronal loss in FTD and ALS likely results from a combination of pathomechanisms including mitochondrial dysfunction, loss of RNA and/or protein homeostasis, oxidative stress and disrupted axonal transport processes. This may explain why single drug approaches have not been effective in patients. Further insights into individual pathomechanisms and their interaction will hopefully uncover possibilities for single or multi-drug based disease modifying therapies. These studies will greatly benefit from *in vivo* biomarkers in preclinical and clinical trials.

## II. Zusammenfassung

Diese Arbeit beschäftigt sich mit Biomakern und Pathomechanismen in zwei familiären Formen der Frontotemporalen Demenz (FTD) und der Amyotrophen Lateralsklerose (ALS). Hierbei fokusierte ich mich insbesondere auf das Ubiquitin-Proteasom-System (UPS), interzellulärer Übertragung von Protein-Aggregaten und mitochondrialer Dysfunktion.

Die häufigste genetische Ursache von FTD und ALS ist eine massive Verlängerung einer sonst kurzen (GGGGCC)<sub>n</sub> Sequenz in der Intronregion von *C9orf72*. Patienten haben hunderte von GGGGCC-Wiederholungen, die bidirektional transkribiert werden. Beide Repeat-Transkripte bilden RNA-Foci im Zellkern und werden auf unkonventionelle Weise in allen Leserahmen in fünf Dipeptid-Repeat (DPR)-Proteine (Poly-GA, Poly-GP, Poly-GR, Poly-PA und Poly-PR) translatiert, die im Gehirn von *C9orf72* Patienten co-aggregieren.

Sowohl in *C9orf72* FTD/ALS als auch in anderen neurodegenerativen Erkrankungen wird eine Dysfunktion des Ubiquitin-Proteasom-Systems (UPS) als Ursache oder Folge von Proteinaggregation diskutiert. Um die Ultrastruktur der Poly-GA-Aggregate zu untersuchen, führten wir Kryoelektronentomographie in primären Neuronen durch. Dabei fanden wir, dass Poly-GA-Aggregate aus dicht gepackten "twisted ribbons" bestehen, an die zahlreiche 26S-Proteasomen binden. Dabei wird das 26S-Proteasom in einem seltenen Übergangszustand blockiert, was auf eine gestörte Degradation hinweist. Ich konnte die Kolo-kalisation von Poly-GA mit dem Proteasom in Zellkultur bestätigen und mit biochemischer Fraktionierung die Sequestrierung des Proteasoms zeigen. Zusammengefasst zeigen diese Ergebnisse, dass Proteasomen in Poly-GA-Aggregaten eingeschlossen und inaktiviert werden und so das zelluläre UPS gestört wird (**Publikation II**).

Die interzelluläre Übertragung von intrazellulären Proteinaggregaten scheint ein gemeinsames Merkmal von neurodegenerativen Erkrankungen zu sein. Im Rahmen einer größeren Studie zur Übertragung von DPR-Proteinen konnte ich in Ko-Kultur Experimenten die Transmission von Poly-GA zwischen primären Neuronen nachweisen. Überraschenderweise induzierte die Überexpression von Poly-GA zudem die RNA-Foci Bildung in *C9orf72*-Fibroblasten, was auf eine positive Rückkopplung der Transkription schließen lässt. Die Übertragung von Poly-GA kann somit nicht-zellautonome Effekte in *C9orf72* FTD/ALS auslösen (**Publikation IV**).

Trotz der Toxizität von DPR-Proteinen in verschiedenen Zellkultur- und Tiermodellen, stellt die fehlende Korrelation der DPR-Protein Verteilung in humanem *post-mortem* Gewebe mit Neurodegeneration ihre kausale Rolle in Frage. Um diesen Widerspruch aufzulösen, wollte ich den zeitlichen Verlauf der DPR-Expression in *C9orf72* Patienten detektieren. Dazu entwickelte ich einen neuartigen Poly-GP-Immunoassay mit monoklonalen Antikörpern und untersuchte damit in

einer Querschnittsstudie Liquor von *C9orf72*-Mutationsträgern. Hier konnte ich Poly-GP, im Vergleich zu gesunden Kontrollen oder Patienten mit anderen neurodegenerativen Erkrankungen, selektiv bei Mutationsträgern nachweisen. Außerdem detektierte ich Poly-GP in einem klinischen Alzheimer Patienten, bei dem ein anschließender Gentest die *C9orf72* Mutation bestätigen konnte. Dies belegt den klinischen Nutzen des neuen Poly-GP Immunoassays. Erstaunlicherweise, waren die Poly-GP Mengen bei symptomatischen und asymptomatischen *C9orf72*-Mutationsträgern nahezu identisch. Dies deutet darauf hin, dass die DPR-Proteine wahrscheinlich bereits im Prodromalstadium den Krankheitsverlauf initiieren, indem sie das UPS überlasten und nicht-zellautonome Effekte auslösen (**Publikation III**).

DPR-Proteine werden zwar mit mitochondrialer Dysfunktion in Verbindung gebracht, allerdings sind Mutationen im mitochondrialen Protein CHCHD10 bisher der stärkste Beweis für eine kausale Rolle dieses Pathomechanismus bei FTD/ALS. Die langsame Progression und unvollständige Penetranz von *CHCHD10*-Mutationen hatten jedoch zu heftigen Debatten geführt. Darüber hinaus sind die molekularen Mechanismen der bisher bekannten *CHCHD10*-Mutationen unklar.

In dieser Arbeit charakterisierte ich eine neue Mutation in *CHCHD10* (Q108P), die bei einem 29 Jahre alten ALS-Patienten mit sehr aggressiver Krankheitsprogression identifiziert wurde. Q108P befindet sich in der CHCH-Domäne und betrifft eine hoch konservierte Aminosäure. Meine *in vitro* Experimente zeigen, dass Q108P den mitochondrialen Import fast vollständig blockiert, was zu einer verringerten Proteinstabilität und einer diffusen zytoplasmatischen Lokalisierung führt. Zusätzlich analysierte ich alle bisher in FTD/ALS Patienten beschriebenen *CHCHD10*-Varianten und entdeckte, dass eine weitere Mutation in der CHCH-Domäne (C122R) auch zu zytoplasmatischer Mislokalisierung führt. Einige Mutationen (G66V und E127K) zeigten normalen mitochondrialen Import, führten jedoch zu mitochondrialer Cluster-Bildung. Somit können *CHCHD10*-Mutationen zu einem Funktionsverlust als auch zu einer toxischen Fehlfunktion des Proteins führen. *CHCHD10* Trunkationen zeigten, dass die CHCH-Domäne für den mitochondrialen Import wichtig ist, und nicht die N-terminale Sequenz, welche bisher als mitochondriales Importsignal postuliert wurde. Entscheidend für den mitochondrialen Import vieler CHCH-Proteine ist eine Mia40-abhängige Bildung von Disulfidbrücken. Mit Hilfe von Knockdown-Experimenten konnte ich in HeLa-Zellen belegen, dass Mia40 auch den mitochondrialen Import von *CHCHD10* vermittelt. Durch Überexpression von Mia40 konnte der mitochondrialen Import von *CHCHD10* Q108P aufgrund verstärkter Bildung von Disulfidbindungen wiederhergestellt werden. Reduzierte mRNA- und Proteinexpression in Patientenlymphoblasten mit Q108stop-Mutation deuten zusätzlich auf Haploinsuffizienz hin. Tatsächlich fand ich eine reduzierte Reserve-Atemkapazität in den Q108stop-Lymphoblasten und in *CHCHD10*-Knockdown-Zellen. Dies bestätigt, dass mitochondriale Dysfunktion wahrscheinlich zur FTD/ALS-Pathogenese beiträgt. Die

Entdeckung einer neuartigen *CHCHD10*-Mutation mit klarem Pathomechanismus unterstützt *CHCHD10* als *bona fide* ALS-Gen. Ein möglicher neuer Therapieansatz für diesen FTD/ALS Subtypen wäre eine Steigerung der Mia40-Aktivität wodurch der CHCHD10-Import und dessen Stabilität erhöht wird (**Publikation I**).

**Zusammengefasst zeigen meine Daten, dass verschiedene Mechanismen wie chronische Beeinträchtigung der Mitochondrien oder des Proteasoms und die Übertragung von Aggregaten zwischen Zellen zur Entwicklung von FTD/ALS beitragen. Darüber hinaus ist Poly-GP ein geeigneter Biomarker für die *C9orf72* FTD/ALS Diagnose und die Überwachung klinischer Therapiestudien.**

### III. Summary

This thesis investigates protein-mediated pathomechanisms and biomarkers in two familial forms of frontotemporal dementia (FTD) and amyotrophic lateral sclerosis (ALS) in cell culture and patient material. I focused on the ubiquitin-proteasome system (UPS), spreading-mechanisms and mitochondrial dysfunction.

The most frequent genetic cause of FTD and ALS is a GGGGCC-repeat expansion mutation in the intronic region of *C9orf72*. Patients harbor hundreds of repeats that are bi-directionally transcribed. Repeat-containing transcripts form nuclear RNA foci and are unconventionally translated in all reading frames into five dipeptide repeat (DPR) proteins (poly-GA, poly-GP, poly-GR, poly-PA and poly-PR). These DPR proteins coaggregate specifically in *C9orf72* patient brains, but their pathogenic nature is still under intense debate.

In *C9orf72* FTD/ALS and other neurodegenerative diseases, dysfunction of the UPS has been discussed as cause or consequence of protein aggregation. To gain deeper insights into the ultrastructure of poly-GA aggregates, we conducted cryo-electron tomography in primary neurons. We found that poly-GA aggregates consist of densely packed twisted ribbons immobilizing numerous 26S proteasomes that are stalled in a rare transition state indicating an unsuccessful degradation attempt. I validated the colocalization of the proteasome with poly-GA and confirmed sequestration of the proteasome by biochemical fractionation. Altogether these results indicate that proteasomes are trapped in poly-GA aggregates and inhibit the UPS (**Publication II**).

Cell-to-cell transmission of intracellular protein aggregates is emerging as a common feature in neurodegenerative diseases. As part of a study on transmission of DPR protein, I conducted co-culture experiments in primary neurons revealing that poly-GA is released and taken up by other neurons. Unexpectedly, I observed that overexpression of poly-GA also induced RNA foci formation in *C9orf72* fibroblasts suggesting a transcriptional feedback mechanism. Together these data suggest cell-to-cell transmission of poly-GA causes non-cell autonomous effects in *C9orf72* FTD/ALS (**Publication IV**).

Despite ample evidence for DPR protein toxicity in cellular and animal models, the lack of correlation between DPR protein expression and neurodegeneration in end-stage tissue have cast doubt on the relevance of DPR proteins for *C9orf72* pathogenesis. To study the temporal course of DPR expression in *C9orf72* FTD/ALS, I established a novel poly-GP immunoassay using monoclonal antibodies. In a cross-sectional study in the CSF from *C9orf72* mutation carrier poly-GP was clearly detected, compared to controls with other neurodegenerative diseases or healthy individuals. Interestingly, poly-GP detection in a clinical AD case and subsequent genetic testing identified a misdiagnosed *C9orf72* case, demonstrating the clinical utility of this immunoassay.

Importantly, I detected similar poly-GP levels in symptomatic and asymptomatic *C9orf72* mutation carriers, suggesting chronic DPR expression in the prodromal stage may trigger subsequent steps in a disease cascade, e.g. by chronic overloading of the UPS, and non-cell autonomous effects through cell-to-cell transmission (**Publication III**).

While DPR proteins have also been linked to mitochondrial dysfunction, mutations in the mitochondrial protein CHCHD10 are so far the strongest evidence for a causal role of this pathomechanism in FTD/ALS. However, most *CHCHD10* mutations described in FTD/ALS patients are associated with late disease onset and slow progression. Incomplete penetrance has raised concerns by some geneticists about the pathogenicity. Moreover, the molecular mechanisms of known *CHCHD10* mutations are unclear.

Here, we identified a novel mutation in CHCHD10 (Q108P) in a 29-year old ALS patient with very aggressive disease progression. Q108P is located in the CHCH domain and affects a highly conserved residue. I discovered that Q108P blocked mitochondrial import nearly completely resulting in decreased protein stability and diffuse cytoplasmic localization *in vitro*. I analyzed all CHCHD10 variants reported in FTD/ALS patients and discovered that another mutation in the CHCH domain (C122R) disrupted mitochondrial localization as well. In contrast, other mutations (G66V and E127K) showed normal mitochondrial import but resulted in mitochondrial clustering. Thus, both loss-of-function and toxic gain-of-function mechanisms might contribute to pathogenesis in *CHCHD10* FTD/ALS. Truncation experiments show that the CHCH domain is critical for import, but not the N-terminal sequence, which has been commonly referred to as a mitochondrial import signal. For other CHCH containing proteins a Mia40-dependent formation of disulfide bonds is critical for mitochondrial import. Using knockdown experiments in HeLa cells, I showed that Mia40 mediates mitochondrial import of CHCHD10. Strikingly, Mia40 overexpression fully rescued mitochondrial import of CHCHD10 Q108P by enhancing disulfide-bond formation and protein stability. Reduced mRNA and protein levels in lymphoblasts from a FTD patient, carrying a Q108stop mutation, further support a loss-of-function mechanism. Interestingly, I also found reduced spare respiratory capacity in the patient Q108stop lymphoblasts and CHCHD10 knockdown cells suggesting that mitochondrial dysfunction can contribute to FTD/ALS pathogenesis. The discovery of a novel *CHCHD10* mutation with a clear pathomechanism strongly supports *CHCHD10* as a bona-fide ALS gene. Enhancing Mia40 activity to boost CHCHD10 import and stability may be a new treatment strategy for this subtype of ALS/FTD (**Publication I**).

**Together, my data show that diverse mechanisms such as chronic impairment of mitochondria or the proteasome, and cell-to-cell transmission of aggregating proteins contribute to the development of FTD/ALS. Furthermore, poly-GP is a suitable biomarker for *C9orf72* FTD/ALS diagnosis and/or monitoring of clinical trials.**

## IV. Results

### 1. Publication I and contribution

*A novel CHCHD10 mutation implicates a Mia40-dependent mitochondrial import deficit in ALS*

published as

**Lehmer C**, Schludi MH, Ransom L, Greiling J, Junghänel M, Exner N, Riemenschneider H, van der Zee J, Van Broeckhoven C, Weydt P, Heneka MT, Edbauer D. A novel CHCHD10 mutation implicates a Mia40-dependent mitochondrial import deficit in ALS. *EMBO Mol Med.* 2018, doi: 10.15252/emmm.201708558



# A novel CHCHD10 mutation implicates a Mia40-dependent mitochondrial import deficit in ALS

Carina Lehmer<sup>1</sup>, Martin H Schludi<sup>1,2</sup>, Linnea Ransom<sup>1</sup>, Johanna Greiling<sup>1</sup>, Michaela Junghänel<sup>1</sup>, Nicole Exner<sup>3</sup>, Henrick Riemenschneider<sup>1</sup>, Julie van der Zee<sup>4,5</sup>, Christine Van Broeckhoven<sup>4,5</sup>, Patrick Weydt<sup>6</sup>, Michael T Heneka<sup>6,7</sup> & Dieter Edbauer<sup>1,2,\*</sup> 

## Abstract

*CHCHD10* mutations are linked to amyotrophic lateral sclerosis, but their mode of action is unclear. In a 29-year-old patient with rapid disease progression, we discovered a novel mutation (Q108P) in a conserved residue within the coiled-coil-helix-coiled-coil-helix (CHCH) domain. The aggressive clinical phenotype prompted us to probe its pathogenicity. Unlike the wild-type protein, mitochondrial import of CHCHD10 Q108P was blocked nearly completely resulting in diffuse cytoplasmic localization and reduced stability. Other CHCHD10 variants reported in patients showed impaired mitochondrial import (C122R) or clustering within mitochondria (especially G66V and E127K) often associated with reduced expression. Truncation experiments suggest mitochondrial import of CHCHD10 is mediated by the CHCH domain rather than the proposed N-terminal mitochondrial targeting signal. Knockdown of Mia40, which introduces disulfide bonds into CHCH domain proteins, blocked mitochondrial import of CHCHD10. Overexpression of Mia40 rescued mitochondrial import of CHCHD10 Q108P by enhancing disulfide-bond formation. Since reduction in CHCHD10 inhibits respiration, mutations in its CHCH domain may cause aggressive disease by impairing mitochondrial import. Our data suggest Mia40 upregulation as a potential therapeutic salvage pathway.

**Keywords** amyotrophic lateral sclerosis; CHCHD10; genetics; mitochondria

**Subject Categories** Genetics, Gene Therapy & Genetic Disease; Neuroscience

**DOI** 10.15252/emmm.201708558 | Received 14 October 2017 | Revised 13 April 2018 | Accepted 18 April 2018

**EMBO Mol Med (2018) e8558**

## Introduction

The recent identification of mutations in *CHCHD10* implicates mitochondrial dysfunction in the pathogenesis of frontotemporal

dementia (FTD) and amyotrophic lateral sclerosis (ALS) (Bannwarth *et al*, 2014). CHCHD10 is a small soluble protein with a positively charged N-terminus commonly referred to as a mitochondrial targeting signal (MTS), a central hydrophobic domain and a C-terminal CHCH domain (Perrone *et al*, 2017). Mutations have been reported mainly in the N-terminus and the central hydrophobic domain. However, the exact molecular function of the protein and the effect of these mutations remain unknown. Electron microscopy and biochemical studies suggest that CHCHD10 resides in the mitochondrial contact site and cristae organizing system (MICOS) in the intermembrane space of mitochondria (Bannwarth *et al*, 2014) although that has been recently disputed by others (Burstein *et al*, 2018). In the MICOS complex, CHCHD10 interacts with mitofusin, CHCHD3, and CHCHD6 and it seems to be required for proper packaging of mitochondrial DNA into the nucleoid structures (Genin *et al*, 2016).

Several *CHCHD10* mutations were identified in association studies from ALS/FTD kindreds. The S59L mutation was found in an extended family with variable clinical presentation including classic motoneuron disease, cerebellar ataxia, and frontal lobar cognitive symptoms (Bannwarth *et al*, 2014). Moreover, S59L patients also show ragged-red fiber myopathy indicative of mitochondrial disease. The subsequent identification of a R15L mutation as the causal mutation in several pedigrees of familial ALS by three independent groups corroborated the link to ALS (Johnson *et al*, 2014; Muller *et al*, 2014; Kurzwelly *et al*, 2015), while a more cautious interpretation of these association studies was put forward by others due to incomplete penetrance (van Rheenen *et al*, 2014). Later, a G66V mutation was associated with ALS (Muller *et al*, 2014), the Jokela type of spinal muscular atrophy (Penttilä *et al*, 2015), and Charcot-Marie-Tooth disease type 2 (Auranen *et al*, 2015). The typical age-of-onset in these families is in the fifties, and patients show variable clinical presentation and disease duration (1–12 years). Sequencing studies identified several other *CHCHD10* mutations in ALS/FTD cohorts, but lack functional characterization to support pathogenicity (Chausseot *et al*,

1 German Center for Neurodegenerative Diseases (DZNE) Munich, Munich, Germany

2 Munich Cluster for Systems Neurology (SyNergy), Munich, Germany

3 Biomedical Center (BMC), Biochemistry, Ludwig-Maximilians-Universität München, Munich, Germany

4 Neurodegenerative Brain Diseases Group, Center for Molecular Neurology, VIB, Antwerp, Belgium

5 Laboratory of Neurogenetics, Institute Born-Bunge, University of Antwerp, Antwerp, Belgium

6 Department of Neurodegenerative Diseases and Geriatric Psychiatry, Bonn University Hospital, Bonn, Germany

7 German Center for Neurodegenerative Disease (DZNE) Bonn, Bonn, Germany

\*Corresponding author. Tel: +49 89 440046 510; E-mail: dieter.edbauer@dzne.de

2014; Dols-Icardo *et al*, 2015; Zhang *et al*, 2015; Jiao *et al*, 2016; Zhou *et al*, 2017; Blauwendraat *et al*, 2018).

Functional studies of CHCHD10 variants are largely limited to the S59L mutation and have so far not revealed a clear mode of action. Patient fibroblasts with the S59L mutation show an altered mitochondrial network structure, but as mitochondrial fusion is normal, this may be secondary to instability of mitochondrial DNA (Bannwarth *et al*, 2014). Overexpression of human wild-type but not R15L or S59L CHCHD10 rescues the shorter lifespan of *Caenorhabditis elegans* lacking the CHCHD10 homolog *har-1* (Woo *et al*, 2017). The reported inhibition of apoptosis by CHCHD10 S59L (Genin *et al*, 2016) has not been replicated by others (Woo *et al*, 2017) and is difficult to reconcile with a neurodegenerative process. The neuropathological features of CHCHD10 cases have not been comprehensively characterized, but CHCHD10 was recently linked to synaptic integrity and nuclear retention of TDP-43 (Woo *et al*, 2017), although the latter has not been replicated (Brockmann *et al*, 2018).

Here, we report a novel Q108P mutation in the CHCH domain of CHCHD10 in a very young patient with rapidly progressing classical ALS symptoms, which is in sharp contrast to the slow progression in most CHCHD10 patients. We show that the Q108P mutation blocks mitochondrial import nearly completely, and examine the mechanism of CHCHD10 mitochondrial import in detail, including rescue strategies. In addition, we analyzed the effect of all other reported missense mutations on protein expression and localization.

## Results

### Identification of CHCHD10 Q108P in an early-onset ALS patient

A 29-year-old male presented with progressive spasticity, starting in the right foot and spreading to the other extremities over 2 years. He reported recurring painful cramps and had recently noticed atrophy in the hand muscles. Neurologic exam revealed spastic tetraparesis, diffuse fasciculations, muscle atrophy in all extremities, hyperactive deep tendon reflexes, a positive Babinski on the right and equivocal on the left. Motor abnormalities were most severe in the right arm. Bulbar, sensory and coordination functions were normal.

The CSF showed slightly elevated proteins (530.2 mg/l) but was otherwise unremarkable. The electrophysiological exam showed chronic and acute neurogenic changes in the cervical, thoracic, and lumbar region.

The family history was unremarkable for neurodegenerative diseases. Both parents are alive and well at 56 and 55 years, respectively. No DNA was available from the parents. Repeat primed PCR detected no *C9orf72* repeat expansion in the index case. Sequencing using a custom panel with genes linked to ALS/FTD and Alzheimer revealed a heterozygous Q108P mutation in CHCHD10, but no mutations in APP, CSF1R, CHMP2B, FUS, GRN, HNRNPA1, HNRNPA2B1, MAPT, MATR3, NEK1, OPTN, PSEN1, PSEN2, SOD1, TARDBP, TBK1, TUBA4A, TREM2, or VCP (see Materials and Methods). Sanger sequencing confirmed a heterozygous Q108P mutation (Fig 1A). Recently, a nonsense variant (Q108\*) was reported at the same position in a case with FTD and atypical Parkinson's disease (Perrone *et al*, 2017). The Q108P variant was not found in the 60,706 control exomes curated in the ExAc database, and the

residue is highly conserved between species (Lek *et al*, 2016). Among the species in the ENSEMBL ortholog list, Q108 is fully conserved apart from yeast (asparagine). While most other reported CHCHD10 variants lie in the N-terminal region (e.g., R15L) and the central hydrophobic domain (e.g., S59L and G66V), the novel Q108P mutation is located in the CHCH domain (Fig 1B).

### CHCHD10 Q108P inhibits mitochondrial import nearly completely

CHCHD10 is localized in the intermembrane space of mitochondria, and several pathogenic mutations are near the putative MTS at the N-terminus. Therefore, we asked, how the Q108P mutation affects the localization and function of CHCHD10, and compared it to the R15L mutation, which was independently discovered in several ALS/FTD kindreds. In HeLa cells, the levels of R15L and especially Q108P were reduced in whole cell lysate compared to HA-tagged wild-type CHCHD10 (Fig EV1A). In immunofluorescence experiments, the wild-type protein showed typical mitochondrial staining and colocalization with the mitochondrial marker protein ATP5A1 (Fig 1C). In contrast, CHCHD10 Q108P was diffusely localized all over the cell, without discernible mitochondrial localization, suggesting that this mutation disrupts the mitochondrial import and/or impairs protein folding/stability. While CHCHD10 R15L levels were also reduced, the residual protein still colocalized with mitochondria similar to the wild-type protein. Line scans confirmed the lack of correlation of CHCHD10 Q108P and mitochondrial signal (Fig EV1B).

In addition, biochemical fractionation showed strongly reduced levels of CHCHD10 Q108P in mitochondria compared to wild-type despite similar cytosolic levels in a quantitative analysis (Fig 1D and E). The mitochondrial levels of CHCHD10 R15L consistently appeared lower than for the wild-type protein without reaching statistical significance. A C-terminal anti-CHCHD10 antibody showed comparable expression of exogenous and endogenous CHCHD10, but poorly detected the Q108P mutant protein. Moreover, transfection of the mutant and wild-type CHCHD10 had no effect on the levels and localization of endogenous CHCHD10 arguing against molecular replacement or dominant negative effects. Next, we transduced primary rat hippocampal neurons with lentivirus expressing CHCHD10 variants. Similar to the results in HeLa cells, wild-type and R15L predominantly localized to mitochondria, while Q108P showed diffuse expression in the soma and neurites (Fig 1F).

Next, we analyzed protein stability, because Q108P and R15L showed reduced protein levels compared to wild-type CHCHD10. Therefore, we treated CHCHD10 expressing cells with cycloheximide (CHX) to block protein translation and analyzed the decay of CHCHD10 over a time course of 24 h (Fig EV1C). Quantification confirmed rapid degradation of CHCHD10 Q108P compared to the wild-type (Fig EV1D), which is reflected in an almost fivefold lower half-life time (Fig EV1E). CHCHD10 R15L showed intermediated stability. Together, these data suggest that the Q108P mutation strongly inhibits mitochondrial import leading to enhanced protein degradation in the cytosol.

### CHCHD10 knockdown impairs cellular respiration

Since mitochondrial CHCHD10 levels are likely reduced in the ALS patient with CHCHD10 Q108P mutation, we addressed the

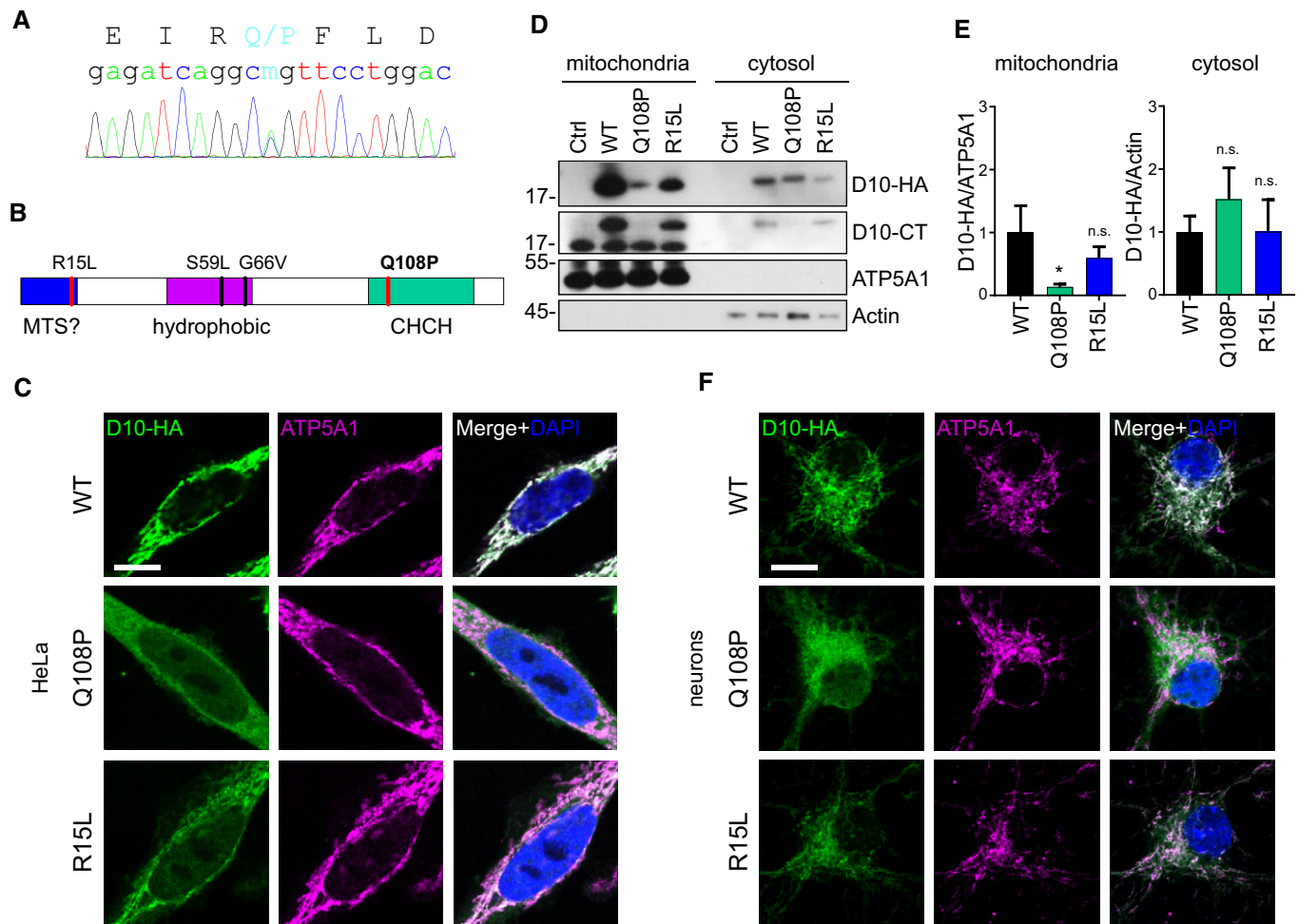


**Figure 1. CHCHD10 Q108P inhibits mitochondrial import.**

A Genomic DNA of an ALS patient was PCR amplified and subjected to Sanger sequencing. The fluorogram revealed a heterozygous Q108P mutation in exon 3 of *CHCHD10*.

B Domain structure and known mutations of CHCHD10. R15L is localized in the putative mitochondrial targeting signal ("MTS?"), S59L and G66V in the hydrophobic region and Q108P in the CHCH domain.

C–F HeLa cells were transfected (C–E) and primary hippocampal neurons were transduced (F) with HA-tagged CHCHD10 (D10-HA) wild-type (WT), Q108P, or R15L (C, F). Mitochondrial localization of CHCHD10-HA (D10-HA) was analyzed by co-staining of a mitochondrial ATP synthase subunit (ATP5A1). Cells with similar expression levels were selected for imaging. Scale bars represent 10  $\mu$ m. (D) Biochemical fractionation of mitochondria and cytosol from transfected HeLa cells. Immunoblot using antibodies against HA, CHCHD10 C-terminus (D10-CT), ATP5A1, and actin. (E) Protein quantification of CHCHD10-HA (D10-HA) in mitochondrial (normalized to ATP5A1) and cytosolic (normalized to actin) fractions. Data are shown as mean  $\pm$  SD. One-way ANOVA (followed by Dunnett's *post hoc* test against WT):  $n = 3$  biological replicates, mitochondrial WT versus Q108P:  $*P = 0.0135$ .

Source data are available online for this figure.

functional role of CHCHD10 focusing on cellular respiration in knockdown experiments using siRNA. CHCHD10 siRNA reduced expression of CHCHD10 mRNA and protein detected by quantitative RT-PCR and immunoblotting in HeLa cells compared to control siRNA (Fig 2A). Using the Seahorse analyzer, we quantified cellular respiration upon CHCHD10 knockdown in HeLa cells. CHCHD10 knockdown cells showed reduced basal respiration and also reduced maximal respiration upon uncoupling with FCCP, resulting in a lower spare respiratory capacity (Fig 2B and C).

Next, we used CRISPR/Cas9 to introduce a frameshift in CHCHD10 in haploid HAP1 cells near Q108. Deletion of 11 base pairs led to a premature stop codon resulting in the deletion of amino acids 110–142 (p.Leu110HisfsTer5, here called

D10 fs). The frame shift caused significant reduction in the CHCHD10 mRNA through nonsense-mediated decay (Fig 2D). While a C-terminal CHCHD10 antibody detected no full-length protein in the edited cells, an N-terminal antibody still detected low levels of truncated CHCHD10 (Fig 2D). D10 fs cells showed reduced spare respiratory capacity (Fig 2E and F), which is consistent with the knockdown data in HeLa cells (Fig 2B and C).

Since primary cells of the Q108P patients were unfortunately not available, we analyzed lymphoblasts from an FTD patient with a heterozygous Q108\* mutation (Perrone *et al*, 2017). Consistent with the reported nonsense-mediated decay of the mutant allele and the findings from the very similar CHCHD10 frame shift allele in HAP1

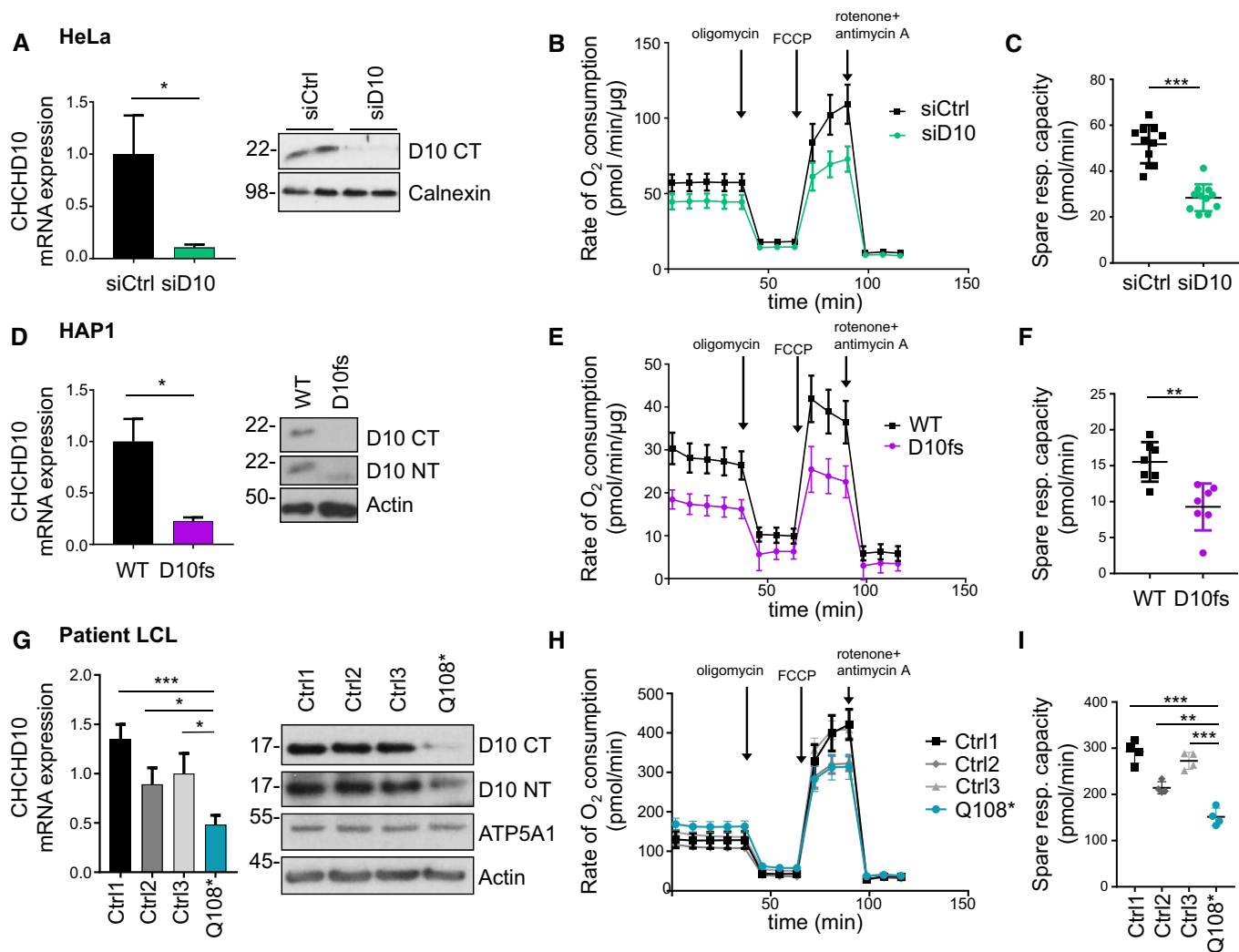


**Figure 2. Partial loss of CHCHD10 reduces spare respiratory capacity.**

A–C HeLa cells were transfected with siRNA targeting CHCHD10 (siD10) or control (siCtrl). (A) Quantitative RT–PCR and immunoblotting (using a C-terminal antibody) show CHCHD10 knockdown. mRNA levels were normalized to *GAPDH* and *B2M* mRNA. Data are shown as mean  $\pm$  SD. Welch's *t*-test was used for statistical analysis:  $n = 3$  biological replicates,  $*P = 0.0102$ . (B, C) Mitochondrial respiration was quantified in real-time using the Seahorse extracellular flux analyzer. The oxygen consumption rate was measured in pmol O<sub>2</sub> per minute and normalized to total protein concentration. After measuring basal respiration, oligomycin was added to inhibit ATP synthase (proton leak), followed by the uncoupling agent FCCP (maximal respiration) and antimycin A/rotenone (non-mitochondrial oxygen consumption). Statistical analysis was done for the spare respiratory capacity (difference of maximal and basal respiration). Data are shown as mean  $\pm$  SD. *T*-test:  $n = 11$  biological replicates,  $***P < 0.0001$ .

D–F CHCHD10 inactivation in haploid HAP1 cells using CRISPR/Cas9 leading to a premature stop codon (p.Leu110HisfsTer5, henceforth abbreviated as D10 fs). (D) Quantitative RT–PCR and immunoblotting (using C- and N-terminal antibodies) show strong reduction of CHCHD10 mRNA expression and loss of full-length protein in D10 fs cells. mRNA levels were normalized to *GAPDH* and *B2M* mRNA. Data are shown as mean  $\pm$  SD. Welch's *t*-test was used for statistical analysis:  $n = 3$  technical replicates,  $*P = 0.0125$ . (E, F) Mitochondrial respiration was analyzed as in (B, C). Statistical analysis was done for spare respiratory capacity (difference of maximal and basal respiration). Data are shown as mean  $\pm$  SD. *T*-Test:  $n = 7$  technical replicates,  $**P = 0.0022$ . A representative experiment of several experiments is shown.

G–I Lymphoblasts from an FTD patient with a Q108\* mutation were compared to three control cases with wild-type CHCHD10. (G) Quantitative RT–PCR and immunoblotting (using C- and N-terminal antibodies) show both reduced CHCHD10 mRNA expression and 50% CHCHD10 protein in Q108\* patient cells. mRNA levels were normalized to *GAPDH* and *B2M* mRNA. Data are shown as mean  $\pm$  SD. One-way ANOVA (followed by Dunnett's *post hoc* test against Q108\*) was used for statistical analysis:  $n = 3$  technical replicates, Q108\* versus Ctr1:  $***P = 0.0004$ , Q108\* versus Ctr2:  $*P = 0.0338$ , Q108\* versus Ctr3:  $*P = 0.0105$ . (H, I) Mitochondrial respiration was analyzed 1 h after plating an equal number of lymphoblasts. Statistical analysis was done for spare respiratory capacity (difference of maximal and basal respiration). Data are shown as mean  $\pm$  SD. One of two independent experiments with similar results was analyzed by one-way ANOVA (followed by Dunnett's *post hoc* test against Q108\*):  $n = 4$  technical replicates, Q108\* versus Ctr1:  $***P = 0.0001$ , Q108\* versus Ctr2:  $**P = 0.0017$ , Q108\* versus Ctr3:  $***P = 0.0001$ .

cells, Q108\* lymphoblasts show reduced CHCHD10 mRNA and protein levels compared to lymphoblasts from controls with wild-type CHCHD10 (Fig 2G). Reduced CHCHD10 expression in these

cells is associated with a reduced spare respiratory capacity compared to the three control lines with wild-type CHCHD10 coding sequence (Fig 2H and I).

Thus, reduced mitochondrial import of CHCHD10 Q108P may decrease mitochondrial function in the early-onset ALS case with only one intact allele.

### The CHCH domain is critical for mitochondrial import

In the current literature, the N-terminus of CHCHD10 is widely referred to as a MTS due to the presence of four interspaced arginine residues. To decipher the contribution of the respective domain to the mitochondrial import mechanism of CHCHD10, we generated truncated CHCHD10 expression constructs and analyzed the mutant proteins by immunofluorescence and biochemical fractionation (Fig 3A–C). Similar to the R15L mutation, truncation of the predicted N-terminal MTS ( $\Delta$ NT, aa 1–16) had little effect on the mitochondrial import. Deleting the C-terminal CHCH domain ( $\Delta$ CHCH, aa  $\Delta$ 92–142) strongly reduced protein levels and

prevented mitochondrial import nearly completely. Importantly, the Q108\* patient variant inhibited mitochondrial import like the Q108P mutation. Both CHCHD10  $\Delta$ CHCH and Q108\* proteins were retained in the cytosolic fraction, confirming that an intact CHCH domain is necessary for mitochondrial import of CHCHD10 (Fig 3B and C). Deleting the N-terminus from the Q108P did not further impair mitochondrial import arguing for a dominant role of the CHCH domain (Fig 3B and C).

To determine which domains of CHCHD10 are sufficient for mitochondrial import, we fused the N-terminus (NT-GFP, amino acids 1–33) or the C-terminus (CHCH-GFP and GFP-CHCH, amino acids 88–142) to GFP. While conventional MTS is widely used in fluorescent mitochondrial reporters, the predicted MTS of CHCHD10 was not sufficient for mitochondrial import when fused to GFP (Fig 3D). Unexpectedly, the CHCH domain fused to either the N- or C-terminus of GFP also failed to drive mitochondrial import.

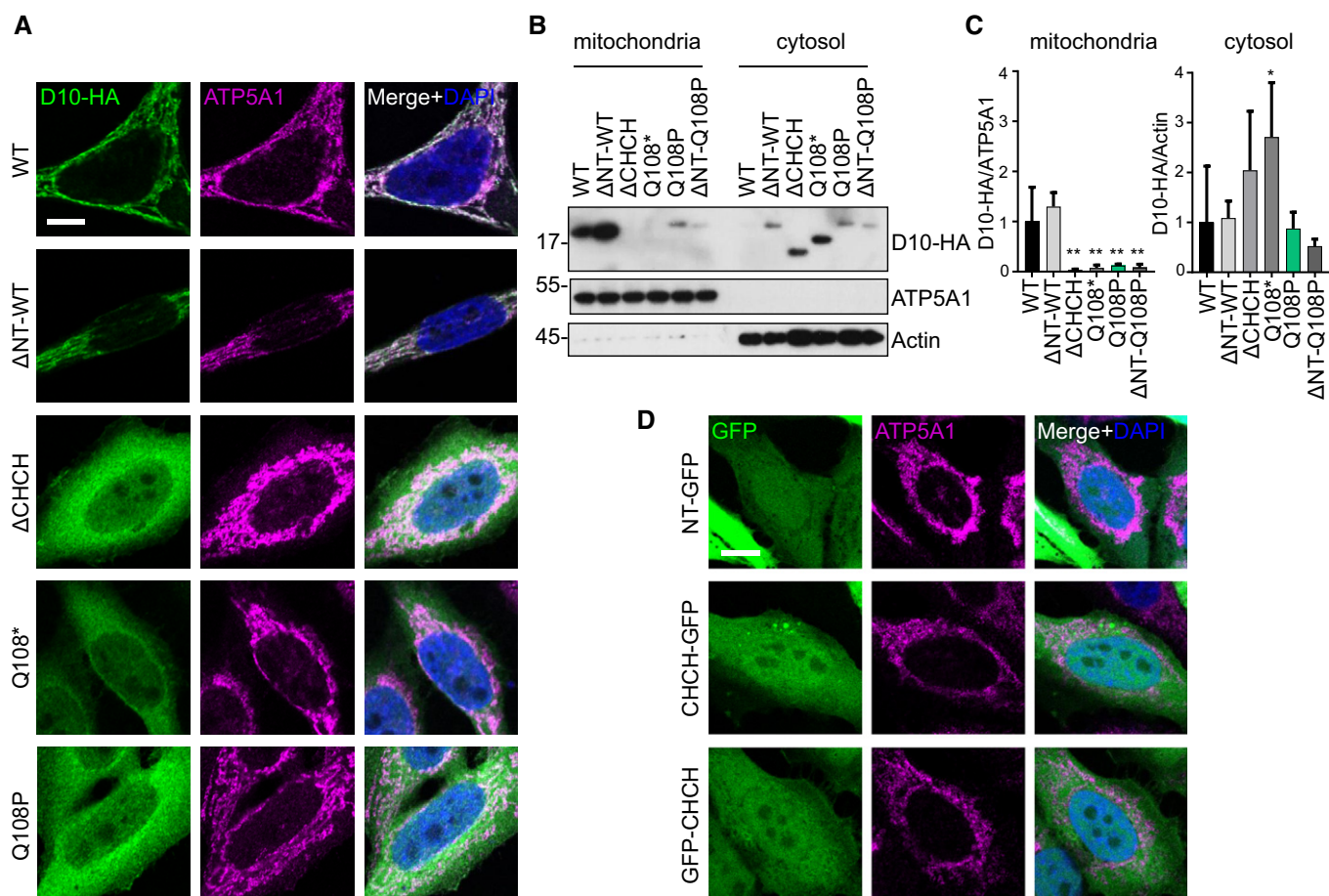


**Figure 3. The CHCH domain is necessary for mitochondrial import of CHCHD10.**

HeLa cells were transfected with the indicated CHCHD10 variants (D10-HA) and GFP-fusion proteins.

A–D (A, D) Double immunofluorescence using ATP5A1 as a mitochondrial marker protein. Cells with similar expression level are shown. Scale bars represent 10  $\mu$ m.

(B, C) Representative immunoblot of biochemical fractionation of mitochondria and cytosol using antibodies against HA, ATP5A1, and actin followed by quantitative analysis of the respective CHCHD10 truncation mutant. Levels of HA-tagged CHCHD10 (D10-HA) were either normalized to ATP5A1 (for mitochondria) or actin (for cytosol). Data are shown as mean  $\pm$  SD. One-way ANOVA (followed by Dunnett's *post hoc* test against WT):  $n = 3$ –4 biological replicates, mitochondrial: WT versus  $\Delta$ CHCH  $**P = 0.0013$ , WT versus Q108\*  $**P = 0.0019$ , WT versus Q108P  $**P = 0.0030$ , WT versus  $\Delta$ NT-Q108P  $**P = 0.0020$ ; Cytosolic: WT versus Q108\*  $*P = 0.0428$ .

Source data are available online for this figure.

However, fusing GFP to the N- or C-terminus of full-length CHCHD10 also blocked mitochondrial import of wild-type CHCHD10 (data not shown), indicating that the CHCH domain-mediated import mechanism may not be compatible with large proteins, which unfortunately precludes definite interpretation of this experiment. The truncation experiments show that mitochondrial import of CHCHD10 is predominantly driven by the CHCH domain.

#### Mutations in the hydrophobic region and the CHCH domain affect subcellular CHCHD10 distribution

To test, whether impaired mitochondrial import is a common pathomechanism, we examined steady state protein levels and localization of all reported missense CHCHD10 variants (Bannwarth *et al*, 2014; Ajroud-Driss *et al*, 2015; Dols-Icardo *et al*, 2015; Jiao *et al*, 2016; Perrone *et al*, 2017; Zhou *et al*, 2017). In public exome sequencing data from ~2,000 ALS patients (ALSdb, Cirulli *et al*, 2015), we discovered two additional CHCHD10 mutations in the CHCH domain that are rare in the ExAc database (Lek *et al*, 2016). One case had a heterozygous mutation of an essential cysteine (C122R), and one case had a charge-altering mutation in a highly conserved residue (E127K) within the CHCH domain, suggesting that such mutations significantly contribute to ALS pathogenesis. In addition, this dataset contained novel R6G and G66S variants. To facilitate site-directed mutagenesis of the highly GC-rich sequence, we used a codon-optimized synthetic gene encoding human CHCHD10 (Fig EV2A). The Q108P and R15L mutants had similar effects on expression and localization, although the synthetic gene allowed higher expression levels (Fig EV2B and C).

Importantly, the C122R mutant showed diffuse cytoplasmic localization similar to Q108P (Figs 4A and EV2C). Consistent with previous reports (Woo *et al*, 2017), CHCHD10 S59L showed small punctate staining in mitochondria in many transfected cells. Even stronger clustering was observed for G66V and E127K in nearly all cells. Other variants in the hydrophobic domain had little (G58R and G66S) or no effect (V57E) on CHCHD10 localization but may have subtle effects on mitochondrial morphology similar to reports for S59L (Bannwarth *et al*, 2014; Woo *et al*, 2017). The other variants showed no gross abnormalities in expression level and localization by immunofluorescence (Fig EV3), highlighting the importance of the hydrophobic region and the CHCH domain.

For a more quantitative analysis, we analyzed CHCHD10 protein levels 3 days after transfection (Fig 4B). CHCHD10 P23S, G58R, G66V, Q108P, and C122R levels were significantly reduced compared to wild-type. Surprisingly, expression of the common P34S variant and R6G, R15S, A32D, and A35D was enhanced arguing against pathogenicity. Biochemical fractionation confirmed that C122R strongly inhibits mitochondrial import similarly to Q108P suggesting that disulfide-bond formation in the CHCH domain is critical for mitochondrial import (Fig 4C and D).

#### Mia40 mediates mitochondrial import of CHCHD10

To test whether CHCHD10 is imported into mitochondria via the Mia40 redox system similar to other CHCH domain containing proteins, we used siRNA to inhibit this pathway, also including the FAD-linked sulfhydryl oxidase Erv1 and AIFM1. RT-qPCR and immunoblotting confirmed the potency and specificity of all siRNAs

(Fig 5A–C). Strikingly, Mia40 knockdown strongly reduced the levels of endogenous CHCHD10 protein despite unchanged mRNA levels. Knockdown of AIFM1 and Erv1 also seemed to decrease CHCHD10 protein levels slightly, however, without reaching statistical significance (Fig 5C). Immunofluorescence confirmed colocalization of endogenous CHCHD10 with mitochondrial cytochrome c oxidase II (MTCO2; Fig 5D). In contrast to control, Mia40 knockdown strongly reduced overall CHCHD10 levels and prevented mitochondrial targeting. Due to the low CHCHD10 protein levels in Mia40 knockdown, we speculate that CHCHD10 mislocalized to the cytosol is degraded rapidly similar to our findings for Q108P (Fig EV1C–E).

Mia40 mediates import of its substrates by direct binding and disulfide-bond formation, which traps the target proteins in the mitochondria (Peleh *et al*, 2016). Therefore, we analyzed interaction of CHCHD10 with Mia40 in cotransfected HeLa cells. Co-immunoprecipitation experiments showed interaction of wild-type, Q108P, and R15L CHCHD10 with Mia40, but no interaction with the  $\Delta$ CHCH construct and only weak interaction with the Q108\* construct (Fig EV4A).

To directly probe Mia40-mediated disulfide-bond formation in the CHCH domain, we treated cell extracts with 4-acetamido-4'-maleimidylstilbene-2,2'-disulfonic acid (AMS), which is covalently linked to free thiol-groups and thus leads to slower migration in SDS-PAGE. AMS treatment of non-reduced extracts had no effect on wild-type CHCHD10 migration indicating that all cysteine residues are oxidized under basal conditions (Fig 5E). Prior reduction with DTT increased the apparent molecular weight of wild-type CHCHD10, particularly upon heating samples to 95°C, presumably due to increased reduction efficiency. Similar results were obtained for endogenous CHCHD10 (Fig EV4B). While CHCHD10 Q108P levels were lower under all conditions, heating the CHCHD10 Q108P extracts during DTT treatment had no additional effect on AMS accessibility in contrast to the wild-type. Thus, the Q108P mutant is completely reduced by DTT already at room temperature indicating that the CHCH domain in the Q108P mutant may be misfolded. Moreover, treating CHCHD10 R15L extract with AMS showed results similar to wild-type, suggesting normal formation of disulfide bonds in the intermembrane space of mitochondria in this mutant.

#### Mia40 overexpression restores mitochondrial import of CHCHD10 Q108P

Since mitochondrial import of wild-type CHCHD10 depends on the integrity of the Mia40 system, we asked how the patient-derived variants are affected by this pathway. First, we analyzed the impact of Mia40 overexpression on the localization of CHCHD10 Q108P in HeLa cells. Strikingly, Mia40 promoted mitochondrial import of CHCHD10 Q108P (Fig 6A). The rescue of mitochondrial import of CHCHD10 Q108P due to Mia40 overexpression was fully replicated in primary neurons (Fig 6B). Additionally, biochemical fractionation and quantification confirmed that overexpression of Mia40 increased the levels of wild-type, Q108P, and R15L CHCHD10 in isolated mitochondria from HeLa cells (Fig 6C and D, also seen in input of Fig EV4A). Overexpressed Mia40 increased also wild-type and mutant CHCHD10 in the cytosolic fraction, which may be explained by partial

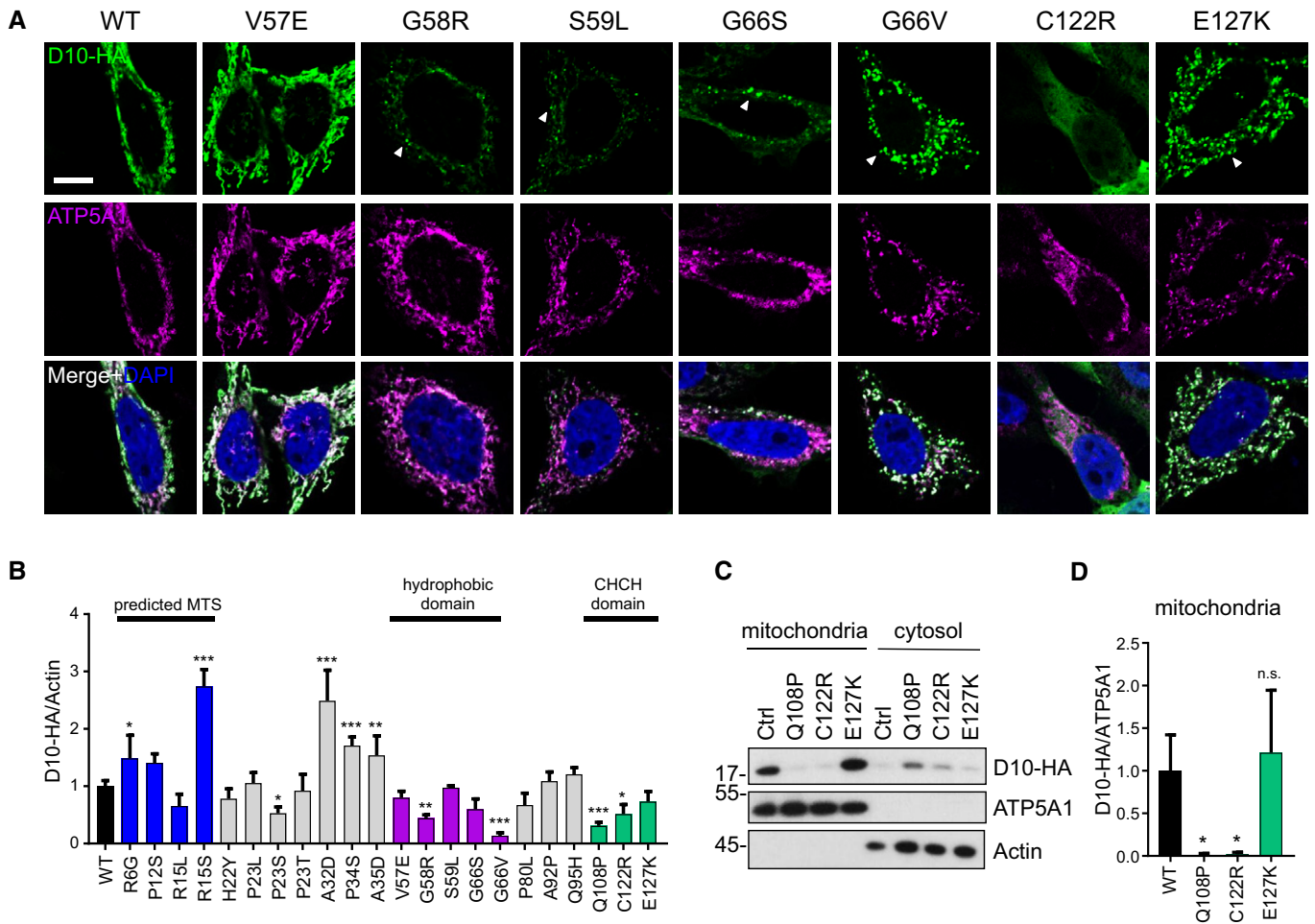


**Figure 4. Differential effect of CHCHD10 patient variants on localization and expression.**

HeLa cells were transfected with HA-tagged CHCHD10 (D10-HA) patient variants.

**A** Immunofluorescence shows expression pattern of CHCHD10-HA variants compared to the mitochondrial marker ATP5A1. Arrowheads indicate clustering of CHCHD10 within mitochondria. Scale bar represents 10  $\mu$ m.

**B** Quantification of CHCHD10 levels from immunoblots of whole cell lysates. Data are shown as mean  $\pm$  SD. One-way ANOVA (followed by Dunnett's *post hoc* test against WT):  $n = 3$ –6 biological replicates, WT versus R6G:  $*P = 0.0145$ , WT versus R15S:  $***P = 0.0001$ , WT versus P23S:  $*P = 0.0189$ , WT versus A32D:  $***P = 0.0001$ , WT versus P34S:  $***P = 0.0001$ , WT versus A35D:  $**P = 0.0044$ , WT versus G58R:  $*P = 0.0029$ , WT versus G66V:  $***P = 0.0001$ , WT versus Q108P:  $***P = 0.0001$ , WT versus C122R:  $*P = 0.0146$ .

**C** Immunoblot of biochemical fractionation of mitochondria and cytosol from transfected HeLa cells expressing different CHCHD10 patient variants using antibodies against HA, ATP5A1, and actin.

**D** Quantification of CHCHD10-HA protein level normalized to mitochondrial ATP5A1. Data are shown as mean  $\pm$  SD. One-way ANOVA (with Dunnett's *post hoc* test against WT):  $n = 4$  biological replicates, Mitochondrial CHCHD10 WT versus Q108P:  $*P = 0.0156$ , WT versus C122R:  $*P = 0.0172$ .

Source data are available online for this figure.

cytosolic localization of excess Mia40 (Fig EV4C). Importantly, Mia40 expression also enhanced CHCHD10 Q108P stability (Fig EV4D and E). Moreover, biochemical analysis of CHCHD10 disulfide-bond formation using AMS treatment confirmed Mia40-induced oxidation and mitochondrial import of Q108P CHCHD10. Without Mia40 overexpression, the CHCHD10 Q108P mutant was poorly expressed (Fig 6E). However, co-expression of Mia40 resulted in higher protein expression and disulfide-bond formation comparable to wild-type CHCHD10, suggesting that oxidation via Mia40 is crucial for the stability and mitochondrial localization of CHCHD10 Q108P. Thus, Mia40 overexpression

likely restores mitochondrial import of CHCHD10 Q108P by promoting disulfide-bond formation.

## Discussion

Unusual phenotypes of genetically determined diseases offer an opportunity to explore molecular pathomechanisms. The known CHCHD10 mutations are usually associated with slow progressing forms of late-onset motoneuron disease and frontotemporal dementia. Here, we identified a novel CHCHD10 mutation in a

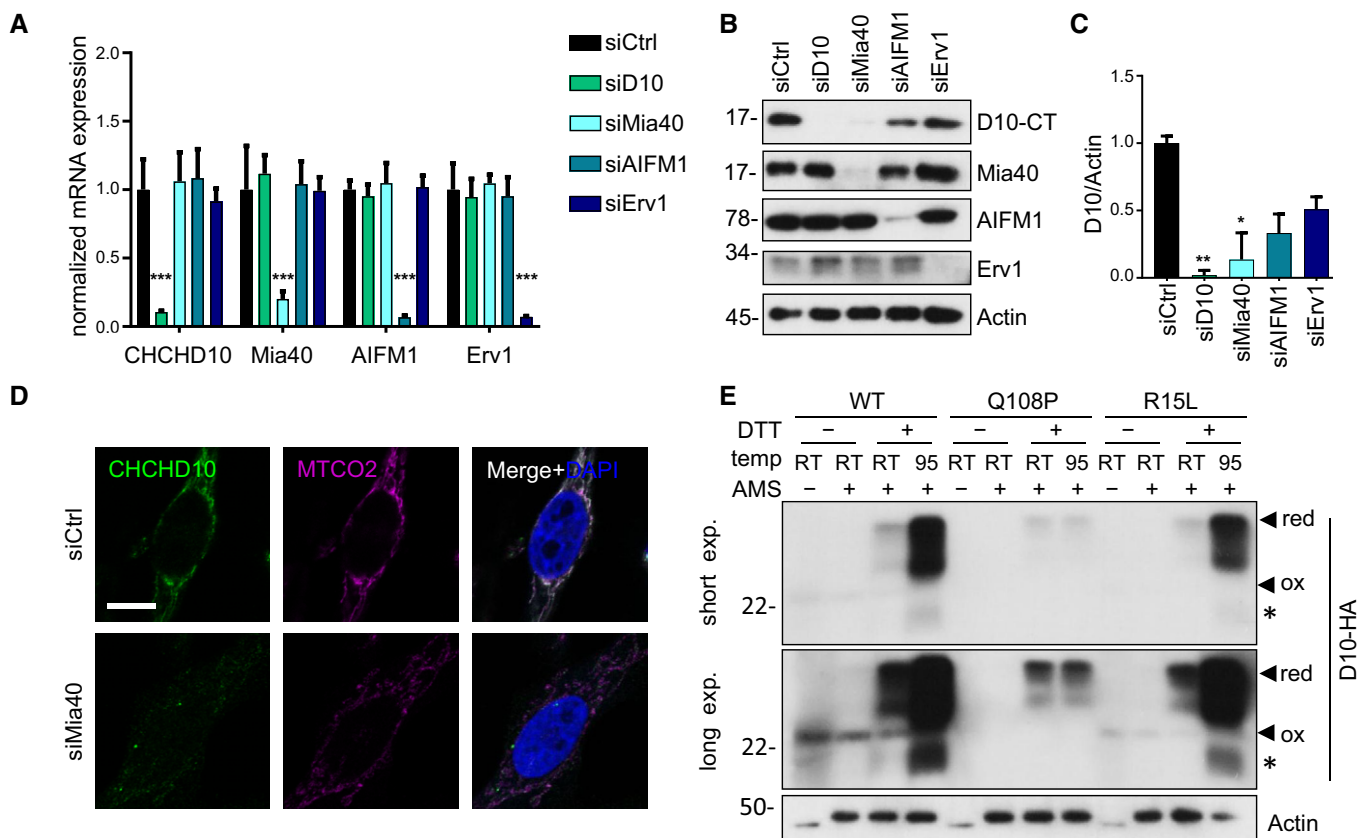


**Figure 5. Mitochondrial import of CHCHD10 depends on Mia40.**

A–D HeLa cells were transfected with siRNA targeting CHCHD10, Mia40, AIFM1, Erv1, or control (siCtrl). (A) Quantitative RT–PCR confirm specific knockdown of CHCHD10, Mia40, AIFM1, and Erv1. mRNA levels were normalized to *GAPDH* and *B2M* mRNA. Data are shown as mean  $\pm$  SD. One-way ANOVA (followed by Dunnett's multiple comparisons test against siCtrl) was used for statistical analysis:  $n = 4$  biological replicates, siCtrl versus siD10  $***P = 0.0001$ , siCtrl versus siMia40  $***P = 0.0001$ , siCtrl versus siAIFM1  $***P = 0.0001$ , siCtrl versus siErv1  $***P = 0.0001$ . (B) Immunoblots with indicated antibodies in siRNA transfected cells. (C) CHCHD10 protein quantification of siRNA transfected cells normalized to actin. Data are shown as mean  $\pm$  SD. Kruskal–Wallis test:  $n = 4$  biological replicates, siCtrl versus siD10:  $**P = 0.0013$ , siCtrl versus siMia40:  $**P = 0.0136$ . (D) Immunostaining of Mia40 knockdown HeLa cells shows overall reduced expression of CHCHD10 compared to control (siCtrl). An antibody against mitochondrially encoded cytochrome c oxidase II (MTCO2) labels mitochondria. Scale bar represents 10  $\mu$ m. (E) AMS assay to assess disulfide-bond formation in whole cell extracts of HeLa cells transfected with CHCHD10-HA wild-type (WT) and mutants (Q108P, R15L). Extracts were treated with the thiol-reactive cross-linker AMS (10 mM, 37°C, 60 min) with or without prior reduction with DTT and heat denaturation (95°C, 10 min), and subjected to immunoblotting to analyze AMS-induced gel shift from oxidized (ox) to reduced (red) forms of CHCHD10. Note that 95°C treatment has no additional effect on AMS accessibility of CHCHD10 Q108P indicating impaired folding compared to wild-type and R15L. Upper and lower panel show short and long exposure of the same blot, respectively. Asterisk denotes degradation product.

Source data are available online for this figure.

young ALS patient with an aggressive disease course and analyze the consequences for protein function. The Q108P mutation inhibits mitochondrial import of CHCHD10 via the Mia40 system nearly completely. Rescue of mitochondrial import by Mia40 overexpression suggests that Q108P reduces binding affinity to Mia40 and can be compensated for by excess Mia40. In contrast, the common R15L mutation had a much smaller effect on protein levels and subcellular distribution, while several mutations in the hydrophobic domain cause clustering of CHCHD10 within mitochondria. Thus, the strong effect of CHCHD10 Q108P on mitochondrial import may explain the aggressive disease in the mutation carrier and suggests that CHCHD10 is important for mitochondrial respiration in motoneurons during healthy aging.

### Mitochondrial import of CHCHD10 via Mia40

To address the pathogenicity of the novel Q108P variant in CHCHD10, we expressed the mutant protein in HeLa cells and primary hippocampal neurons and noticed diffuse localization all over the cell compared to predominantly mitochondrial localization of the wild-type. Our findings suggest that impaired mitochondrial import is the main pathogenic mechanism for the CHCHD10 Q108P variant and led us to investigate the mitochondrial import mechanisms of wild-type and mutant CHCHD10 in more detail.

Apart from the 13 proteins encoded on the mitochondrial DNA, all other  $\sim 1,500$  mitochondrial proteins are synthesized in the cytosol and require active transport into mitochondria (Wiedemann & Pfanner, 2017). The vast majority of nuclear encoded proteins

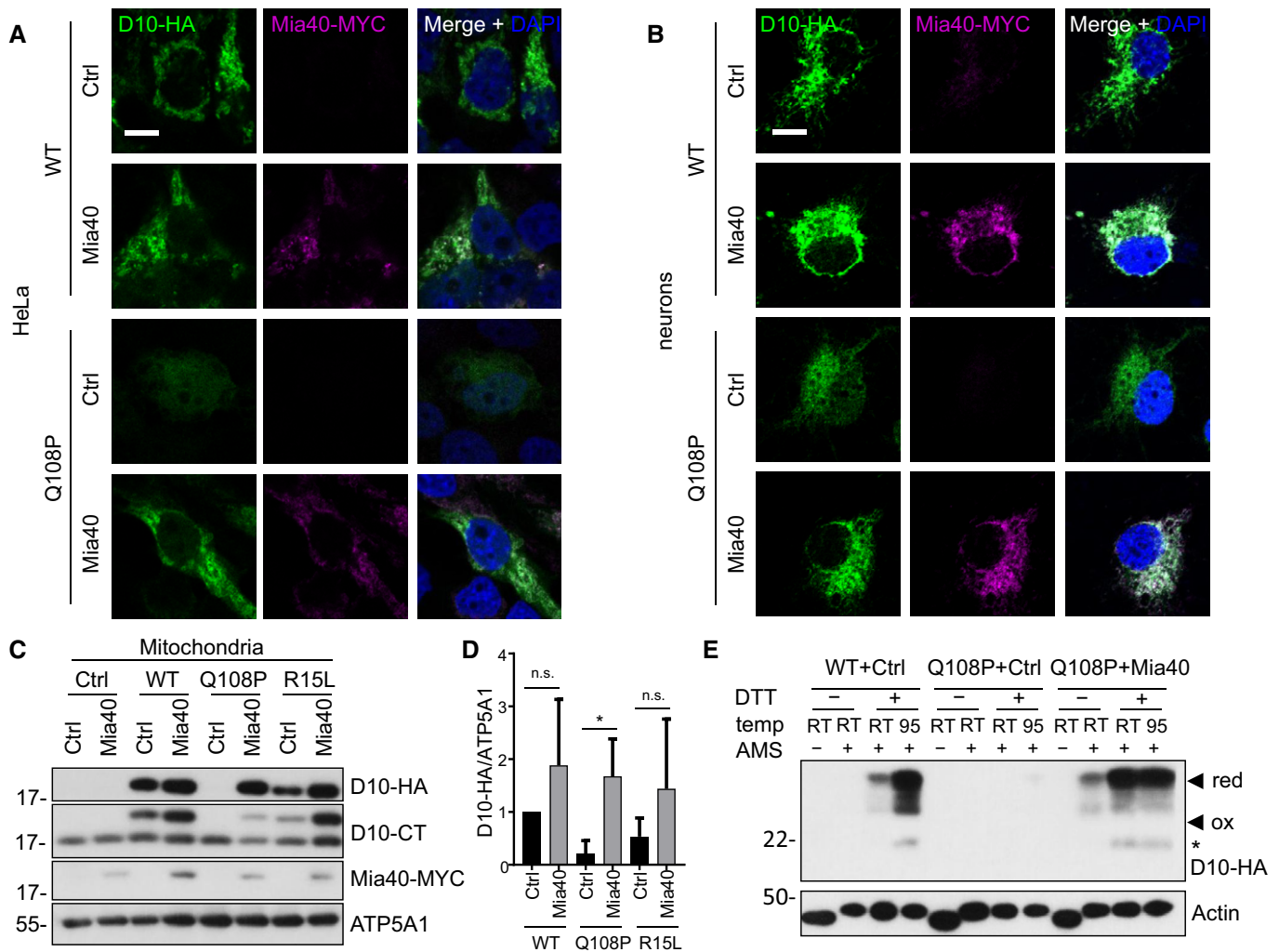


**Figure 6. Mia40 overexpression rescues CHCHD10 mutants.**

Co-transfection of HeLa cells (A, C, D, E) and co-transduction of primary hippocampal rat neurons (B) with the indicated HA-tagged CHCHD10 (D10-HA) variants and Mia40-MYC or empty vector (Ctrl).

A, B Immunofluorescence shows colocalization of wild-type CHCHD10 with Mia40. Scale bars represent 10  $\mu$ m. Overexpression of Mia40 promotes expression and mitochondrial localization of CHCHD10 Q108P.

C, D Immunoblot and quantification of mitochondrial fraction confirms CHCHD10 stabilization and increased mitochondrial localization upon Mia40 expression compared to empty vector. Quantification normalized to ATP5A1. Data are shown as mean  $\pm$  SD. Kruskal–Wallis test:  $n = 4$  biological replicates. Q108P Ctrl versus Q108P Mia40 \* $P = 0.0126$ .

E AMS treatment visualizes disulfide-bond formation in CHCHD10 Q108P upon Mia40 expression comparable to wild-type CHCHD10 (with endogenous Mia40 levels). Actin is used as loading control. Note that DTT treatment has no effect on AMS cross-linking of actin, because all its cysteines are reduced in the cytoplasmic environment. Asterisk denotes degradation product.

Source data are available online for this figure.

have to pass through the translocator of the outer membrane (TOM). Distinct machinery directs these proteins further to their final destination in the outer membrane, the intermembrane space, the inner membrane or the matrix, depending on additional sequence motifs. The classical import pathway is triggered by an amphipathic N-terminal MTS recognized by the TOM complex. For CHCHD10, the NCBI annotation and bioinformatic predictions tools (e.g., Psort2 and MitoProt II) suggest the presence of a classical N-terminal MTS with interspaced conserved arginines (amino acids 1–16). So far, the N-terminal region has been interpreted as an MTS in several papers without rigorous experimental validation

(e.g., Perrone *et al*, 2017). Disruption of this putative MTS could potentially explain pathogenicity of the common N-terminal mutations. However, the R15L mutant was still localized to mitochondria and expression levels and stability of CHCHD10 were only slightly reduced, which is consistent with previous colocalization data for this mutant (Woo *et al*, 2017). Other tested N-terminal variants (R6G, P12S) did not reduce expression levels noticeable or even increased expression (R15S). The dramatic reduction of endogenous CHCHD10 levels in Mia40 knockdown cells suggests that cytosolic CHCHD10 lacking the characteristic disulfide bonds is misfolded and rapidly degraded. We therefore cannot exclude that the reduced

expression of R15L is due to slightly less efficient mitochondrial import. Indeed, consistent with other recent reports, CHCHD10 R15L has a shorter half-life time than wild-type (Brockmann *et al*, 2018). The N-terminal arginine-rich sequence may enhance mitochondrial import although it is neither necessary nor sufficient for mitochondrial import by itself. Truncation of the N-terminus did not further impair mitochondrial import in Q108P. The more dramatic effect of the Q108P mutation on mitochondrial import and half-life time may explain the early age of onset in our patient.

Deletion of the whole CHCH domain completely abolished mitochondrial import of CHCHD10. The Mia40 redox system mediates import of proteins with twin CX<sub>3</sub>C and CX<sub>9</sub>C motifs into the intermembrane space, including CHCH domain proteins (Mesecke *et al*, 2005). We show that mitochondrial import of CHCHD10 critically depends on Mia40. Strikingly, overexpression of Mia40 promotes import of not only wild-type CHCHD10 but also the Q108P and R15L mutants. In yeast, Mia40 levels are rate limiting for mitochondrial import suggesting it acts as a trans-site receptor for import (Peleh *et al*, 2016). In addition, disulfide-bond formation is impaired in the Q108P mutant, which may be due to disturbed  $\alpha$ -helix formation in the CHCH domain because proline is a strong helix breaker (Darshi *et al*, 2012). Interestingly, exome sequencing of ~2,000 mostly sporadic ALS cases revealed a mutation (C122R) in one of the critical cysteines in the CHCH domain that also impaired mitochondrial import (ALSdb, Cirulli *et al*, 2015).

Our analysis of all reported missense CHCHD10 variants suggests that mutations within the hydrophobic region (G58R, S59L, G66V, and G66S) might invoke additional pathomechanisms because they still allow mitochondrial targeting but lead to intra-mitochondrial clustering. Surprisingly, a similar localization pattern was observed for the E127K variant, but not for other variants in the CHCH domain.

Recently, partial nuclear localization and transcriptional effects of CHCHD10 and a homologous protein, CHCHD2, have been reported (Aras *et al*, 2015, 2017; Woo *et al*, 2017), particularly under stress conditions such as TDP-43 overexpression or oxidative stress. We detected some nuclear staining (Figs 1B and 3A) for CHCHD10 Q108P and other variants with strongly impaired mitochondrial import, suggesting they might additionally cause a gain of toxic function.

### Relevance of CHCHD10 impairment for ALS/FTD

Mitochondrial dysfunction has long been implicated in the pathogenesis of ALS (Smith *et al*, 2017). ALS-causing mutations in SOD1 inhibit respiration and cause mitochondrial damages (Magrane *et al*, 2009), and poly-Gly-Arg/Pro-Arg translated from the expanded *C9orf72* hexanucleotide repeat induce oxidative stress and disrupt mitochondrial architecture (Lopez-Gonzalez *et al*, 2016). Furthermore, pathogenic OPTN mutations impair mitochondrial clearance by mitophagy (Wong & Holzbaur, 2014). Mitochondrial dysfunction has been linked to other neurodegenerative diseases and may explain the broad clinical symptoms associated with CHCHD10 mutations. Interestingly, we noticed reduced spare respiratory capacity upon CHCHD10 knockdown or CRISPR/Cas9-mediated truncation consistent with findings in patient fibroblasts with CHCHD10 S59L (Genin *et al*, 2016). Importantly, spare respiratory capacity was also reduced in lymphoblasts showing reduced CHCHD10 expression due to nonsense-mediated decay caused by a

Q108\* mutation in an FTD patient (Perrone *et al*, 2017). This may impair ATP synthesis in patient motoneurons or muscle and may be accompanied by enhanced formation of damaging reactive oxygen species. Several previous reports of conflicting findings of respiratory function in CHCHD10 cellular models (mutant, knockdown, and overexpression) and the recent finding of impaired respiration in muscle but not in whole brain of homozygous CHCHD10 knock-out mice suggest cell type-specific effects are at play (Burstein *et al*, 2018; Straub *et al*, 2018). Interestingly, CHCHD10 knockdown in zebrafish also causes muscle pathology (Brockmann *et al*, 2018). Altered metabolism in muscle may promote to ALS pathogenesis (Loeffler *et al*, 2016). AIFM1, which is required for mitochondrial targeting of Mia40, and thus indirectly of CHCHD10, has been linked to mitochondrial encephalopathy and axonal neuropathy (Ghezzi *et al*, 2010; Rinaldi *et al*, 2012). AIFM1 knockdown appeared to reduce CHCHD10 levels after 3 days (without reaching statistical significance), but longer knockdown may be required for a more severe effect due to its indirect action via Mia40.

Together, our data demonstrate that the Q108P mutation almost completely prevents mitochondrial import and perturbed mitochondrial function may ultimately lead to motoneuron degeneration. The stronger effect of Q108P on mitochondrial import compared to previously characterize pathogenic variants may explain the early onset and aggressive course of ALS in our patient. Our findings have implications for genetic counseling of novel CHCHD10 variants and suggest future therapeutic approaches: (i) Variants in conserved residues of the CHCH domain and nonsense mutations (e.g., the previously reported Q108\*) are likely pathogenic. Variants in the hydrophobic region primarily alter CHCHD10 distribution within mitochondria. Thus, analyzing mitochondrial import and clustering within mitochondria may be used to assess pathogenicity of novel variants. (ii) Unless the mutant CHCHD10 causes a toxic gain-of-function phenotype, epigenetic boosting of CHCHD10 expression may rescue haploinsufficiency by increasing expression of the wild-type allele. (iii) It may be possible to pharmacologically activate the Mia40/Erv1 disulfide relay system using small redox-compounds. Boosting Mia40 activity or expression may promote import of mutant and wild-type CHCHD10 and thus restore its function within mitochondrial respiration. Most importantly, our report of a novel aggressive mutation with clear functional consequences strongly supports the genetic linkage of CHCHD10 to ALS/FTD pathogenesis.

## Materials and Methods

### Patient materials, clinical history, and sequencing

All procedures on human subjects were in accordance with the WGA Declaration of Helsinki and the Department of Health and Human Services Belmont Report. The Q108P patient consented to diagnostic DNA testing for ALS mutations. All information was obtained from the hospital files. No experiments were done on the patient or using patient material. Genomic DNA was sequenced with a TruSeq Custom Amplicon kit on a MiSeq (Illumina) according to the protocol from the manufacturer. The custom gene panel covered all exons of CHCHD10, CHMP2B, GRN, MAPT, NEK1, OPTN, PSEN1, PSEN2, SOD1, TARDBP, TBK1, TUBA4A, TREM2 and the exons with known pathogenic mutations of APP (exons 12–15),

CSF1R (exon 13–21), FUS (exon 6, 14, 15), HNRNPA1 (exon 9), HNRNPA2B1 (exon 10), MATR3 (exon 1), VCP (exons 3, 5, 6, 11). The CHCHD10 Q108P mutation was confirmed by Sanger Sequencing of genomic DNA (primers GTGGCCCCAGGTTTGGAAAC and CAATCTGGTGTGTGGTCTGG). Repeat primed PCR for *C9orf72* repeat expansion was performed as described previously (van der Zee *et al*, 2013).

Epstein–Barr virus (EBV)-transformed lymphoblast cell lines were established according to standard procedures for previously reported patients and controls (Perrone *et al*, 2017). All subjects had given informed consent.

### DNA constructs, siRNA, and transfection

CHCHD10 and Mia40/CHCHD4 were amplified from HEK293T cDNA and cloned in the FUW3a lentiviral expression vector containing a C-terminal HA or myc epitope tag. As controls we used the empty vectors containing only the epitope tag. The following CHCHD10 truncations were generated:  $\Delta 1$ –16 ( $\Delta$ NT),  $\Delta 108$ –142 (Q108\*),  $\Delta 92$ –142 ( $\Delta$ CHCH). Q108P and R15L were introduced by standard mutagenesis. For Figs 4 and EV2, we introduced several patient variants in a codon-optimized synthetic gene with reduced GC-content encoding human CHCHD10. All constructs were sequence verified. We used Silencer Select siRNA targeting human Mia40/CHCHD4 (s43607, Thermo Fisher Scientific), human CHCHD10 (s53406, Thermo Fisher Scientific), human Erv1/Gfer (s5704, Thermo Fisher Scientific), human AIFM1 (s17440, Thermo Fisher Scientific), and the Silencer Select Negative Control No. 1 (#4390844, Thermo Fisher Scientific). HeLa cells were transfected using Lipofectamine 2000 (Thermo Fisher Scientific).

### CRISPR/Cas9 genome editing

HAP1 cells (Horizon Discovery) were transfected with Cas9 (Addgene plasmid #52962) and sgRNA (TCTGAGTGGTGGAA CAGTCC in Addgene plasmid #41824) using Lipofectamine 3000 (Thermo Fisher Scientific). After 12 h, medium was exchanged for 24 h before splitting into selection medium containing 8  $\mu$ g/ml blasticidin and 400  $\mu$ g/ml Zeocin. After 3 days, selection medium was removed and cultured for 10–14 days till single cell clones were visible. Individual clones were picked and cultured in 96 wells. For screening, genomic DNA was extracted with the NucleoSpin Tissue 96 well kit (Macherey-Nagel) according to manufacturer's instructions. The region of CHCHD10 targeted by the sgRNA was PCR amplified (GGTTTGGAAACGCACCTCCAG and AGGTGCAAGAGGA GGGTTG) using the Q5 High-Fidelity Master Mix (New England Biolabs) and analyzed by Sanger sequencing.

### Antibodies

The following primary antibodies were used: anti-HA (clone 3F10, Thermo Fisher - IF 1:10, WB 1:50), anti-myc (9E10 hybridoma supernatant, WB 1:15, supernatant of clone 9E10, IF 1:200, purified), anti-ATP5A1 (WB 1:1,000, IF 1:250, clone 15H4C4, abcam 14748), anti-CHCHD10 (C-terminal WB 1:500, IF 1:100, abcam 121196), anti-CHCHD10 (N-terminal, WB 1:500, abcam ab124186), anti-MTCO2 (IF 1:100, abcam 3298), anti-actin (WB 1:3,000, clone A5316, Sigma), anti-calnexin (WB 1:7,000, clone SPA-860, Enzo Life

Sciences), anti-CHCHD4 (Mia40, WB: 1:1,000, Proteintech 21090-1-AP) anti-AIF (AIFM1, WB 1:1,000, abcam ab32516), anti-Gfer (Erv1, WB 1:200, Atlas Antibodies HPA041227).

### Cell culture, mitochondrial fractionation

HeLa cells were transfected with plasmids and siRNA using Lipofectamine 2000 (Thermo Fisher Scientific) according to the manufacturer's instructions. Three days after transfection, mitochondria were isolated using the Qproteome Mitochondria Isolation Kit (Qiagen). The cytosolic fraction was precipitated with four volumes of ice-cold acetone and incubated for 15 min on ice. After centrifugation (10 min, 12,000 g, 4°C), the pellet was washed twice with acetone and air dried. The cytosolic pellet and the highly purified mitochondrial pellet were resuspended in RIPA buffer (137 mM NaCl, 20 mM Tris pH 7.5, 0.1% SDS, 10% glycerol, 1% Triton X-100, 0.5% deoxycholate, 2 mM EDTA) containing protease inhibitor cocktails (1:100, Sigma), incubated for 20 min on ice, and sonicated for 10s. Afterward, the protein concentration was determined using BCA assay (Interchim). After adding 4 $\times$  Laemmli buffer (Bio-Rad) containing 2-mercaptoethanol, samples were denatured (95°C, 10 min) and loaded with the same protein amount on Novex 10–20% Tris-Tricine gels (Life Technologies).

### Protein stability and immunoblotting

For protein stability analysis, HeLa cells were treated 2 days after transfection with 150  $\mu$ g/ml cycloheximide dissolved in DMSO or DMSO only for 0, 4, 8, and 24 h.

For immunoblotting of the whole cell lysates, cells were lysed in RIPA buffer (137 mM NaCl, 20 mM Tris pH 7.5, 0.1% SDS, 10% glycerol, 1% Triton X-100, 0.5% deoxycholate, 2 mM EDTA) with protease inhibitor cocktails (1:100, Sigma) and incubated on ice (20 min). After centrifugation (18,000 g, 15 min), the supernatant was transferred into a new tube, protein concentration was determined by BCA assay (Interchim), and 4 $\times$  Laemmli buffer (Bio-Rad) containing 2-mercaptoethanol was added. Samples were denatured at 95°C for 10 min and loaded on Novex 10–20% Tris-Tricine gels (Life Technologies) or 12.5% SDS–PAGE gels.

### Immunoprecipitation

HeLa cells were lysed at 4°C for 20 min in lysis buffer (120 mM NaCl, 1 mM EDTA, 0.5% NP-40, 20 mM Tris–HCL pH 8) supplemented with protease and phosphatase inhibitors and centrifuged at 13,000 g for 10 min. HA-labeled magnetic beads (Thermo Fischer 88836) were washed with 4°C lysis buffer; 5% of the cell lysate was used as an input control and the rest of the cell lysate was incubated at 4°C with HA-labeled beads overnight. Beads were washed three times with 4°C lysis buffer supplemented with protease and phosphatase inhibitors, boiled in 50  $\mu$ l Laemmli buffer (Bio-Rad) containing 2-mercaptoethanol, and analyzed by immunoblotting on Novex 10–20% Tris-Tricine gels (Life Technologies).

### Neuronal cell culture and lentivirus production

Primary hippocampal cultures were prepared from E19 rats as described previously and plated on glass coverslips coated with

poly-D-lysine (Guo *et al*, 2018). Lentivirus was packaged in HEK293FT cells as described (Guo *et al*, 2018).

### Immunofluorescence

After washing once with PBS, HeLa cells (2 days after transfection) and transduced primary hippocampal rat neurons (DIV3 + 4) were fixed for 10 min at room temperature (4% paraformaldehyde and 4% sucrose in PBS). Primary and secondary antibodies were diluted in GDB buffer (0.1% gelatin, 0.3% Triton X-100, 450 mM NaCl, 16 mM sodium phosphate pH 7.4). For visualizing the nucleus, cells were stained with DAPI (1:5,000 in PBS, 10 min, RT). After mounting the coverslips with Fluoromount™ Aqueous Mounting medium (Sigma), images were taken with LSM710 confocal microscope (Carl Zeiss, Jena) using a 63× oil immersion objective (NA 1.4).

### RNA isolation and quantitative RT-PCR

After 3 days of transfection, RNA isolation was conducted with the RNeasy- and QIAshredder kit (Qiagen) following the manufacturer's instructions. cDNA was generated using the TaqMan MicroRNA Reverse Transcription Kit (Applied Biosystems) with random hexamer primers according to the manufacturer's instructions. RT-qPCR was performed on the CFX384-Real-Time system (Bio-Rad) using following primers: CHCHD10 (Hs01369775\_g1, Thermo Fisher), Mia40/CHCHD4 (Hs01027804\_g1, Thermo Fisher), AIFM1 (Hs00377585\_m1, Thermo Fisher), Erv1/GFER (Hs00193365\_m1, Thermo Fisher), B2M (4326319E, Thermo Fisher), GAPDH (Hs02758991\_g1, Thermo Fisher). Signals were normalized to GAPDH and B2M with the CFX Manager program (Bio-Rad) according to the  $\Delta\Delta C_T$  method.

### Analysis of disulfide-bond formation

We used thiol-reactive 4-acetamido-4'-maleimidylstilbene-2,2'-disulfonic acid (AMS, Thermo Fisher) to analyze disulfide-bond formation following the protocol by (Gross *et al*, 2011). HeLa cells were lysed in RIPA buffer (137 mM NaCl, 20 mM Tris pH 7.5, 0.1% SDS, 10% glycerol, 1% Triton X-100, 0.5% deoxycholate, 2 mM EDTA) for 20 min on ice. After centrifugation (18,000 g, 15 min, 4°C), the supernatant was divided and incubated at room temperature or 95°C for 10 min with or without 15 mM dithiothreitol (DTT). Afterwards, proteins were precipitated with trichloroacetic acid (TCA). Here, one volume of a 8 M TCA stock solution was added to four volumes of protein sample, incubated at 4°C for 10 min, and centrifuged (18,000 g, 5 min, 4°C). After removing the supernatant, the pellet was washed with ice-cold acetone and again centrifuged (18,000 g, 5 min, 4°C). These washing steps were repeated twice, and the remaining pellet was dried at 95°C for 5–10 min. After acetone evaporation, the pellet was resolved in buffer (2% SDS, 100 mM Tris pH 8, 100 mM NaCl, 10 mM EDTA) and 10 mM AMS or distilled water was added. The samples were incubated for 60 min at 37°C in the dark. After adding 50 mM iodoacetic acid (IAA), Laemmli buffer (Bio-Rad) was added and the proteins were analyzed by immunoblotting using 12.5% SDS-PAGE gels.

### The paper explained

#### Problem

Several mutations in CHCHD10 have been reported in familial and sporadic cases of amyotrophic lateral sclerosis (ALS), frontotemporal dementia (FTD), spinal muscular atrophy, and mitochondrial myopathy, but their mode of action is unclear. Since disease progression in mutation carriers is usually slow and penetrance is incomplete, some geneticists raised concerns, whether CHCHD10 mutations are truly pathogenic. CHCHD10 is a small protein localized to the intramembrane space of mitochondria. It is involved in organizing cristae morphology and has been linked to stability of mitochondrial DNA. Loss-of-function and gain-of-function pathomechanisms have been discussed. Several patient mutations, including R15L, are located in the proposed N-terminal mitochondrial targeting signal (MTS), but the mitochondrial import mechanism of CHCHD10 has not been carefully analyzed experimentally, although restoring mitochondrial import of CHCHD10 may be a therapeutic strategy.

#### Results

We discovered a novel CHCHD10 mutation (Q108P) in a highly conserved residue within the coiled-coil-helix-coiled-coil-helix (CHCH) domain in a young ALS patient with aggressive disease progression and analyzed its pathogenicity in transfected heterologous cells and primary rat neurons. The Q108P mutation blocked mitochondrial import nearly completely suggesting a loss-of-function mechanism. Moreover, reduced CHCHD10 expression in heterologous and patient cells inhibited mitochondrial respiration. The R15L mutation had only a small effect on overall protein levels, but largely spared mitochondrial localization. Several other CHCHD10 variants reported in ALS/FTD patients showed diffuse cytoplasmic localization (C122R) or dot-like clustering within mitochondria (G58R, S59L, G66V, G66S, E127K) and reduced stability and/or expression (R15L, P23S, G58R, G66V, Q108P, Q108\*, C122R). Mitochondrial import of CHCHD10 is predominantly driven by Mia40-dependent disulfide-bond formation in the CHCH domain rather than the putative N-terminal MTS. Overexpression of Mia40 strikingly boosts mitochondrial import of CHCHD10 Q108P.

#### Impact

The identification of a novel CHCHD10 mutation resulting in aggressive ALS and a clear loss-of-function phenotype *in vitro* strongly supports the genetic role of CHCHD10 in ALS pathogenesis. This unusual mutation revealed Mia40-dependent mitochondrial import of CHCHD10 and suggests that activation of the Mia40-dependent mitochondrial import pathway could be a novel therapeutic strategy. Our data supports the pathogenicity of several previously uncharacterized CHCHD10 variants found in ALS/FTD patients via a loss-of-function mechanism (R15L, P23S, G58R, G66V, Q108P, Q108\*, C122R) and/or gain-of-function mechanism (G58R, S59L, G66V, G66S, E127K).

### Quantitative analysis of respiration

Oxygen consumption rate (OCR) was measured using the Seahorse XF96 extracellular flux analyzer (Agilent). The day before, siCHCHD10 knockdown or control siRNA transfected HeLa cells were plated in growth medium in 96-well plates (Agilent). For OCR measurements, growth medium was replaced with pre-warmed XF assay medium (Agilent) supplemented with 10 mM glucose and 10 mM pyruvate, and cells were incubated at 37°C without CO<sub>2</sub> for 60 min. To measure OCR in patient lymphoblastoid cells, 96-well plates (Agilent) were coated with 30  $\mu$ l of poly-D-lysine (50  $\mu$ g/ml) in 0.1 M borate buffer (pH 8.5) for 2 h and washed twice with cell culture-grade water. One hour before the measurement,

lymphoblasts were plated ( $1.1 \times 10^5$  cells/well) in pre-warmed XF assay medium (Agilent) and incubated at 37°C without CO<sub>2</sub>. Oligomycin (final concentration 1 μM), FCCP (0.75 μM), and rotenone and antimycin A (10 μM each) were diluted with pre-warmed assay medium and loaded into injector ports. Assay cycles included 4 min of mixing, followed by 4 min of measurement.

**Expanded View** for this article is available online.

## Acknowledgements

We thank Hannelore Hartmann, Bettina Schmid, Harald Steiner, Johannes Trambauer, Matias Wagner, and Qihui Zhou for critical comments to the manuscript. This work was supported by NOMIS Foundation and the Hans und Ilse Breuer Foundation (D.E.), the Munich Cluster of Systems Neurology (SyNergy) (D.E.), the European Community's Health Seventh Framework Programme under Grant agreement no. 617198 [DPR-MODELS] (D.E.) and the general legacy of Mrs. Ammer (N.E.).

## Author contributions

DE, MTH, and CL designed the study and interpreted the results with additional help from NE and PW. CL performed experiments with help from MHS, LR, JG, MJ, and HR. JvdZ and CVB provided genetically characterized patient lymphoblasts. MTH identified the patient. DE, CL, and PW wrote the manuscript with input from all co-authors.

## Conflict of interest

The authors declare that they have no conflict of interest.

## References

- Ajroud-Driss S, Fecto F, Ajroud K, Lalani I, Calvo SE, Mootha VK, Deng HX, Siddique N, Tahmouh AJ, Heiman-Patterson TD *et al* (2015) Mutation in the novel nuclear-encoded mitochondrial protein CHCHD10 in a family with autosomal dominant mitochondrial myopathy. *Neurogenetics* 16: 1–9
- ALSDb (2018) New York City, NY (<http://alsdb.org>) Accessed January.
- Aras S, Bai M, Lee I, Springett R, Huttemann M, Grossman LI (2015) MNRR1 (formerly CHCHD2) is a bi-organellar regulator of mitochondrial metabolism. *Mitochondrion* 20: 43–51
- Aras S, Arrabi H, Purandare N, Huttemann M, Kamholz J, Zuchner S, Grossman LI (2017) Abl2 kinase phosphorylates Bi-organellar regulator MNRR1 in mitochondria, stimulating respiration. *Biochim Biophys Acta* 1864: 440–448
- Auranen M, Ylikallio E, Shcherbii M, Paetau A, Kiuru-Enari S, Toppila JP, Tyynismaa H (2015) CHCHD10 variant p.(Gly66Val) causes axonal Charcot-Marie-Tooth disease. *Neurol Genet* 1: e1.
- Bannwarth S, Ait-El-Mkadem S, Chausseot A, Genin EC, Lacas-Gervais S, Fragaki K, Berg-Alonso L, Kageyama Y, Serre V, Moore DG *et al* (2014) A mitochondrial origin for frontotemporal dementia and amyotrophic lateral sclerosis through CHCHD10 involvement. *Brain* 137: 2329–2345
- Blauwendraat C, Wilke C, Simon-Sanchez J, Jansen IE, Reifschneider A, Capell A, Haass C, Castillo-Lizardo M, Biskup S, Maetzler W *et al* (2018) The wide genetic landscape of clinical frontotemporal dementia: systematic combined sequencing of 121 consecutive subjects. *Genet Med* 20: 240–249
- Brockmann SJ, Freischmidt A, Oeckl P, Muller K, Ponna SK, Helferich AM, Paone C, Reinders J, Kojer K, Orth M *et al* (2018) CHCHD10 mutations p.R15L and p.G66V cause motoneuron disease by haploinsufficiency. *Hum Mol Genet* 27: 706–715
- Burstein SR, Valsecchi F, Kawamata H, Bourens M, Zeng R, Zuberi A, Milner TA, Cloonan SM, Lutz C, Barrientos A *et al* (2018) *In vitro* and *in vivo* studies of the ALS-FTLD protein CHCHD10 reveal novel mitochondrial topology and protein interactions. *Hum Mol Genet* 27: 160–177
- Chausseot A, Le Ber I, Ait-El-Mkadem S, Camuzat A, de Septenville A, Bannwarth S, Genin EC, Serre V, Auge G, French research network on FTD and Ftd ALS, Brice A, Pouget J, Paquis-Flucklinger V (2014) Screening of CHCHD10 in a French cohort confirms the involvement of this gene in frontotemporal dementia with amyotrophic lateral sclerosis patients. *Neurobiol Aging* 35: 2884 e1–4
- Cirulli ET, Lasseigne BN, Petrovski S, Sapp PC, Dion PA, Leblond CS, Couthouis J, Lu YF, Wang Q, Krueger BJ *et al* (2015) Exome sequencing in amyotrophic lateral sclerosis identifies risk genes and pathways. *Science* 347: 1436–1441
- Darshi M, Trinh KN, Murphy AN, Taylor SS (2012) Targeting and import mechanism of coiled-coil helix coiled-coil helix domain-containing protein 3 (ChChd3) into the mitochondrial intermembrane space. *J Biol Chem* 287: 39480–39491
- Dols-Icardo O, Nebot I, Gorostidi A, Ortega-Cubero S, Hernandez I, Rojas-Garcia R, Garcia-Redondo A, Povedano M, Llado A, Alvarez V *et al* (2015) Analysis of the CHCHD10 gene in patients with frontotemporal dementia and amyotrophic lateral sclerosis from Spain. *Brain* 138: e400
- Genin EC, Plutino M, Bannwarth S, Villa E, Cisneros-Barroso E, Roy M, Ortega-Vila B, Fragaki K, Lespinasse F, Pinero-Martos E *et al* (2016) CHCHD10 mutations promote loss of mitochondrial cristae junctions with impaired mitochondrial genome maintenance and inhibition of apoptosis. *EMBO Mol Med* 8: 58–72
- Ghezzi D, Sevrioukova I, Invernizzi F, Lamperti C, Mora M, D'Adamo P, Novara F, Zuffardi O, Uziel G, Zeviani M (2010) Severe X-linked mitochondrial encephalomyopathy associated with a mutation in apoptosis-inducing factor. *Am J Hum Genet* 86: 639–649
- Gross DP, Burgard CA, Reddehase S, Leitch JM, Culotta VC, Hell K (2011) Mitochondrial Ccs1 contains a structural disulfide bond crucial for the import of this unconventional substrate by the disulfide relay system. *Mol Biol Cell* 22: 3758–3767
- Guo Q, Lehmer C, Martinez-Sanchez A, Rudack T, Beck F, Hartmann H, Perez-Berlanga M, Frottin F, Hipp MS, Hartl FU *et al* (2018) *In situ* structure of neuronal C9orf72 Poly-GA aggregates reveals proteasome recruitment. *Cell* 172: 696–705.e12
- Jiao B, Xiao T, Hou L, Gu X, Zhou Y, Zhou L, Tang B, Xu J, Shen L (2016) High prevalence of CHCHD10 mutation in patients with frontotemporal dementia from China. *Brain* 139: e21
- Johnson JO, Glynn SM, Gibbs JR, Nalls MA, Sabatelli M, Restagno G, Drory VE, Chio A, Rogaeva E, Traynor BJ (2014) Mutations in the CHCHD10 gene are a common cause of familial amyotrophic lateral sclerosis. *Brain* 137: e311
- Kurzweily D, Kruger S, Biskup S, Heneka MT (2015) A distinct clinical phenotype in a German kindred with motor neuron disease carrying a CHCHD10 mutation. *Brain* 138: e376
- Lek M, Karczewski KJ, Minikel EV, Samocha KE, Banks E, Fennell T, O'Donnell-Luria AH, Ware JS, Hill AJ, Cummings BB *et al* (2016) Analysis of protein-coding genetic variation in 60,706 humans. *Nature* 536: 285–291
- Loeffler JP, Picchiarrelli G, Dupuis L, Gonzalez De Aguilar JL (2016) The role of skeletal muscle in amyotrophic lateral sclerosis. *Brain Pathol* 26: 227–236
- Lopez-Gonzalez R, Lu Y, Gendron TF, Karydas A, Tran H, Yang D, Petrucelli L, Miller BL, Almeida S, Gao FB (2016) Poly(GR) in C9ORF72-Related ALS/FTD

- compromises mitochondrial function and increases oxidative stress and DNA damage in iPSC-derived motor neurons. *Neuron* 92: 383–391
- Magrane J, Hervias I, Henning MS, Damiano M, Kawamata H, Manfredi G (2009) Mutant SOD1 in neuronal mitochondria causes toxicity and mitochondrial dynamics abnormalities. *Hum Mol Genet* 18: 4552–4564
- Mesecke N, Terziyska N, Kozany C, Baumann F, Neupert W, Hell K, Herrmann JM (2005) A disulfide relay system in the intermembrane space of mitochondria that mediates protein import. *Cell* 121: 1059–1069
- Muller K, Andersen PM, Hubers A, Marroquin N, Volk AE, Danzer KM, Meitinger T, Ludolph AC, Strom TM, Weishaupt JH (2014) Two novel mutations in conserved codons indicate that CHCHD10 is a gene associated with motor neuron disease. *Brain* 137: e309
- Peleh V, Cordat E, Herrmann JM (2016) Mia40 is a trans-site receptor that drives protein import into the mitochondrial intermembrane space by hydrophobic substrate binding. *Elife* 5: e16177
- Penttila S, Jokela M, Bouquin H, Saukkonen AM, Toivanen J, Udd B (2015) Late onset spinal motor neuronopathy is caused by mutation in CHCHD10. *Ann Neurol* 77: 163–172
- Perrone F, Nguyen HP, Van Mossevelde S, Moisse M, Sieben A, Santens P, De Bleecker J, Vandenbulcke M, Engelborghs S, Baets J et al (2017) Investigating the role of ALS genes CHCHD10 and TUBA4A in Belgian FTD-ALS spectrum patients. *Neurobiol Aging* 51: 177.e9–177.e16
- van Rheenen W, Diekstra FP, van den Berg LH, Veldink JH (2014) Are CHCHD10 mutations indeed associated with familial amyotrophic lateral sclerosis? *Brain* 137: e313
- Rinaldi C, Grunseich C, Sevrioukova IF, Schindler A, Horkayne-Szakaly I, Lamperti C, Landoure G, Kennerson ML, Burnett BG, Bonnemann C et al (2012) Cowchock syndrome is associated with a mutation in apoptosis-inducing factor. *Am J Hum Genet* 91: 1095–1102
- Smith EF, Shaw PJ, De Vos KJ (2017) The role of mitochondria in amyotrophic lateral sclerosis. *Neurosci Lett* DOI:10.1016/j.neulet.2017.06.052
- Straub IR, Janer A, Weraarpachai W, Zinman L, Robertson J, Rogaeva E, Shoubridge EA (2018) Loss of CHCHD10-CHCHD2 complexes required for respiration underlies the pathogenicity of a CHCHD10 mutation in ALS. *Hum Mol Genet* 27: 178–189
- Wiedemann N, Pfanner N (2017) Mitochondrial machineries for protein import and assembly. *Annu Rev Biochem* 86: 685–714
- Wong YC, Holzbaur EL (2014) Optineurin is an autophagy receptor for damaged mitochondria in parkin-mediated mitophagy that is disrupted by an ALS-linked mutation. *Proc Natl Acad Sci USA* 111: E4439–E4448
- Woo JA, Liu T, Trotter C, Fang CC, De Narvaez E, LePochat P, Maslar D, Bukhari A, Zhao X, Deonarine A et al (2017) Loss of function CHCHD10 mutations in cytoplasmic TDP-43 accumulation and synaptic integrity. *Nat Commun* 8: 15558
- van der Zee J, Gijssels I, Dillen L, Van Langenhove T, Theuns J, Engelborghs S, Philtjens S, Vandenbulcke M, Slegers K, Sieben A et al (2013) A Pan-European study of the C9orf72 repeat associated with FTL: geographic prevalence, genomic instability and intermediate repeats. *Hum Mutat* 34: 363–373
- Zhang M, Xi Z, Zinman L, Bruni AC, Maletta RG, Curcio SA, Rainero I, Rubino E, Pinessi L, Nacmias B et al (2015) Mutation analysis of CHCHD10 in different neurodegenerative diseases. *Brain* 138: e380
- Zhou Q, Chen Y, Wei Q, Cao B, Wu Y, Zhao B, Ou R, Yang J, Chen X, Hadano S et al (2017) Mutation screening of the CHCHD10 gene in Chinese patients with amyotrophic lateral sclerosis. *Mol Neurobiol* 54: 3189–3194



**License:** This is an open access article under the terms of the Creative Commons Attribution 4.0 License, which permits use, distribution and reproduction in any medium, provided the original work is properly cited.

## Expanded View Figures

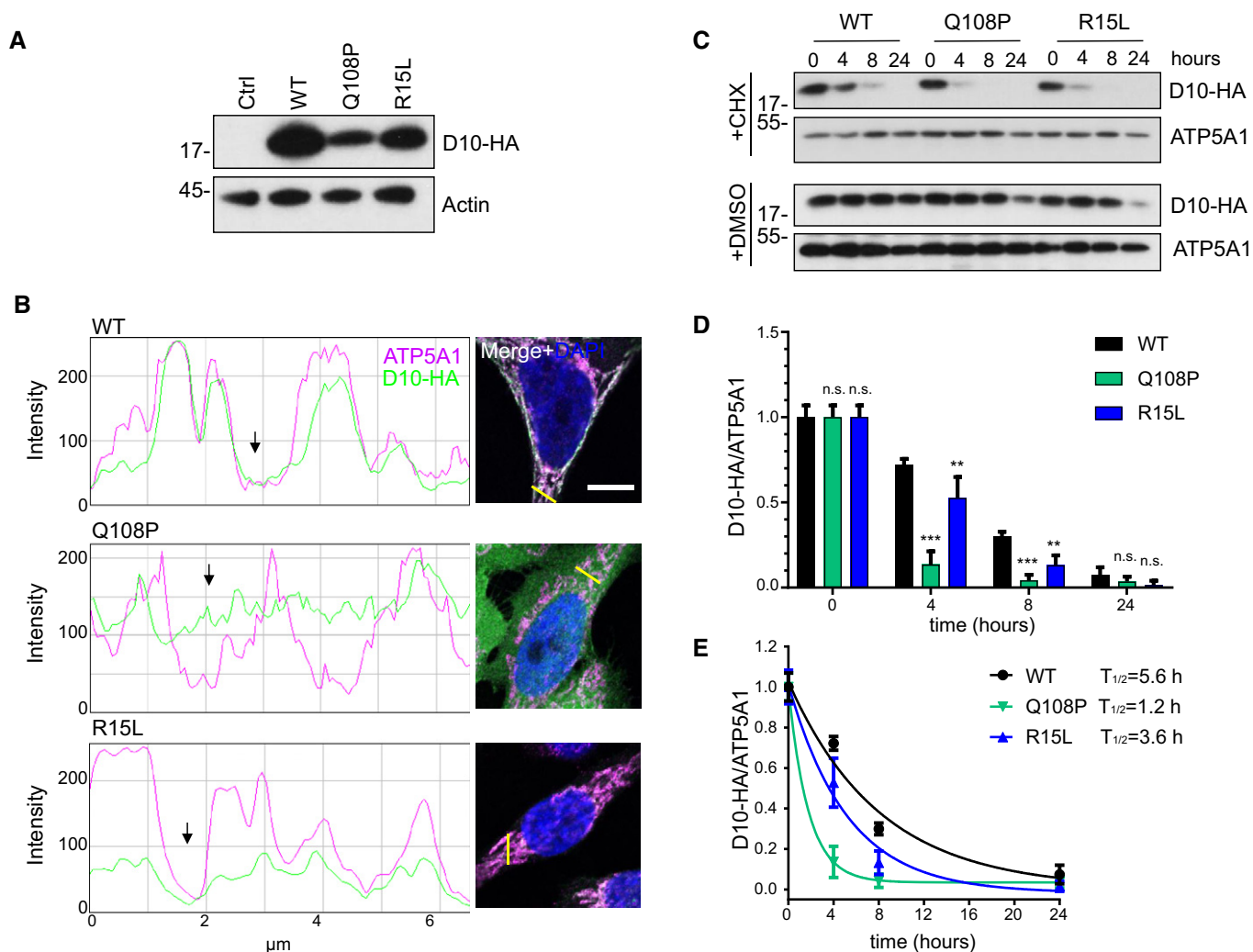


**Figure EV1. CHCHD10 mutants are less stable.**

A CHCHD10-HA (D10-HA) level in whole cell lysates of HeLa cells transfected with empty vector (Ctrl) or HA-tagged CHCHD10 variants (WT, Q108P, or R15L).

B Line scans of CHCHD10-HA (D10-HA) and ATP5A1 intensity in immunofluorescence pictures (right) of HeLa cells transfected with the indicated HA-tagged CHCHD10 constructs. Intensities of the red (ATP5A1, here shown in magenta) and the green (D10-HA) channels were measured along a 6.5- $\mu\text{m}$ -long line (yellow), and diagrams were generated with the plugin RGB-profiler in ImageJ. Scale bar represents 10  $\mu\text{m}$ .

C Protein stability of HA-tagged CHCHD10 (WT, Q108P, or R15L) was measured in HeLa cells transfected for 2 days and then treated with cycloheximide (+CHX) or vehicle (+DMSO) and harvested after 0, 4, 8, and 24 h. Note that steady state levels of CHCHD10 Q108P and R15L in DMSO-treated cells are also lower at 24 h, i.e. 3 days after transfection.

D Quantification of HA-tagged CHCHD10 (D10-HA) protein levels normalized to ATP5A1. Transfected HeLa cells were treated with cycloheximide for 0, 4, 8, and 24 h. Data are shown as mean  $\pm$  SD. Two-way ANOVA (followed by Turkey's multiple comparison):  $n = 3$  biological replicates,  $t = 4$  h WT versus Q108P: \*\*\* $P < 0.0001$ ,  $t = 4$  h WT versus R15L: \*\* $P = 0.002$ ,  $t = 8$  h WT versus Q108P: \*\*\* $P < 0.0001$ ,  $t = 8$  h WT versus R15L: \*\* $P = 0.0076$ .

E Half-life analysis of the respective CHCHD10 variant was calculated by nonlinear regression analysis. Data are shown as mean  $\pm$  SD.  $n = 3$  biological replicates.

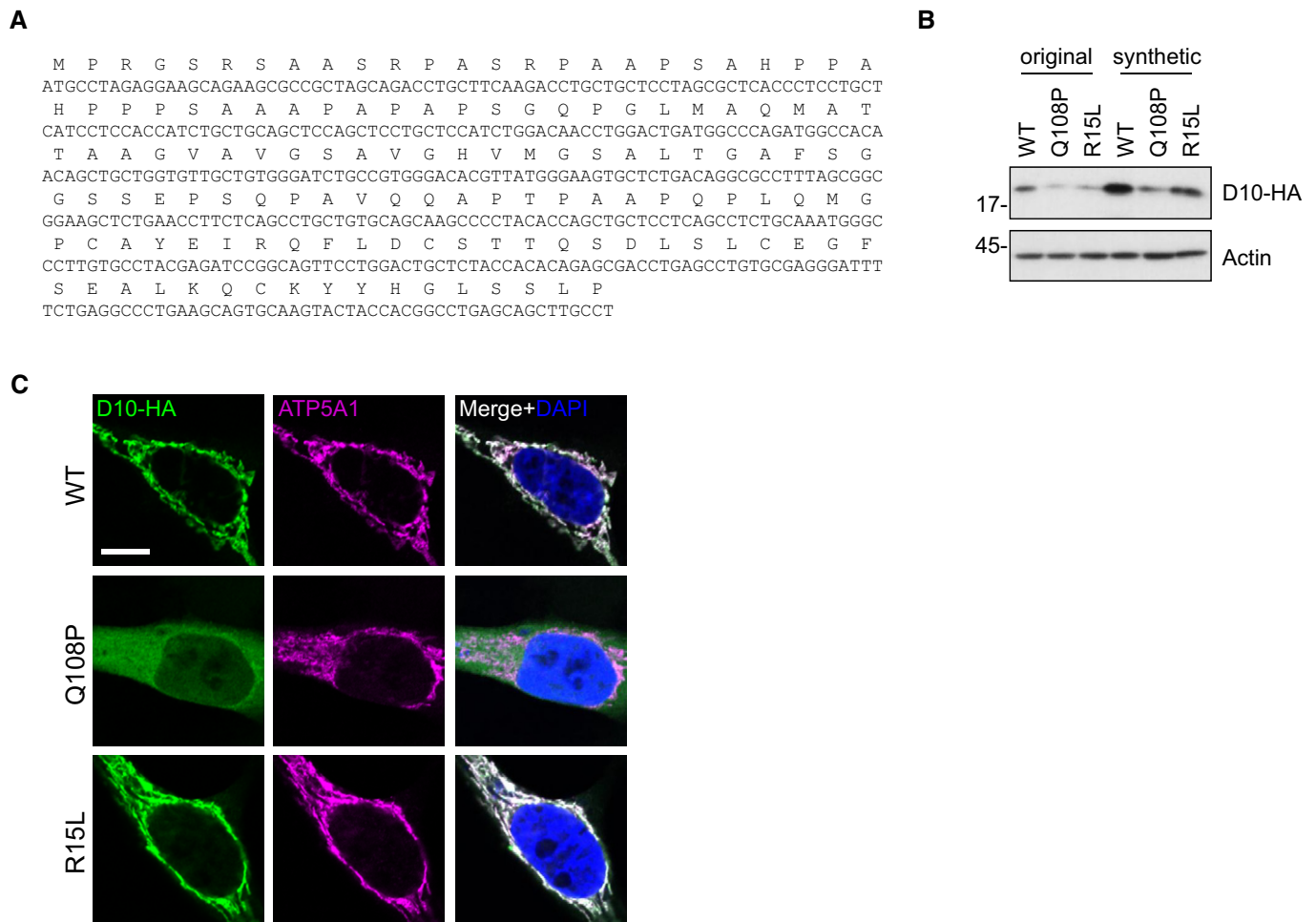


**Figure EV2. Import deficit of CHCHD10 Q108P is replicated with a high-expressing synthetic gene.**

- A Sequence of the codon-optimized synthetic CHCHD10 gene used to reduce GC-content in order to facilitate cloning of many patient-derived variants.
- B Comparison of HA-tagged CHCHD10 (D10-HA) protein levels in whole cell lysates of HeLa cells transfected with CHCHD10 constructs harboring either the original or the codon-optimized synthetic cDNA.
- C Mitochondrial localization of synthetic CHCHD10-HA (D10-HA) was analyzed in transfected HeLa cells by co-staining with a mitochondrial marker (ATP5A1). Scale bar represents 10  $\mu$ m.

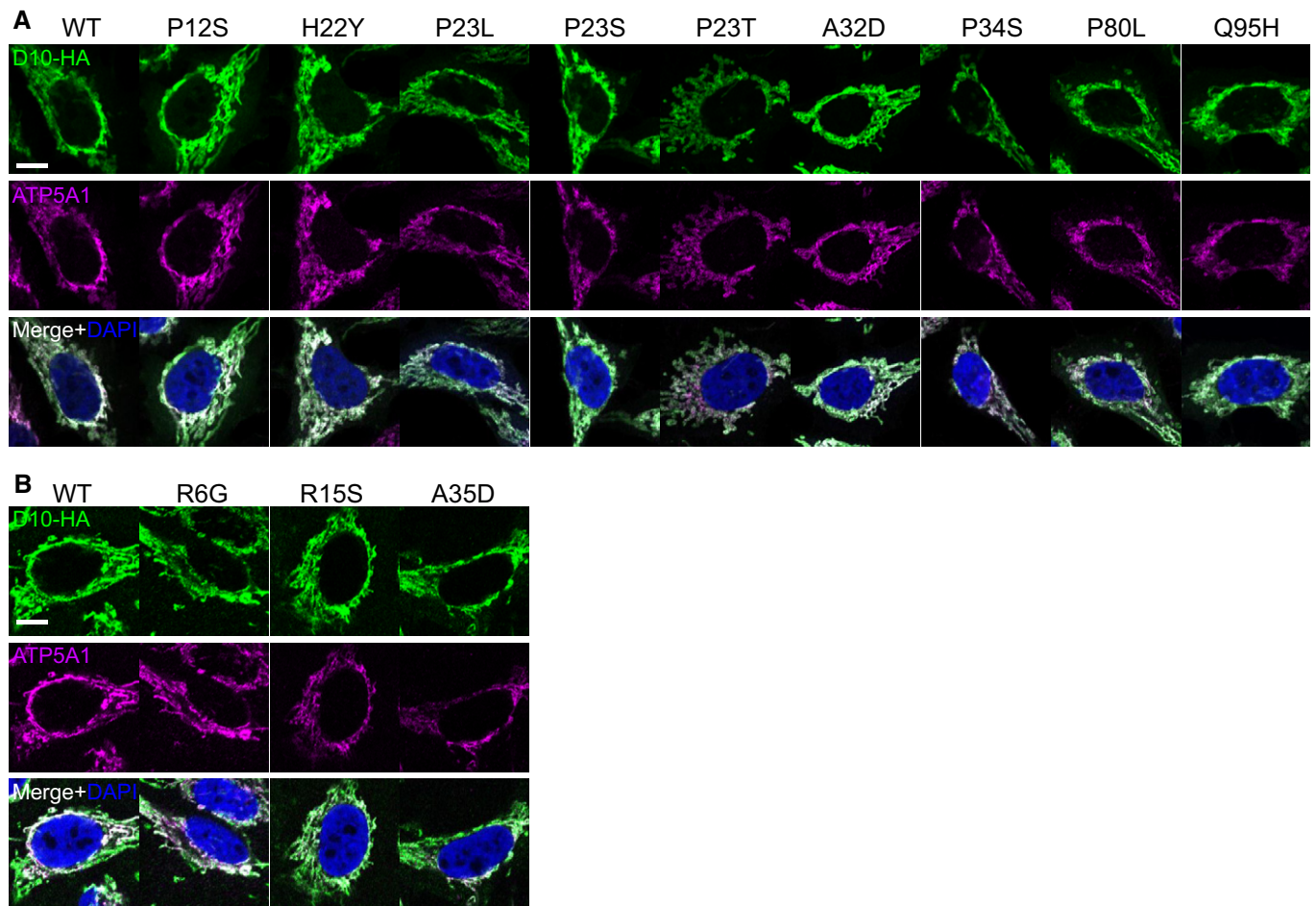


**Figure EV3. Subcellular distribution of CHCHD10 patient variants.**

A, B HeLa cells were transfected with HA-tagged CHCHD10 (D10-HA) patient variants in two sets (A and B). Immunofluorescence shows expression pattern of CHCHD10-HA (D10-HA) variants compared to the mitochondrial marker ATP5A1. Scale bars represent 10  $\mu$ m.

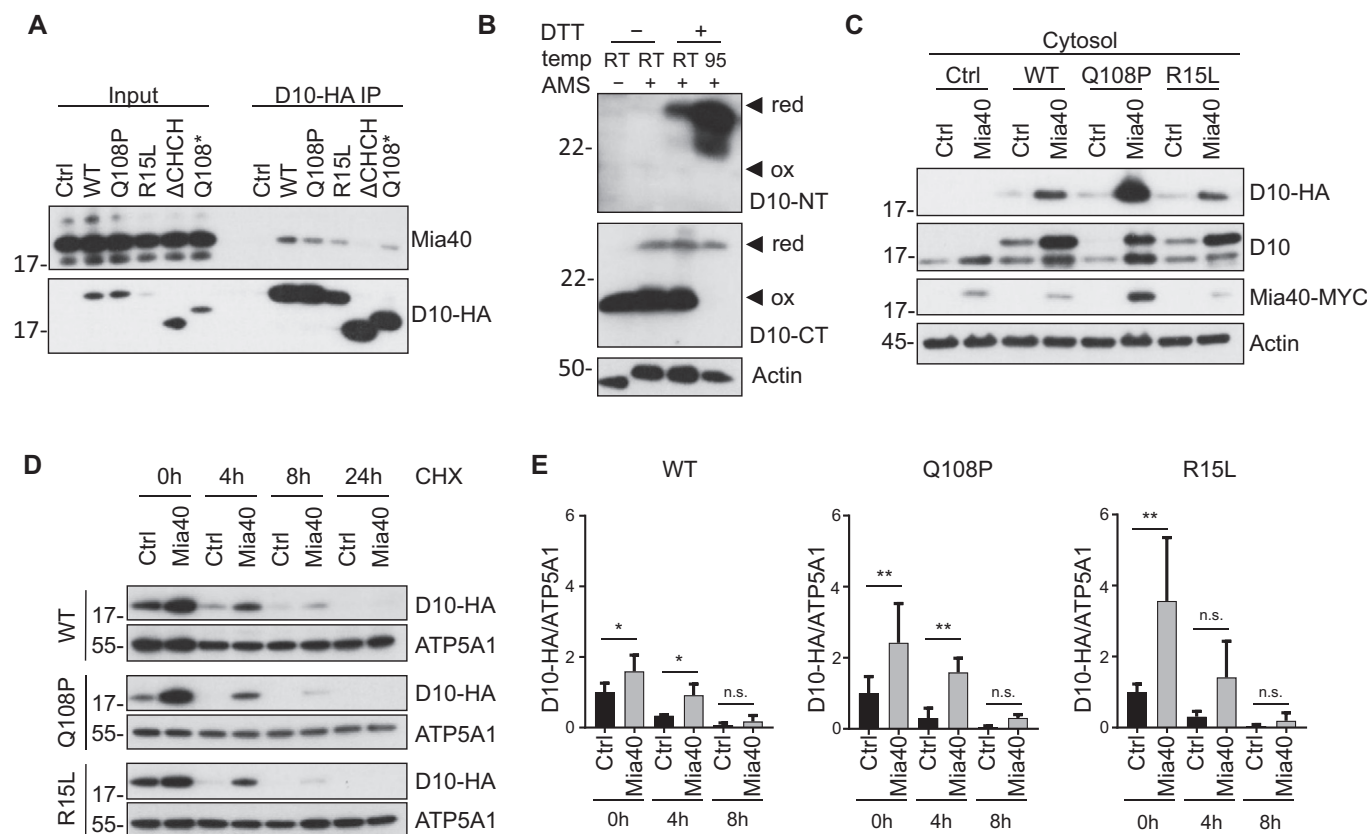


**Figure EV4. Mia40 binds and stabilizes CHCHD10.**

- A** Co-immunoprecipitation of Mia40-MYC and CHCHD10-HA (D10-HA) wild-type (WT), variants (Q108P, R15L, ΔCHCH, Q108\*), or empty vector (Ctrl) from transfected HeLa cells. Input represents 5% of the whole cell lysate used for immunoprecipitation. Immunoblot of the co-immunoprecipitation was detected with antibodies against Mia40 and HA. Low binding may be explained by the transient interaction of the oxidoreductase Mia40 with its substrate CHCHD10.
- B** AMS treatment shows disulfide-bond formation of endogenous CHCHD10 in HeLa cells. Note that endogenous CHCHD10, detected with an N-terminal antibody (D10-NT), shows a similar pattern. The C-terminal CHCHD10 antibody poorly detects AMS coupled endogenous CHCHD10 indicating that the epitope overlaps with the cysteine residues. Actin is used as loading control. Note that DTT treatment has no effect on AMS cross-linking of actin, because all its cysteines are reduced in the cytoplasmic environment.
- C** Immunoblotting shows elevation of CHCHD10 upon Mia40 expression also in cytosolic fractions with indicated antibodies.
- D, E** Protein stability of HA-tagged CHCHD10 (WT, Q108P, or R15L) upon Mia40 overexpression was measured in HeLa cells treated with cycloheximide (+CHX) and compared to empty vector co-transfection (Ctrl). Cells were harvested after 0, 4, 8, and 24 h. Quantification of CHCHD10-HA (D10-HA) protein levels normalized to ATP5A1. Data are shown as mean ± SD. Two-way ANOVA (with Sidak's multiple comparisons test):  $n = 4$  biological replicates, WT:  $t = 0$  h Ctrl versus Mia40:  $*P = 0.0146$ ,  $t = 4$  h Ctrl versus Mia40  $*P = 0.0168$ ; Q108P:  $t = 0$  h Ctrl versus Mia40:  $**P = 0.0039$ ,  $t = 4$  h Ctrl versus Mia40  $**P = 0.0089$ ; R15L:  $t = 0$  h Ctrl versus Mia40:  $**P = 0.0014$ .

## **Contribution to Publication I**

As first author of this publication, I contributed to the study design, manuscript writing and conducted the majority of experiments. I performed all experiments of this publication with some exceptions: Fig. EV1C, Fig. EV4A, Fig. EV4D.

## 2. Publication II and contribution

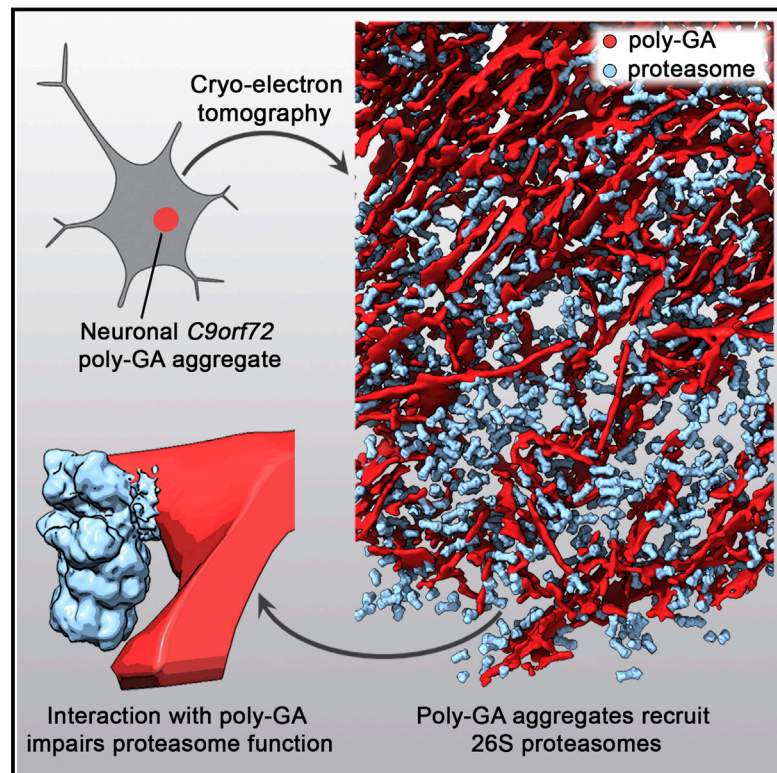
*In situ structure of neuronal C9orf72 poly-GA aggregates reveals proteasome recruitment*

published as

Guo Q, **Lehmer C**, Martínez-Sánchez A, Rudack T, Beck F, Hartmann H, Pérez-Berlanga M, Frottin F, Hipp MS, Hartl FU, Edbauer D, Baumeister W, Fernández-Busnadiego R. In Situ Structure of Neuronal C9orf72 Poly-GA Aggregates Reveals Proteasome Recruitment. *Cell*. 2018, doi: 10.1016/j.cell.2017.12.030

# In Situ Structure of Neuronal *C9orf72* Poly-GA Aggregates Reveals Proteasome Recruitment

## Graphical Abstract



## Authors

Qiang Guo, Carina Lehmer, Antonio Martínez-Sánchez, ..., Dieter Edbauer, Wolfgang Baumeister, Rubén Fernández-Busnadiego

## Correspondence

dieter.edbauer@dzne.de (D.E.),  
baumeist@biochem.mpg.de (W.B.),  
ruben@biochem.mpg.de (R.F.-B.)

## In Brief

Neuronal poly-GA aggregates linked to amyotrophic lateral sclerosis and frontotemporal dementia selectively sequester proteasomes.

## Highlights

- Neuronal *C9orf72* poly-GA aggregates were analyzed by cryoelectron tomography
- Poly-GA aggregates in neurons consist of planar twisted ribbons
- Poly-GA aggregates recruit proteasomes while excluding other large macromolecules
- Interactions with poly-GA aggregates lead to proteasome stalling



Guo et al., 2018, *Cell* 172, 696–705  
February 8, 2018 © 2018 Elsevier Inc.  
<https://doi.org/10.1016/j.cell.2017.12.030>

# In Situ Structure of Neuronal *C9orf72* Poly-GA Aggregates Reveals Proteasome Recruitment

Qiang Guo,<sup>1</sup> Carina Lehmer,<sup>2,3,8</sup> Antonio Martínez-Sánchez,<sup>1,8</sup> Till Rudack,<sup>4,5,8</sup> Florian Beck,<sup>1</sup> Hannelore Hartmann,<sup>2,3</sup> Manuela Pérez-Berlanga,<sup>6</sup> Frédéric Frottin,<sup>6</sup> Mark S. Hipp,<sup>3,6</sup> F. Ulrich Hartl,<sup>3,6</sup> Dieter Edbauer,<sup>2,3,7,\*</sup> Wolfgang Baumeister,<sup>1,9,\*</sup> and Rubén Fernández-Busnadiego<sup>1,\*</sup>

<sup>1</sup>Department of Molecular Structural Biology, Max Planck Institute of Biochemistry, 82152 Martinsried, Germany

<sup>2</sup>German Center for Neurodegenerative Diseases (DZNE), 81377 Munich, Germany

<sup>3</sup>Munich Cluster for Systems Neurology (SyNergy), 80336 Munich, Germany

<sup>4</sup>Department of Biophysics, Ruhr University Bochum, 44780 Bochum, Germany

<sup>5</sup>NIH Center for Macromolecular Modeling and Bioinformatics, Beckman Institute for Advanced Science and Technology, University of Illinois at Urbana-Champaign, Champaign, IL 61801, USA

<sup>6</sup>Department of Cellular Biochemistry, Max Planck Institute of Biochemistry, 82152 Martinsried, Germany

<sup>7</sup>Ludwig-Maximilians University Munich, 81377 Munich, Germany

<sup>8</sup>These authors contributed equally

<sup>9</sup>Lead Contact

\*Correspondence: dieter.edbauer@dzne.de (D.E.), baumeist@biochem.mpg.de (W.B.), ruben@biochem.mpg.de (R.F.-B.)

<https://doi.org/10.1016/j.cell.2017.12.030>

## SUMMARY

Protein aggregation and dysfunction of the ubiquitin-proteasome system are hallmarks of many neurodegenerative diseases. Here, we address the elusive link between these phenomena by employing cryo-electron tomography to dissect the molecular architecture of protein aggregates within intact neurons at high resolution. We focus on the poly-Gly-Ala (poly-GA) aggregates resulting from aberrant translation of an expanded GGGGCC repeat in *C9orf72*, the most common genetic cause of amyotrophic lateral sclerosis and frontotemporal dementia. We find that poly-GA aggregates consist of densely packed twisted ribbons that recruit numerous 26S proteasome complexes, while other macromolecules are largely excluded. Proximity to poly-GA ribbons stabilizes a transient substrate-processing conformation of the 26S proteasome, suggesting stalled degradation. Thus, poly-GA aggregates may compromise neuronal proteostasis by driving the accumulation and functional impairment of a large fraction of cellular proteasomes.

## INTRODUCTION

The ubiquitin-proteasome system (UPS) is the main cellular pathway for targeted protein degradation (Collins and Goldberg, 2017; Hershko et al., 2000). UPS alterations have been implicated in many human diseases, including multiple neurodegenerative disorders (Dantuma and Bott, 2014; Hipp et al., 2014; Schmidt and Finley, 2014). In particular, frontotemporal dementia (FTD) and amyotrophic lateral sclerosis (ALS) have been associated with mutations in UPS components (Deng et al., 2011; Johnson et al., 2010; Watts et al., 2004) and altered UPS

function (Cheroni et al., 2009; Tashiro et al., 2012). However, the contribution of UPS dysfunction to neurodegeneration and its underlying mechanisms are not yet well understood.

UPS impairment also has been linked to *C9orf72* mutations, the most common genetic cause of ALS/FTD (Edbauer and Haass, 2016; Freibaum and Taylor, 2017; Gendron and Petrucelli, 2017; Lin et al., 2017). A massive expansion of a GGGGCC ( $G_4C_2$ ) repeat in a non-coding region of the *C9orf72* gene to up to several thousand copies is found in 10%–50% of familial ALS/FTD cases and in 5%–7% of patients with sporadic disease (DeJesus-Hernandez et al., 2011; Majounie et al., 2012; Renton et al., 2011; van der Zee et al., 2013). Three non-mutually exclusive mechanisms have been suggested to mediate the toxicity of the  $G_4C_2$  repeat expansion: (1) loss of native function of the *C9orf72* protein due to reduced transcription of the mutant allele, (2) aberrant RNA interactions, and (3) production of toxic translation products and aggregates via repeat-associated non-ATG (RAN) translation (Zu et al., 2011).

Although the  $G_4C_2$  repeat is found in a non-coding region of the *C9orf72* gene, sense and anti-sense transcripts are unconventionally translated in all reading frames into five dipeptide-repeat proteins (Ash et al., 2013; Gendron et al., 2013; Mori et al., 2013a, 2013b; Zu et al., 2013): poly-GA, poly-GR, poly-GP, poly-PR, and poly-PA. While all five proteins form TDP-43-negative, p62-positive inclusions in ALS/FTD patient brain, the vast majority of these aggregates contain poly-GA (Mackenzie et al., 2015; Mori et al., 2013b; Zhang et al., 2014).

Poly-GA expression leads to toxicity in heterologous cells, primary neuron cultures, and mice (Jovičić et al., 2015; May et al., 2014; Schludi et al., 2017; Yamakawa et al., 2015; Zhang et al., 2014, 2016). Similar to other toxic aggregating proteins (Olzsha et al., 2011; Park et al., 2013), poly-GA aggregates sequester critical cellular factors including Unc119 and multiple UPS components (May et al., 2014; Zhang et al., 2016). UPS impairment is critically involved in poly-GA-mediated toxicity (Yamakawa et al., 2015; Zhang et al., 2014, 2016), but our

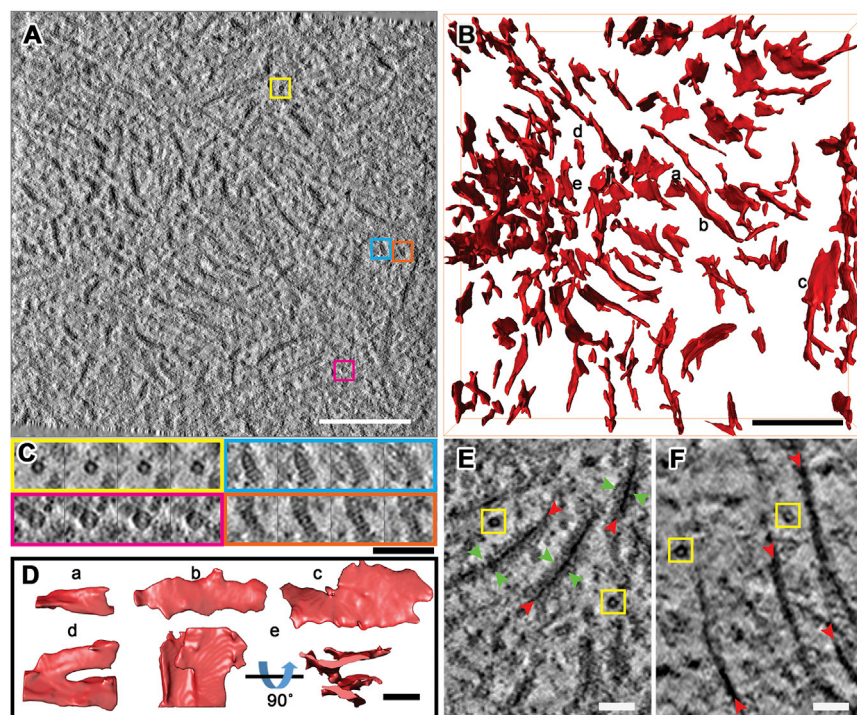


**Figure 1. *In Situ* Neuronal Poly-GA Aggregates Form Twisted Ribbons**

(A) Tomographic slice of an aggregate within a (GA)<sub>175</sub>-GFP-transduced neuron (DIV 5 + 5). Colored boxes show macromolecules magnified in (C).

(B) 3D rendering of the aggregate shown in (A). Selected poly-GA ribbons (red) magnified in (D) are indicated.

(C) Series of higher magnification tomographic slices of representative protein complexes detected in the tomogram shown in (A). Yellow and magenta boxes show the typical smaller (yellow) and larger (magenta) ring-like structures found in the aggregate region. Blue and orange boxes show side views of single-capped (blue) and double-capped (orange) 26S proteasomes.

(D) Selected ribbons from (B) rotated and magnified for visualization. Note the variable width of the ribbons (a-c). Some ribbons show bifurcations (d and e).

(E and F) Higher magnification tomographic slices of aggregates within neurons transduced with (GA)<sub>175</sub>-GFP (DIV 5 + 5) (E) or untagged (GA)<sub>175</sub> (DIV 5 + 5) (F). Yellow boxes mark similar small ring-like structures like in (A). Note that (GA)<sub>175</sub>-GFP ribbons (red arrowheads) are decorated by additional densities (green arrowheads), which are missing from untagged (GA)<sub>175</sub> ribbons. Tomographic slices are 5 nm thick.

Scale bars, 200 (A and B) and 50 nm (C–F).

See also [Figure S1](#).

understanding of the underlying mechanisms remains incomplete. This is aggravated by the limited structural information currently available on poly-GA aggregates, especially within an unperturbed cellular context.

Here, we address these challenges using state-of-the-art cryo-electron tomography (cryo-ET) technologies, which allow 3D imaging of the cell interior in close-to-native conditions and at molecular resolution (Beck and Baumeister, 2016). We reveal the structure and cellular interactions of poly-GA aggregates within intact neurons to an unprecedented level of detail. Interestingly, we find that poly-GA aggregates consist of densely packed twisted ribbons that recruit large numbers of 26S proteasome complexes. Structural analysis of these proteasome complexes by subtomogram averaging and classification into functional states provides mechanistic insights into proteasomal dysfunction in *C9orf72* ALS/FTD.

## RESULTS

### Poly-GA Aggregates Contain Densely Packed Twisted Ribbons

To study neuronal poly-GA aggregates without interference from *C9orf72* loss-of-function and RNA-mediated toxicity, we transduced primary rat neuronal cultures with a GFP-tagged codon-modified synthetic construct expressing (GA)<sub>175</sub>-GFP using an ATG start codon (May et al., 2014). We have previously shown that lentiviral poly-GA expression results in inclusions of similar size and poly-GA intensity as in *C9orf72* patient tissue (May et al., 2014). Neurons were transduced at day *in vitro* (DIV) 5 and allowed to express the protein for another

5 days (DIV 5 + 5). The cultures were then vitrified and subsequently imaged by cryo-light microscopy to locate cellular poly-GA inclusions (Figure S1A). Correlative microscopy allowed the production of 100 to 200 nm-thick lamellas at the location of these aggregates using cryo-focused ion beam milling (Bauerlein et al., 2017; Rigort et al., 2012) (Figures S1B–S1D). Lastly, the samples were transferred to a cryo-transmission electron microscope for high-resolution 3D imaging by cryo-ET (Figures S1E and S1F).

Poly-GA aggregate cross-sections were typically ~3 μm in diameter and consisted of a dense network of elongated polymorphic ribbons (Figures 1A and 1B). Whereas the thickness of the ribbons was well defined (13–15 nm), their length (100 nm–1 μm) and width (20–80 nm) varied considerably (Figure 1D, top). Our measurements likely underestimate ribbon length, as the parts of ribbons oriented perpendicular to the electron beam were not reliably detected because of missing information along this direction (Lucić et al., 2005). The ribbons were twisted along their axis with a variable helical pitch, and often bifurcated and/or associated laterally with neighboring ribbons (Figure 1D, bottom). This polymorphism contrasts with the uniform fibrils forming polyQ-expanded huntingtin exon 1 aggregates in mammalian cells (Bauerlein et al., 2017). Poly-GA ribbons were also more densely packed than polyQ fibrils, which occupied a lower fraction of the inclusion volume (poly-GA, ≥ 10%; polyQ, ≤ 4%). Thus, different amyloids adopt different morphologies *in situ*.

However, similarly to GFP-tagged polyQ fibrils, GFP-labeled poly-GA ribbons were decorated by additional densities (Figure 1E). To investigate the nature of these densities, neurons

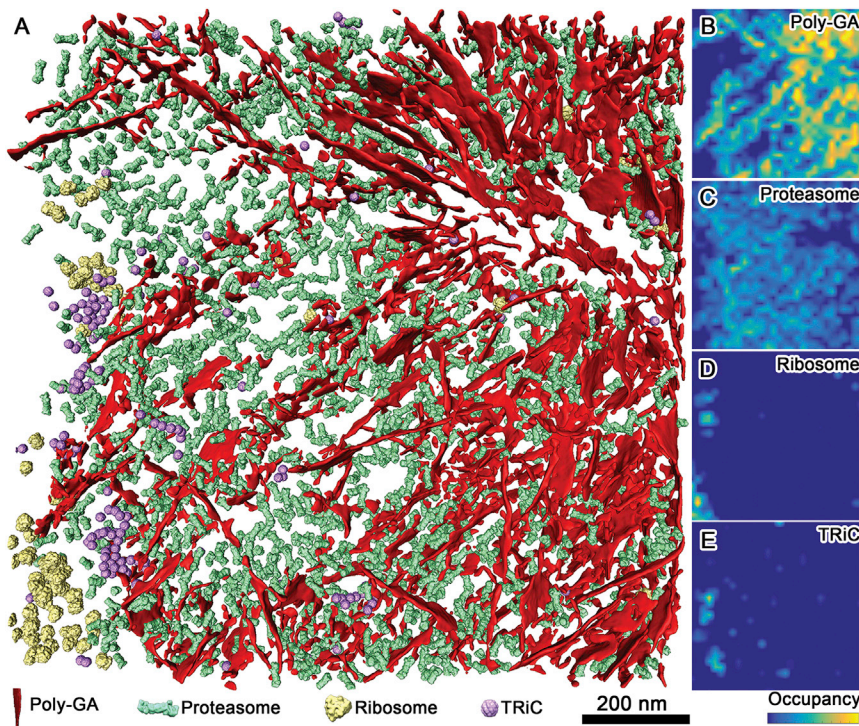


**Figure 2. Mapping Macromolecules within Poly-GA Aggregates Shows a Substantial Recruitment of 26S Proteasomes**

(A) 3D rendering of an aggregate within a neuron transduced with (GA)<sub>175</sub>-GFP (DIV 5 + 5) showing different macromolecules found either within or at the periphery of the aggregate. Red, poly-GA ribbons; green, 26S proteasomes; yellow, ribosomes; purple, TRiC/CCT chaperonins. The macromolecules are mapped in their original locations and orientations, computationally determined by template matching and subtomogram averaging.

(B–E) Maximum intensity projection heatmaps of the molecular species shown in (A). Note that the proteasomes (C) are mostly found in between poly-GA ribbons (B), whereas ribosomes (D) almost exclusively occur outside of the aggregate. TRiC/CCT molecules (E) mostly populate the aggregate periphery, but some can also be found between poly-GA ribbons.

See also Figures S2–S5 and Movie S1.

were co-transduced with untagged poly-GA and tagRFP-p62, as p62 co-localizes with poly-GA aggregates (May et al., 2014; Mori et al., 2013b; Yamakawa et al., 2015; Zhang et al., 2014) and allows targeting untagged poly-GA by correlative microscopy. As for polyQ fibrils (Bauerlein et al., 2017), the decorating densities were absent from untagged poly-GA ribbons (Figure 1F), demonstrating that these additional densities require GFP for their formation and that the ribbons consisted indeed of poly-GA aggregates. Thus, poly-GA forms amyloid-like ribbons in neurons.

### 26S Proteasomes Are Recruited to Poly-GA Aggregates

Unlike polyQ fibrils (Bauerlein et al., 2017), poly-GA ribbons did not visibly interact with cellular endomembranes. However, both the aggregate interior and periphery were densely populated by macromolecular complexes (Figures 1A, 1C, 1E, and 1F). Ribosomes were abundant around poly-GA aggregates but largely absent from their interior. In contrast, the space between poly-GA ribbons was densely populated with macromolecules that appeared as ~10-nm rings in tomographic cross-sections. Larger (~20 nm) cross-sectioned rings were also found at the aggregate periphery and occasionally in the interior. To investigate the identity of these macromolecules, we performed unbiased subtomogram averaging (Figure S2A). A small set of particles were hand-picked from the tomogram, aligned, and averaged. The resultant average was used as a template to computationally search the tomogram for additional occurrences of the same structure. These additional particles were then visually inspected, aligned, classified, and averaged again to produce a higher resolution average. The iterative application of this procedure yielded an average structure unequivocally corre-

ones (Figures 2, 3, and S3A–S3C; Movie S1). Other large UPS components, such as p97/VCP, did not appear abundant at poly-GA aggregates.

The abundance of TRiC/CCT complexes was not significantly different around poly-GA aggregates compared to the cell body of control neurons (untransduced or transduced with GFP only). However, the estimated concentration of proteasomes within the aggregate (~7 μM) was approximately 30-fold higher than in the cell body (Figure S4B) or the processes (Asano et al., 2015) of control cells. Given that poly-GA expression did not increase overall proteasome expression levels (Figure S4C), these data suggest that proteasomes are removed from other regions of the cell to accumulate within poly-GA aggregates. This is consistent with immunofluorescence staining (Figure S4A) and biochemical fractionation experiments showing reduced levels of Triton-soluble neuronal proteasomes (Figure S4C). Furthermore, our tomograms showed that 26S proteasomes almost exclusively accumulated within the aggregate interior (Figures 2 and S5A–S5D). Taken together, these results show that a substantial fraction of neuronal 26S proteasomes is sequestered into poly-GA aggregates.

To test the influence of the poly-GA expression level on proteasome recruitment, we analyzed aggregates formed in neurons at an earlier time point after transduction (DIV 5 + 3). Although these aggregates were smaller, they contained a similar concentration of proteasomes in their interior (Figure S5E). Importantly, analogous observations were made for poly-GA aggregates generated from a RAN-translated (G<sub>4</sub>C<sub>2</sub>)<sub>73</sub> construct, which more closely mimics the C9orf72 patient situation (Figures S4E and S5F). Thus, poly-GA aggregate morphology and proteasome recruitment were comparable in all the experimental conditions tested.

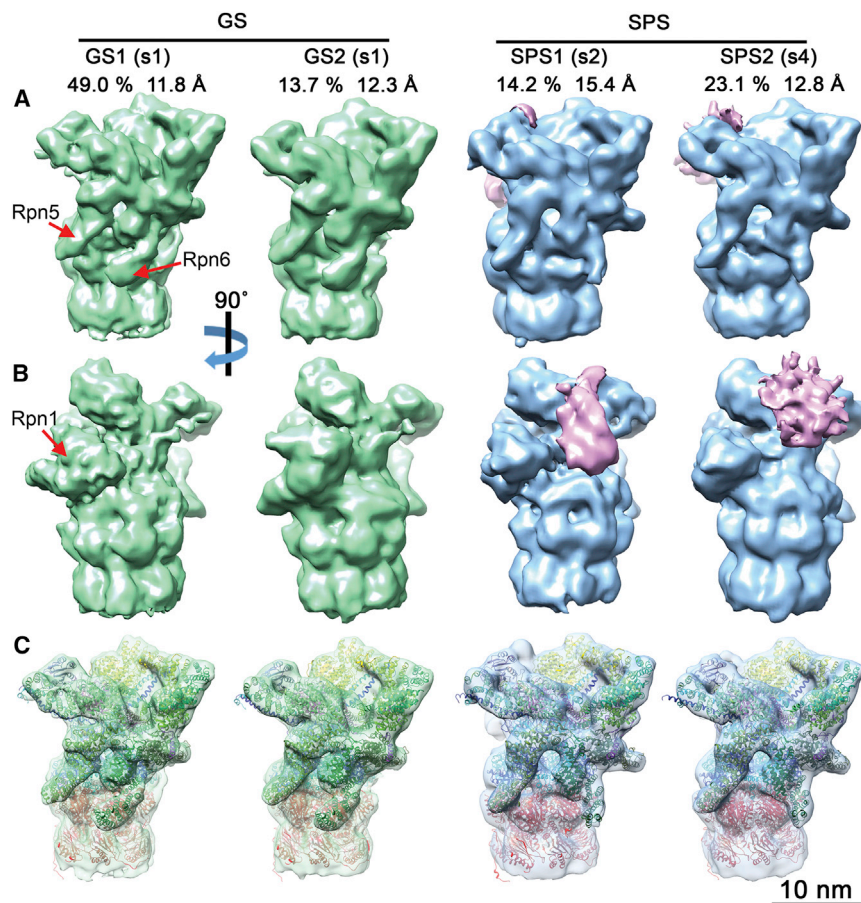


**Figure 3. Subtomogram Classification of 26S Proteasomes Reveals Enrichment of Substrate Processing Conformations**

(A–C) To analyze the functional state of proteasome regulatory particles, we cut single- and double-capped proteasomes by the half of the CP. The resultant half proteasomes were classified according to RP conformation into ground- or substrate-processing states (Asano et al., 2015), yielding two ground states (GS1, GS2) and two substrate-processing classes (SPS1, SPS2).

(A and B) The four density maps are displayed in solid surface representation in two different views. The positions of the Rpn1, Rpn5, and Rpn6 subunits are indicated. Prominent densities in the substrate binding region of SPS1 and SPS2 are colored in pink. For each class, the percentage of the total number of classified particles and the global resolution are indicated.

(C) Same view as (A), with semi-transparent maps superimposed with the atomic models generated by MDFF. The classes, respectively, represent the s1 state with different Rpn1 positions (GS1, GS2), the s2 state (SPS1), and the s4 state (SPS2). Atomic models are colored by subunits: Rpn1 (brown), Rpn2 (yellow), Rpn9/5/6/7/3/12 (different shades of green), Rpn8/Rpn11 (light/dark magenta), Rpn10 and Rpn13 (purple), AAA-ATPase hexamer (blue), and CP (red).

See also Figures S2 and S3 and Table S1.

### Poly-GA Aggregation Alters Proteasome Structure

The 26S proteasome consists of a barrel-shaped 20S core particle (CP) that harbors the catalytic activity, bound to one or two 19S regulatory particles (RP). Regulatory particles are responsible for substrate recognition, unfolding, and translocation into the CP for proteolysis. Recent single-particle cryoelectron microscopy (cryo-EM) studies have revealed how RP conformational dynamics are coupled to the functional cycle of the 26S complex (Chen et al., 2016a; Unverdorben et al., 2014; Wehmer et al., 2017). Initial binding of substrates to the 26S proteasome presumably occurs in a low-energy ground state (s1) (see also Lu et al., 2015). Bound substrates are committed for degradation (s2 state) and then translocated into the CP (s3–s4 states). In the s4 state, the gate of the 20S CP is open, allowing the substrates to access the proteolytic chamber. We took advantage of the large number of proteasome complexes recruited to poly-GA aggregates to investigate their functional states *in situ* by subtomogram averaging and classification (Figure S2B).

We first sorted 26S proteasomes according to the number of regulatory particles (one or two) bound per CP. Previous structural (Asano et al., 2015) and biochemical (Tai et al., 2010) data indicated that in control neurons the large majority of 26S proteasomes contain only one RP (single-capped 26S). In striking contrast, 76% of poly-GA-associated 26S proteasomes were double-capped (Figures S3D and S3F). Therefore, the labile

interaction between the proteasome core and regulatory particles (Kleijnen et al., 2007) is apparently stabilized within poly-GA aggregates.

We further classified 26S proteasomes by RP conformation (Asano et al., 2015; Unverdorben et al., 2014). This yielded four well-defined classes, two of which (GS1, GS2) were consistent with the RP ground state conformation (s1), whereas the other two (SPS1, SPS2) corresponded to substrate processing states (s2–s4) (Figure 3). Interestingly, 37% of all 26S proteasomes belonged to substrate processing classes, almost twice the number than in control neurons (Asano et al., 2015) (Figures S3E and S3G). Thus, poly-GA aggregates recruit a large number of 26S proteasome regulatory particles, a substantial fraction of which adopts substrate processing conformations.

The relatively high resolution of the classes (11.8–15.4 Å) (Figures 3 and S3H) enabled us to assign each class to a functional state. To this end we employed molecular dynamics flexible fitting (MDFF) (Trabuco et al., 2009) initiated through the atomic models of the s1–s4 states of the yeast 26S proteasome (Figure 3C) (Wehmer et al., 2017). The s1 state was clearly the best fit for the GS1 and GS2 classes (Table S1). The yeast s1 structure fitted GS1 (49% of the total number of particles) without large discrepancies except for the position of the Rpn1 subunit, which in GS1 was similar to that observed in the human 26S proteasome (Chen et al., 2016a; Huang et al., 2016; Schweitzer et al., 2016). Also, in agreement with these studies, no prominent density was visible in our data for the Rpn13 subunit. The GS2 class (13.7% of particles) was overall similar to

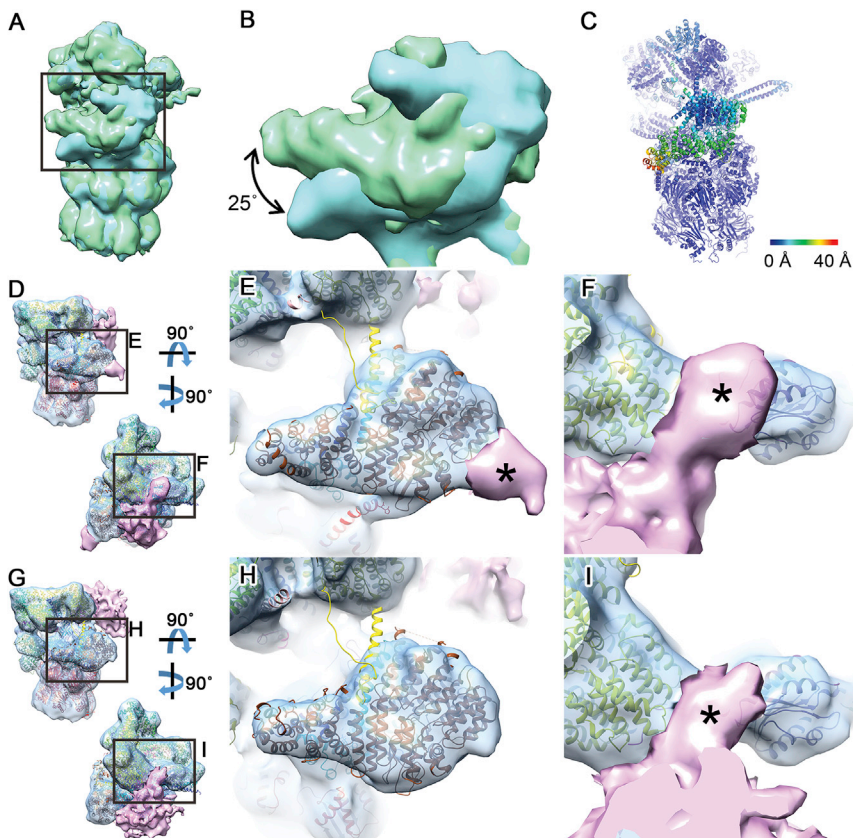


**Figure 4. Detailed Structural Differences between 26S Proteasome Conformations Highlight Its *In Situ* Structural Dynamics and Interactions**

(A) Superimposition of GS1 (green) and GS2 (cyan) density maps aligned by their CP. Both classes are consistent with the s1 state and differ only in the position of Rpn1.

(B) Magnified view of the region boxed in (A) showing a 25° rotation of the Rpn1 subunit in the GS2 map.

(C) Atomic model of the GS2 class colored according to the root-mean-square deviation (RMSD) from the GS1 model. Note that the only substantial differences are found in the Rpn1 region.

(D) Two views of the SPS1 map (consistent with the s2 state) shown in surface representation superimposed with its atomic model. A prominent density in the substrate binding region is colored in pink.

(E and F) Magnified view of the regions boxed in (D). The atomic models of Rpn1 (E), Rpn2, and Rpn10 (F) are shown in brown, yellow, and purple, respectively. Parts of the additional density denoted by asterisks may correspond to proteasome-bound ubiquitin or UBL domain proteins.

(G) Two views of the SPS2 map (consistent with the s4 state) shown in surface representation superimposed with its atomic model. A prominent density in the substrate binding region is colored in pink.

(H and I) Magnified view of the regions boxed in (G). Note that the density in the Rpn2/10 region is similar in the SPS1 and SPS2 class averages (I), whereas no additional density was found on the Rpn1 region of the SPS2 map (H).

GS1, but the Rpn1 subunit pivoted 25° on its N-terminal region to shift its C terminus toward the CP with respect to GS1 (Figures 4A–4C). This is a novel conformation of Rpn1, a particularly dynamic subunit (Asano et al., 2015; Huang et al., 2016; Schweitzer et al., 2016; Wehmer et al., 2017) that serves as binding hub for 26S regulatory cofactors containing ubiquitin-like (UBL) domains (Elsasser et al., 2002; Leggett et al., 2002) and was recently identified as an ubiquitin receptor (Shi et al., 2016).

SPS1 proteasomes (14.2% of particles) were most similar to the substrate commitment state s2 (Table S1). In contrast, the SPS2 class (23.1% of particles) was best fitted by the s4 model of actively translocating proteasomes (Table S1). This is remarkable because, *in vitro*, the s4 state was only recently discovered in proteasomes incubated with non-hydrolyzable nucleotide analogs (Wehmer et al., 2017), suggesting that it is normally a highly transient conformation. Thus, the interaction of poly-GA aggregates with the proteasome appears to stall its s4 conformation.

Both substrate processing classes showed prominent additional densities in the substrate binding region of the proteasome, in contact with the ATPase ring (Figure 3). In SPS1 the density was well defined (Figure 3), indicating a relatively stable interaction with the 26S complex that may in part correspond to bound UBL domain proteins (Aufderheide et al., 2015; Bashore et al., 2015). The density contacted Rpn1 (Figures 3, 4D, and 4E), consistent with the bound UBL domains of Rad23 or the ubiquitin C-terminal hydrolase 6 (Ubp6)/USP14 (Chen et al.,

2016b; Shi et al., 2016), and extended to another binding site of Rad23 at the Rpn10 subunit (Hiyama et al., 1999; Mueller and Feigon, 2003; Walters et al., 2002) (Figures 4D and 4F). Interestingly, similar to our SPS1 class, Ubp6-bound proteasomes have been shown to mainly adopt the s2 conformation (Aufderheide et al., 2015). Because the Rpn1 and Rpn10 UBL binding sites also interact with ubiquitin, proteasome-bound ubiquitinated substrates may also contribute to the extra density. Consistent with this notion, the estimated molecular mass of the density (~70 kDa) was larger than Ubp6 (56 kDa) or Rad23 (40/44 kDa for Rad23A/B). For the SPS2 class, the additional density contacted the Rpn10 subunit but not Rpn1 (Figures 4G–4I). The density was overall less well defined than for SPS1, indicating a more dynamic interaction, perhaps involving a more extensive participation of substrates (see below). Therefore, both substrates and cofactors may contribute to the additional densities found on substrate processing proteasomes.

### Direct Interactions with Poly-GA Aggregates Impair Proteasome Function

To address the physiological role of the different proteasome conformations observed, we investigated their cellular distribution by mapping the particles back into the tomograms (Figure 5). We found that proteasome conformation correlated with the distance to poly-GA ribbons (Figures 5B–5E,  $p < 0.001$ , chi-square test,  $n = 6,080$  regulatory particles from 4 tomograms).

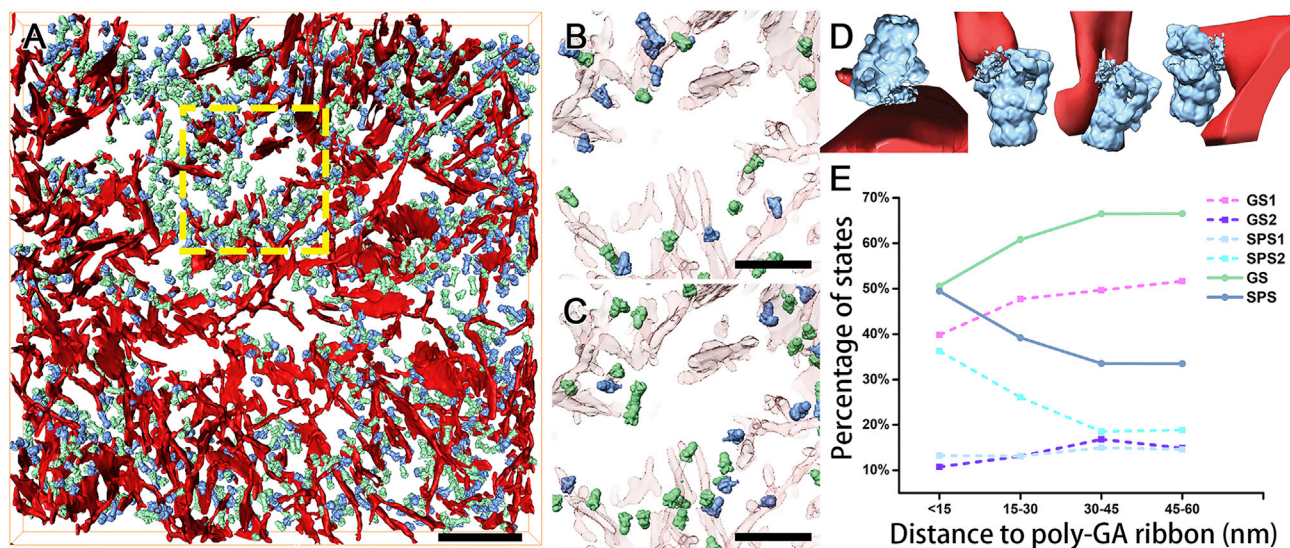


**Figure 5. Spatial Mapping of Proteasomes within Poly-GA Aggregates Reveals Poly-GA Influence on Proteasome Conformation**

(A) 3D rendering of an aggregate within a neuron transduced with (GA)<sub>175</sub>-GFP (DIV 5 + 5). Poly-GA ribbons (red), proteasomes in ground state (green), and proteasomes in substrate processing states (blue). Proteasome location and orientation were determined by template matching and subtomogram averaging. (B and C) Magnification of the region boxed in (A) showing only proteasomes less than 15 nm away from poly-GA ribbons (B) or 30–45 nm away (C). Poly-GA ribbons are shown as a transparent red surface. Note that substrate processing proteasomes are more abundant close to poly-GA ribbons.

(D) Examples of SPS2 proteasomes directly touching poly-GA ribbons in the tomogram shown in (A). The additional density in the substrate binding region overlaps with the poly-GA ribbons.

(E) Plot of proteasome conformation versus distance to poly-GA ribbons. The influence of the distance to poly-GA ribbons in proteasome conformation was statistically significant ( $p < 0.001$ , chi-square test,  $n = 6,080$  regulatory particles from 4 tomograms).

Scale bars, 200 nm (A) and 100 nm (B and C).

See also Figure S4.

For proteasomes directly touching (Figure 5D) or very close to ribbons, the SPS2 class was overrepresented (36% versus 23% of the total proteasomes (Figure 5E), whereas the fraction of GS1 proteasomes was smaller than within the total (40% versus 49%) (Figure 5E). The fraction of GS1 proteasomes increased with their distance to ribbons, whereas SPS2 proteasomes followed the opposite trend. For SPS2 proteasomes associated with poly-GA ribbons, the contact interface was consistent with the location of the additional density observed in this class (Figures 3 and 4G–4I). Only small variations were found in the fractions of GS2 and SPS1 particles with respect to the distance to poly-GA ribbons (Figure 5E). These results indicate that association with poly-GA aggregates modifies the functional state of the 26S proteasome.

In agreement with this notion, functional measurements show that poly-GA expression impairs proteasome function (Figure S4D) (Yamakawa et al., 2015; Zhang et al., 2014). Interestingly, GA-rich sequences have been reported to slow or even stall proteasomal substrate processing in the context of the Epstein-Barr virus-encoded nuclear antigen 1 protein (Hoyt et al., 2006; Kraut, 2013; Levitskaya et al., 1997). Whereas *in vitro* the s4 state was only observed in the presence of non-hydrolysable nucleotide analogs (Wehmer et al., 2017), 23% of all proteasomes within neuronal poly-GA aggregates, and 36% of the proteasomes located in the immediate vicinity of poly-GA ribbons adopted the s4 conformation *in situ* (SPS2 class). Therefore, our results suggest that proteasomal degradation is slowed

down by poly-GA-mediated stalling of the otherwise highly transient s4 state. This may play an important role in the proteostasis impairment observed in poly-GA models.

## DISCUSSION

Previous studies using classical EM reported that cellular poly-GA inclusions consist of a network of filaments 15–17 nm in diameter (Zhang et al., 2014, 2016). Our 3D imaging of unstained fully hydrated neurons shows that rather than filaments, poly-GA forms twisted ribbons similar to those observed *in vitro* for (GA)<sub>15</sub> (Chang et al., 2016). Whereas most amyloids are believed to be largely unbranched (Knowles et al., 2014), poly-GA ribbons bifurcated extensively. Together with their variable width, this suggests that *in situ* poly-GA ribbons are formed by different numbers of laterally stacked protofilaments. Furthermore, the similar morphology of (GA)<sub>15</sub> (Chang et al., 2016) and (GA)<sub>175</sub> (this study) ribbons is consistent with a molecular arrangement in which stacked GA-repeats give rise to the long axis of the protofilament.

Poly-GA aggregates recruited striking numbers of 26S proteasomes, whereas other macromolecules were excluded from the aggregate interior. This is remarkably different from our recent observations on polyQ inclusions, which interact with and may disrupt the membranes of the endoplasmic reticulum (ER) and other organelles, but do not harbor substantial numbers of 26S proteasomes or other large macromolecules (Bauerlein et al., 2017). This difference is surprising as proteasomes were also

reported to colocalize with polyQ aggregates (Bennett et al., 2005; Waelter et al., 2001). Thus, different aggregating proteins may trigger UPS dysfunction and cellular toxicity by distinct mechanisms, and how proteasomes associate with other disease-related aggregates remains to be elucidated (Deriziotis et al., 2011; Myeku et al., 2016). Future work should also address the extent of proteasome recruitment by aggregates of poly-GA proteins expressed at endogenous levels, as well as by other *C9orf72* dipeptide-repeat proteins.

UPS impairment is known to play an important role in poly-GA induced toxicity (Yamakawa et al., 2015; Zhang et al., 2014, 2016). The proteasome and other UPS components are major poly-GA interactors in neurons (May et al., 2014), and poly-GA expression leads to reduced proteasome activity (Yamakawa et al., 2015; Zhang et al., 2014; our results). Our data provide mechanistic insights into these phenomena. First, poly-GA aggregates sequester a large fraction of cellular proteasomes, depleting them from other cellular functions critical for proteostasis maintenance, such as ER-associated degradation (Zhang et al., 2014). This may be particularly damaging to neurons given their extended morphology. Second, many of the poly-GA associated proteasomes may be functionally impaired. The fraction of double-capped proteasomes and proteasome RPs in substrate processing conformations was much higher within poly-GA aggregates than in control cells. Given that CP/RP interactions are stabilized during substrate degradation (Kleijnen et al., 2007), these data suggest that many poly-GA-associated proteasomes are processing substrates or stalled in the process. Consistently, our analysis shows that contact with poly-GA ribbons causes the proteasomes to adopt the s4 conformation, an otherwise highly transient intermediate state of substrate translocation (Wehmer et al., 2017). This is in line with previous reports that GA-rich sequences slow proteasomal translocation or even stall it (Kraut, 2013; Levitskaya et al., 1997). Interestingly, despite the strong association between proteasomes and poly-GA aggregates observed here, inhibiting proteasomal degradation does not affect poly-GA levels (Yamakawa et al., 2015). Therefore, the recruitment of proteasomes to poly-GA aggregates may be unproductive and may not lead to poly-GA degradation. The mechanisms driving such recruitment, which may involve ubiquitination of poly-GA and/or of associated factors, require further investigation.

Our data may also provide insights into the cellular mechanisms of proteasome regulation in the presence of protein aggregates. Poly-GA-associated proteasomes in substrate processing states showed additional densities that may correspond to bound ubiquitin and/or UBL domain-containing cofactors such as the deubiquitinating enzyme Ubp6/USP14 or the substrate shuttle factor Rad23 (Aufderheide et al., 2015; Bashore et al., 2015; Chen et al., 2016b; Shi et al., 2016). Although the binding of these factors to poly-GA-associated proteasomes remains to be conclusively demonstrated, several UBL domain proteins (Rad23, ubiquilin2, or Bag6) were highly enriched in the poly-GA interactome (May et al., 2014), and Rad23 is an important regulator of poly-GA induced toxicity (Zhang et al., 2016). UBL domain proteins strongly modulate proteasome activity (Finley et al., 2016) and have recently been implicated in neurodegeneration and aggregate clearance (Deng et al., 2011; Hjerpe et al.,

2016). Our results are consistent with the notion that UBL domain cofactors regulate the interactions of the proteasome with protein aggregates.

## STAR★METHODS

Detailed methods are provided in the online version of this paper and include the following:

- KEY RESOURCES TABLE
- CONTACT FOR REAGENT AND RESOURCE SHARING
- EXPERIMENTAL MODEL AND SUBJECT DETAILS
  - Cell Culture
- METHOD DETAILS
  - Lentivirus Packaging
  - Generation of pcDNA3.1 – STOP-GA(G<sub>4</sub>C<sub>2</sub>)<sub>73</sub>-GFP
  - Immunofluorescence and Cellular Fractionation
  - Flow Cytometry
  - Cryo-EM Sample Preparation
  - Cryo-Fluorescent Light Microscopy and Cryo-FIB Microscopy
  - Cryo-Electron Tomography and Reconstruction
  - Template Matching and Subtomogram Averaging
  - Atomic Model Fitting
  - Segmentation of Poly-GA Aggregates and Distance Measurement
- QUANTIFICATION AND STATISTICAL ANALYSES
- DATA AND SOFTWARE AVAILABILITY

## SUPPLEMENTAL INFORMATION

Supplemental Information includes five figures, one table, and one movie and can be found with this article online at <https://doi.org/10.1016/j.cell.2017.12.030>.

## ACKNOWLEDGMENTS

We thank Radostin Danev, Günter Pfeifer, Jürgen Plitzko, and Miroslava Schaffer for electron microscopy support, as well as Irina Dudanova and Eri Sakata for helpful discussions. The psPAX2 plasmid (Addgene plasmid # 12260) was a gift from Didier Trono. Q.G. is the recipient of postdoctoral fellowships from EMBO (EMBO ALTF 73-2015) and the Alexander von Humboldt Foundation. A.M.-S. is the recipient of a postdoctoral fellowship from the Séneca Foundation. This research has received funding from the European Commission (FP7 GA ERC-2012-SyG\_318987-ToPAG and FP7 GA ERC-2013-CoG\_617198 DPR-MODELS), the German Science Foundation (Excellence Cluster Center for Integrated Protein Science Munich [CIPSM]), Munich Cluster for Systems Neurology (SyNergy) (SFB-1035/Project A01), the NOMIS Foundation, the Helmholtz Association, and the NIH (Center for Macromolecular Modeling and Bioinformatics, grant 9P41GM104601).

## AUTHOR CONTRIBUTIONS

Q.G. performed the electron microscopy experiments, computationally analyzed the data, and prepared the figures. C.L., H.H., and M.S.H. performed the cell culture and biochemistry experiments. A.M.-S. developed the software procedures for the data analysis. T.R. constructed the structural models. F.B. contributed to the computational analysis of the data. M.P.-B. and F.F. contributed the reagents. Q.G., M.S.H., F.-U.H., D.E., W.B., and R.F.-B. designed the research. D.E. and R.F.-B. supervised the experiments. Q.G., M.S.H., F.-U.H., D.E., W.B., and R.F.-B. wrote the manuscript.

## DECLARATION OF INTERESTS

D.E. has a pending patent application on “Dipeptide-repeat proteins as therapeutic target in neurodegenerative diseases with hexanucleotide repeat expansion.”

Received: August 9, 2017

Revised: November 7, 2017

Accepted: December 20, 2017

Published: February 1, 2018

## REFERENCES

- Asano, S., Fukuda, Y., Beck, F., Aufderheide, A., Förster, F., Danev, R., and Baumeister, W. (2015). Proteasomes. A molecular census of 26S proteasomes in intact neurons. *Science* *347*, 439–442.
- Ash, P.E., Bieniek, K.F., Gendron, T.F., Caulfield, T., Lin, W.L., DeJesus-Hernandez, M., van Blitterswijk, M.M., Jansen-West, K., Paul, J.W., 3rd, Rademakers, R., et al. (2013). Unconventional translation of C9ORF72 GGGGCC expansion generates insoluble polypeptides specific to c9FTD/ALS. *Neuron* *77*, 639–646.
- Aufderheide, A., Beck, F., Stengel, F., Hartwig, M., Schweitzer, A., Pfeifer, G., Goldberg, A.L., Sakata, E., Baumeister, W., and Förster, F. (2015). Structural characterization of the interaction of Ubp6 with the 26S proteasome. *Proc. Natl. Acad. Sci. USA* *112*, 8626–8631.
- Bashore, C., Dambacher, C.M., Goodall, E.A., Matyskiela, M.E., Lander, G.C., and Martin, A. (2015). Ubp6 deubiquitinase controls conformational dynamics and substrate degradation of the 26S proteasome. *Nat. Struct. Mol. Biol.* *22*, 712–719.
- Bauerlein, F.J.B., Saha, I., Mishra, A., Kalemans, M., Martinez-Sanchez, A., Klein, R., Dudanova, I., Hipp, M.S., Hartl, F.U., Baumeister, W., et al. (2017). In situ architecture and cellular interactions of polyQ inclusions. *Cell* *171*, 179–187.e10.
- Beck, M., and Baumeister, W. (2016). Cryo-electron tomography: can it reveal the molecular sociology of cells in atomic detail? *Trends Cell Biol.* *26*, 825–837.
- Bennett, E.J., Bence, N.F., Jayakumar, R., and Kopito, R.R. (2005). Global impairment of the ubiquitin-proteasome system by nuclear or cytoplasmic protein aggregates precedes inclusion body formation. *Mol. Cell* *17*, 351–365.
- Bharat, T.A., and Scheres, S.H. (2016). Resolving macromolecular structures from electron cryo-tomography data using subtomogram averaging in RELION. *Nat. Protoc.* *11*, 2054–2065.
- Chang, Y.J., Jeng, U.S., Chiang, Y.L., Hwang, I.S., and Chen, Y.R. (2016). The glycine-alanine dipeptide repeat from C9orf72 hexanucleotide expansions forms toxic amyloids possessing cell-to-cell transmission properties. *J. Biol. Chem.* *291*, 4903–4911.
- Chen, S., Wu, J., Lu, Y., Ma, Y.B., Lee, B.H., Yu, Z., Ouyang, Q., Finley, D.J., Kirschner, M.W., and Mao, Y. (2016a). Structural basis for dynamic regulation of the human 26S proteasome. *Proc. Natl. Acad. Sci. USA* *113*, 12991–12996.
- Chen, X., Randles, L., Shi, K., Tarasov, S.G., Aihara, H., and Walters, K.J. (2016b). Structures of Rpn1 T1:Rad23 and hRpn13:hPLIC2 reveal distinct binding mechanisms between substrate receptors and shuttle factors of the proteasome. *Structure* *24*, 1257–1270.
- Cheroni, C., Marino, M., Tortarolo, M., Veglianesi, P., De Biasi, S., Fontana, E., Zuccarello, L.V., Maynard, C.J., Dantuma, N.P., and Bendotti, C. (2009). Functional alterations of the ubiquitin-proteasome system in motor neurons of a mouse model of familial amyotrophic lateral sclerosis. *Hum. Mol. Genet.* *18*, 82–96.
- Collins, G.A., and Goldberg, A.L. (2017). The logic of the 26S proteasome. *Cell* *169*, 792–806.
- Dantuma, N.P., and Bott, L.C. (2014). The ubiquitin-proteasome system in neurodegenerative diseases: precipitating factor, yet part of the solution. *Front. Mol. Neurosci.* *7*, 70.
- Dantuma, N.P., Lindsten, K., Glas, R., Jellne, M., and Masucci, M.G. (2000). Short-lived green fluorescent proteins for quantifying ubiquitin/proteasome-dependent proteolysis in living cells. *Nat. Biotechnol.* *18*, 538–543.
- De Smet, F., Saiz Rubio, M., Hompes, D., Naus, E., De Baets, G., Langenberg, T., Hipp, M.S., Houben, B., Claes, F., Charbonneau, S., et al. (2017). Nuclear inclusion bodies of mutant and wild-type p53 in cancer: a hallmark of p53 inactivation and proteostasis remodelling by p53 aggregation. *J. Pathol.* *242*, 24–38.
- DeJesus-Hernandez, M., Mackenzie, I.R., Boeve, B.F., Boxer, A.L., Baker, M., Rutherford, N.J., Nicholson, A.M., Finch, N.A., Flynn, H., Adamson, J., et al. (2011). Expanded GGGGCC hexanucleotide repeat in noncoding region of C9ORF72 causes chromosome 9p-linked FTD and ALS. *Neuron* *72*, 245–256.
- Deng, H.X., Chen, W., Hong, S.T., Boycott, K.M., Gorrie, G.H., Siddique, N., Yang, Y., Fecto, F., Shi, Y., Zhai, H., et al. (2011). Mutations in UBQLN2 cause dominant X-linked juvenile and adult-onset ALS and ALS/dementia. *Nature* *477*, 211–215.
- Deriziotis, P., André, R., Smith, D.M., Goold, R., Kinghorn, K.J., Kristiansen, M., Nathan, J.A., Rosenzweig, R., Krutauz, D., Glickman, M.H., et al. (2011). Misfolded PrP impairs the UPS by interaction with the 20S proteasome and inhibition of substrate entry. *EMBO J.* *30*, 3065–3077.
- Edbauer, D., and Haass, C. (2016). An amyloid-like cascade hypothesis for C9orf72 ALS/FTD. *Curr. Opin. Neurobiol.* *36*, 99–106.
- Elsasser, S., Gali, R.R., Schwickart, M., Larsen, C.N., Leggett, D.S., Müller, B., Feng, M.T., Tübing, F., Dittmar, G.A., and Finley, D. (2002). Proteasome subunit Rpn1 binds ubiquitin-like protein domains. *Nat. Cell Biol.* *4*, 725–730.
- Fernandez, J.J., Laugks, U., Schaffer, M., Bäuerlein, F.J., Khoshouei, M., Baumeister, W., and Lucic, V. (2016). Removing contamination-induced reconstruction artifacts from cryo-electron tomograms. *Biophys. J.* *110*, 850–859.
- Finley, D., Chen, X., and Walters, K.J. (2016). Gates, channels, and switches: Elements of the [proteasome machine]. *Trends Biochem. Sci.* *41*, 77–93.
- Freibaum, B.D., and Taylor, J.P. (2017). The role of dipeptide repeats in C9ORF72-related ALS-FTD. *Front. Mol. Neurosci.* *10*, 35.
- Gendron, T.F., and Petrucelli, L. (2017). Disease mechanisms of C9ORF72 repeat expansions. *Cold Spring Harb. Perspect. Med.*, a024224.
- Gendron, T.F., Bieniek, K.F., Zhang, Y.J., Jansen-West, K., Ash, P.E., Caulfield, T., Daugherty, L., Dunmore, J.H., Castaneda-Casey, M., Chew, J., et al. (2013). Antisense transcripts of the expanded C9ORF72 hexanucleotide repeat form nuclear RNA foci and undergo repeat-associated non-ATG translation in c9FTD/ALS. *Acta Neuropathol.* *126*, 829–844.
- Goh, B.C., Hadden, J.A., Bernardi, R.C., Singharoy, A., McGreevy, R., Rudack, T., Cassidy, C.K., and Schulten, K. (2016). Computational methodologies for real-space structural refinement of large macromolecular complexes. *Annu. Rev. Biophys.* *45*, 253–278.
- Hershko, A., Ciechanover, A., and Varshavsky, A. (2000). Basic medical research award. The ubiquitin system. *Nat. Med.* *6*, 1073–1081.
- Hipp, M.S., Bersuker, K., and Kopito, R.R. (2012a). Live-cell imaging of ubiquitin-proteasome system function. *Methods Mol. Biol.* *832*, 463–472.
- Hipp, M.S., Patel, C.N., Bersuker, K., Riley, B.E., Kaiser, S.E., Shaler, T.A., Brandeis, M., and Kopito, R.R. (2012b). Indirect inhibition of 26S proteasome activity in a cellular model of Huntington’s disease. *J. Cell Biol.* *196*, 573–587.
- Hipp, M.S., Park, S.H., and Hartl, F.U. (2014). Proteostasis impairment in protein-misfolding and -aggregation diseases. *Trends Cell Biol.* *24*, 506–514.
- Hiyama, H., Yokoi, M., Masutani, C., Sugawara, K., Maekawa, T., Tanaka, K., Hoeijmakers, J.H., and Hanaoka, F. (1999). Interaction of hHR23 with S5a. The ubiquitin-like domain of hHR23 mediates interaction with S5a subunit of 26 S proteasome. *J. Biol. Chem.* *274*, 28019–28025.
- Hjerpe, R., Bett, J.S., Keuss, M.J., Solovyova, A., McWilliams, T.G., Johnson, C., Sahu, I., Varghese, J., Wood, N., Wightman, M., et al. (2016). UBQLN2 mediates autophagy-independent protein aggregate clearance by the proteasome. *Cell* *166*, 935–949.
- Hoyt, M.A., Zich, J., Takeuchi, J., Zhang, M., Govaerts, C., and Coffino, P. (2006). Glycine-alanine repeats impair proper substrate unfolding by the proteasome. *EMBO J.* *25*, 1720–1729.

- Hrabe, T., Chen, Y., Pfeffer, S., Cuellar, L.K., Mangold, A.V., and Förster, F. (2012). PyTom: a python-based toolbox for localization of macromolecules in cryo-electron tomograms and subtomogram analysis. *J. Struct. Biol.* *178*, 177–188.
- Huang, X., Luan, B., Wu, J., and Shi, Y. (2016). An atomic structure of the human 26S proteasome. *Nat. Struct. Mol. Biol.* *23*, 778–785.
- Humphrey, W., Dalke, A., and Schulten, K. (1996). VMD: visual molecular dynamics. *J. Mol. Graph.* *14*, 33–38, 27–38.
- Johnson, J.O., Mandrioli, J., Benatar, M., Abramzon, Y., Van Deerlin, V.M., Trojanowski, J.Q., Gibbs, J.R., Brunetti, M., Gronka, S., Wu, J., et al.; ITALSGEN Consortium (2010). Exome sequencing reveals VCP mutations as a cause of familial ALS. *Neuron* *68*, 857–864.
- Jovičić, A., Mertens, J., Boeynaems, S., Bogaert, E., Chai, N., Yamada, S.B., Paul, J.W., 3rd, Sun, S., Herdy, J.R., Bieri, G., et al. (2015). Modifiers of C9orf72 dipeptide repeat toxicity connect nucleocytoplasmic transport defects to FTD/ALS. *Nat. Neurosci.* *18*, 1226–1229.
- Khatter, H., Myasnikov, A.G., Natchiar, S.K., and Klaholz, B.P. (2015). Structure of the human 80S ribosome. *Nature* *520*, 640–645.
- Kleijnen, M.F., Roelofs, J., Park, S., Hathaway, N.A., Glickman, M., King, R.W., and Finley, D. (2007). Stability of the proteasome can be regulated allosterically through engagement of its proteolytic active sites. *Nat. Struct. Mol. Biol.* *14*, 1180–1188.
- Knowles, T.P., Vendruscolo, M., and Dobson, C.M. (2014). The amyloid state and its association with protein misfolding diseases. *Nat. Rev. Mol. Cell Biol.* *15*, 384–396.
- Kraut, D.A. (2013). Slippery substrates impair ATP-dependent protease function by slowing unfolding. *J. Biol. Chem.* *288*, 34729–34735.
- Kremer, J.R., Mastronarde, D.N., and McIntosh, J.R. (1996). Computer visualization of three-dimensional image data using IMOD. *J. Struct. Biol.* *116*, 71–76.
- Kuhn, P.H., Wang, H., Dislich, B., Colombo, A., Zeitschel, U., Ellwart, J.W., Kremmer, E., Rossner, S., and Lichtenthaler, S.F. (2010). ADAM10 is the physiologically relevant, constitutive alpha-secretase of the amyloid precursor protein in primary neurons. *EMBO J.* *29*, 3020–3032.
- Lee, Y.B., Chen, H.J., Peres, J.N., Gomez-Deza, J., Attig, J., Stalekar, M., Troakes, C., Nishimura, A.L., Scotter, E.L., Vance, C., et al. (2013). Hexanucleotide repeats in ALS/FTD form length-dependent RNA foci, sequester RNA binding proteins, and are neurotoxic. *Cell Rep.* *5*, 1178–1186.
- Leggett, D.S., Hanna, J., Borodovsky, A., Crosas, B., Schmidt, M., Baker, R.T., Walz, T., Ploegh, H., and Finley, D. (2002). Multiple associated proteins regulate proteasome structure and function. *Mol. Cell* *10*, 495–507.
- Leitner, A., Joachimiak, L.A., Bracher, A., Mönkemeyer, L., Walzthoeni, T., Chen, B., Pechmann, S., Holmes, S., Cong, Y., Ma, B., et al. (2012). The molecular architecture of the eukaryotic chaperonin TRiC/CCT. *Structure* *20*, 814–825.
- Levitskaya, J., Sharipo, A., Leonchiks, A., Ciechanover, A., and Masucci, M.G. (1997). Inhibition of ubiquitin/proteasome-dependent protein degradation by the Gly-Ala repeat domain of the Epstein-Barr virus nuclear antigen 1. *Proc. Natl. Acad. Sci. USA* *94*, 12616–12621.
- Li, X., Mooney, P., Zheng, S., Booth, C.R., Braunfeld, M.B., Gubbens, S., Agard, D.A., and Cheng, Y. (2013). Electron counting and beam-induced motion correction enable near-atomic-resolution single-particle cryo-EM. *Nat. Methods* *10*, 584–590.
- Lin, G., Mao, D., and Bellen, H.J. (2017). Amyotrophic lateral sclerosis pathogenesis converges on defects in protein homeostasis associated with TDP-43 mislocalization and proteasome-mediated degradation overload. *Curr. Top. Dev. Biol.* *121*, 111–171.
- Lu, Y., Lee, B.H., King, R.W., Finley, D., and Kirschner, M.W. (2015). Substrate degradation by the proteasome: a single-molecule kinetic analysis. *Science* *348*, 1250834.
- Lucić, V., Yang, T., Schweikert, G., Förster, F., and Baumeister, W. (2005). Morphological characterization of molecular complexes present in the synaptic cleft. *Structure* *13*, 423–434.
- Mackenzie, I.R., Arzberger, T., Kremmer, E., Troost, D., Lorenzi, S., Mori, K., Weng, S.M., Haass, C., Kretschmar, H.A., Edbauer, D., and Neumann, M. (2013). Dipeptide repeat protein pathology in C9ORF72 mutation cases: clinico-pathological correlations. *Acta Neuropathol.* *126*, 859–879.
- Mackenzie, I.R., Frick, P., Grässer, F.A., Gendron, T.F., Petrucelli, L., Cashman, N.R., Edbauer, D., Kremmer, E., Prudlo, J., Troost, D., and Neumann, M. (2015). Quantitative analysis and clinico-pathological correlations of different dipeptide repeat protein pathologies in C9ORF72 mutation carriers. *Acta Neuropathol.* *130*, 845–861.
- Majounie, E., Renton, A.E., Mok, K., Dopper, E.G., Waite, A., Rollinson, S., Chiò, A., Restagno, G., Nicolaou, N., Simon-Sanchez, J., et al.; Chromosome 9-ALS/FTD Consortium; French research network on FTL/FTLD/ALS; ITALSGEN Consortium (2012). Frequency of the C9orf72 hexanucleotide repeat expansion in patients with amyotrophic lateral sclerosis and frontotemporal dementia: a cross-sectional study. *Lancet Neurol.* *11*, 323–330.
- Martinez-Sanchez, A., Garcia, I., Asano, S., Lucic, V., and Fernandez, J.J. (2014). Robust membrane detection based on tensor voting for electron tomography. *J. Struct. Biol.* *186*, 49–61.
- Mastronarde, D.N. (2005). Automated electron microscope tomography using robust prediction of specimen movements. *J. Struct. Biol.* *152*, 36–51.
- May, S., Hornburg, D., Schludi, M.H., Arzberger, T., Rentzsch, K., Schwenk, B.M., Grässer, F.A., Mori, K., Kremmer, E., Banzhaf-Strathmann, J., et al. (2014). C9orf72 FTL/ALS-associated Gly-Ala dipeptide repeat proteins cause neuronal toxicity and Unc119 sequestration. *Acta Neuropathol.* *128*, 485–503.
- Mori, K., Arzberger, T., Grässer, F.A., Gijssels, I., May, S., Rentzsch, K., Weng, S.M., Schludi, M.H., van der Zee, J., Cruts, M., et al. (2013a). Bidirectional transcripts of the expanded C9orf72 hexanucleotide repeat are translated into aggregating dipeptide repeat proteins. *Acta Neuropathol.* *126*, 881–893.
- Mori, K., Weng, S.M., Arzberger, T., May, S., Rentzsch, K., Kremmer, E., Schmid, B., Kretschmar, H.A., Cruts, M., Van Broeckhoven, C., et al. (2013b). The C9orf72 GGGGCC repeat is translated into aggregating dipeptide-repeat proteins in FTL/ALS. *Science* *339*, 1335–1338.
- Mueller, T.D., and Feigon, J. (2003). Structural determinants for the binding of ubiquitin-like domains to the proteasome. *EMBO J.* *22*, 4634–4645.
- Myeku, N., Clelland, C.L., Emrani, S., Kukushkin, N.V., Yu, W.H., Goldberg, A.L., and Duff, K.E. (2016). Tau-driven 26S proteasome impairment and cognitive dysfunction can be prevented early in disease by activating cAMP-PKA signaling. *Nat. Med.* *22*, 46–53.
- Nickell, S., Förster, F., Linaroudis, A., Net, W.D., Beck, F., Hegerl, R., Baumeister, W., and Plitzko, J.M. (2005). TOM software toolbox: acquisition and analysis for electron tomography. *J. Struct. Biol.* *149*, 227–234.
- Olszcha, H., Schermann, S.M., Woerner, A.C., Pinkert, S., Hecht, M.H., Tartaglia, G.G., Vendruscolo, M., Hayer-Hartl, M., Hartl, F.U., and Vabulas, R.M. (2011). Amyloid-like aggregates sequester numerous metastable proteins with essential cellular functions. *Cell* *144*, 67–78.
- Park, S.H., Kukushkin, Y., Gupta, R., Chen, T., Konagai, A., Hipp, M.S., Hayer-Hartl, M., and Hartl, F.U. (2013). PolyQ proteins interfere with nuclear degradation of cytosolic proteins by sequestering the Sis1p chaperone. *Cell* *154*, 134–145.
- Petterson, E.F., Goddard, T.D., Huang, C.C., Couch, G.S., Greenblatt, D.M., Meng, E.C., and Ferrin, T.E. (2004). UCSF Chimera—a visualization system for exploratory research and analysis. *J. Comput. Chem.* *25*, 1605–1612.
- Phillips, J.C., Braun, R., Wang, W., Gumbart, J., Tajkhorshid, E., Villa, E., Chipot, C., Skeel, R.D., Kalé, L., and Schulten, K. (2005). Scalable molecular dynamics with NAMD. *J. Comput. Chem.* *26*, 1781–1802.
- Renton, A.E., Majounie, E., Waite, A., Simón-Sánchez, J., Rollinson, S., Gibbs, J.R., Schymick, J.C., Laaksovirta, H., van Swieten, J.C., Myllykangas, L., et al.; ITALSGEN Consortium (2011). A hexanucleotide repeat expansion in C9ORF72 is the cause of chromosome 9p21-linked ALS-FTD. *Neuron* *72*, 257–268.
- Ribeiro, J.V., Bernardi, R.C., Rudack, T., Stone, J.E., Phillips, J.C., Freddolino, P.L., and Schulten, K. (2016). QwikMD-Integrative molecular dynamics toolkit for novices and experts. *Sci. Rep.* *6*, 26536.

- Rigort, A., Bäuerlein, F.J., Villa, E., Eibauer, M., Laugks, T., Baumeister, W., and Plitzko, J.M. (2012). Focused ion beam micromachining of eukaryotic cells for cryoelectron tomography. *Proc. Natl. Acad. Sci. USA* *109*, 4449–4454.
- Scheres, S.H., and Chen, S. (2012). Prevention of overfitting in cryo-EM structure determination. *Nat. Methods* *9*, 853–854.
- Schindelin, J., Arganda-Carreras, I., Frise, E., Kaynig, V., Longair, M., Pietzsch, T., Preibisch, S., Rueden, C., Saalfeld, S., Schmid, B., et al. (2012). Fiji: an open-source platform for biological-image analysis. *Nat. Methods* *9*, 676–682.
- Schludi, M.H., Becker, L., Garrett, L., Gendron, T.F., Zhou, Q., Schreiber, F., Popper, B., Dimou, L., Strom, T.M., Winkelmann, J., et al. (2017). Spinal poly-GA inclusions in a C9orf72 mouse model trigger motor deficits and inflammation without neuron loss. *Acta Neuropathol.* *134*, 241–254.
- Schmidt, M., and Finley, D. (2014). Regulation of proteasome activity in health and disease. *Biochim. Biophys. Acta* *1843*, 13–25.
- Schroeder, W., Martin, K.M., and Lorensen, W.E. (2006). The Visualization Toolkit: an object-oriented approach to 3D graphics (Kitware).
- Schweitzer, A., Aufderheide, A., Rudack, T., Beck, F., Pfeifer, G., Plitzko, J.M., Sakata, E., Schulten, K., Förster, F., and Baumeister, W. (2016). Structure of the human 26S proteasome at a resolution of 3.9 Å. *Proc. Natl. Acad. Sci. USA* *113*, 7816–7821.
- Shi, Y., Chen, X., Elsasser, S., Stocks, B.B., Tian, G., Lee, B.H., Shi, Y., Zhang, N., de Poot, S.A., Tuebing, F., et al. (2016). Rpn1 provides adjacent receptor sites for substrate binding and deubiquitination by the proteasome. *Science* *351*, pii: aad9421.
- Tai, H.C., Besche, H., Goldberg, A.L., and Schuman, E.M. (2010). Characterization of the brain 26S proteasome and its interacting proteins. *Front. Mol. Neurosci.* *3*, 12.
- Tashiro, Y., Urushitani, M., Inoue, H., Koike, M., Uchiyama, Y., Komatsu, M., Tanaka, K., Yamazaki, M., Abe, M., Misawa, H., et al. (2012). Motor neuron-specific disruption of proteasomes, but not autophagy, replicates amyotrophic lateral sclerosis. *J. Biol. Chem.* *287*, 42984–42994.
- Tivol, W.F., Briegel, A., and Jensen, G.J. (2008). An improved cryogen for plunge freezing. *Microsc. Microanal.* *14*, 375–379.
- Trabuco, L.G., Villa, E., Schreiner, E., Harrison, C.B., and Schulten, K. (2009). Molecular dynamics flexible fitting: a practical guide to combine cryo-electron microscopy and X-ray crystallography. *Methods* *49*, 174–180.
- Unverdorben, P., Beck, F., Śledź, P., Schweitzer, A., Pfeifer, G., Plitzko, J.M., Baumeister, W., and Förster, F. (2014). Deep classification of a large cryo-EM dataset defines the conformational landscape of the 26S proteasome. *Proc. Natl. Acad. Sci. USA* *111*, 5544–5549.
- van der Zee, J., Gijssels, I., Dillen, L., Van Langenhove, T., Theuns, J., Engelborghs, S., Philtjens, S., Vandenbulcke, M., Sleegers, K., Sieben, A., et al.; European Early-Onset Dementia Consortium (2013). A pan-European study of the C9orf72 repeat associated with FTL: geographic prevalence, genomic instability, and intermediate repeats. *Hum. Mutat.* *34*, 363–373.
- Waelter, S., Boeddrich, A., Lurz, R., Scherzinger, E., Lueder, G., Lehrach, H., and Wanker, E.E. (2001). Accumulation of mutant huntingtin fragments in aggresome-like inclusion bodies as a result of insufficient protein degradation. *Mol. Biol. Cell* *12*, 1393–1407.
- Walters, K.J., Kleijnen, M.F., Goh, A.M., Wagner, G., and Howley, P.M. (2002). Structural studies of the interaction between ubiquitin family proteins and proteasome subunit S5a. *Biochemistry* *41*, 1767–1777.
- Watts, G.D., Wymer, J., Kovach, M.J., Mehta, S.G., Mumm, S., Darvish, D., Pestronk, A., Whyte, M.P., and Kimonis, V.E. (2004). Inclusion body myopathy associated with Paget disease of bone and frontotemporal dementia is caused by mutant valosin-containing protein. *Nat. Genet.* *36*, 377–381.
- Wohmer, M., Rudack, T., Beck, F., Aufderheide, A., Pfeifer, G., Plitzko, J.M., Förster, F., Schulten, K., Baumeister, W., and Sakata, E. (2017). Structural insights into the functional cycle of the ATPase module of the 26S proteasome. *Proc. Natl. Acad. Sci. USA* *114*, 1305–1310.
- Yamakawa, M., Ito, D., Honda, T., Kubo, K., Noda, M., Nakajima, K., and Suzuki, N. (2015). Characterization of the dipeptide repeat protein in the molecular pathogenesis of c9FTD/ALS. *Hum. Mol. Genet.* *24*, 1630–1645.
- Zang, Y., Jin, M., Wang, H., Cui, Z., Kong, L., Liu, C., and Cong, Y. (2016). Staggered ATP binding mechanism of eukaryotic chaperonin TRiC (CCT) revealed through high-resolution cryo-EM. *Nat. Struct. Mol. Biol.* *23*, 1083–1091.
- Zhang, Y.J., Jansen-West, K., Xu, Y.F., Gendron, T.F., Bieniek, K.F., Lin, W.L., Sasaguri, H., Caulfield, T., Hubbard, J., Daugherty, L., et al. (2014). Aggregation-prone c9FTD/ALS poly(GA) RAN-translated proteins cause neurotoxicity by inducing ER stress. *Acta Neuropathol.* *128*, 505–524.
- Zhang, Y.J., Gendron, T.F., Grima, J.C., Sasaguri, H., Jansen-West, K., Xu, Y.F., Katzman, R.B., Gass, J., Murray, M.E., Shinohara, M., et al. (2016). C9ORF72 poly(GA) aggregates sequester and impair HR23 and nucleocytoplasmic transport proteins. *Nat. Neurosci.* *19*, 668–677.
- Zu, T., Gibbens, B., Doty, N.S., Gomes-Pereira, M., Huguet, A., Stone, M.D., Margolis, J., Peterson, M., Markowski, T.W., Ingram, M.A., et al. (2011). Non-ATG-initiated translation directed by microsatellite expansions. *Proc. Natl. Acad. Sci. USA* *108*, 260–265.
- Zu, T., Liu, Y., Bañez-Coronel, M., Reid, T., Pletnikova, O., Lewis, J., Miller, T.M., Harms, M.B., Falchook, A.E., Subramony, S.H., et al. (2013). RAN proteins and RNA foci from antisense transcripts in C9ORF72 ALS and frontotemporal dementia. *Proc. Natl. Acad. Sci. USA* *110*, E4968–E4977.

## STAR★METHODS

## KEY RESOURCES TABLE

REAGENT or RESOURCE	SOURCE	IDENTIFIER
<b>Antibodies</b>		
Rabbit polyclonal anti-PSMC4	Bethyl Laboratories	Cat# A303-850A; RRID: AB_2620201
Goat anti rabbit Alexa 555	Thermo Fisher Scientific	Cat# A-21429; RRID: AB_2535850
Goat anti mouse Alexa 555	Thermo Fisher Scientific	Cat# A-21424; RRID: AB_141780
Goat anti rabbit Alexa 647	Thermo Fisher Scientific	Cat# A-21245; RRID: AB_2535813
Mouse monoclonal GFP	NeuroMab	Cat# 75-131; RRID: AB_10671445
Mouse monoclonal anti-GA	<a href="#">Mackenzie et al., 2013</a>	N/A
Rabbit polyclonal anti-Calnexin	Enzo Life Sciences	Cat# ADI-SPA-860; RRID: AB_10616095
<b>Chemicals, Peptides, and Recombinant Proteins</b>		
4x Laemmli buffer	Biorad	Cat# 1610747
B27	Thermo Fisher Scientific	Cat# 17504044
Borax anhydrous	Sigma	Cat# 71996
Bovine serum albumin	Sigma	Cat# BQ3716
DMEM, high glucose, GlutaMAX	Thermo Fisher Scientific	Cat# 10566-016
DNase	Sigma	Cat# DN25
Fetal calf serum	Sigma-Aldrich	Cat# F7524
Gelatin	Sigma-Aldrich	Cat# G9391
HEPES	Biomol	Cat# 05288
L-Glutamine	Thermo Fisher Scientific	Cat# 25030081
Lipofectamine 2000	Thermo Fisher Scientific	Cat# 11668-019
MEM non-essential amino acids solution	Thermo Fisher Scientific	Cat# 11140050
MgCl <sub>2</sub>	Merck	Cat# 105833
NaCl	Merck	Cat# 106404
Na <sub>2</sub> HPO <sub>4</sub> * 2 H <sub>2</sub> O	Merck	Cat# 106580
Neurobasal medium	Thermo Fisher Scientific	Cat# 21103049
Opti-MEM reduced serum medium	Thermo Fisher Scientific	Cat# 31985070
Paraformaldehyde	Sigma-Aldrich	Cat# 76240
Penicillin-streptomycin	Thermo Fisher Scientific	Cat# 15140122
Poly-D-lysine	Sigma	Cat# P1149
Protease inhibitor cocktail	Sigma	Cat# P8340
Sucrose	Sigma Aldrich	Cat# S9378
Tricine gels	Thermo Fisher Scientific	Cat# EC66252BOX
Dulbecco's modified Eagle medium (DMEM)	Biochrom	Cat# F0435
Fetal bovine serum	GIBCO	Cat# 10270-106
L-Glutamine	GIBCO	Cat# 25030-024
Non-essential amino acids	GIBCO	Cat# 11140-035
Trypsin	GIBCO	Cat# 12605-010
PBS	GIBCO	Cat# 20012-068
FuGENE 6	Promega	Cat# E2691
<b>Deposited Data</b>		
Cryo-EM model of the <i>S. cerevisiae</i> 26S proteasome (s1 state)	<a href="#">Wehmer et al., 2017</a>	PDB: 5MP9, 5MPD
Cryo-EM model of the <i>S. cerevisiae</i> 26S proteasome (s2 state)	<a href="#">Wehmer et al., 2017</a>	PDB: 5MPA, 5MPE
Cryo-EM model of the <i>S. cerevisiae</i> 26S proteasome (s3 state)	<a href="#">Wehmer et al., 2017</a>	PDB: 5MPB
Cryo-EM model of the <i>S. cerevisiae</i> 26S proteasome (s4 state)	<a href="#">Wehmer et al., 2017</a>	PDB: 5MPC

(Continued on next page)

**Continued**

REAGENT or RESOURCE	SOURCE	IDENTIFIER
Hybrid model of the <i>S. cerevisiae</i> TRiC/CCT	<a href="#">Leitner et al., 2012</a>	PDB: 4V94
Cryo-EM map of the human 80S ribosome	<a href="#">Khatler et al., 2015</a>	EMDB: 2938
<i>In situ</i> subtomogram average of the GS1 conformation of the 26S proteasome from rat neurons	This paper	EMDB: EMD-3916
Fitted model of the GS1 conformation of the 26S proteasome from rat neurons	This paper	PDB: 6EPF
<i>In situ</i> subtomogram average of the GS2 conformation of the 26S proteasome from rat neurons	This paper	EMDB: EMD-3913
Fitted model of the GS2 conformation of the 26S proteasome from rat neurons	This paper	PDB: 6EPC
<i>In situ</i> subtomogram average of the SPS1 conformation of the 26S proteasome from rat neurons	This paper	EMDB: EMD-3914
Fitted model of the SPS1 conformation of the 26S proteasome from rat neurons	This paper	PDB: 6EPD
<i>In situ</i> subtomogram average of the SPS2 conformation of the 26S proteasome from rat neurons	This paper	EMDB: EMD-3915
Fitted model of the SPS2 conformation of the 26S proteasome from rat neurons	This paper	PDB: 6EPE
<i>In situ</i> subtomogram average of TRiC from rat neurons	This paper	EMDB: EMD-3917
<i>In situ</i> cryo-electron tomogram of C9ORF72 poly-GA aggregates within a rat neuron	This paper	EMDB: EMD-4191
Experimental Models: Cell Lines		
HEK293FT	Thermo Fisher Scientific	Cat# R70007
UbG76V-GFP HEK293 stable cell line	<a href="#">De Smet et al., 2017</a>	N/A
Experimental Models: Organisms/Strains		
Primary neuronal cultures from CD (SD) IGS rats	Charles River	CD-SIFA; RRID: RGD_734476
Recombinant DNA		
Plasmid: FhSynW-GFP	<a href="#">May et al., 2014</a>	N/A
Plasmid: FhSynW-175xGA-GFP	<a href="#">May et al., 2014</a>	N/A
Plasmid: FU3a-tagRFP-T2 human p62	This paper	N/A
Plasmid: FhSynW -GA149stop	This paper	N/A
Plasmid: pcDNA3.1-VSVG	<a href="#">Kuhn et al., 2010</a>	N/A
Plasmid: psPAX2	Gift from Didier Trono (unpublished data)	Addgene Cat# 12260
Plasmid: pcDNA3.1-STOP-GA(G <sub>4</sub> C <sub>2</sub> ) <sub>73</sub> -GFP	This paper	N/A
Software and Algorithms		
SerialEM	<a href="#">Mastronarde, 2005</a>	<a href="http://bio3d.colorado.edu/SerialEM/">http://bio3d.colorado.edu/SerialEM/</a>
TomSegMemTV	<a href="#">Martinez-Sanchez et al., 2014</a>	<a href="https://sites.google.com/site/3demimageprocessing/tomosegmemtv">https://sites.google.com/site/3demimageprocessing/tomosegmemtv</a>
MaskTomRec	<a href="#">Fernandez et al., 2016</a>	<a href="https://sites.google.com/site/3demimageprocessing/masktomrec">https://sites.google.com/site/3demimageprocessing/masktomrec</a>
K2Align	Dimitry Tegunov	<a href="https://github.com/dtegunov/k2align">https://github.com/dtegunov/k2align</a>
Pytom	<a href="#">Hrabe et al., 2012</a>	<a href="http://pytom.org/">http://pytom.org/</a>
RELION	<a href="#">Bharat and Scheres, 2016</a>	<a href="http://www2.mrc-lmb.cam.ac.uk/relion/index.php/Main_Page">http://www2.mrc-lmb.cam.ac.uk/relion/index.php/Main_Page</a>
UCSF CHIMERA	<a href="#">Pettersen et al., 2004</a>	<a href="http://www.cgl.ucsf.edu/chimera">http://www.cgl.ucsf.edu/chimera</a>
OriginPro	OriginLab	<a href="https://www.originlab.com/index.aspx?go=Products/Origin">https://www.originlab.com/index.aspx?go=Products/Origin</a>
MATLAB	MathWorks	<a href="https://www.mathworks.com/">https://www.mathworks.com/</a>
IMOD	<a href="#">Kremer et al., 1996</a>	<a href="http://bio3d.colorado.edu/imod/">http://bio3d.colorado.edu/imod/</a>

(Continued on next page)

**Continued**

REAGENT or RESOURCE	SOURCE	IDENTIFIER
VTK	N/A	<a href="https://www.vtk.org">https://www.vtk.org</a> ; RRID: SCR_015013
Python scripts used to measure the distance between proteasomes and poly-GA aggregates	This paper	<a href="https://github.com/anmartinez/poly-GA">https://github.com/anmartinez/poly-GA</a>
QwikMD	Ribeiro et al., 2016	<a href="http://www.ks.uiuc.edu/Research/qwikmd/">http://www.ks.uiuc.edu/Research/qwikmd/</a>
VMD	Humphrey et al., 1996	<a href="http://www.ks.uiuc.edu/Research/vmd/">http://www.ks.uiuc.edu/Research/vmd/</a>
NAMD	Phillips et al., 2005	<a href="http://www.ks.uiuc.edu/Research/namd/">http://www.ks.uiuc.edu/Research/namd/</a>
TOM toolbox	Nickell et al., 2005	<a href="https://www.biochem.mpg.de/tom">https://www.biochem.mpg.de/tom</a>
Amira	Thermo Fisher Scientific	<a href="https://www.fei.com/software/amira-3d-for-life-sciences/">https://www.fei.com/software/amira-3d-for-life-sciences/</a> ; RRID: SCR_014305
Other		
Quantifoil grids 200 mesh Gold R2/1	Quantifoil Micro Tools	N/A
Whatman filter paper #1	Whatman	Cat# 1001090
Nunc 12 well plates	Thermo Fisher	Cat# 150628
Glass coverslips	VWR	Cat# 631-1581

**CONTACT FOR REAGENT AND RESOURCE SHARING**

Further information and requests for resources and reagents should be directed to and will be fulfilled by the Lead Contact, Wolfgang Baumeister ([baumeist@biochem.mpg.de](mailto:baumeist@biochem.mpg.de)).

**EXPERIMENTAL MODEL AND SUBJECT DETAILS****Cell Culture**

HEK293 cells (female) stably expressing UbG76V-GFP (Dantuma et al., 2000; De Smet et al., 2017) were cultured in Dulbecco's modified Eagle's medium (DMEM; Biochrom) supplemented with 10% (v/v) fetal bovine serum (GIBCO), 2 mM L-glutamine (GIBCO), penicillin-streptomycin (Thermo Fisher) and non-essential amino acids (GIBCO). Transfection was carried out using FuGENE 6 (Promega).

Rats (IGS background, Charles River; RRID:RGD\_734476) were housed in a pathogen-free facility with 12:12 h light/dark cycle and food/water available *ad libitum*. All animal experiments were performed in compliance with institutional policies approved by the government of Upper Bavaria following §11 Ab.1 TierSchG for the DZNE animal facility (Inst.-Nr. 04-26). Primary cortical neurons were prepared from embryonic day 19 animals of both sexes. Neocortex and hippocampus were dissected in ice-cold dissection media (HBBS, penicillin-streptomycin, 10 mM HEPES pH 7.3). The tissue was enzymatically dissociated at 37°C (for cortices 20 min in 0.2% trypsin, 0.7 mg/ml DNase I; for hippocampi 15 min in 0.25% trypsin in dissection media) followed by gentle trituration.

For EM analysis, 250,000 cells/ml cortical neurons were plated on EM grids and cultured in Neurobasal medium containing 2% B27 (Thermo Fisher), penicillin-streptomycin, 0.5 mM L-glutamine (Thermo Fisher). For biochemical analysis, 250,000 cells/ml cortical neurons were plated on 12-well plates (Thermo Fisher) and cultured in Neurobasal medium. For immunofluorescence experiments, 85,000 cells/ml hippocampal neurons were plated on 12-well plates containing glass coverslips (VWR) coated with poly-D-lysine and cultured in Neurobasal medium supplemented with 12.5  $\mu$ M glutamate.

**METHOD DETAILS****Lentivirus Packaging**

HEK293FT cells (female; from Thermo Fisher) of low passage number were plated in three 10 cm dishes (5,000,000 cells/dish) and cultured in DMEM (Thermo Fisher), penicillin-streptomycin, 1% non-essential amino acids (Thermo Fisher) and 10% fetal bovine serum (Sigma). A transfection mix was set up as follows: 18.6  $\mu$ g transfer vector (FhSynW-(GA)<sub>175</sub>-GFP, FhSynW (GA)<sub>149</sub>, FU3a-tagRFP-p62 or FhSynW-GFP), 11  $\mu$ g pSPAX2 and 6.4  $\mu$ g pVSVg in 4.5 mL Opti-MEM were combined with 108  $\mu$ l Lipofectamine 2000 in 4.5 mL Opti-MEM (Thermo Fisher) and incubated for 20 minutes. Cell media was replaced with 5 mL Opti-MEM and 3 mL of transfection mix were added per dish. The transfection media was replaced after 6 h by plating media supplemented with 13 mg/ml bovine serum albumin, and the supernatant was collected after additional 24 h. Lentiviral particles were harvested by ultracentrifugation using a Sw28 rotor (22,000 rpm, 2 h), resuspended in 150  $\mu$ l Neurobasal media on a rocking platform overnight and stored in aliquots at  $-80^{\circ}$ C.

### Generation of pcDNA3.1 – STOP-GA(G<sub>4</sub>C<sub>2</sub>)<sub>73</sub>-GFP

The method to generate the construct was adapted from [Lee et al. \(2013\)](#). Complementary G<sub>4</sub>C<sub>2</sub> repeat oligonucleotides with phosphorylated ends (5'-PHOS-(G<sub>4</sub>C<sub>2</sub>)<sub>5</sub>-3' and 5'-PHOS-CC(G<sub>2</sub>C<sub>4</sub>)<sub>4</sub>GGCC-3') were energetically optimized to maximize heterodimer formation. After initial denaturation for 5 min at 95°C in T4 ligase buffer (New England Biolabs), the complementary oligonucleotides were allowed to anneal by slow cool down to room temperature during 2 h. Hybridized oligonucleotides were then self-ligated for 1 h to extend the G<sub>4</sub>C<sub>2</sub> DNA sequence. Adaptor oligonucleotides containing NheI (5') and BamHI (3') restriction sites (5' adaptor oligonucleotides containing NheI: 5'-GCCGTCAAGGCCGCATCTAGTAGCTAGC-3' and 5'-PHOS-CCGCTAGCTACTAGATGCGGCCTT GACGGC-3'; 3' adaptor oligonucleotides containing BamHI: 5'-PHOS-GGGATCCCTAGTACTGGCCTCATGGGC-3' and 5'-GCC CATGAGGCCAGTACTAGGGATC-3') were separately hybridized and sequentially added in excess to the ligation reaction mix to stop G<sub>4</sub>C<sub>2</sub> elongation. Ligation products were separated in a 1.25% agarose gel, and bands running at the desired molecular size were excised. The DNA was then purified with the ZymoClean Gel DNA recovery kit (Zymo Research) according to the manufacturer's guidelines. The resulting blunt-end fragments were phosphorylated and cloned into a dephosphorylated SmaI-restricted pUC18 plasmid for amplification. Colonies were screened for G<sub>4</sub>C<sub>2</sub> repeat length, and a construct with 73 G<sub>4</sub>C<sub>2</sub> repeats was chosen for further experiments. The selected sequence was subcloned into the mammalian expression vector pcDNA3.1(+)/myc-His between NheI and BamHI in front of a GFP-encoding region. Finally, multiple stop codons were added by site-directed mutagenesis in every reading frame at the 5' of the sequence of interest, thereby removing all initiator codons between the T7 promoter and the sequence of interest. The sequence was verified by multiple sequencing reactions as well as restriction digest.

### Immunofluorescence and Cellular Fractionation

Immunofluorescence stainings were performed on primary hippocampal neurons 5 days after infection with (GA)<sub>175</sub>-GFP or GFP lentivirus on day 5, or 3 days upon transfection with G<sub>4</sub>C<sub>2</sub> on day 3 using Lipfectamine 2000 (Thermo Fisher). Cells were fixed for 10 min at room temperature (4% paraformaldehyde, 4% sucrose in PBS). Anti-PSMC4 (Bethyl Laboratories, 1:250, RRID:AB\_2620201) or anti-GA ([Mackenzie et al., 2013](#), 1:200) primary antibodies as well as secondary antibodies (Alexa 555, Alexa 647, Thermo Fisher, 1:400, RRID:AB\_2535850, RRID:AB\_141780, RRID:AB\_2535813) were diluted in staining buffer (0.1% gelatin, 0.3% Triton X-100, 450 mM NaCl, 16 mM sodium phosphate pH 7.4). After mounting the coverslips, images were taken using a LSM710 confocal microscope (Carl Zeiss, Jena) with a 63 × oil immersion objective.

Biochemical experiments were performed on primary cortical neurons 10 days after infection with either (GA)<sub>175</sub>-GFP or GFP lentivirus on day 3. Cells were lysed (PBS with 1% Triton X-100, 15 mM MgCl<sub>2</sub>, 0.2 mg/ml DNase with protease inhibitor cocktail). Upon centrifugation (18,000 xg, 4°C for 30 min) the soluble fraction was collected from the supernatant. The pellets were washed twice with lysis buffer yielding the insoluble fraction. After adding 4x Laemmli buffer (Bio-Rad), samples were denaturated (95°C for 10 min) and loaded on Tricine gradient gels (Thermo Fisher). The following antibodies were used: Anti-PSMC4 (Bethyl Laboratories, 1:1000), anti-GFP (NeuroMab, 1:5000, RRID:AB\_10671445) and anti-Calnexin (Enzo Life Sciences, 1:7000, RRID:AB\_10616095). The data in [Figure S4C](#) was normalized to the total proteasome levels in GFP-transduced control neurons.

### Flow Cytometry

HEK293 cells stably expressing UbG76V-GFP were harvested 72 h after transient transfection with (GA)<sub>175</sub>-tagRFP or tagRFP as control and analyzed with a BD FACSAriaIII flow cytometer, as described previously ([Hipp et al., 2012a, 2012b](#)). In brief, to ensure a sufficient number of cells with elevated levels of the transfected proteins > 100,000 events were analyzed per condition. To plot the level of the reporter protein versus the level of the transfected protein, a set of gates was established in the tagRFP channel. HEK293 cells transfected with tagRFP were used as single-color control to compensate the bleed-through between GFP and tag-RFP individually for each gate, and to correct for effects due to high expression of tagRFP. The compensated mean fluorescence of the reporter protein UbG76V-GFP in each of these gates was plotted on the y axis and the gate number (corresponding to the log of fluorescence intensity of the transfected protein) was plotted on the x axis. The data shown in [Figure S4D](#) are from a single representative experiment out of three independent repeats. Cells expressing low levels of tagRFP (gates 1-9) and gates with < 1000 events were not included in the analysis. Raw flow cytometry data were analyzed using FlowJo software (version 9.9; Tree Star).

### Cryo-EM Sample Preparation

Quantifoil grids (R2/1, Au 200 mesh grid, Quantifoil Micro Tools, Germany) were coated with an additional carbon layer (~20 nm thick) using a carbon evaporator (MED 020, BAL-TEC). Before use, the grids were glow discharged using a plasma cleaner (PDC-3XG, Harrick) for 20 s and neurons were seeded as described above. Neurons were vitrified 5 days after transduction with GFP or tagRFP-p62/untagged (GA)<sub>175</sub> on day 5, 3 or 5 days after transduction with (GA)<sub>175</sub>-GFP on day 5, and 3 days after transfection with (G<sub>4</sub>C<sub>2</sub>)<sub>73</sub> on day 3. Untransduced and untransfected control neurons were vitrified on DIV 10.

For vitrification, the grids were blotted for 10 s from the back side using filter paper and immediately plunged into a liquid ethane/propane mixture ([Tivol et al., 2008](#)) using a manual plunge freezer. Grids were transferred to sealed boxes and stored in liquid nitrogen until usage.

### Cryo-Fluorescent Light Microscopy and Cryo-FIB Microscopy

EM grids were mounted onto modified Autogrid (FEI, Hillsboro, OR, USA) sample carriers, allowing subsequent FIB milling with a shallow incident ion beam (Rigort et al., 2012), and then transferred to the cryo-stage of an FEI CorrSight microscope for cryo-light microscopy. Overview images of the grid and poly-GA-GFP/tagRFP-p62 signal were respectively acquired in transmitted light and the spinning disk confocal modes using a 20x lens (air, N.A. 0.8). Image acquisition was done with FEI MAPS software. The samples were then transferred into a FEI Scios dual beam cryo-FIB/scanning electron microscope (SEM) using a cryo-transfer system.

To improve the sample conductivity, a layer of organometallic platinum was deposited onto the grid using the *in situ* gas injection system with the following parameters: 10 mm working distance, 26°C pre-heating temperature, and 8 s gas injection time. MAPS software allowed correlation between cryo-light microscopy and SEM images via the 3-point alignment method. Thin lamellas were prepared in the regions of poly-GA-GFP/tagRFP-p62 fluorescence signal using the Ga<sup>2+</sup> ion beam at 30 kV under a 20° stage tilt angle. 0.5 nA beam current was used for rough milling, followed by sequentially lower currents during the thinning procedure. A current of 30 pA was used for the final polishing step to reach a final lamella thickness of 150-200 nm. SEM imaging was used to monitor the milling progress.

### Cryo-Electron Tomography and Reconstruction

The specimens were examined at liquid nitrogen temperature in an FEI Titan Krios cryo-electron microscope operated at 300 kV and equipped with a field emission gun and a Gatan post column energy filter. Lamellas were loaded vertical to the tilt axis, and were precisely aligned by adjusting the  $\beta$  angle of the cryo-stage. Images were collected using a 4 k x 4 k K2 Summit (Gatan) direct detector camera operated in dose fractionation mode (0.4 s, 0.3 electrons/Å<sup>2</sup> per frame). Tilt series were recorded using SerialEM software (Mastrorade, 2005) at a nominal magnification of 42,000 X, resulting in a pixel size of 3.42 Å at the specimen level. Unidirectional tomographic tilt series were recorded from -50° to +70° with an increment of 2°. On average, 6 frames were collected for each image resulting in a total dose between 100 e<sup>-</sup>/Å<sup>2</sup> to 110 e<sup>-</sup>/Å<sup>2</sup> per tilt series. K2 frames were aligned using in house software (K2Align) based on previous work (Li et al., 2013). Tilt series were aligned using fiducial-less patch tracking, and the tomograms were reconstructed by weighted back projection using the IMOD software package (Kremer et al., 1996). For tomograms of lamellas superficially contaminated by ice crystals, a surface cleaning procedure was employed after alignment (Fernandez et al., 2016). The resulting tilt series were then aligned and reconstructed again to obtain the final reconstructions.

### Template Matching and Subtomogram Averaging

To identify the macromolecules found in the tomograms, a *de novo* subtomogram averaging procedure without any external structural information was developed (Figure S2A). The MATLAB (Mathworks) TOM toolbox (Nickell et al., 2005) was used as general platform for image processing. First, all the tomograms were binned twice (13.68 Å<sup>3</sup> per voxel) for processing. In one tomogram, several identical small ring-like structures were hand-picked, aligned and averaged to obtain a first tube-like average structure. This was used as an initial template for template matching in all the binned tomograms using PyTom (Hrabe et al., 2012). The resulting subtomograms were cropped, CTF-corrected and classified using Relion (Bharat and Scheres, 2016). The resulting structure clearly showed a 20S proteasome core complex, but because of the missing wedge and the preferred orientation induced by the initial template, the 19S regulatory particles (RP) were not well resolved. This structure was used to perform a new round of template matching and classification, which clearly resolved proteasomes either single- or double-capped. The single-capped proteasomes were low-pass filtered to 40 Å and used as a reference for template matching again to produce the final dataset. In total, 10,367 proteasome subtomograms of 180<sup>3</sup> pixel volume were picked for further analysis from 9 tomograms containing large (GA)<sub>175</sub>-GFP aggregates (DIV 5 + 5). The same template matching procedure was applied to tomograms of control neurons, either untransduced (16 tomograms) or transduced with GFP only (17 tomograms).

The subtomograms were then 3D classified using Relion (Figure S2B). They were first divided into single-capped and double-capped proteasomes. To further rule out reference bias, a single-capped proteasome, a double-capped proteasome and a mirrored single-capped proteasome were used as references for classification. The results were similar, indicating negligible reference bias during classification. To further analyze the conformational status of the 19S regulatory particles, all subtomograms were cut *in silico* between the  $\beta$ -rings of the 20S, resulting in two independent particles for the double-capped proteasomes (Asano et al., 2015). All cut-out half proteasomes were merged into a new dataset for another round of classification. Ground state and substrate processing state structures were distinguished by the relative orientation of the Rpn5 and Rpn6 subunits (Asano et al., 2015; Unverdorben et al., 2014). Ground state and substrate processing state structures were further classified by applying a soft sphere mask in the RP region only. Identical subclasses were merged resulting in two ground state and two substrate processing state classes, which were further refined to achieve the final structures. A similar analysis could not be applied to control neurons (GFP-transduced or untransduced) due to the low numbers of proteasomes found in these samples. Therefore, the results from untransduced neurons from a previous study (Asano et al., 2015) were used as reference. Visualization of the subtomogram averages was performed in UCSF Chimera (Pettersen et al., 2004). Resolution was determined using the 0.143 criterion according to the gold standard Fourier Shell Correlation (Scheres and Chen, 2012).

To identify the larger ring-like structures found in the tomograms, a similar template matching procedure was employed. A spherical structure was generated after processing, which showed a clear eight-fold symmetry by rotational correlation coefficient analysis (Figure S3B). Furthermore, the size of the average fitted well with the crystal structure of TRiC/CCT (PDB: 4V94) (Leitner et al., 2012),

indicating that these larger rings correspond to the TRiC/CCT chaperonin. A total of 1,366 TRiC subtomograms were used for averaging. For ribosome template matching, a human 80S ribosome structure (EMDB 2938) (Khatter et al., 2015) was filtered to 40 Å and used as a template.

### Atomic Model Fitting

The *S. cerevisiae* proteasome models of the states s1 (PDB: 5MP9, 5MPD), s2 (PDB: 5MPA, 5MPE), s3 (PDB: 5MPB), and s4 (PDB: 5MPC) (Wehmer et al., 2017) were used as initial models. The core particles of the models were fitted into each of the groups obtained by classification of the poly-GA proteasome dataset using rigid body docking within UCSF Chimera. For each class, MDFF was performed to refine the s1-4 models according to the density maps. Then, the RMSD between the best fitting atomic models and the initial s1-4 state models was calculated (Table S1). This showed that the GS1 class reflected the s1 state with the Rpn1 positioning of the human s1 state (PDB: 5L5K) (Schweitzer et al., 2016), GS2 reflected the s1 state with a rotated Rpn1 position, SPS1 reflected the s2 state and SPS2 reflected the s4 state. To obtain the final atomic rat models, the best fitting yeast structures for each class were used as templates for comparative modeling and real-space structure refinement (Goh et al., 2016). MDFF simulations were prepared using QwikMD (Ribeiro et al., 2016), analyzed with VMD (Humphrey et al., 1996), and carried out with NAMD (Phillips et al., 2005).

### Segmentation of Poly-GA Aggregates and Distance Measurement

Poly-GA ribbons are locally planar and were consequently segmented using a filter based on tensor voting, which distinguishes planar-like from line- and blob-like structures (Martinez-Sanchez et al., 2014). The filter outputs a scalar map, where voxel intensity value is proportional to the local similarity with a plane. The final segmentation was generated by thresholding the filter output combined with a manually generated mask to discard other locally planar structures like membranes and correct minor artifacts. Due to the missing information along the electron beam direction (Lucić et al., 2005), poly-GA ribbons were not clearly visible when oriented within the xy plane. Segmentations were visualized using Amira (Thermo Fischer, RRID:SCR\_014305).

For Figure 5, proteasome regulatory particles and poly-GA ribbons were represented by an isosurface, properly placed and oriented in their original tomogram. For regulatory particles, surfaces were obtained by applying the marching cubes algorithm, implemented in the VTK Open Source library (<https://www.vtk.org/>; RRID:SCR\_015013; Schroeder et al., 2006), on the corresponding subtomogram average. Isosurface threshold was set manually for every case with the criterion of choosing the minimum value avoiding noisy features. For poly-GA ribbons, isosurfaces were generated from the output of the planar filter using the marching cubes algorithm. The final ribbon surfaces were obtained by masking the isosurface with the corresponding ribbon segmentation from the tomogram. To calculate the fraction of the volume of poly-GA inclusions occupied by poly-GA ribbons, total ribbon volume was measured from the segmentations and divided by the total tomogram volume. For this calculation, tomograms ( $n = 4$ , (GA)<sub>175</sub>-GFP transduced neurons at DIV 5 + 5) were selected in which the large majority of the volume contained poly-GA aggregates.

RP to poly-GA ribbon distance was defined as the shortest Euclidean distance between the center of the RP to any surface point of any ribbon in the same tomogram. A custom Python software package was developed to measure RP-to-ribbon distance for every RP in all tomograms. The results were grouped by particle class to facilitate statistical analysis. The shortest distance among surfaces was computed with the help of a VTK library (Schroeder et al., 2006).

## QUANTIFICATION AND STATISTICAL ANALYSES

To measure proteasome concentration, for each tomogram ( $n = 9$ , (GA)<sub>175</sub>-GFP transduced neurons, DIV 5 + 5;  $n = 17$ , GFP transduced neurons;  $n = 16$ , untransduced neurons) the number of proteasomes found by template matching and subtomogram averaging was divided by the total tomogram volume. Because other cellular structures (such as poly-GA aggregates, other macromolecules or cellular organelles) were also present in the tomogram volume, this calculation underestimates the cytosolic concentration of proteasomes. For poly-GA aggregates, only tomograms with more than half volume occupied by aggregates were considered for the concentration calculation. In Figure S4B, the top and bottom boundaries of the boxes indicate  $\pm 2x$  standard error, and whiskers extend to the maximum and minimum values. Statistical analysis was performed by the non-parametric Mann-Whitney test, as not all data was normally distributed according to the Shapiro-Wilk test.

For the analysis of proteasome conformation as a function of the distance to poly-GA ribbons (Figures 5B, 5C, and 5E), 6080 regulatory particles from 4 tomograms of (GA)<sub>175</sub>-GFP transduced neurons (DIV 5 + 5) were analyzed. The data were divided in a 4x4 Table (4 RP states x 4 distance bins) resulting in 9 degrees of freedom. Statistical analysis was performed by Chi-square test.

The proteasome levels in the total, soluble and insoluble fractions of (GA)<sub>175</sub>-GFP transduced neurons were quantified from western blots by measuring the gray levels using Fiji (Schindelin et al., 2012). Error bars in Figure S4C indicate standard error. All data was normally distributed according to the Shapiro-Wilk test (95% confidence level). Statistical analysis was performed by two-sided paired t test ( $n = 6$  replicates from 4 independent experiments). All graphs were plotted using OriginPro (OriginLab).

## DATA AND SOFTWARE AVAILABILITY

The Python scripts used to calculate the distance between proteasomes and poly-GA ribbons are available at <https://github.com/anmartinez/poly-GA>.

The tomogram analyzed in [Figure 2](#) has been deposited at the Electron Microscopy Data Base with accession number EMD-4191. The structures of the proteasome and TRiC/CCT obtained by *in situ* subtomogram averaging have been deposited at EMD-4191 with the following accession numbers: EMD-3916 (GS1 proteasome), EMD-3913 (GS2 proteasome), EMD-3914 (SPS1 proteasome), EMD-3915 (SPS2 proteasome), EMD-3917 (TRiC/CCT). The fitted atomic models of the different proteasome states have been deposited at the Protein Data Base with the following accession numbers: PDB: 6EPF (GS1), 6EPC (GS2), 6EPD (SPS1), 6EPE (SPS2).

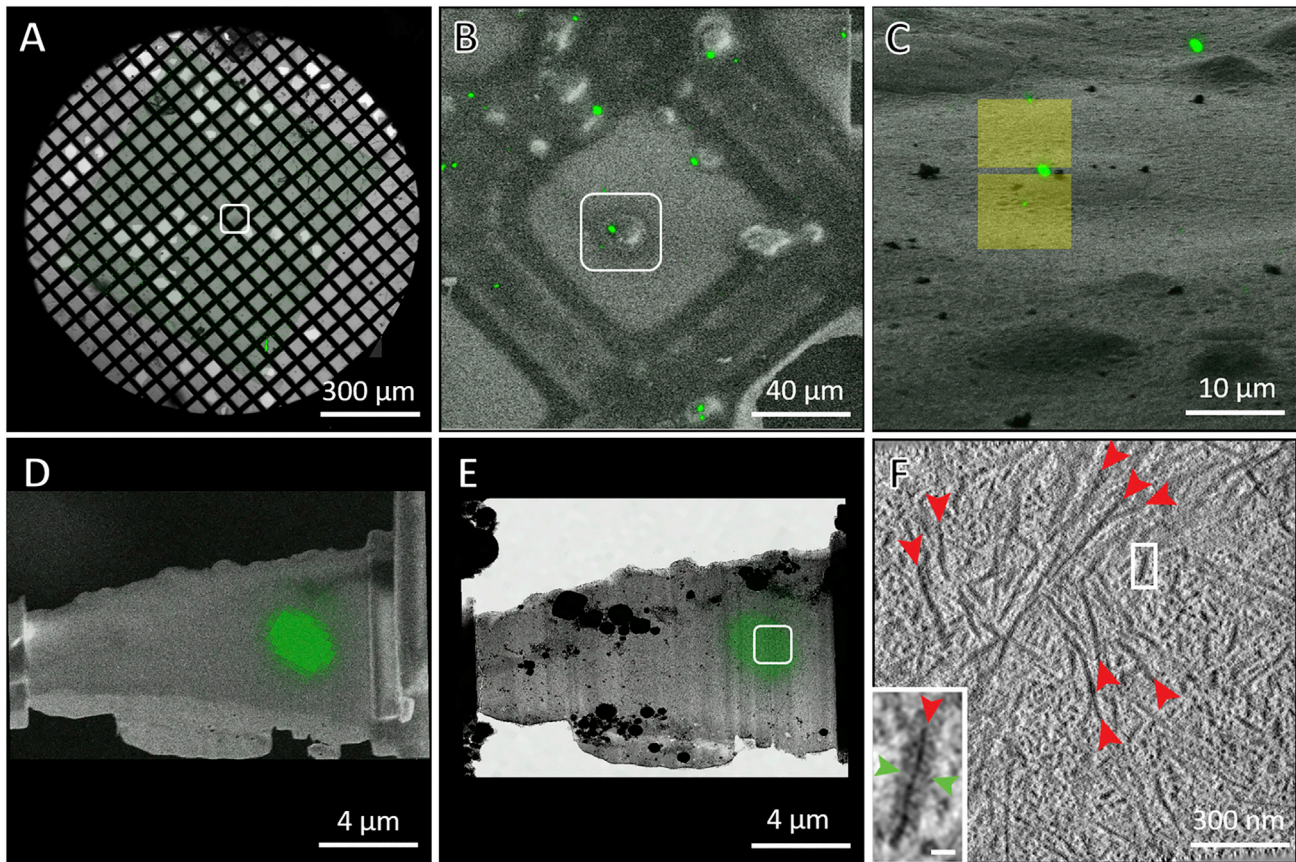


**Figure S1. Correlative Cryo-light and Cryoelectron Microscopy Workflow, Related to Figure 1**

(A) Rat cortical neurons were cultured on EM grids and transduced with (GA)<sub>175</sub>-GFP on day 5. Upon vitrification by plunge freezing 5 days after transfection, the grids were imaged by cryo-light microscopy. (A) shows an overlay of phase and GFP channels.

(B) EM grids were transferred to a cryo-FIB/SEM microscope. To locate cells of interest (boxed), SEM images were aligned and superimposed with the GFP signal from the cryo-LM image.

(C) FIB-induced secondary electron image of the cell shown in (B), superimposed with the GFP signal. Yellow boxes mark the regions of the cell removed by FIB to produce a lamella containing the GFP-positive region.

(D) SEM image of the lamella resulting from FIB milling, with a final thickness of ~200 nm, superimposed with the GFP signal.

(E) Cryo-TEM low magnification image of the lamella shown in (D).

(F) 5 nm-thick tomographic slice of a tomogram recorded in the area marked by a white square in (E), containing the GFP signal. A dense network of poly-GA-GFP ribbons (red arrowheads) is visible. The inset shows a high magnification of a poly-GA-GFP ribbon decorated by GFP-associated additional densities (green arrowheads). Scale bar: 20 nm.

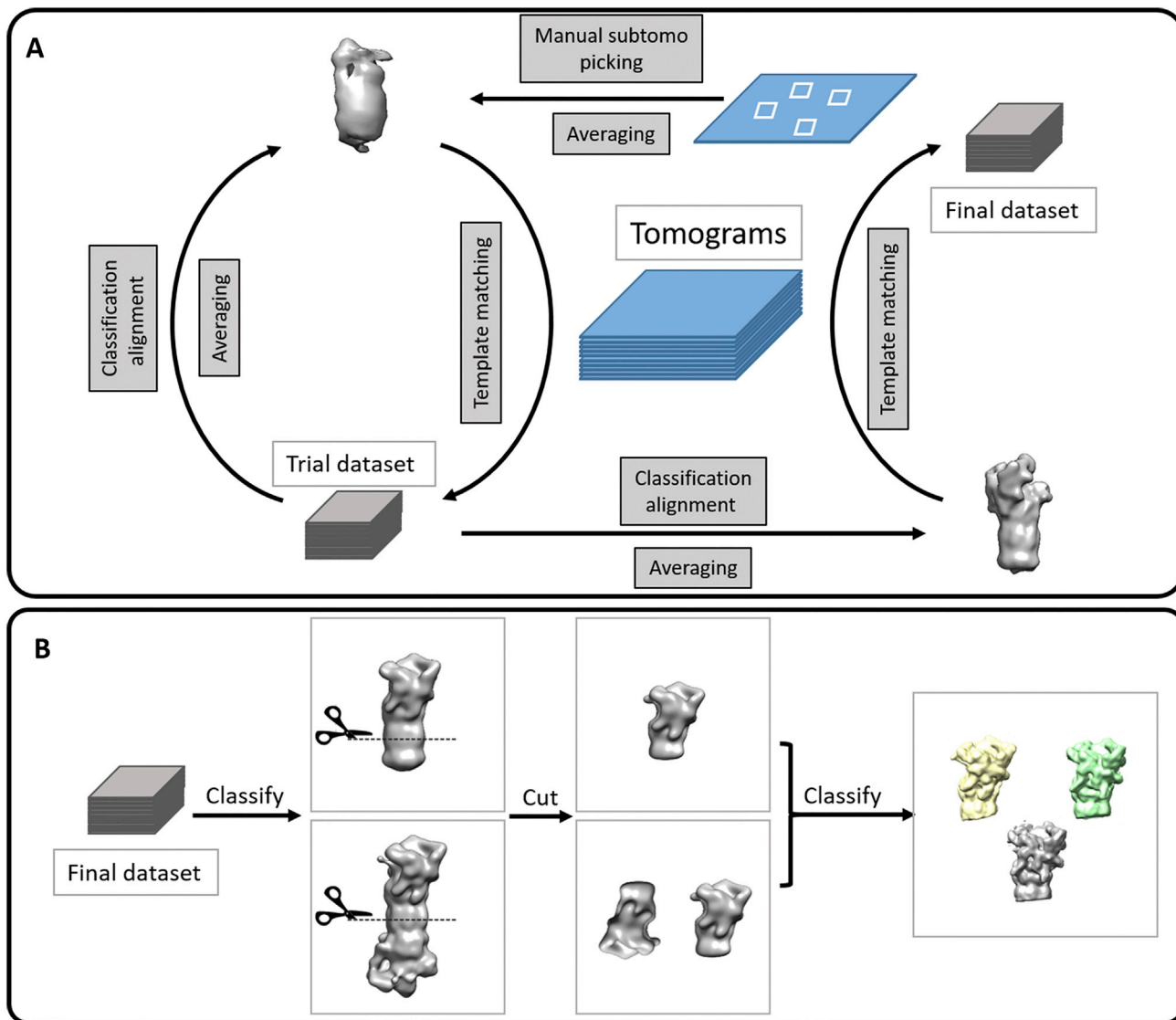


**Figure S2. Subtomogram Averaging and Classification Workflow, Related to Figures 2 and 3**

(A) Unbiased template matching procedure. Several identical structures were first hand-picked from one tomogram, aligned and averaged. The resulting average was used as a template to search more tomograms for additional occurrences of the same structure. These additional particles were then visually inspected, aligned, classified and averaged again to produce a higher resolution average. This average was low-pass filtered and used as a template to search all the tomograms to produce the final subtomogram dataset.

(B) All proteasome subtomograms were first classified into single-capped or double-capped. To further analyze the conformational status of the regulatory particles, all the subtomograms were cut *in silico* between the  $\beta$ -rings of the core particle (Asano et al., 2015), resulting in two independent particles for double-capped proteasomes. Cut out caps from all proteasomes were merged and subjected to a further round of classification.

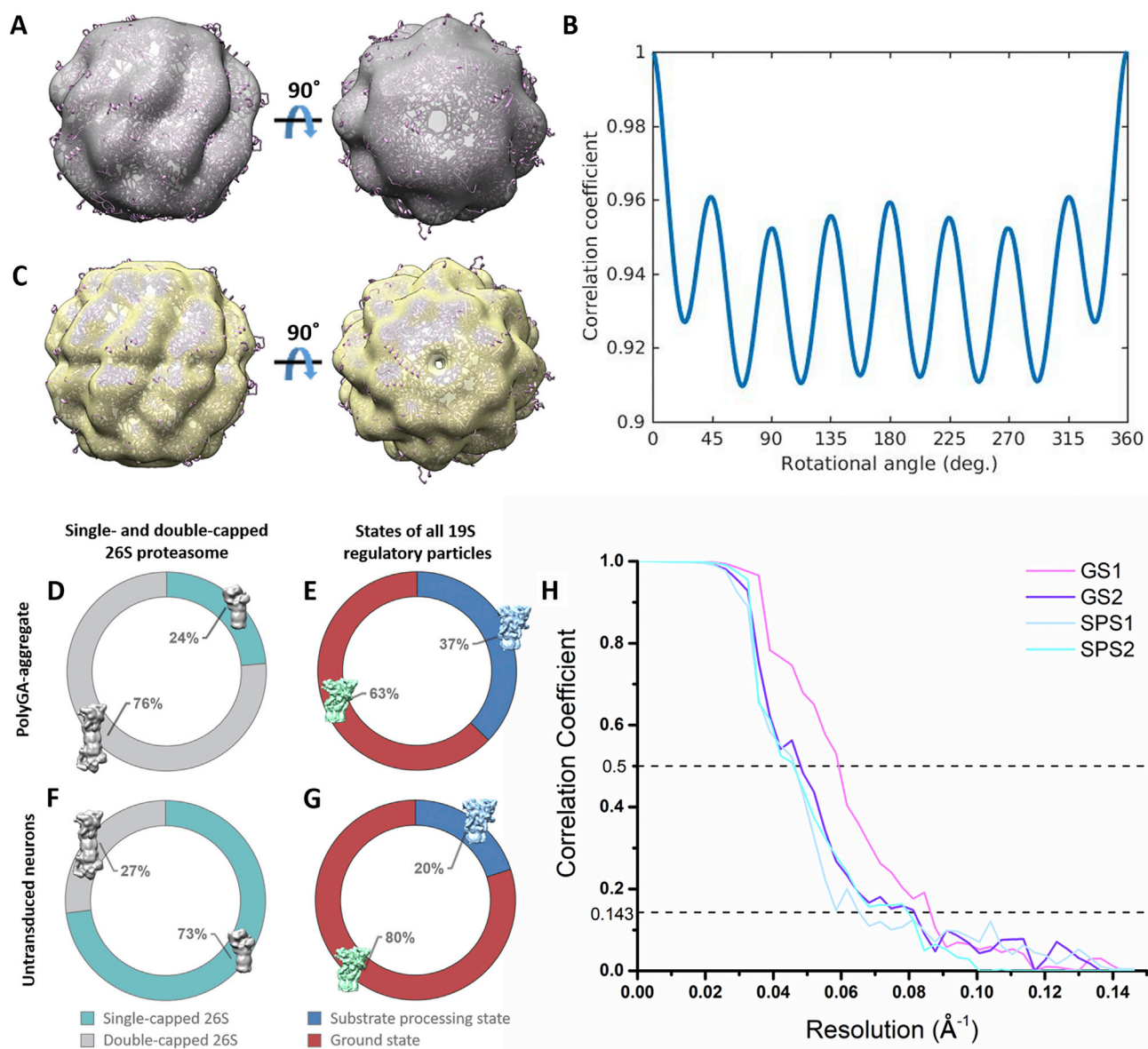


**Figure S3. Subtomogram Averaging and Classification for TRiC/CCT and the 26S Proteasome, Related to Figures 2 and 3**

(A) Unsymmetrized average structure of TRiC/CCT at a resolution of 20.5 Å superimposed on its atomic model (purple; PDB: 4V94).  
 (B) Rotational correlation coefficient analysis of (A) indicating 8-fold symmetry.  
 (C) Average structure of TRiC/CCT at a resolution of 17.1 Å upon application of D8 symmetry to (A) superimposed on its atomic model. Resolutions were estimated by gold-standard Fourier shell correlation using the 0.143 criterion.  
 (D and F) Overall distribution of single-capped and double-capped 26S proteasomes within aggregates in (GA)<sub>175</sub>-GFP transduced neurons (D) and untransduced neurons (Asano et al., 2015) (F).  
 (E and G) Distribution of the ground and substrate processing states for all regulatory particles within aggregates in neurons transduced with (GA)<sub>175</sub>-GFP (E) and untransduced (Asano et al., 2015) (G).  
 (H) Gold-standard Fourier shell correlation curves of the four proteasome structures, yielding the following resolution estimations: 11.8 Å (GS1), 12.3 Å (GS2), 15.4 Å (SPS1) and 12.8 Å (SPS2).

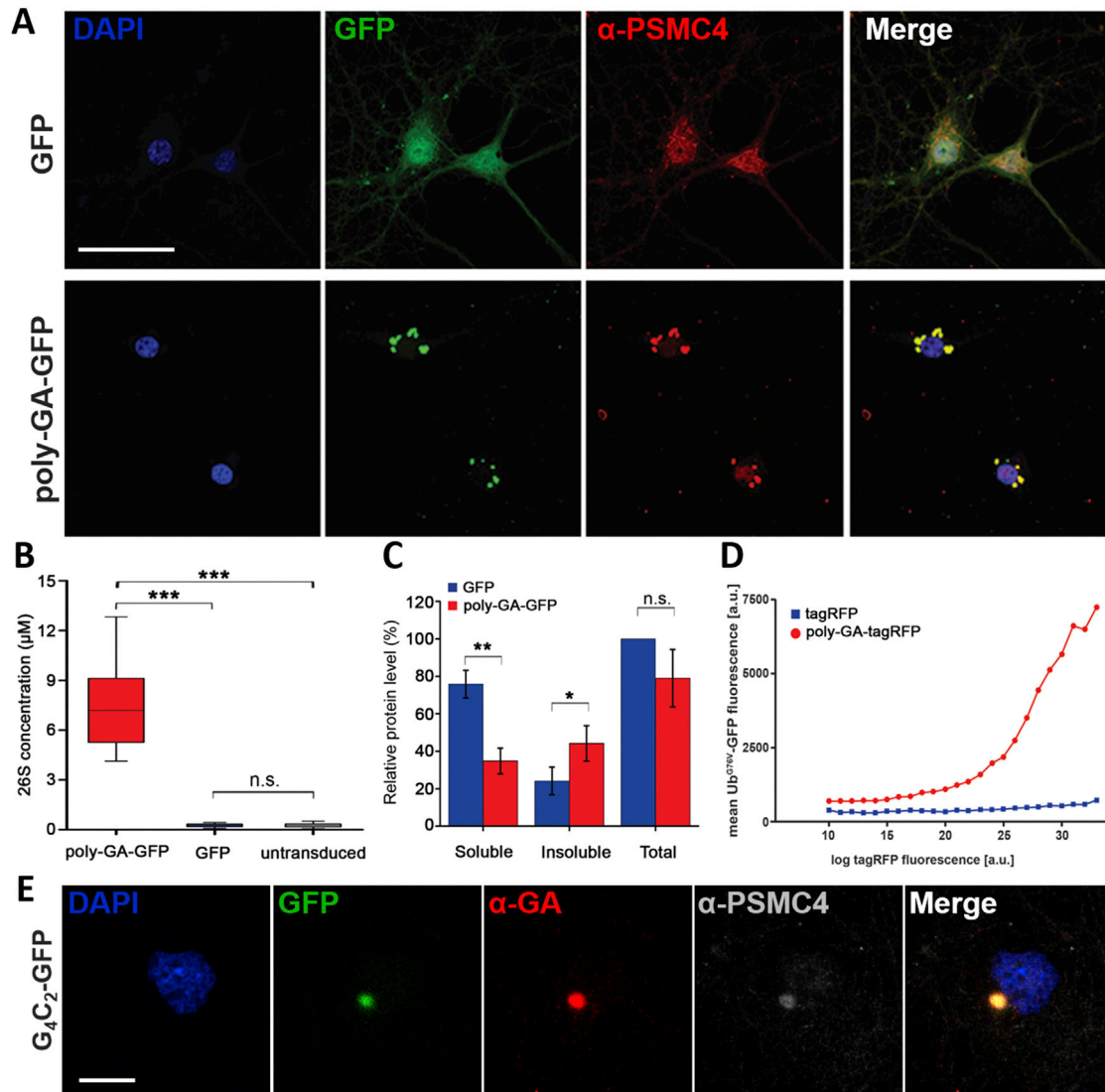


**Figure S4. Proteasome Abundance and Function at Poly-GA Aggregates, Related to Figures 2 and 5**

(A) Poly-GA-GFP aggregates (green) in primary neurons expressing a synthetic (GA)<sub>175</sub>-GFP construct with a start codon colocalize with proteasomes detected with a PSMC4/Rpt3 antibody (red). Proteasome staining is diffuse in GFP-expressing control cells. Nuclei are labeled with DAPI (blue). Scale bar: 50  $\mu$ m.

(B) Proteasome concentration for (GA)<sub>175</sub>-GFP aggregates (DIV 5 + 5), control neurons transduced with GFP only (DIV 5 + 5) or untransduced (DIV 10) ( $n = 9$  tomograms, (GA)<sub>175</sub>-GFP;  $n = 17$ , GFP;  $n = 16$ , untransduced). For poly-GA aggregates, only tomograms with more than half volume occupied by aggregates were considered for the concentration calculation. The top and bottom boundaries of the boxes indicate  $\pm 2x$  standard error, and whiskers extend to the maximum and minimum values. Proteasome concentration within poly-GA aggregates was significantly higher than in control conditions (\*\* $p < 0.001$  by Mann-Whitney test), whereas the difference between GFP-transfected and untransfected control neurons was not significant (n. s.).

(C) Quantification of proteasome levels in the soluble and insoluble fractions as well as total, analyzed by immunoblotting. The data was normalized to the total proteasome levels in GFP-transduced control neurons. Error bars indicate standard error. \* and \*\* indicate respectively  $p < 0.05$  and  $p < 0.01$  by paired t test ( $n = 6$  replicates from 4 independent experiments). Proteasomes are enriched in the insoluble fraction in the presence of poly-GA aggregates.

(D) Poly-GA expression leads to the stabilization of a reporter for the ubiquitin-proteasome system. HEK293 cells stably expressing an unstable green fluorescent reporter for the ubiquitin-proteasome system (UbG76V-GFP) were transfected with the indicated constructs. After 72 h, UbG76V-GFP levels were analyzed by flow cytometry. The relationship between poly-GA-tagRFP levels on the x axis and of UbG76V-GFP on the y axis shows a concentration-dependent accumulation of UbG76V-GFP in the presence of poly-GA. The data shown are from a single representative experiment out of three independent repeats.

(E) Poly-GA-GFP aggregates (green) in primary neurons expressing a non-ATG (G<sub>4</sub>C<sub>2</sub>)<sub>73</sub> construct containing a downstream GFP in the poly-GA reading frame. RAN translation-derived poly-GA-GFP aggregates are stained by a poly-GA antibody (red) and colocalize with proteasomes detected with a PSMC4/Rpt3 antibody (white). Nuclei are labeled with DAPI (blue). Scale bar: 10  $\mu$ m.

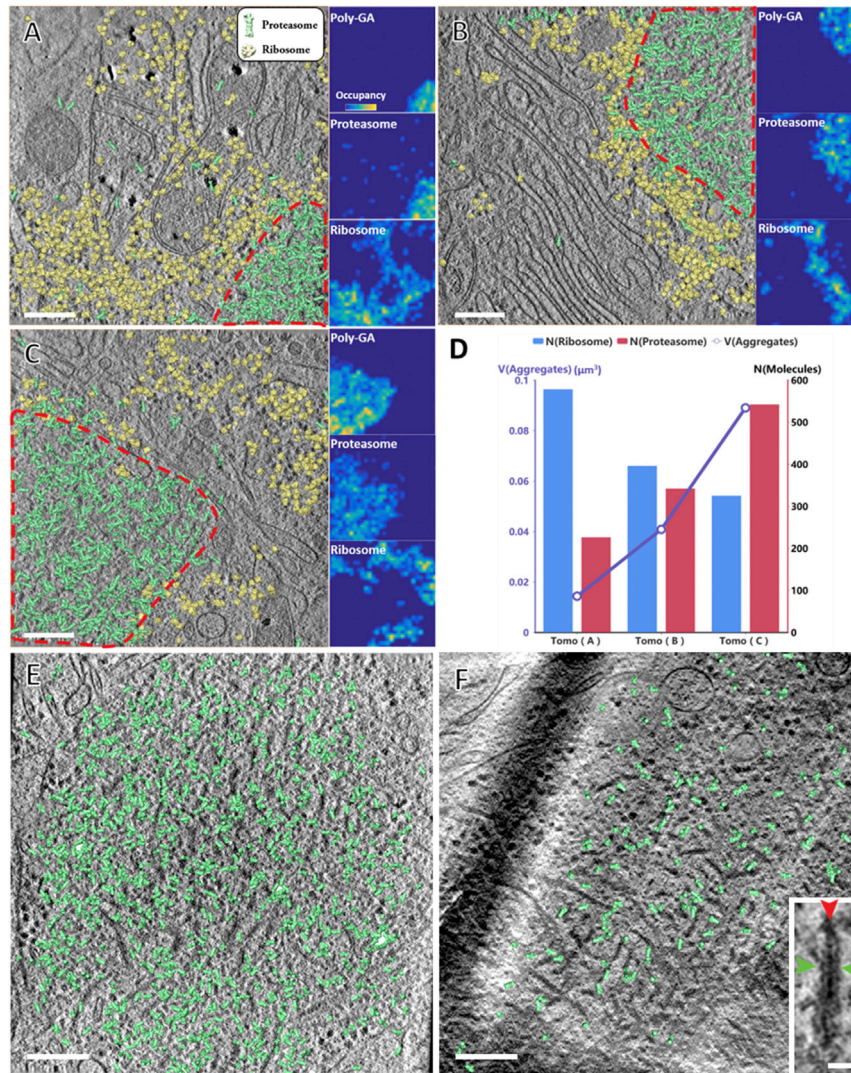


**Figure S5. Macromolecule Mapping in Different Poly-GA Aggregates, Related to Figure 2**

(A–C) Tomographic slices of aggregates within neurons transduced with  $(\text{GA})_{175}$ -GFP (main panels) and analyzed at DIV 5 + 5. Regions containing poly-GA ribbons are outlined in red. For the whole tomogram, proteasomes (green) and ribosomes (yellow) are mapped to their original positions and orientations by template matching and subtomogram averaging. For each tomogram, maximum intensity projection heatmaps of poly-GA ribbons, proteasomes and ribosomes were generated (right column of each panel).

(D–F) Numbers of proteasomes and ribosomes detected in the tomograms shown in (A)–(C) plotted versus the volume of the region containing poly-GA aggregates. The number of proteasomes detected shows a positive correlation with poly-GA aggregate volume. (E and F) Tomographic slices and mapped 26S proteasomes of aggregates within neurons transduced with  $(\text{GA})_{175}$ -GFP at an earlier time point (DIV 5 + 3) (E), or transfected with a RAN-translated  $(\text{G}_4\text{C}_2)_{73}$  construct with GFP in the poly-GA reading frame (F). Note that despite the smaller size compared to DIV 5 + 5  $(\text{GA})_{175}$ -GFP aggregates, similar concentrations of proteasomes accumulated within these aggregates ( $\sim 7 \mu\text{M}$  for  $(\text{GA})_{175}$ -GFP, DIV 5 + 3;  $\sim 5 \mu\text{M}$  for  $\text{G}_4\text{C}_2$ ). Due to the lower thickness of the cryo-FIB lamella (70 nm versus 100–200 nm in all other cases) fewer proteasomes are visible in (F). The inset in (F) shows a high magnification of a poly-GA ribbon (red arrowhead) decorated by GFP-associated additional densities (green arrowheads). Note that the morphology of RAN-translated poly-GA ribbons is indistinguishable from aggregates formed by the  $(\text{GA})_{175}$ -GFP construct. Tomographic slices are 7 nm thick. Scale bars: 200 nm in main panels, 20 nm in inset.

## **Contribution to Publication II**

As second author of this publication, I was involved in the initiation of this project, where I infected primary rat neurons for all cryo-EM experiments. Furthermore, I validated the cryo-EM findings in primary rat neurons, including immunofluorescence (Fig. S4A and E) and biochemical fractionation experiments (Fig. S4C).

### 3. Publication III and contribution

*Poly-GP in cerebrospinal fluid links C9orf72-associated dipeptide repeat expression to the asymptomatic phase of ALS/FTD*

published as

**Lehmer C**, Oeckl P, Weishaupt JH, Volk AE, Diehl-Schmid J, Schroeter ML, Lauer M, Kornhuber J, Levin J, Fassbender K, Landwehrmeyer B; German Consortium for Frontotemporal Lobar Degeneration, Schludi MH, Arzberger T, Kremmer E, Flatley A, Feederle R, Steinacker P, Weydt P, Ludolph AC, Edbauer D, Otto M. Poly-GP in cerebrospinal fluid links C9orf72-associated dipeptide repeat expression to the asymptomatic phase of ALS/FTD. *EMBO Mol Med.* 2017, doi: 10.15252/emmm.201607486



# Poly-GP in cerebrospinal fluid links *C9orf72*-associated dipeptide repeat expression to the asymptomatic phase of ALS/FTD

Carina Lehmer<sup>1,†</sup>, Patrick Oeckl<sup>2,†</sup>, Jochen H Weishaupt<sup>2</sup>, Alexander E Volk<sup>3</sup>, Janine Diehl-Schmid<sup>4</sup>, Matthias L Schroeter<sup>5,6</sup>, Martin Lauer<sup>7</sup>, Johannes Kornhuber<sup>8</sup>, Johannes Levin<sup>1,9</sup>, Klaus Fassbender<sup>10</sup>, Bernhard Landwehrmeyer<sup>2</sup>, German Consortium for Frontotemporal Lobar Degeneration<sup>‡</sup>, Martin H Schludi<sup>1</sup>, Thomas Arzberger<sup>1,11,12</sup>, Elisabeth Kremmer<sup>13</sup>, Andrew Flatley<sup>14</sup>, Regina Feederle<sup>1,14</sup>, Petra Steinacker<sup>2</sup>, Patrick Weydt<sup>2,15</sup>, Albert C Ludolph<sup>2</sup>, Dieter Edbauer<sup>1,†,\*</sup>  & Markus Otto<sup>2,†,\*\*</sup> 

## Abstract

The *C9orf72* GGGGCC repeat expansion is a major cause of amyotrophic lateral sclerosis and frontotemporal dementia (c9ALS/FTD). Non-conventional repeat translation results in five dipeptide repeat proteins (DPRs), but their clinical utility, overall significance, and temporal course in the pathogenesis of c9ALS/FTD are unclear, although animal models support a gain-of-function mechanism. Here, we established a poly-GP immunoassay from cerebrospinal fluid (CSF) to identify and characterize *C9orf72* patients. Significant poly-GP levels were already detectable in asymptomatic *C9orf72* mutation carriers compared to healthy controls and patients with other neurodegenerative diseases. The poly-GP levels in asymptomatic carriers were similar to symptomatic c9ALS/FTD cases. Poly-GP levels were not correlated with disease onset, clinical scores, and CSF levels of neurofilaments as a marker for axonal damage. Poly-GP determination in CSF revealed a *C9orf72* mutation carrier in our cohort and may thus be used as a diagnostic marker in addition to genetic testing to screen patients. Presymptomatic expression of poly-GP and likely other DPR species may

contribute to disease onset and thus represents an alluring therapeutic target.

**Keywords** amyotrophic lateral sclerosis; biomarker; *C9orf72*; cerebrospinal fluid; frontotemporal dementia

**Subject Categories** Biomarkers & Diagnostic Imaging; Genetics, Gene Therapy & Genetic Disease; Neuroscience

**DOI** 10.15252/emmm.201607486 | Received 19 December 2016 | Revised 27 March 2017 | Accepted 28 March 2017 | Published online 13 April 2017

**EMBO Mol Med (2017) 9: 859–868**

See also: R Balendra *et al* (July 2017)

## Introduction

Amyotrophic lateral sclerosis (ALS) and frontotemporal dementia (FTD) are neurodegenerative diseases with similar neuropathological features and overlapping clinical symptoms and pathomechanisms (Ling *et al*, 2013). To date, a genetic cause can be identified in

- 1 German Center for Neurodegenerative Diseases (DZNE) and Munich Cluster for System Neurology (SyNergy), Munich, Germany
  - 2 Department of Neurology, Ulm University Hospital, Ulm, Germany
  - 3 Institute of Human Genetics, University Medical Centre Hamburg-Eppendorf, Hamburg, Germany
  - 4 Department of Psychiatry and Psychotherapy, Technical University of Munich, München, Germany
  - 5 Clinic for Cognitive Neurology, University Clinic Leipzig, Leipzig, Germany
  - 6 Max Planck Institute for Human Cognitive and Brain Sciences, Leipzig, Germany
  - 7 Department of Psychiatry, Psychosomatics and Psychotherapy, University Hospital of Würzburg, Würzburg, Germany
  - 8 Department of Psychiatry and Psychotherapy, Friedrich-Alexander-University of Erlangen-Nuremberg, Erlangen, Germany
  - 9 Department of Neurology, Ludwig-Maximilians-Universität München, Munich, Germany
  - 10 Department of Neurology, Saarland University, Homburg, Germany
  - 11 Center for Neuropathology and Prion Research, Ludwig-Maximilians-University Munich, Munich, Germany
  - 12 Department of Psychiatry and Psychotherapy, Ludwig-Maximilians-University Munich, Munich, Germany
  - 13 Institute of Molecular Immunology, Helmholtz Zentrum München, German Research Center for Environmental Health (GmbH), Munich, Germany
  - 14 Monoclonal Antibody Core Facility and Research Group, Institute for Diabetes and Obesity, Helmholtz Zentrum München, German Research Center for Environmental Health (GmbH), Munich, Germany
  - 15 Department of Neurodegenerative Diseases and Gerontopsychiatry, Bonn University Hospital, Bonn, Germany
- \*Corresponding author. Tel: +49 89 4400 46510; E-mail: dieter.edbauer@dzne.de  
 \*\*Corresponding author. Tel: +49 731 500 63010; Fax: +49 731 500 63012; E-mail: markus.otto@uni-ulm.de  
 †These authors contributed equally to this work  
 ‡For the German Consortium for Frontotemporal Lobar Degeneration: Adrian Danek, Emily Feneberg, Sarah Anderl-Straub, Christine von Arnim, Holger Jahn, Anja Schneider, Manuel Maler, Maryna Polyakova, Lina Riedl, Jens Wiltfang, Georg Ziegler

around two-thirds of familial and 10% of sporadic ALS (Renton *et al*, 2014). Similarly, a genetic cause is described in about 25% of familial and 10% of sporadic FTD (Belzil *et al*, 2016). The most frequent genetic cause of ALS, FTD, or a combination of both is a large GGGGCC repeat expansion in the *C9orf72* gene (c9ALS/FTD). Three non-mutually exclusive mechanisms are discussed to mediate the effects of the hexanucleotide expansion. The *C9orf72* protein has been linked to autophagy and its expression is reduced in ALS/FTD patients (Sellier *et al*, 2016). While *C9orf72* knockout mice show no neurodegeneration, repeat expressing mice develop neuron loss and TDP-43 pathology depending on the expression levels (Hayes & Rothstein, 2016; Jiang *et al*, 2016; O'Rourke *et al*, 2016). Formation of repeat RNA foci in the nucleus and the accompanying sequestration of RNA-binding proteins are thought to alter RNA processing (DeJesus-Hernandez *et al*, 2011). The expanded repeat is translated into aggregating dipeptide repeat proteins (DPRs) by a non-conventional mechanism termed repeat-associated non-ATG (RAN) translation (Ash *et al*, 2013; Mori *et al*, 2013b; Zu *et al*, 2013), which was first discovered for expanded CAG repeats (Zu *et al*, 2011).

Five DPR species result from the translation from sense (poly-GA, poly-GP, poly-GR) and antisense RNA (poly-PA, poly-PR, and further poly-GP) in all reading frames (Gendron *et al*, 2013; Mori *et al*, 2013a; Zu *et al*, 2013). DPRs accumulate in p62-positive but TDP-43-negative neuronal inclusions in the brain, a pathognomonic feature of c9ALS/FTD (Al-Sarraj *et al*, 2011; Mori *et al*, 2013b). *In vitro* and *in vivo* studies showed toxicity of the different DPR species by inhibition of gene expression, nucleocytoplasmic transport, and the ubiquitin-proteasome system (May *et al*, 2014; Zhang *et al*, 2014; Jovicic *et al*, 2015). Poly-GA is the most abundant DPR species in the brain whereas overexpression of the arginine-containing species (poly-GR/-PR) causes the most severe toxicity in cellular and fly models (Mizielinska *et al*, 2014; Schludi *et al*, 2015).

However, in end-stage brains DPR pathology does not correlate with the degree of neurodegeneration, which challenges the concept of DPRs as the driving force of acute neurodegeneration as overly simplistic (Mackenzie *et al*, 2013), although mouse models strongly support a gain-of-function mechanism (Chew *et al*, 2015; Jiang *et al*, 2016; Liu *et al*, 2016). However, post-mortem studies cannot provide conclusions on the temporal sequence of events (DPR/TDP-43 deposition and neurodegeneration). Neuropathological reports from rare cases suggest that DPRs accumulate in the brain prior to TDP-43 pathology early in disease or even prior its onset (Baborie *et al*, 2014; Proudfoot *et al*, 2014; Vatsavayai *et al*, 2016). Thus, the study of DPR expression in the asymptomatic phase of *C9orf72* mutation carriers is essential to clarify the role of DPRs in the pathogenesis of c9ALS/FTD. So far only poly-GP has been detected in cerebrospinal fluid (CSF) in a small case series of symptomatic c9ALS patients (Su *et al*, 2014). It is unclear how accurately CSF levels of poly-GP reflect the overall DPR load, but it is currently the only way to analyze RAN translation in living patients.

Therefore, we performed a cross-sectional study of CSF samples of patients in different stages of the disease, even before onset of either dementia or motor symptoms to elucidate the temporal course of poly-GP expression in c9ALS/FTD pathogenesis. In addition, we correlated poly-GP levels with clinical scores (ALSFRS-R, FTLDCDR), markers of neurodegeneration/axonal damage (neurofilament light chain, NfL; phosphorylated neurofilament heavy chain, pNfH),

age at disease onset, disease duration at CSF collection, and estimated repeat length to assess the interaction between DPR load and disease severity.

## Results

### Monoclonal antibodies specifically detect poly-GP

To develop an anti-GP sandwich immunoassay with optimal sensitivity, we rescreened all our monoclonal anti-GP clones from rat for affinity as a capture antibody (Schludi *et al*, 2015). As expected, the two best anti-GP clones 18H8 and 3F9 specifically detected neuronal cytoplasmic poly-GP inclusions by immunohistochemistry in a c9ALS/FTD patient, but not in a *C9orf72*-negative ALS/FTD case (Fig 1A). An optimized immunoassay using these antibodies reliably detected GST-GP<sub>15</sub> down to a concentration of 0.03 ng/ml (Figs 1B and EV1). No cross-reactivity with other GST-DPR fusion proteins was observed even at 1 µg/ml (Fig 1C). Due to the different number of epitopes in the GST-GP<sub>15</sub> and endogenous poly-GP from patients with variable repeat length, we present only background-corrected raw values of CSF samples. To confirm assay stability, we repeatedly measured the concentration of four recombinant GST-GP<sub>15</sub> calibration samples ranging from 0.0064 to 0.8 ng/ml (Fig EV1). The coefficient of variance was between 1.59 and 9.41% for intra-plate replicates, between 7.36 and 15.95% for inter-plates replicates, and between 4.77 and 14.53% for day-to-day replicates, suggesting the assay is sufficiently accurate for diagnostic use.

### Poly-GP is detectable in the CSF of asymptomatic and symptomatic c9ALS/FTD

Poly-GP levels were measured in CSF in a group of 125 clinically well-characterized patients and controls from the German FTLDC Consortium. The demographic characteristics of the participants are listed in Table 1. The sample includes 30 subjects with evidence of a repeat *C9orf72* expansion (C9-F1, *n* = 10; c9ALS, *n* = 9; c9FTD, *n* = 11) in the peripheral blood. The median response in the poly-GP immunoassay in the CSF of all 30 *C9orf72* patients was > 35-fold higher than in ND-CON and NonC9-F1 controls (median 140.3, interquartile range 66.5 to 335.3 vs. median 4.0, interquartile range -1.25 to 24.9), which indicates a specific response (Fig 2A). We performed receiver operating characteristic (ROC) curve analysis of all *C9orf72* mutation carriers vs. all other samples. The area under the curve (AUC) was 0.95 (95% CI: 0.92–0.99) (Fig 2B) and at a cutoff of 43.5 the sensitivity was 93.3% (95% CI: 77.9–99.2%) and the specificity was 91.6% (95% CI: 84.1–96.3%).

Of note, we detected poly-GP signal in eight out of 95 from patients in the *C9orf72*-negative groups. One patient who eventually received the clinical diagnosis of sporadic ALS and was initially seen under the differential diagnosis of hereditary spastic paraplegia (HSP) showed elevated poly-GP levels in CSF. One ND-CON patient with very high poly-GP signal had undergone a lumbar puncture in order to exclude a chronic inflammatory process. This patient presented with dysaesthesia of the lower limbs, a small spinal lesion in MRI, but without oligoclonal bands or motor and frontal signs. The other patients included four patients with a clinical diagnosis of AD and two control patients with the clinical diagnosis of a

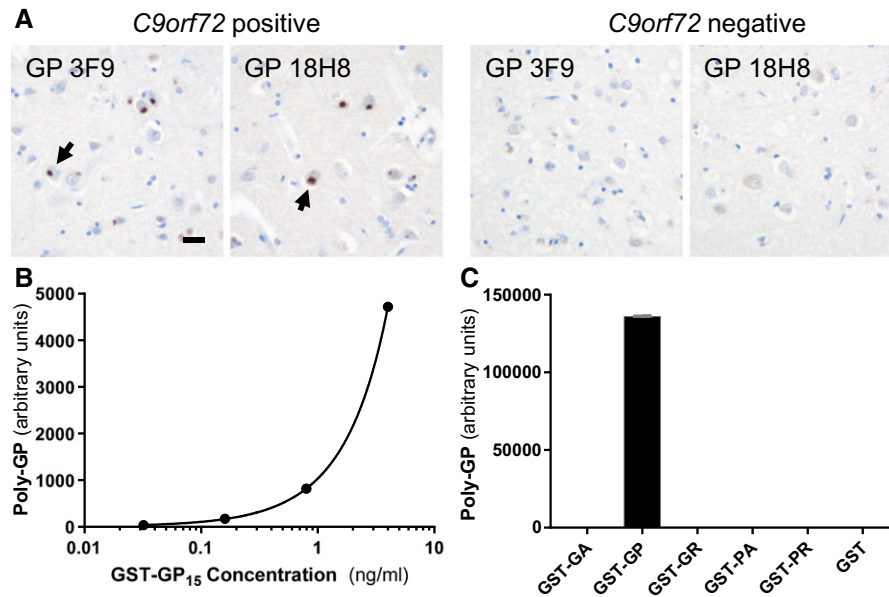


**Figure 1. Validation of a novel poly-GP-specific immunoassay.**

**A** Immunohistochemistry of frontal cortex from ALS/FTD cases with or without *C9orf72* repeat expansion using poly-GP antibodies 18H8 and 3F9. Both antibodies detect neuronal cytoplasmic inclusions specifically in the *C9orf72* case (arrows). Hybridoma supernatants were used at 1:250 dilution as described previously (Schludi *et al*, 2015). Scale bar 20  $\mu$ m.

**B, C** Poly-GP sandwich immunoassay with anti-GP antibodies 18H8 and 3F9 detects purified GST-GP<sub>15</sub> below 0.03 ng/ml (B), but no other 15-mer DPRs fused to GST at 1  $\mu$ g/ml. Data are shown as mean  $\pm$  SD ( $n = 2$ ) (C). A four-parameter logistic curve was used to fit the dose–response using Prism 7.01 software.

vestibular neuritis and a polyneuritis. However, for the latter two patients, the poly-GP levels were just above the calculated cutoff level. In these patients, there was no clinical sign for a neurodegenerative disease. The genetic *C9orf72* status of these patients was (re)analyzed except for the two control patients with vestibular neuritis and polyneuritis, where no DNA was available. We did not detect a *C9orf72* repeat expansion in peripheral blood, but cannot rule out a somatic mosaicism in the brain as autopsy samples were not available for a definitive diagnosis. In an additional poly-GP-positive AD case, genotyping indeed revealed a *C9orf72* mutation, which led to reclassification as c9FTD (Fig 2A, red dot).

Importantly, there was no significant difference in the poly-GP levels of asymptomatic and symptomatic *C9orf72* mutation carriers and also not between c9ALS and c9FTD cases. In contrast, only c9ALS and sALS patients, but not C9-F1 cases, showed increased CSF concentrations of pNfH and NfL (Fig 2C and D). Thus, poly-GP in CSF is a biomarker for the identification of both symptomatic and asymptomatic *C9orf72* mutation carriers, while neurofilament levels in CSF are associated with the symptomatic but not the premanifest phase of the disease.

#### Association of poly-GP with other CSF biomarkers and clinical scales

Next, we analyzed the correlation of poly-GP levels in the CSF of c9ALS/FTD cases with different markers of neurodegeneration and disease severity (Fig 3). There was no significant correlation of poly-GP levels with the axonal damage markers NfL ( $r = -0.02$ ,  $P = 0.98$  in c9ALS;  $r = 0.04$ ,  $P = 0.92$  in c9FTD) and pNfH ( $r = 0.13$ ,

$P = 0.74$  in c9ALS;  $r = -0.41$ ,  $P = 0.21$  in c9FTD) (Fig 3A and B). Furthermore, no significant correlation was observed with clinical scores ( $r = 0.12$ ,  $P = 0.79$  for ALSFRS-R in c9ALS;  $r = -0.10$ ,  $P = 0.81$  for FTLD-CDR in c9FTD), disease duration at the time of CSF collection ( $r = 0.67$ ,  $P = 0.06$  in c9ALS;  $r = -0.18$ ,  $P = 0.63$  in c9FTD) (Fig 3C and D), and age at disease onset ( $r = 0.29$ ,  $P = 0.44$  in c9ALS;  $r = -0.38$ ,  $P = 0.28$  in c9FTD) (Fig 3E and F). Current technologies allow only a rough estimate of the repeat length, because the expanded allele presents as a smear rather than a distinct band in Southern blots and somatic variability between blood and brain DNA is well described (Nordin *et al*, 2015). Given these limitations, no significant correlation of poly-GP levels with the estimated repeat length from blood (available for 11 patients) was identified ( $r = 0.58$ ,  $P = 0.07$  for c9ALS and c9FTD combined) (Fig 3G).

Despite being a cross-sectional study, we used a similar approach as that used in the GENFI study (Rohrer *et al*, 2015) in order to determine the changes of CSF poly-GP throughout the evolution of the disease. That is, we used parental age of onset as a proxy to calculate the estimated years to disease onset. We did not find any association between the estimated years to disease onset and CSF poly-GP ( $r = 0.28$ ,  $P = 0.46$ ) (Fig 3H). Thus, poly-GP expression starts at least several years prior to clinical disease onset and remains unchanged in late stages.

## Discussion

Using a novel immunoassay, we measured poly-GP in the CSF from *C9orf72* ALS and bvFTD cases and carefully selected control groups.

Table 1. Patient characteristics.

Characteristic	ND-CON (n = 20)	NonC9-F1 (n = 8)	AD (n = 24)	PD (n = 14)	sALS (n = 18)	sFTD (n = 11)	C9-F1 (n = 10)	c9ALS (n = 9)	c9FTD (n = 11)
Age (years) <sup>a</sup>	63.5 (52.8 to 70.0)	42.3 (34.6 to 48.0) <sup>b</sup>	67.5 (56.6 to 70.2)	72.5 (67.0 to 77.0)	60.0 (52.0 to 67.5)	64.0 (53.0 to 68.0)	44.8 (39.4 to 51.2) <sup>b</sup>	65.1 (54.4 to 71.1)	56.3 (44.9 to 61.1)
Gender (F/M)	11/9	3/5	14/10	5/9	6/12	4/7	8/2	3/6	4/7
ALSFRS-R <sup>a</sup>	n.a.	n.a.	n.a.	n.a.	41.0 (32.0 to 44.0)	n.a.	n.a.	39.0 (36.3 to 44.0)	n.a.
FTLD-CDR <sup>a</sup>	n.a.	n.a.	n.a.	n.a.	n.a.	4.5 (1.0 to 5.5)	n.a.	n.a.	7.0 (3.8 to 11.8)
Disease duration at LP (months) <sup>a</sup>	n.a.	n.a.	n.a.	n.a.	14.5 (8.8 to 26.0)	21.0 (15.0 to 39.0)	n.a.	11.3 (4.8 to 29.9)	56.0 (23.4 to 163) <sup>c</sup>
Poly-GP in CSF (arbitrary units) <sup>a</sup>	4.0 (−1.3 to 24.9)	−1.8 (−5.5 to 7.0)	6.0 (3.6 to 16.3) <sup>d</sup>	−10.5 (−18.9 to −3.6)	−1.3 (−9.6 to 5.3)	−13.5 (−16.0 to 7.0)	129 (68.0 to 393) <sup>e</sup>	113 (80.0 to 279) <sup>f</sup>	151 (51.5 to 333) <sup>e</sup>
NfL in CSF (pg/ml) <sup>a</sup>	909 (759 to 2,297)	720 (581 to 1,093)	2,232 (1,768 to 2,655)	2,911 (2,185 to 5,907) <sup>g</sup>	6,319 (3,000 to 27,013) <sup>h</sup>	4,455 (2,515 to 8,397) <sup>i</sup>	716 (620 to 1,043)	13,644 (9,313 to 29,818) <sup>j</sup>	2,614 (1,903 to 3,771)
pNfH in CSF (pg/ml) <sup>a</sup>	264 (188 to 474)	188 (188 to 188)	353 (254 to 495) <sup>k</sup>	499 (343 to 675) <sup>l</sup>	1,593 (790 to 5,325) <sup>m</sup>	309 (241 to 768)	188 (188 to 188)	3,740 (2,028 to 5,487) <sup>n</sup>	303 (246 to 485)

AD, Alzheimer's disease; ALS, amyotrophic lateral sclerosis; ALSFRS-R, ALS Functional Rating Scale—revised; bvFTD, behavioral variant of frontotemporal dementia; C9-F1, asymptomatic *C9orf72* mutation carriers; c9ALS, symptomatic ALS *C9orf72* mutation carriers; c9FTD, symptomatic bvFTD *C9orf72* mutation carriers; CSF, cerebrospinal fluid; F, female; FTLD-CDR, Frontotemporal Lobar Degeneration-specific Clinical Dementia Rating; LP, lumbar puncture; M, male; n.a., not available; ND-CON, age-matched control population without signs of a neurodegenerative disease; NfL, neurofilament light chain; NonC9-F1, *C9orf72*-negative offspring of a *C9orf72* mutation carrier; PD, Parkinson's disease; pNfH, phosphorylated neurofilament heavy chain; sALS, sporadic ALS; sFTD, sporadic bvFTD.

<sup>a</sup>Values are median and interquartile range.

<sup>b</sup> $P < 0.05$  vs. ND-CON,  $P < 0.01$  vs. AD,  $P < 0.001$  vs. PD.

<sup>c</sup> $P < 0.05$  vs. sFTD.

<sup>d</sup> $P < 0.01$  vs. PD.

<sup>e</sup> $P < 0.05$  vs. ND-CON, NonC9-F1,  $P < 0.001$  vs. sFTD, PD, sALS.

<sup>f</sup> $P < 0.05$  vs. ND-CON, NonC9-F1,  $P < 0.001$  vs. sALS, sFTD, PD.

<sup>g</sup> $P < 0.05$  vs. NonC9-F1,  $P < 0.01$  vs. C9-F1.

<sup>h</sup> $P < 0.01$  vs. ND-CON,  $P < 0.001$  vs. NonC9-F1, C9-F1.

<sup>i</sup> $P < 0.001$  vs. C9-F1, NonC9-F1.

<sup>j</sup> $P < 0.01$  vs. AD,  $P < 0.001$  vs. ND-CON, NonC9-F1, C9-F1.

<sup>k</sup> $P < 0.05$  vs. C9-F1.

<sup>l</sup> $P < 0.05$  vs. NonC9-F1,  $P < 0.01$  vs. C9-F1.

<sup>m</sup> $P < 0.01$  vs. ND-CON,  $P < 0.001$  vs. NonC9-F1, C9-F1.

<sup>n</sup> $P < 0.05$  vs. ND-CON,  $P < 0.001$  vs. NonC9-F1, C9-F1.

Our main results were as follows: (i) Significant poly-GP levels are detectable in the CSF of 93.3% of the *C9orf72* ALS and bvFTD cases but not in 91.6% of the control cases; (ii) rapid poly-GP immunoassay is useful to detect individuals with a *C9orf72* expansion misdiagnosed with other diseases (e.g. AD); and (iii) poly-GP levels are already increased in asymptomatic stages of the disease, suggesting DPRs may be most important for the early pathogenic events in *C9orf72* ALS/FTD rather than driving acute neurodegeneration in late-stage patients.

### Poly-GP immunoassay from CSF

Previously, poly-GP had been detected in CSF of c9ALS cases by immunoassay using polyclonal antibodies (Su *et al*, 2014). Here, we developed an analogous immunoassay using two monoclonal anti-GP antibodies. The monoclonal antibodies allow standardized analysis and are not vulnerable to limited antibody availability or batch-to-batch variation, which will be critical for the use as a

therapeutic biomarker for repeat-directed clinical trials (Jiang *et al*, 2016). The repeat expansion in *C9orf72* patients seems to vary mostly between 400 and > 5,000 (GGGGCC)<sub>n</sub> repeats (Beck *et al*, 2013; Fratta *et al*, 2013) and is notoriously difficult to determine precisely (Akimoto *et al*, 2014). We present raw responses instead of absolute poly-GP concentrations, because the repeat length affects epitope numbers and thus likely capture and detection of poly-GP antigens in the immunoassay (compare Fig 3G). While low-level release and intercellular transmission of all five DPR species have been reported in cell culture systems (Westergard *et al*, 2016), we have so far not been able to detect the other DPR species in patient CSF using a similar approach suggesting that these species might be released into the CSF at lower levels.

### Poly-GP signal in apparently *C9orf72*-negative cases

Using ROC analysis, we established a cutoff that allows sensitive and specific discrimination of most *C9orf72* cases from controls.

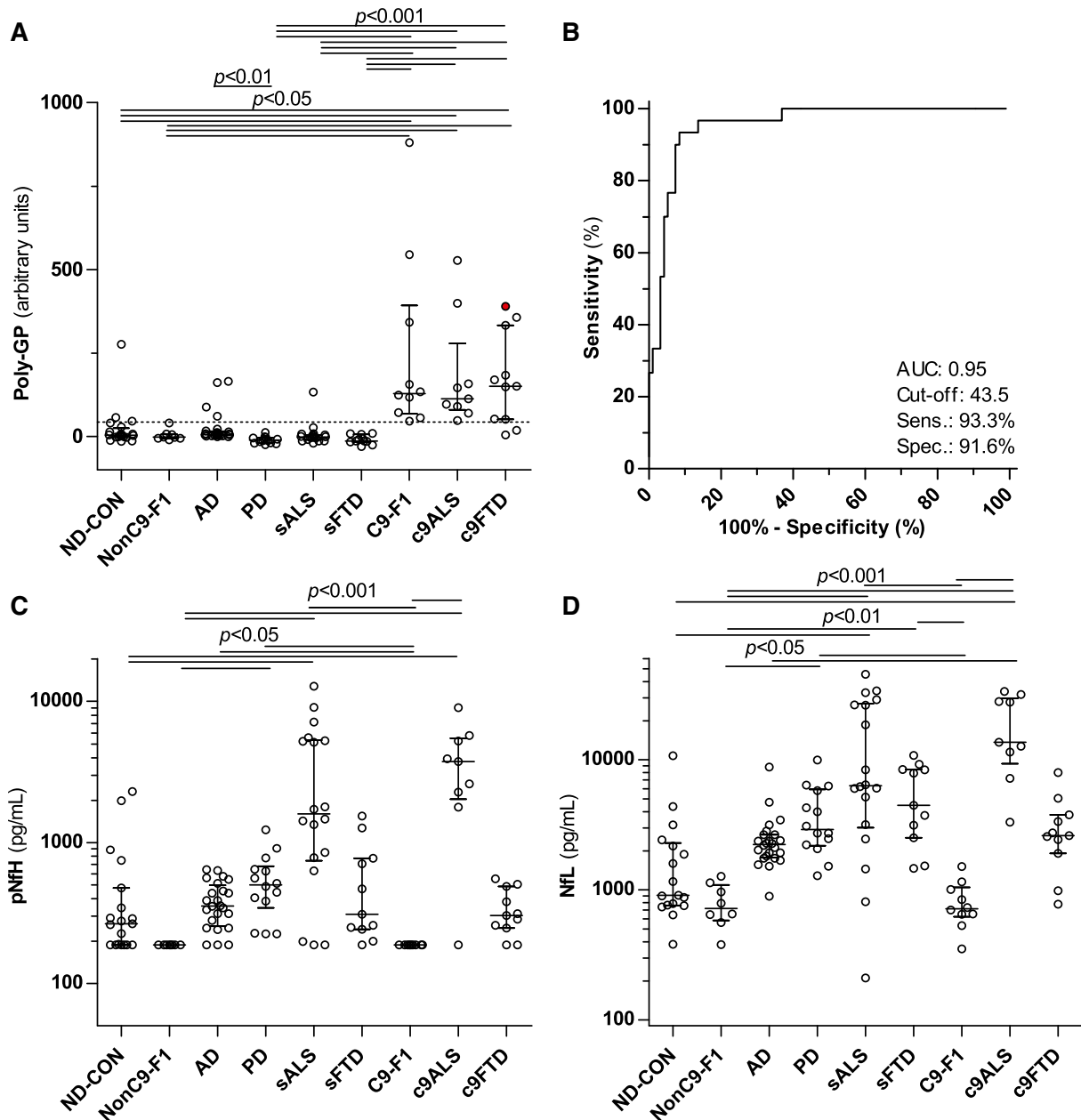


**Figure 2. Poly-GP expression is increased in CSF of asymptomatic and symptomatic *C9orf72* mutation carriers.**

- A** Poly-GP was measured using immunoassay in an age-matched control population without signs of a neurodegenerative disease (ND-CON,  $n = 18$ –20), *C9orf72*-negative offspring of *C9orf72* mutation carriers (NonC9-F1,  $n = 8$ ) in patients with other neurodegenerative diseases, that is, Alzheimer's (AD,  $n = 24$ ) and Parkinson's disease (PD,  $n = 14$ ), sporadic ALS (sALS,  $n = 18$ ) and FTD (sFTD,  $n = 11$ ) patients, and asymptomatic (C9-F1,  $n = 10$ ) and symptomatic *C9orf72* mutation carriers with ALS (c9ALS,  $n = 9$ ) and FTD (c9FTD,  $n = 11$ ). The c9FTD patient indicated by the filled, red circle was initially seen under the differential diagnosis of AD, but after poly-GP measurement followed by *C9orf72* genotyping reclassified as c9FTD.
- B** Receiver operating characteristic (ROC) curve analysis of poly-GP levels for the discrimination of *C9orf72* mutation carriers vs. non-carriers. The cutoff (43.5) was calculated using the Youden index and is shown as a dotted line in (A). AUC, area under the curve; Sens, sensitivity; Spec, specificity.
- C, D** (C) Phosphorylated neurofilament heavy chain (pNfH) and (D) neurofilament light chain (NfL) were measured using an established ELISA.

Data information: Groups were compared by Kruskal–Wallis test and Dunn's *post hoc* test. Bars and whiskers are median and interquartile range, and circles are individual values. Exact *P*-values poly-GP (A): ND-CON vs. c9FTD:  $P = 0.0477$ ; PD vs. AD:  $P = 0.0053$ ; ND-CON vs. c9ALS:  $P = 0.0483$ ; ND-CON vs. C9-F1:  $P = 0.0236$ ; NonC9-F1 vs. c9FTD:  $P = 0.0365$ ; NonC9-F1 vs. c9ALS:  $P = 0.0334$ ; NonC9-F1 vs. C9-F1:  $P = 0.0194$ ; sALS vs. c9FTD:  $P = 0.0006$ ; sALS vs. c9ALS:  $P = 0.0007$ ; sALS vs. C9-F1:  $P = 0.0003$ ; sFTD vs. c9FTD, sFTD vs. c9ALS, sFTD vs. C9-F1, PD vs. c9FTD, PD vs. c9ALS, and PD vs. C9-F1:  $P < 0.0001$ . Exact *P*-values pNfH (C): PD vs. C9-F1:  $P = 0.0121$ ; PD vs. NonC9-F1:  $P = 0.0261$ ; sALS vs. ND-CON:  $P = 0.0103$ ; C9-F1 vs. AD:  $P = 0.0334$ ; ND-CON vs. c9ALS:  $P = 0.0142$ ; NonC9-F1 vs. c9ALS, C9-F1 vs. c9ALS, sALS vs. C9-F1, and sALS vs. NonC9-F1:  $P < 0.0001$ . Exact *P*-values NfL (D): sFTD vs. C9-F1:  $P = 0.0013$ ; sFTD vs. NonC9-F1:  $P = 0.0038$ ; PD vs. C9-F1:  $P = 0.0122$ ; PD vs. NonC9-F1:  $P = 0.0245$ ; c9ALS vs. AD:  $P = 0.0107$ ; sALS vs. ND-CON:  $P = 0.0017$ ; sALS vs. NonC9-F1:  $P = 0.0001$ ; sALS vs. C9-F1, ND-CON vs. c9ALS, NonC9-F1 vs. c9ALS, and C9-F1 vs. c9ALS:  $P < 0.0001$ .

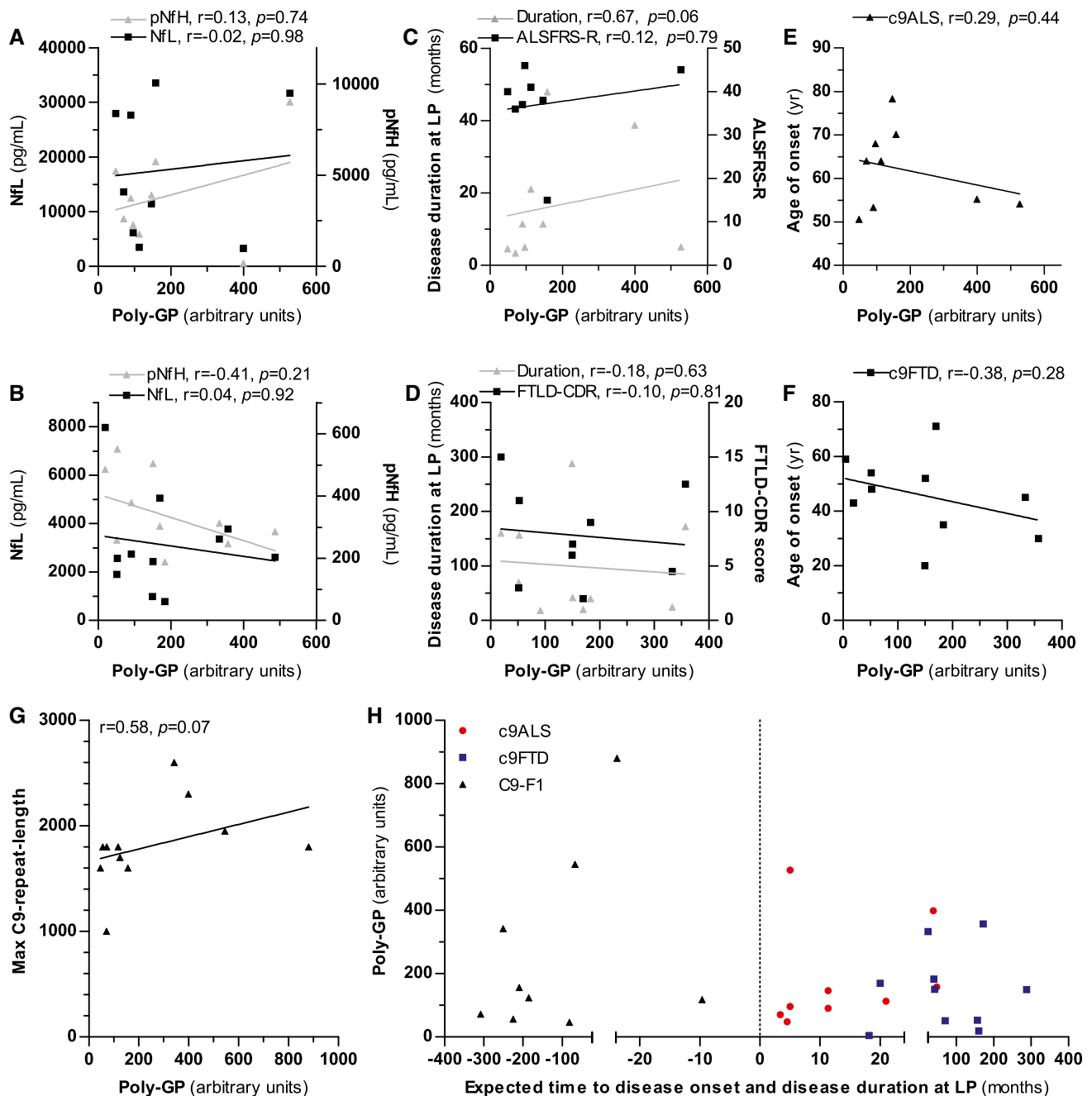


**Figure 3.** Poly-GP expression in CSF correlates neither with markers of neurodegeneration nor with clinical disease severity.

A–F Correlation analysis of poly-GP levels in CSF of c9ALS (A, C, E) and c9FTD cases (B, D, F). Correlation with phosphorylated neurofilament heavy chain (pNfH) and neurofilament light chain (NfL) (A, B), with disease duration at lumbar puncture (LP) and the ALSFRS-R or FTLD-CDR score (C, D) and with age at disease onset (E, F).

G Correlation of poly-GP levels in CSF with the largest repeat length estimated by Southern blotting.

H Association of poly-GP levels in CSF with disease duration at LP in c9ALS/FTD patients and with time to expected disease onset in C9-F1 cases. Time to expected disease onset was calculated using parental age at disease onset.

Data information: Correlation analysis was performed using Spearman's rank correlation coefficient.

Only two of our genetically verified c9ALS/FTD cases had low poly-GP levels in CSF. In contrast, some of the non-mutation carriers (one sALS, four AD, and one ND-CON) showed strongly elevated poly-GP signals. We offer three potential explanations. First, the repeat length in *C9orf72* patients is known to vary

widely between different tissues (Nordin *et al*, 2015) and it is possible that the repeat length is normal in blood lymphocytes, but pathological in the central nervous system. Thus, somatic mosaicism could prevent detection of *bona fide* *C9orf72* cases using genotyping from peripheral blood. Emerging single-cell

genome data show an unexpected degree of mosaicism in health and disease (Forsberg *et al*, 2016). Second, other pathologically expanded repeats in the genome, for example, the intronic (GGCCTG)<sub>n</sub> repeat expansion in the gene for the nucleolar protein *NOP56* causing spinocerebellar ataxia type 36 (SCA36), could result in poly-GP expression (Kobayashi *et al*, 2011). Third, other CSF proteins with short poly-GP stretches that are upregulated preferentially in a subgroup of AD patients may cross-react in the immunoassay.

### High poly-GP levels in presymptomatic *C9orf72* carriers

Animal models support a predominant gain-of-function mechanism for *C9orf72* pathogenesis, but the role of DPR proteins in disease initiation and progression in human ALS and FTD patients remains unresolved. Here, we show that poly-GP is already elevated in CSF of asymptomatic *C9orf72* mutation carriers ~14 years younger than the symptomatic group, suggesting that DPR expression is present in the earliest disease phase (compare Table 1). This is in agreement with the neuropathological detection of DPRs in presymptomatic *C9orf72* cases at young age (Baborie *et al*, 2014; Proudfoot *et al*, 2014; Vatsavayai *et al*, 2016). Interestingly, cross-sectional data from the GENFI cohort show subtle brain volume loss and behavioral changes in *C9orf72* carriers already 20 years prior to the expected disease onset, while *MAPT* (microtubule-associated protein tau) and *GRN* (granulin) mutation carriers show the first significant differences much closer to the disease onset (Rohrer *et al*, 2015). Presymptomatic DPR expression suggests that DPRs may be most critical for initially triggering the disease, while progression may largely depend on TDP-43 pathology (Edbauer & Haass, 2016).

Moreover, poly-GP levels are similar in c9ALS and c9FTD although disease duration is much shorter in ALS. Poly-GP levels in CSF of c9ALS/FTD cases did not correlate with markers of neurodegeneration such as the axonal damage markers NfL and pNfH and with markers of disease severity (clinical scores, disease duration, and onset). This is consistent with neuropathological findings showing no spatial correlation of DPR pathology with neurodegeneration (Mackenzie *et al*, 2013; Schludi *et al*, 2015). It is unclear how CSF levels of poly-GP correlate the amounts of poly-GP and the other DPR species within the neuronal inclusions. Although the total DPR levels vary between patients, we are not aware of cases with vastly different ratios of the different DPR species (Mackenzie *et al*, 2015; Schludi *et al*, 2015).

Since poly-GR/PR and poly-GA are by far more toxic than poly-GP in cellular and animal models (Mizielinska *et al*, 2014), it will be critical to determine their levels during disease progression to better address the role of DPRs in c9ALS/FTD pathogenesis.

In conclusion, poly-GP determination in CSF may be used as an alternative or addition to genetic testing to identify *C9orf72* mutation carriers. Our data indicate that poly-GP expression is already present in the presymptomatic phase of c9ALS/FTD, and thus, DPRs may predominantly contribute to triggering the disease rather than driving acute neurodegeneration in late-stage patients. This has implications for developing drugs and designing clinical trials. A standardized monoclonal-based anti-GP immunoassay will be critical to determine whether antisense oligonucleotide treatment in patients reduces DPR expression in patients similar to the preclinical trials in mice (Su *et al*, 2014).

## Materials and Methods

### Patients

We investigated nine different patient groups: (i) symptomatic ALS *C9orf72* mutation carriers (c9ALS), (ii) symptomatic patients of the behavioral variant of FTD (bvFTD) *C9orf72* mutation carriers (c9FTD), (iii) asymptomatic *C9orf72* mutation carriers (C9-F1), (iv) *C9orf72*-negative offspring of a *C9orf72* mutation carrier (NonC9-F1), (v) sporadic ALS patients (sALS), (vi) sporadic FTD patients (sFTD), two groups of other neurodegenerative diseases, namely (vii) Parkinson's disease (PD) and (viii) Alzheimer's disease (AD), and (ix) an age-matched control population without clinical signs of a neurodegenerative disease (non-neurodegenerative control, ND-CON). Diagnosis was made according to standard criteria.

*C9orf72* ALS cases and NonC9-F1 cases were recruited from the German Presymptomatic (GPS)-ALS cohort (Weydt *et al*, 2016). AD and bvFTD patients (including *C9orf72* cases) were enrolled at different clinical centers coordinated by the German FTLD consortium (Erlangen, Leipzig, Munich, Ulm, Würzburg). All other patients were recruited at the Department of Neurology, Ulm University Hospital, Germany. Group size for the groups ND-CON, PD, sALS, and sFTD was estimated by experience because no preliminary data were available. For the groups NonC9-F1, AD, C9-F1, c9ALS, and c9FTD, all samples available from the cohorts of the GPS-ALS and FTLD consortium were used. All patients gave written informed consent. All procedures were in accordance with the WGA Declaration of Helsinki and the Department of Health and Human Services Belmont Report. The ethics committees of the participating centers approved the study (Otto *et al*, 2011).

All patients underwent neuropsychological testing using standard procedures. Disease severity in ALS patients was assessed using the ALS Functional Rating Scale—revised (ALSFRS-R) and in bvFTD patients using the FTLD-specific Clinical Dementia Rating (FTLD-CDR) score. PCR-based screening methods were used for the detection of *C9orf72* repeat expansion. If enough DNA was available, Southern blot analyses were conducted (Akimoto *et al*, 2014).

Cerebrospinal fluid was collected by lumbar puncture, centrifuged, and stored within 2 h at  $-80^{\circ}\text{C}$  following standard operating procedures at all sites.

### Poly-GP sandwich immunoassay from CSF

By immunizing Lou/c rats with synthetic GP<sub>10</sub> peptides, the poly-GP-specific monoclonal antibodies 18H8 (IgG1/ $\kappa$ ) and 3F9 (IgG2a/ $\kappa$ ) were raised using previously described protocols (Mackenzie *et al*, 2013). These new monoclonal antibodies against poly-GP had higher affinity than the previously described clone 7A5 (Schludi *et al*, 2015). An immunoassay was performed using the Meso Scale Discovery platform (MSD). Streptavidin plates (MSD Gold 96-well Streptavidin) were coated with biotinylated 18H8 antibody (capture antibody, 1:8,000) in PBS, washed three times (0.05% Tween-20, PBS) using a Biotek 405US Microplate washer, and blocked for 1 h at room temperature (0.05% Tween-20, 1% BSA in PBS). Plates were incubated with 80  $\mu\text{l}$ /well of CSF samples diluted with one volume of RIPA buffer (137 mM NaCl, 20 mM Tris pH = 7.5, 10% glycerol, 1% Triton X-100, 0.5% sodium

**The paper explained****Problem**

A massive expansion of a GGGGCC repeat upstream of the *C9orf72* coding region is the most common genetic cause of ALS and behavioral variant FTLD. The expanded repeat is translated in all reading frames into five aggregating dipeptide repeat (DPR) proteins poly-GA, poly-GP, poly-GR, poly-PA, and poly-PR. Reliable detection of these proteins *in vivo* would be a desirable clinical biomarker for diagnosis and therapeutic studies. Several DPRs are clearly toxic in cellular and animal models, but their role in human pathogenesis remains controversial. Therefore, we asked how the levels of DPRs differ between asymptomatic carriers and patients with manifest ALS and bvFTD.

**Results**

We developed an immunoassay for poly-GP in the CSF using two monoclonal antibodies and measured poly-GP in 125 samples from nine groups, including Parkinson and Alzheimer cases. Screening by immunoassay revealed one misdiagnosed *C9orf72* carrier among the AD cohort. The poly-GP levels in asymptomatic carriers and ALS/FTD patients are similar, suggesting widespread early expression of DPR proteins consistent with rare autopsy reports. Poly-GP levels show no correlation with clinical disease stage or other established markers for axonal loss in CSF.

**Impact**

The poly-GP immunoassay is a useful biomarker for *C9orf72* ALS/FTD cases. DPR expression in the presymptomatic stage may explain the early prodromal brain volume loss and behavior alterations previously observed in *C9orf72* mutation carriers.

deoxycholate, 0.1% SDS, 2 mM EDTA) and supplemented with a protease inhibitor cocktail (Sigma) for 2 h at room temperature on a shaking platform. Pseudonymized samples were randomly distributed on the plate and measured blindly in two replicates. After three washing steps, the plates were incubated with MSD sulfo-tag-labeled 3F9 antibody (detection antibody, 1:1,000) for 2 h at room temperature on a shaking platform followed by three final washing steps. Upon adding 100  $\mu$ l MSD Read Buffer T, the plates were immediately measured. The electrochemical signal was detected using a MSD SECTOR Imager 2400. 15-mer GST-DPR fusion proteins were purified from *Escherichia coli* as described (Mori *et al*, 2013b). After background correction, data are presented in arbitrary units.

**Measurement of neurofilament levels**

Neurofilament, that is, NfL and pNfH, levels were measured using commercial ELISA kits from Quanterix, Lexington (NfL), and BioVendor (pNfH) (Steinacker *et al*, 2016a,b). Values of pNfH below the detection limit (188 pg/ml) were set to 188 pg/ml to permit statistical analysis.

**Statistics**

Statistical analysis was performed using GraphPad Prism 5.0 and JMP software 11.1.1. The data did not follow a normal distribution, and therefore, non-parametric tests were used. Groups were compared by Kruskal–Wallis test and Dunn's *post hoc* test (> 2 groups) or Mann–Whitney test. Correlation analysis was

performed with Spearman's rank correlation coefficient. ROC curve analysis was used to calculate sensitivity and specificity of poly-GP expression, and a threshold to separate *C9orf72* mutation carriers and non-carriers was selected using the Youden index. A *P*-value < 0.05 was regarded as statistically significant.

**Expanded View** for this article is available online.

**Acknowledgements**

We are grateful to all study participants. We thank Mehtap Bulut-Karac, Sandra Hübsch, Marika Pusch, Ingrid Goebel, and Dagmar Schattauer for their excellent technical assistance. We thank Christian Haass and Marc Suárez-Calvet for critical comments to the manuscript. This study was supported by the JPND networks SOPHIA (01ED1202A), BiomarkAPD (01ED1203F), PreFrontAls (01ED1512), STRENGTH (01ED1408), the German Federal Ministry of Education and Research (FTLDC 01G11007A, MND-Net 01GM1103A), the EU (NADINE 246513, FAIR-PARK II 633190, DPR-MODELS grant 617198), the German research foundation/DFG (VO2028), the foundation of the state Baden-Württemberg (D.3830), BIU (D.5009), Departmental Funds (GPS-ALS Study), the Charcot Foundation for ALS, and the NOMIS Foundation.

**Author contributions**

DE and MO were responsible for conception and design of the study. All authors participated in acquisition and analysis of data. CL, PO, MO, and DE drafted the manuscript and figures.

**Conflict of interest**

The authors declare that they have no conflict of interest.

**References**

- Akimoto C, Volk AE, van Blitterswijk M, Van den Broeck M, Leblond CS, Lumbroso S, Camu W, Neitzel B, Onodera O, van Rheenen W *et al* (2014) A blinded international study on the reliability of genetic testing for GGGGCC-repeat expansions in *C9orf72* reveals marked differences in results among 14 laboratories. *J Med Genet* 51: 419–424
- Al-Sarraj S, King A, Troakes C, Smith B, Maekawa S, Bodi I, Rogelj B, Al-Chalabi A, Hortobagyi T, Shaw CE (2011) p62 positive, TDP-43 negative, neuronal cytoplasmic and intranuclear inclusions in the cerebellum and hippocampus define the pathology of *C9orf72*-linked FTLD and MND/ALS. *Acta Neuropathol* 122: 691–702
- Ash PE, Bieniek KF, Gendron TF, Caulfield T, Lin WL, DeJesus-Hernandez M, van Blitterswijk MM, Jansen-West K, Paul JW III, Rademakers R *et al* (2013) Unconventional translation of *C9ORF72* GGGGCC expansion generates insoluble polypeptides specific to c9FTD/ALS. *Neuron* 77: 639–646
- Baborie A, Griffiths TD, Jaros E, Perry R, McKeith IG, Burn DJ, Masuda-Suzukake M, Hasegawa M, Rollinson S, Pickering-Brown S *et al* (2014) Accumulation of dipeptide repeat proteins predates that of TDP-43 in Frontotemporal Lobar Degeneration associated with hexanucleotide repeat expansions in *C9ORF72* gene. *Neuropathol Appl Neurobiol* 41: 601–612
- Beck J, Poulter M, Hensman D, Rohrer JD, Mahoney CJ, Adamson G, Campbell T, Uphill J, Borg A, Fratta P *et al* (2013) Large *C9orf72* hexanucleotide repeat expansions are seen in multiple neurodegenerative syndromes and are more frequent than expected in the UK population. *Am J Hum Genet* 92: 345–353

- Belzil VV, Katzman RB, Petrucelli L (2016) ALS and FTD: an epigenetic perspective. *Acta Neuropathol* 132: 487–502
- Chew J, Gendron TF, Prudencio M, Sasaguri H, Zhang YJ, Castanedes-Casey M, Lee CW, Jansen-West K, Kurti A, Murray ME et al (2015) Neurodegeneration. C9ORF72 repeat expansions in mice cause TDP-43 pathology, neuronal loss, and behavioral deficits. *Science* 348: 1151–1154
- DeJesus-Hernandez M, Mackenzie IR, Boeve BF, Boxer AL, Baker M, Rutherford NJ, Nicholson AM, Finch NA, Flynn H, Adamson J et al (2011) Expanded GGGGCC hexanucleotide repeat in noncoding region of C9ORF72 causes chromosome 9p-linked FTD and ALS. *Neuron* 72: 245–256
- Edbauer D, Haass C (2016) An amyloid-like cascade hypothesis for C9orf72 ALS/FTD. *Curr Opin Neurobiol* 36: 99–106
- Forsberg LA, Gisselsson D, Dumanski JP (2016) Mosaicism in health and disease – clones picking up speed. *Nat Rev Genet* 18: 128–142
- Fratta P, Poulter M, Lashley T, Rohrer JD, Polke JM, Beck J, Ryan N, Hensman D, Mizielinska S, Waite AJ et al (2013) Homozygosity for the C9orf72 GGGGCC repeat expansion in frontotemporal dementia. *Acta Neuropathol* 126: 401–409
- Gendron TF, Bieniek KF, Zhang YJ, Jansen-West K, Ash PE, Caulfield T, Daugherty L, Dunmore JH, Castanedes-Casey M, Chew J et al (2013) Antisense transcripts of the expanded C9ORF72 hexanucleotide repeat form nuclear RNA foci and undergo repeat-associated non-ATG translation in c9FTD/ALS. *Acta Neuropathol* 126: 829–844
- Hayes LR, Rothstein JD (2016) C9ORF72-ALS/FTD: transgenic mice make a come-BAC. *Neuron* 90: 427–431
- Jiang J, Zhu Q, Gendron TF, Saberi S, McAlonis-Downes M, Seelman A, Stauffer JE, Jafar-Nejad P, Drenner K, Schulte D et al (2016) Gain of toxicity from ALS/FTD-linked repeat expansions in C9ORF72 is alleviated by antisense oligonucleotides targeting GGGGCC-containing RNAs. *Neuron* 90: 535–550
- Jovicic A, Mertens J, Boeynaems S, Bogaert E, Chai N, Yamada SB, Paul JW III, Sun S, Herdy JR, Bieri G et al (2015) Modifiers of C9orf72 dipeptide repeat toxicity connect nucleocytoplasmic transport defects to FTD/ALS. *Nat Neurosci* 18: 1226–1229
- Kobayashi H, Abe K, Matsuura T, Ikeda Y, Hitomi T, Akechi Y, Habu T, Liu W, Okuda H, Koizumi A (2011) Expansion of intronic GGCTG hexanucleotide repeat in NOP56 causes SCA36, a type of spinocerebellar ataxia accompanied by motor neuron involvement. *Am J Hum Genet* 89: 121–130
- Ling SC, Polymenidou M, Cleveland DW (2013) Converging mechanisms in ALS and FTD: disrupted RNA and protein homeostasis. *Neuron* 79: 416–438
- Liu Y, Pattamatta A, Zu T, Reid T, Bardhi O, Borchelt DR, Yachnis AT, Ranum LP (2016) C9orf72 BAC mouse model with motor deficits and neurodegenerative features of ALS/FTD. *Neuron* 90: 521–534
- Mackenzie IR, Arzberger T, Kremmer E, Troost D, Lorenz S, Mori K, Weng SM, Haass C, Kretzschmar HA, Edbauer D et al (2013) Dipeptide repeat protein pathology in C9ORF72 mutation cases: clinico-pathological correlations. *Acta Neuropathol* 126: 859–879
- Mackenzie IR, Frick P, Grasser FA, Gendron TF, Petrucelli L, Cashman NR, Edbauer D, Kremmer E, Prudlo J, Troost D et al (2015) Quantitative analysis and clinico-pathological correlations of different dipeptide repeat protein pathologies in C9ORF72 mutation carriers. *Acta Neuropathol* 130: 845–861
- May S, Hornburg D, Schludi MH, Arzberger T, Rentzsch K, Schwenk BM, Grasser FA, Mori K, Kremmer E, Banzhaf-Strathmann J et al (2014) C9orf72 FTL/ALS-associated Gly-Ala dipeptide repeat proteins cause neuronal toxicity and Unc119 sequestration. *Acta Neuropathol* 128: 485–503
- Mizielinska S, Gronke S, Niccoli T, Ridler CE, Clayton EL, Devoy A, Moens T, Norona FE, Woollacott IO, Pietrzyk J et al (2014) C9orf72 repeat expansions cause neurodegeneration in *Drosophila* through arginine-rich proteins. *Science* 345: 1192–1194
- Mori K, Arzberger T, Grasser FA, Gijssels I, May S, Rentzsch K, Weng SM, Schludi MH, van der Zee J, Cruts M et al (2013a) Bidirectional transcripts of the expanded C9orf72 hexanucleotide repeat are translated into aggregating dipeptide repeat proteins. *Acta Neuropathol* 126: 881–893
- Mori K, Weng SM, Arzberger T, May S, Rentzsch K, Kremmer E, Schmid B, Kretzschmar HA, Cruts M, Van Broeckhoven C et al (2013b) The C9orf72 GGGGCC repeat is translated into aggregating dipeptide-repeat proteins in FTL/ALS. *Science* 339: 1335–1338
- Nordin A, Akimoto C, Wuolikainen A, Alstermark H, Jonsson P, Birve A, Marklund SL, Graffmo KS, Forsberg K, Brannstrom T et al (2015) Extensive size variability of the GGGGCC expansion in C9orf72 in both neuronal and non-neuronal tissues in 18 patients with ALS or FTD. *Hum Mol Genet* 24: 3133–3142
- O'Rourke JG, Bogdanik L, Yanez A, Lall D, Wolf AJ, Muhammad AK, Ho R, Carmona S, Vit JP, Zarrow J et al (2016) C9orf72 is required for proper macrophage and microglial function in mice. *Science* 351: 1324–1329
- Otto M, Ludolph AC, Landwehrmeyer B, Forstl H, Diehl-Schmid J, Neumann M, Kretzschmar HA, Schroeter M, Kornhuber J, Danek A, Consortium F (2011) German consortium for frontotemporal lobar degeneration. *Nervenarzt* 82: 1002–1005
- Proudfoot M, Gutowski NJ, Edbauer D, Hilton DA, Stephens M, Rankin J, Mackenzie IR (2014) Early dipeptide repeat pathology in a frontotemporal dementia kindred with C9ORF72 mutation and intellectual disability. *Acta Neuropathol* 127: 451–458
- Renton AE, Chio A, Traynor BJ (2014) State of play in amyotrophic lateral sclerosis genetics. *Nat Neurosci* 17: 17–23
- Rohrer JD, Nicholas JM, Cash DM, van Swieten J, Doppler E, Jiskoot L, van Minkelen R, Rombouts SA, Cardoso MJ, Clegg S et al (2015) Presymptomatic cognitive and neuroanatomical changes in genetic frontotemporal dementia in the Genetic Frontotemporal dementia Initiative (GENFI) study: a cross-sectional analysis. *Lancet Neurol* 14: 253–262
- Schludi MH, May S, Grasser FA, Rentzsch K, Kremmer E, Kupper C, Klopstock T, German Consortium for Frontotemporal Lobar Degeneration, Bavarian Brain Banking Alliance, Arzberger T, Edbauer D (2015) Distribution of dipeptide repeat proteins in cellular models and C9orf72 mutation cases suggests link to transcriptional silencing. *Acta Neuropathol* 130: 537–555
- Sellier C, Campanari ML, Julie Corbier C, Gaucherot A, Kolb-Cheynet I, Oulad-Abdelghani M, Ruffenach F, Page A, Ciura S, Kabashi E et al (2016) Loss of C9ORF72 impairs autophagy and synergizes with polyQ Ataxin-2 to induce motor neuron dysfunction and cell death. *EMBO J* 35: 1276–1297
- Steinacker P, Blennow K, Halbgebauer S, Shi S, Ruf V, Oeckl P, Giese A, Kuhle J, Slivarchova D, Zetterberg H et al (2016a) Neurofilaments in blood and CSF for diagnosis and prediction of onset in Creutzfeldt-Jakob disease. *Sci Rep* 6: 38737
- Steinacker P, Feneberg E, Weishaupt J, Bretschneider J, Tumani H, Andersen PM, von Arnim CA, Bohm S, Kassubek J, Kubisch C et al (2016b) Neurofilaments in the diagnosis of motoneuron diseases: a prospective study on 455 patients. *J Neural Neurosurg Psychiatry* 87: 12–20
- Su Z, Zhang Y, Gendron TF, Bauer PO, Chew J, Yang WY, Fostvedt E, Jansen-West K, Belzil VV, Desaro P et al (2014) Discovery of a biomarker and lead small molecules to target r(GGGGCC)-associated defects in c9FTD/ALS. *Neuron* 83: 1043–1050
- Vatsavayai SC, Yoon SJ, Gardner RC, Gendron TF, Vargas JN, Trujillo A, Pribadi M, Phillips JJ, Gaus SE, Hixson JD et al (2016) Timing and significance of

- pathological features in C9orf72 expansion-associated frontotemporal dementia. *Brain* 139: 3202–3216
- Westergard T, Jensen BK, Wen X, Cai J, Kropf E, Iacovitti L, Pasinelli P, Trotti D (2016) Cell-to-cell transmission of dipeptide repeat proteins linked to C9orf72-ALS/FTD. *Cell Rep* 17: 645–652
- Weydt P, Oeckl P, Huss A, Muller K, Volk AE, Kuhle J, Knehr A, Andersen PM, Prudlo J, Steinacker P et al (2016) Neurofilament levels as biomarkers in asymptomatic and symptomatic familial amyotrophic lateral sclerosis. *Ann Neurol* 79: 152–158
- Zhang YJ, Jansen-West K, Xu YF, Gendron TF, Bieniek KF, Lin WL, Sasaguri H, Caulfield T, Hubbard J, Daugherty L et al (2014) Aggregation-prone c9FTD/ALS poly(GA) RAN-translated proteins cause neurotoxicity by inducing ER stress. *Acta Neuropathol* 128: 505–524
- Zu T, Gibbens B, Doty NS, Gomes-Pereira M, Huguet A, Stone MD, Margolis J, Peterson M, Markowski TW, Ingram MA et al (2011) Non-ATG-initiated translation directed by microsatellite expansions. *Proc Natl Acad Sci USA* 108: 260–265
- Zu T, Liu Y, Banez-Coronel M, Reid T, Pletnikova O, Lewis J, Miller TM, Harms MB, Falchook AE, Subramony SH et al (2013) RAN proteins and RNA foci from antisense transcripts in C9ORF72 ALS and frontotemporal dementia. *Proc Natl Acad Sci USA* 110: E4968–E4977



**License:** This is an open access article under the terms of the Creative Commons Attribution 4.0 License, which permits use, distribution and reproduction in any medium, provided the original work is properly cited.

## Expanded View Figures

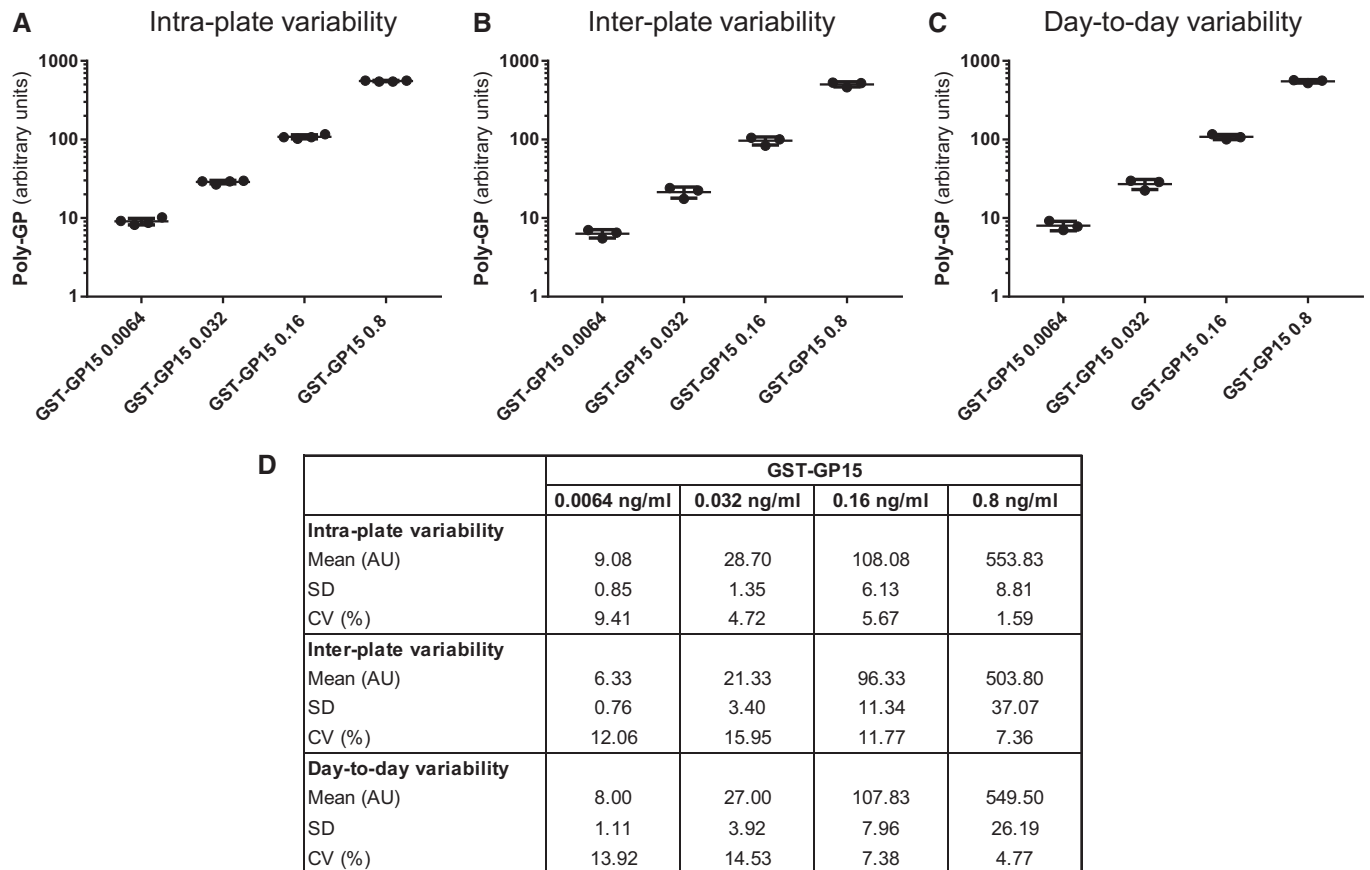


**Figure EV1. The poly-GP immunoassay is reproducible.**

A–D Poly-GP sandwich immunoassay with anti-GP antibodies 18H8 and 3F9 was used to analyze the GST-GP<sub>15</sub> standard at four concentrations. Background-corrected absolute values, mean, and standard deviation (SD) for  $n = 4$  GST-GP<sub>15</sub> intra-plate replicates (A),  $n = 3$  inter-plate replicates (B), and  $n = 3$  day-to-day replicates (C). Mean, SD, and the coefficient of variance (CV) for all conditions are listed in (D).

### **Contribution to Publication III**

As first author of this publication, I established the novel poly-GP immunoassay with new monoclonal antibodies. Most importantly, I conducted all poly-GP measurements in the patient cohort, which was the key experiment of this publication.

#### 4. Publication IV and contribution

*Antibodies inhibit transmission and aggregation of C9orf72  
poly-GA dipeptide repeat proteins*

published as

Zhou Q, **Lehmer C**, Michaelsen M, Mori K, Alterauge D, Baumjohann D, Schludi MH, Greiling J, Farny D, Flatley A, Feederle R, May S, Schreiber F, Arzberger T, Kuhm C, Klopstock T, Hermann A, Haass C, Edbauer D. Antibodies inhibit transmission and aggregation of C9orf72 poly-GA dipeptide repeat proteins. EMBO Mol Med. 2017, doi: 10.15252/emmm.201607054.

# Antibodies inhibit transmission and aggregation of *C9orf72* poly-GA dipeptide repeat proteins

Qihui Zhou<sup>1,2</sup>, Carina Lehmer<sup>1</sup>, Meike Michaelsen<sup>1</sup>, Kohji Mori<sup>3,4</sup> , Dominik Alterauge<sup>5</sup>, Dirk Baumjohann<sup>5</sup> , Martin H Schludi<sup>1,2</sup>, Johanna Greiling<sup>1</sup>, Daniel Farny<sup>1</sup>, Andrew Flatley<sup>6</sup>, Regina Feederle<sup>1,2,6</sup>, Stephanie May<sup>1</sup>, Franziska Schreiber<sup>1</sup>, Thomas Arzberger<sup>1,7,8</sup>, Christoph Kuhm<sup>1,2,9</sup>, Thomas Klopstock<sup>1,2,9</sup>, Andreas Hermann<sup>10</sup>, Christian Haass<sup>1,2,3</sup> , & Dieter Edbauer<sup>1,2,3,\*</sup> 

## Abstract

Cell-to-cell transmission of protein aggregates is an emerging theme in neurodegenerative disease. Here, we analyze the dipeptide repeat (DPR) proteins that form neuronal inclusions in patients with hexanucleotide repeat expansion *C9orf72*, the most common known cause of amyotrophic lateral sclerosis (ALS) and frontotemporal lobar degeneration (FTLD). Sense and antisense transcripts of the (G4C2)<sub>n</sub> repeat are translated by repeat-associated non-ATG (RAN) translation in all reading frames into five aggregating DPR proteins. We show that the hydrophobic DPR proteins poly-GA, poly-GP, and poly-PA are transmitted between cells using co-culture assays and cell extracts. Moreover, uptake or expression of poly-GA induces nuclear RNA foci in (G4C2)<sub>80</sub>-expressing cells and patient fibroblasts, suggesting an unexpected positive feedback loop. Exposure to recombinant poly-GA and cerebellar extracts of *C9orf72* patients increases repeat RNA levels and seeds aggregation of all DPR proteins in receiver cells expressing (G4C2)<sub>80</sub>. Treatment with anti-GA antibodies inhibits intracellular poly-GA aggregation and blocks the seeding activity of *C9orf72* brain extracts. Poly-GA-directed immunotherapy may thus reduce DPR aggregation and disease progression in *C9orf72* ALS/FTD.

**Keywords** amyotrophic lateral sclerosis; *C9orf72*; immunotherapy; RAN translation; seeding

**Subject Category** Neuroscience

**DOI** 10.15252/emmm.201607054 | Received 12 September 2016 | Revised 23 February 2017 | Accepted 24 February 2017 | Published online 28 March 2017

**EMBO Mol Med (2017) 9: 687–702**

## Introduction

Intracellular protein aggregation is a common feature of Alzheimer's disease and many other neurodegenerative disorders. Cell-to-cell transmission of intracellular protein aggregates has been described for intracellular tau and  $\alpha$ -synuclein aggregates forming amyloid fibrils (Chai *et al*, 2012; Sanders *et al*, 2014). The secretion and reuptake mechanisms are largely unknown, but the transmitted small aggregates seem to act as nucleation seeds that template further aggregation in the receiving cell (Jucker & Walker, 2011). The spreading of aggregates between cells is thought to cause the stereotypic progression of tau pathology through synaptically connected brain regions during disease progression (Braak *et al*, 2006; Iba *et al*, 2015; Takeda *et al*, 2015). Ongoing preclinical and clinical trials aim to interrupt the spreading of intraneuronal pathology using mostly passive vaccination (Yanamandra *et al*, 2013).

In 2011, a (G4C2)<sub>n</sub> repeat expansion upstream of the coding region of *C9orf72* was found to cause frontotemporal lobar degeneration (FTLD) and/or amyotrophic lateral sclerosis (ALS) in about 10% of all Caucasian patients with these related fatal neurodegenerative conditions (DeJesus-Hernandez *et al*, 2011; Renton *et al*, 2011; Gijssels *et al*, 2012). *C9orf72* haploinsufficiency, toxic nuclear RNA foci, and translation into toxic dipeptide repeat (DPR) proteins have been suggested as drivers of pathogenesis (Edbauer & Haass, 2016). Animal models expressing the repeat expansion strongly support a gain-of-function mechanism (Mizielinska *et al*, 2014; Chew *et al*, 2015; Jiang *et al*, 2016; Liu *et al*, 2016). Repeat RNA accumulates in nuclear foci and sequesters several RNA-binding proteins (Mori *et al*, 2013b), but even high level expression of the repeat RNA from an intron is not toxic in *Drosophila* models

- 1 German Center for Neurodegenerative Diseases (DZNE), Munich, Germany
  - 2 Munich Cluster of Systems Neurology (SyNergy), Munich, Germany
  - 3 Biomedical Center, Biochemistry, Ludwig Maximilians-Universität München, Planegg-Martinsried, Germany
  - 4 Department of Psychiatry, Osaka University Graduate School of Medicine, Osaka, Japan
  - 5 Institute for Immunology, Biomedical Center Munich, Ludwig Maximilians-Universität München, Planegg-Martinsried, Germany
  - 6 Monoclonal Antibody Core Facility and Research Group, Institute for Diabetes and Obesity, Helmholtz Zentrum München, German Research Center for Environmental Health (GmbH), Munich, Germany
  - 7 Center for Neuropathology and Prion Research, Ludwig Maximilians-Universität München, Planegg-Martinsried, Germany
  - 8 Department of Psychiatry and Psychotherapy, Ludwig Maximilians-Universität München, Planegg-Martinsried, Germany
  - 9 Department of Neurology, Friedrich-Baur-Institute, Ludwig Maximilians-Universität München, Planegg-Martinsried, Germany
  - 10 Department of Neurology and Center for Regenerative Therapies Dresden (CRTD), Technische Universität Dresden and German Center for Neurodegenerative Diseases (DZNE), Dresden, Germany
- \*Corresponding author. Tel: +49 89 440046510; E-mail: dieter.edbauer(at)dzne.de

(Tran *et al*, 2015). Sense and antisense repeat transcripts are translated in all reading frames into five aggregating DPR proteins (Ash *et al*, 2013; Mori *et al*, 2013a,c) by an unconventional mechanism. This so-called repeat-associated non-ATG (RAN) translation was first described for expanded CAG repeats and seems to require formation of RNA hairpins (Zu *et al*, 2011). Poly-GA is abundantly expressed in the *C9orf72* brains, followed by poly-GP and poly-GR, while poly-PA and poly-PR resulting from translation of the antisense transcript are rare. In addition to RNA foci and DPR pathology, *C9orf72* patients also develop TDP-43 pathology that correlates well with neurodegeneration like in other forms of FTL/ALS (Mackenzie *et al*, 2013), but it is still unclear how the *C9orf72* repeat expansion triggers TDP-43 pathology. In contrast, several neuropathology studies failed to detect a strong correlation of the different DPR species (or RNA foci) with the region-specific neurodegeneration seen in *C9orf72* ALS and FTL/ALS patients (Mackenzie *et al*, 2013; Schludi *et al*, 2015), suggesting an interplay of several factors and/or non-cell autonomous effects such as spreading and seeding may be crucial for pathogenesis. Interestingly, GA<sub>15</sub> peptides form amyloid-like fibrils that are taken up by N2a cells (Chang *et al*, 2016).

Thus, we asked whether poly-GA and the other DPR species are transmitted between cells and how DPR uptake affects the receiving cells. We detected cell-to-cell transmission of all hydrophobic DPR species and show that poly-GA boosts repeat RNA levels and DPR expression, suggesting DPR transmission may trigger a vicious cycle. Treating cells with anti-GA antibodies reduced intracellular aggregation of DPRs. Poly-GA antibodies blocked the seeding activity of *C9orf72* brain extracts which further supports the therapeutic potential of our discovery.

## Results

### Poly-GA and poly-PR differentially affect repeat RNA expression and translation

To allow better interpretation of DPR seeding experiments, we first analyzed DPR protein co-localization in cell lines co-expressing repeat RNA and synthetic DPR constructs. Thus, we cotransfected ATG-initiated synthetic DPR expression plasmids with GFP tag together with a (G4C2)<sub>80</sub> expression vector driven by the strong CMV promoter (Mori *et al*, 2016). As expected, RAN translation leads to GA<sub>80</sub>-flag aggregation under all conditions. We observed co-aggregation of GA<sub>80</sub>-flag with GA<sub>175</sub>-GFP, but little specific co-localization with the other DPR proteins, which were mainly diffusely localized in the cytoplasm as reported previously (May *et al*, 2014; Zhang *et al*, 2014). Compared to the GFP co-expression, GA<sub>80</sub>-flag aggregates appeared larger particularly in GA<sub>175</sub>-GFP- and PR<sub>175</sub>-GFP-expressing cells and to a lesser extent also with the other DPR proteins (Fig 1A). Quantification confirmed the increased size of GA<sub>80</sub>-flag aggregates in GA<sub>175</sub>-GFP- and PR<sub>175</sub>-GFP-expressing cells and showed no significant effects on the number of aggregates upon co-expression of any DPR species (Fig 1B and C). Similarly, filter-trap analysis showed enhanced aggregation of GA<sub>80</sub>-flag particularly in GA<sub>175</sub>-GFP- and PR<sub>175</sub>-GFP-expressing cells (Fig 1D and E).

Since poly-PR binds RNA and RNA-binding proteins (Kwon *et al*, 2014; Kanekura *et al*, 2016) and thus might affect mRNA

expression, we quantified the expression levels of the repeat mRNA (Fig 1F). Poly-PR had no significant effect on the repeat RNA, suggesting it may mainly induce RAN translation. In contrast, poly-GA expression unexpectedly also increased the levels of the (G4C2)<sub>n</sub> RNA.

Together, these data indicate that especially poly-GA and poly-PR proteins promote repeat transcription and/or RAN translation. In contrast to patient tissue, poly-GA did not specifically co-aggregate with the other DPR species under our conditions. Thus, uptake of poly-GA may affect both expression and nucleation in receiver cells.

### Poly-GA, poly-GP, and poly-PA are transmitted between cells

To address whether large DPR proteins are transmitted between cells, we performed co-culture experiments. HEK293 cells were first transfected separately with either DPR-GFP, GFP, or RFP expression vectors. After 24 h, RFP-transfected cells were resuspended and mixed with GFP- or DPR-GFP-transfected cells. Double-positive cells were quantified using flow cytometry analysis immediately after mixing or after 24 h of co-culture (Fig 2A and B). In mixtures of GFP- and RFP-transfected cells, double-positive cells were extremely rare (~0.3%) at both time points. In contrast, GA<sub>175</sub>-GFP was detected in 1–2% of RFP-positive cells after 24 h of co-culture indicating transmission of GA<sub>175</sub>-GFP to RFP-transfected neighboring cells (Fig 2C and D). Furthermore, double-positive cells were sorted to image GFP-tagged DPR proteins in RFP-positive receiver cells (Fig EV1), thus implying secretion and uptake of poly-GA by neighboring cells. We detected even higher intercellular transmission of GP<sub>47</sub>-GFP and PA<sub>175</sub>-GFP, which show mostly diffuse cytoplasmic expression (May *et al*, 2014; Zhang *et al*, 2014).

In contrast, positively charged GFP-GR<sub>149</sub> and PR<sub>175</sub>-GFP, which localize to cytoplasm and nucleus, were not detected in the RFP-positive receiving cells above background levels. To compensate for the different transfection and expression levels of the GFP-DPR proteins, we also normalized the double-positive cells to the total population of GFP-positive cells (Fig 2D), which showed a similar result compared to the absolute fraction of double-positive cells (Fig 2C). Thus, the hydrophobic cytoplasmic DPR proteins are transmitted between cells regardless of their aggregation properties.

### GA<sub>175</sub> aggregates seed further poly-GA aggregates in repeat RNA-expressing cells

To test whether transmitted DPR proteins act as a seed for further aggregation, we next used (G4C2)<sub>80</sub>-transfected cells as receiving cells in co-culture experiments. We first confirmed that (G4C2)<sub>80</sub>-transfected cells also take up GA<sub>175</sub>-GFP by co-staining of GA<sub>80</sub>-flag and GA-GFP for analysis by flow cytometry after 3 days of co-culture to allow sufficient levels of RAN translation (Fig 3A and B). We detected a similar fraction of double-positive cells for co-culture of (G4C2)<sub>80</sub> and GA<sub>175</sub>-GFP-, GP<sub>47</sub>-GFP-, or PA<sub>175</sub>-GFP-expressing cells as with RFP-positive receiver cells (compare Figs 2 and 3B). Since (G4C2)<sub>80</sub> drives mainly poly-GA expression (Mori *et al*, 2016), we focused on this DPR species for the following experiments.

To further increase the load of transmissible DPR proteins, we incubated (G4C2)<sub>80</sub>-transfected cells for 3 days with GA<sub>175</sub>-RFP aggregates (Fig 3C). Immunofluorescence confirmed intracellular uptake of GA<sub>175</sub>-RFP aggregates (Fig 3D). The exogenous aggregates

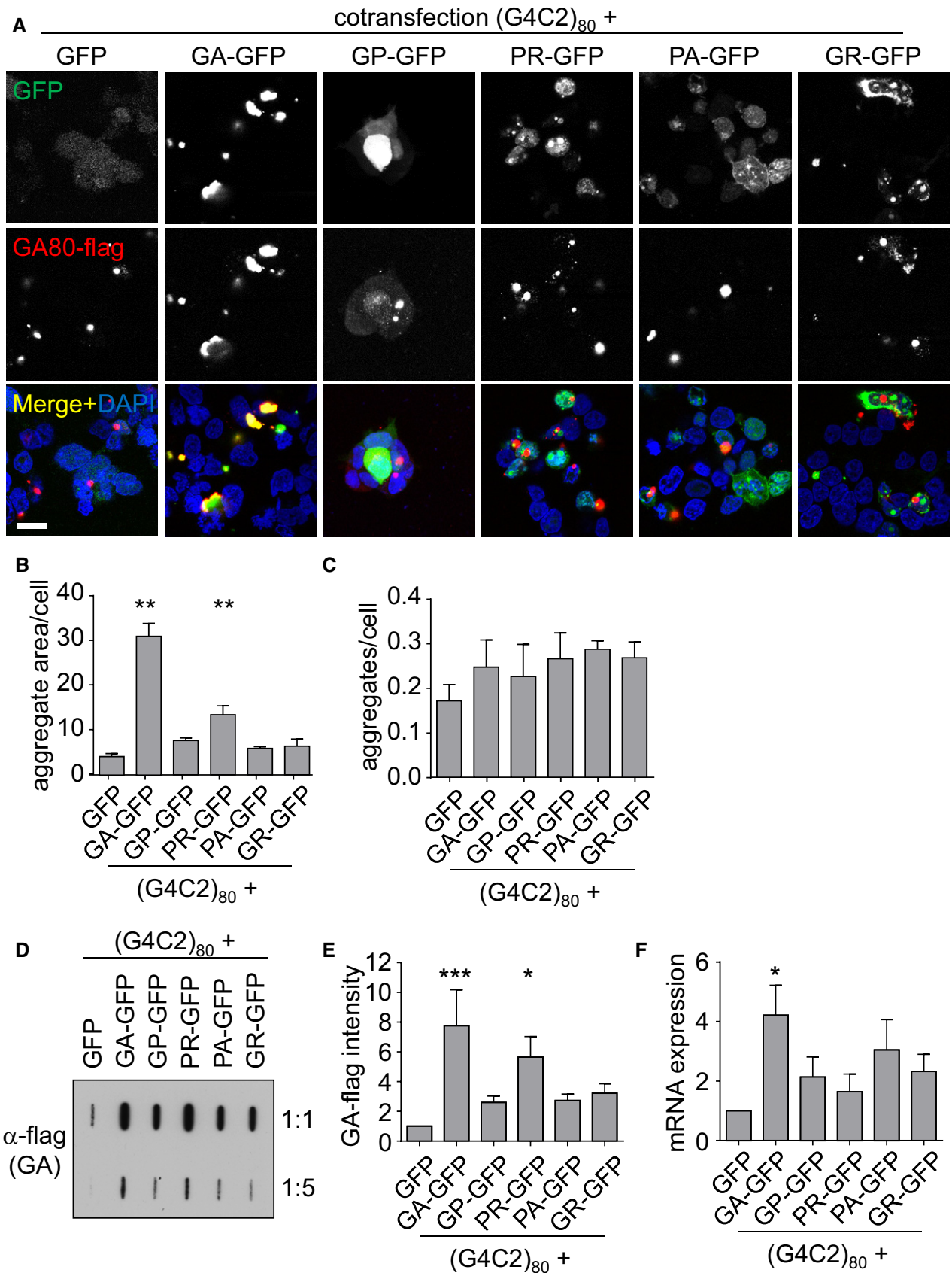


Figure 1.

**Figure 1. DPR expression promotes RAN translation from (G4C2)<sub>80</sub>.**

HEK293 cells cotransfected with (G4C2)<sub>80</sub> containing a flag-tag in the poly-GA reading frame and GFP or DPR-GFP for 3 days to analyze effects on RAN translation.

- A Immunofluorescence for the GFP-tagged proteins and RAN translation-derived GA<sub>80</sub>-flag. DAPI labels nuclei. Scale bar 20 μm.
- B, C Quantification of GA<sub>80</sub>-flag aggregate area and number from  $n = 4$  independent experiments with five images each (containing 60–90 cells per image). Aggregate and cell number were counted manually, and aggregate size was determined by thresholding. Data are shown as mean ± SD. One-way ANOVA with Dunnett's multiple comparisons test; GFP vs. GA-GFP  $P = 0.0025$ ; GFP vs. PR-GFP  $P = 0.0095$ ; \*\*\* $P < 0.01$ .
- D Filter-trap analysis of GA<sub>80</sub>-flag in two dilutions. A representative of four experiments is shown.
- E Quantification of GA<sub>80</sub>-flag from four independent experiments. Data are shown as mean ± SD. Statistics were performed by one-way ANOVA with Dunnett's multiple comparisons test; GFP vs. GA-GFP  $P = 0.0009$ ; GFP vs. PR-GFP  $P = 0.0325$ ; \* $P < 0.05$ , \*\*\* $P < 0.001$ .
- F Expression of the G4C2<sub>80</sub> RNA was measured by qPCR targeting the 3' region of the repeat sequence. RNA levels were normalized to GAPDH mRNA. Data are shown as mean ± SD ( $n = 3$ ). Statistics were performed by one-way ANOVA with Dunnett's multiple comparisons test; GFP vs. GA-GFP  $P = 0.0241$ ; \* $P < 0.05$ .

co-localized with GA<sub>80</sub>-flag derived from the (G4C2)<sub>80</sub> vector (Fig 3D, arrow), indicating that transmitted poly-GA can seed further aggregation. Importantly, even cells without prominent GA<sub>175</sub>-RFP staining showed increased GA<sub>80</sub>-flag levels compared to cells treated with RFP extracts, suggesting that even trace amounts of GA<sub>175</sub>-RFP can accelerate poly-GA aggregation in the receiving cells (Fig 3D, arrowhead). Importantly, also the fraction of GA<sub>80</sub>-flag-positive cells increased significantly, suggesting that genuine seeding occurred (Fig 3E).

Filter-trap experiments and flow cytometry analysis confirmed increased expression/aggregation of RAN translation-derived GA<sub>80</sub>-flag and to a lesser extent also of GR<sub>80</sub>-HA and GP<sub>80</sub>-myc in GA-RFP-treated cells on a biochemical level (Fig 3F and G). Similar to direct poly-GA expression (Fig 1F), exposure to GA<sub>175</sub>-RFP lysates also increased the levels of the (G4C2)<sub>80</sub> mRNA transcripts (Fig 3H), indicating that poly-GA may affect transcription or stability of the expanded *C9orf72* repeat RNA. Taken together, uptake of poly-GA promotes further aggregation of poly-GA, poly-GR, and poly-GP in cells expressing the *C9orf72* repeat expansion.

**Dipeptide repeat proteins promote repeat RNA foci formation**

To corroborate the effect of poly-GA on repeat RNA levels, we analyzed nuclear RNA foci, which are another disease hallmark of *C9orf72* FTL/ALS. We switched from HEK293 to HeLa cells, because they attach better to glass coverslips and can sustain the harsh washing steps for *in situ* hybridization. As (G4C2)<sub>80</sub> expression resulted in many coalescing RNA foci, which made counting their number unreliable, we analyzed the size of RNA foci. Cotransfection of GA<sub>175</sub>-GFP, PA<sub>175</sub>-GFP, and GFP-GR<sub>149</sub> significantly increased foci size compared to GFP control, while GP<sub>47</sub>-GFP and PR<sub>175</sub>-GFP expression had no effect (Fig 4A and B). The effects of DPR proteins on RNA foci in HeLa cells are comparable to their effects on repeat RNA levels in HEK293 cells (compare Figs 4B and 1F).

To verify the effects of DPR proteins on the repeat RNA under physiological conditions, we used primary fibroblasts derived from patients with expanded G4C2 repeats and transduced them with individual DPR-GFP-expressing lentiviruses. Since DPR expression in primary patient-derived cells (including induced pluripotent stem cells) is extremely low, we investigated the effect on RNA foci formation. Consistent with the effects of DPR proteins on RNA foci in HeLa cells (Fig 4B), expression of poly-GA, poly-PA, and poly-GR increased the number of foci per cell (Fig 4C and D), whereas poly-PR had no effect on foci formation. Thus, poly-GA, poly-PA, and poly-GR seem to promote transcription or stability of the expanded repeat RNA.

**Poly-GA is transmitted between neurons**

To replicate our data in primary neurons, we transduced donor and receiver cells on separate coverslips for 3 days and co-cultured both coverslips with spacers from paraffin dots for another 4 days. We focused on poly-GA and used both (G4C2)<sub>80</sub> and empty vector-transduced receiver cells. Unfortunately, repeat-transduced neurons show only low GA<sub>80</sub>-flag expression, presumably due to poor packaging efficiency of the repeat RNA (Fig 5A). In contrast, lentiviral transduction of primary neurons with GA<sub>175</sub>-GFP results in inclusions of size and intensity comparable to the aggregates in cortex of *C9orf72* patients (May et al, 2014).

Consistent with Figs 2 and 3, we did not detect transmission from the GFP control donor to the receiver cells (Fig 5A, first row). In contrast, we detect GA<sub>175</sub>-GFP inclusions in several receiver neurons after 4 days of co-culture (Fig 5A, second row), suggesting that neurons can release and take up poly-GA similar to HEK293 cells. In addition, we noticed co-localization of transmitted GA<sub>175</sub>-GFP and RAN-translated GA<sub>80</sub>-flag in some receiver cells expressing (G4C2)<sub>80</sub> (Fig 5A, fourth row).

To directly assess poly-GA release from neurons, we collected conditioned media every 24 h and performed a poly-GA immunoassay. We first detected poly-GA levels in GA<sub>175</sub>-GFP-transduced cells compared to GFP controls 48 h after transduction (Fig 5B), but poly-GA release was significantly higher on the third and fourth day. Thus, neurons are able to release and take up low levels of poly-GA similar to tau and other intracellular aggregates.

**Brain lysates from *C9orf72* mutation carriers seed poly-GA aggregates in repeat RNA-expressing cells**

Next, we asked whether patient-derived DPR aggregates can induce seeding. Therefore, we homogenized cerebella of FTL/ALS patients with or without *C9orf72* mutation, because in this brain region, DPR levels are very high and TDP-43 aggregation is virtually absent (Mackenzie et al, 2013). Similar to established protocols for tau seeding, we used liposome-mediated transfection to promote aggregate uptake in (G4C2)<sub>80</sub>-expressing cells (Nonaka et al, 2010; Sanders et al, 2014).

Cerebellar extracts from *C9orf72* patients increased the number of GA<sub>80</sub>-flag-positive cells compared to *C9orf72*-negative controls as quantified by flow cytometry (Fig 6A and B). Filter trap confirmed the enhanced GA<sub>80</sub>-flag aggregate levels in cells treated with extracts from a *C9orf72* patient compared to a *C9orf72*-negative control (Fig 6C and D). Cerebellar extracts from a *C9orf72* patient also increased the levels of GR<sub>80</sub>-HA and GP<sub>80</sub>-myc (Fig 6C and D).

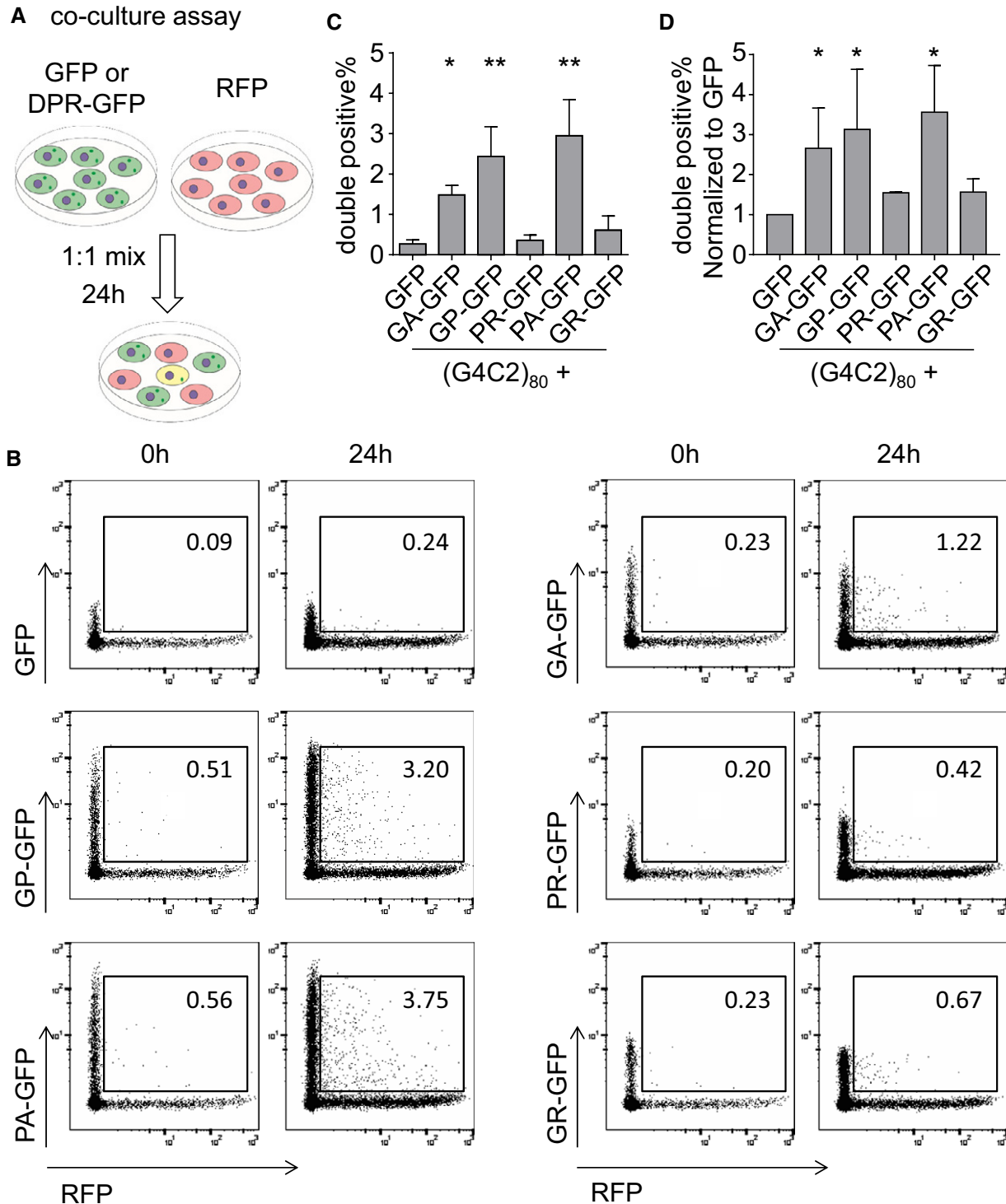


**Figure 2. Hydrophobic DPR proteins are transmitted between cells in co-culture assays.**

HEK293 cells were transfected with RFP, GFP, or DPR-GFP for 24 h and mixed in the indicated combinations. Co-cultures were analyzed by flow cytometry immediately after mixing or 24 h later. Gating was performed on RFP-expressing cells compared to mixture of all green fluorescent cells.

A Schematic overview of experimental flow.

B The fraction of double-positive cells is indicated in percent. A representative of three experiments is shown.

C Absolute frequency of double-positive cells after 24 h of co-culture. Data are shown as mean  $\pm$  SD ( $n = 4$ ). GFP vs. GA-GFP  $P = 0.0482$ ; GFP vs. GP-GFP  $P = 0.0019$ ; GFP vs. PA-GFP  $P = 0.0012$ ; \* $P < 0.05$ , \*\* $P < 0.01$  by one-way ANOVA with Dunnett's multiple comparisons test.

D Relative frequency of double-positive cells to total GFP-expressing cells after 24 h of co-culture. Data are shown as mean  $\pm$  SD ( $n = 4$ ). GFP vs. GA-GFP  $P = 0.0473$ ; GFP vs. GP-GFP  $P = 0.0327$ ; GFP vs. PA-GFP  $P = 0.0166$ ; \* $P < 0.05$  by one-way ANOVA with Dunnett's multiple comparisons test.

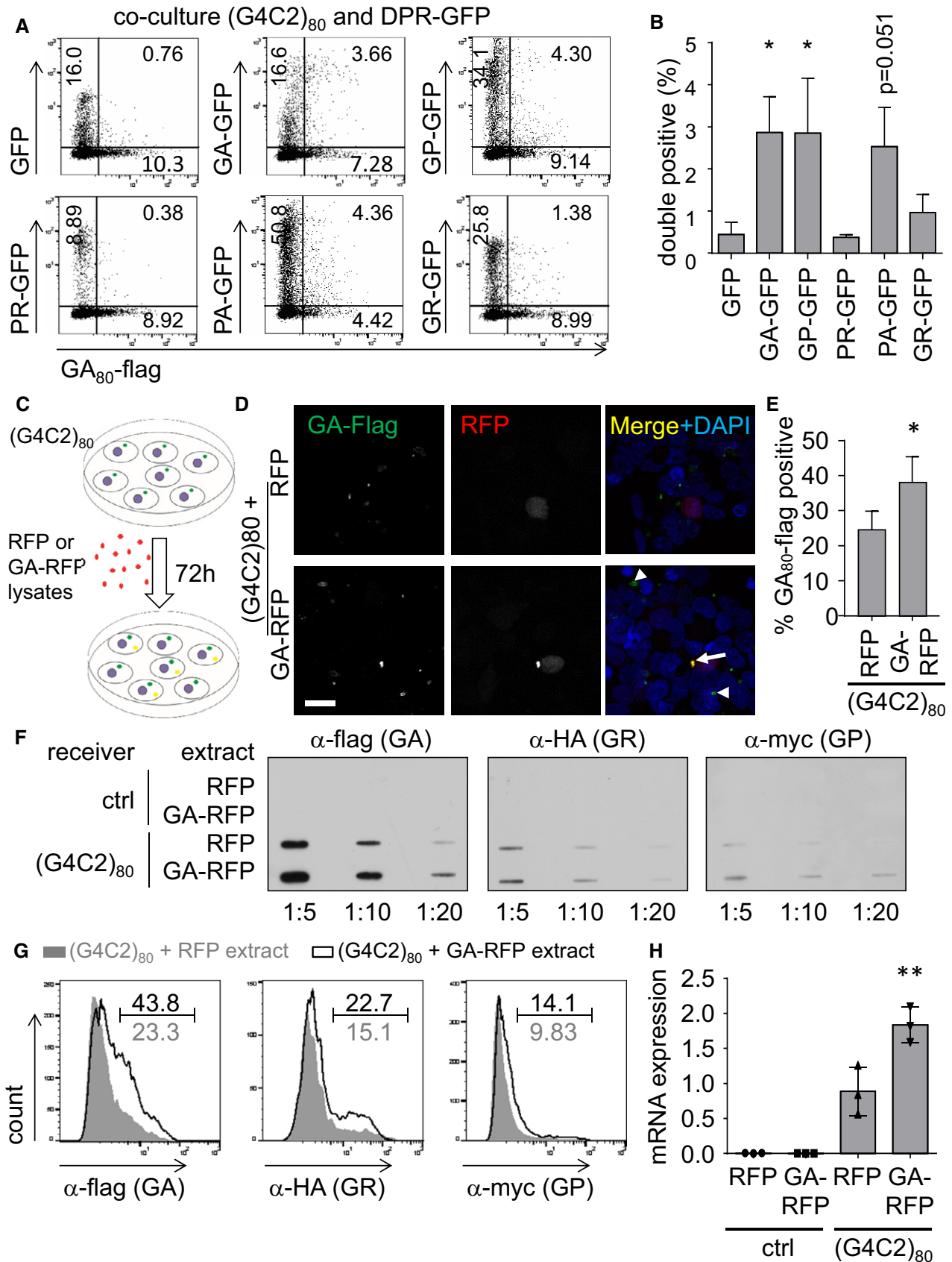


Figure 3.

**Figure 3. Poly-GA uptake seeds DPR aggregation and induces repeat RNA expression.**

A, B Co-culture assay in HEK293 cells. 24 h after transfection with either (G4C2)<sub>80</sub>, GFP, or DPR-GFP, cells were mixed in the indicated combination. After 72 h of co-culture, cells were fixed, permeabilized, and stained with anti-flag to detect GA<sub>80</sub>-flag for flow cytometry analysis. Flow cytometry dot plots are shown based on levels of GA<sub>80</sub>-flag (x-axis) and GFP (y-axis) expression. The fraction of indicated populations is indicated in percent. Graphs shows mean ± SD fraction of double-positive cells from three independent experiments. Statistics were performed by one-way ANOVA with Dunnett's multiple comparisons test; GFP vs. GA-GFP  $P = 0.0316$ ; GFP vs. GP-GFP  $P = 0.0331$ ; GFP vs. PA-GFP  $P = 0.0513$ ; \* $P < 0.05$ .

C–H HEK293 cells transfected with (G4C2)<sub>80</sub> for 48 h were treated for 72 h with cell lysates from HEK293 transfected with RFP or GA<sub>175</sub>-RFP as depicted in (C). The RAN-translated GA<sub>80</sub>-flag, GR<sub>80</sub>-HA, GP<sub>80</sub>-myc are detected by anti-flag immunofluorescence (D) and quantified (E). Arrowheads indicate GA<sub>80</sub>-flag aggregates in cells without prominent GA<sub>175</sub>-RFP uptake, arrows indicate co-localization of exogenous GA<sub>175</sub>-RFP with GA<sub>80</sub>-flag. Results from  $n = 4$  independent experiments with five images each quantified and analyzed by two-tailed unpaired t-test. Data are shown as mean ± SD.  $P = 0.0061$ ; \* $P < 0.05$ . Scale bar 20 μm. Filter trap (F) and flow cytometry analysis (G) confirmed the increased levels of GA<sub>80</sub>-flag in GA<sub>175</sub>-RFP-treated cells. The percentage of DPR-positive cells in GA-RFP-treated cells compared to the RFP control is indicated. A representative of three independent experiments is shown. (H) Expression of the (G4C2)<sub>80</sub> RNA in DPR-treated cells was measured by qPCR targeting the tag region downstream of the repeat sequence. RNA levels were normalized to GAPDH mRNA. Data are shown as mean ± SD ( $n = 3$ ). Statistics were performed by one-way ANOVA with Dunnett's multiple comparisons test; (G4C2)<sub>80</sub> + RFP vs. (G4C2)<sub>80</sub> + GA-RFP  $P = 0.007$ ; \*\* $P < 0.01$ .

Similar to the experiments with cell lysates, this was associated with an upregulation of (G4C2)<sub>80</sub> mRNA expression in the cells receiving extracts from different *C9orf72* mutant patients (Fig 6E). Thus, uptake of patient-derived DPR proteins induces DPR aggregation in (G4C2)-repeat-expressing cells by seeding aggregation and increasing repeat RNA levels.

**Treatment with specific antibodies blocks poly-GA aggregation and seeding**

Since antibody treatment has been shown to reduce intracellular aggregation of tau and  $\alpha$ -synuclein, which are also known to be transmitted between cells (Boutajangout *et al*, 2011; Chai *et al*, 2011, 2012; Yanamandra *et al*, 2013), we tested whether anti-GA antibodies could inhibit aggregation in our cell culture model. Treating GA<sub>175</sub>-GFP-transfected HEK293 cells with anti-GA reduced GA<sub>175</sub>-GFP aggregation compared to isotype control (Fig 7A and B). Filter-trap assays using a stable cell line expressing GA<sub>149</sub>-GFP confirmed that anti-GA reduced poly-GA aggregate levels compared to isotype control antibodies (Fig 7C). To analyze the efficacy of anti-GA antibodies in neurons, we transduced primary neurons with GA<sub>175</sub>-GFP and treated with antibodies for 6 days (Fig 7D). Treatment with anti-GA significantly reduced poly-GA levels compared to an isotype control (Fig 7E).

We next assessed the ability of anti-GA antibodies to block the seeding activity of brain extracts from *C9orf72* patients on repeat-expressing cells. Brain lysates were pre-incubated with anti-GA or IgG2a control for 16 h and then added to (G4C2)<sub>80</sub>-expressing HEK293 cells for 48 h before measurement. We detected increased expression of GA<sub>80</sub>-flag in cells receiving cerebellar extracts from a *C9orf72* patient (compare Figs 7F and G, and 6A–D). Pre-incubation with anti-GA antibodies reduced the GA<sub>80</sub>-flag expression to control levels, without affecting expression of GR<sub>80</sub>-HA or the repeat RNA levels (Fig EV2), indicating that poly-GA is crucial for the seeding activity of *C9orf72* brains.

Together, these data suggest that anti-GA immunotherapy may prevent seeding and spreading of poly-GA in *C9orf72* disease.

**Discussion**

We demonstrate intercellular spreading and seeding of the hydrophobic DPR species poly-GA, poly-GP, and poly-PA. Uptake of poly-GA from transfected cells or from brain homogenates

promotes expression of the expanded repeat RNA and RAN translation products, suggesting a vicious cycle of DPR expression and repeat RNA expression. Anti-GA antibodies block the seeding activity of *C9orf72* brain extracts and reduce poly-GA aggregation in cell lines, suggesting immunotherapy may be a useful therapeutic option to treat the DPR component of *C9orf72* disease.

**Hydrophobic DPR proteins are transmitted between cells**

Using co-culture assays, we show intercellular transmission of the hydrophobic DPR species poly-GA, poly-GP, and poly-PA in cell lines (Fig 1) and we confirmed poly-GA release and uptake in rat primary neurons (Fig 5). Moreover, cells treated with poly-GA-containing cell extract or *C9orf72* brain homogenates show induced aggregation of RAN-translated GA<sub>80</sub>-flag (Figs 3, 6, and 7).

Our data add to previous reports that fibrillar GA<sub>15</sub> peptides are taken up by N2a cells and promote intracellular poly-GA aggregation (Chang *et al*, 2016), because we show intercellular transmission of much larger synthetic poly-GA and even patient-derived poly-GA. In contrast to A $\beta$  seeding, which is very inefficient with synthetic peptides and seems to require an elusive cofactor from patient brain (Stohr *et al*, 2012), at least poly-GA seeding seems to work with synthetic peptides and lysates from cell culture or cerebellum. In addition, we detected intercellular spreading of poly-GP and poly-PA. Poly-GP is readily detectable in CSF of *C9orf72* patients (Su *et al*, 2014), but whether extracellular poly-GP in the CSF originates from active secretion or cellular debris is unclear. Our co-culture data rather point to unconventional secretion or passive release of small amounts of hydrophobic DPR proteins as it has been shown for intracellular tau or  $\alpha$ -synuclein (Chai *et al*, 2012), because DPR expression is not toxic in HEK293 cells under our conditions (May *et al*, 2014). We did not find significant transmission of arginine-rich DPRs at physiological levels, although synthetic GR<sub>20</sub> and PR<sub>20</sub> peptides are taken up by cells and cause toxicity by interfering with RNA expression and splicing when applied at 10 μM (Kwon *et al*, 2014).

While this manuscript was under review, Westergard *et al* reported cell-to-cell transmission of the hydrophobic DPR 50-mers, GR<sub>50</sub>-GFP, and in case of direct cell contact also of PR<sub>50</sub>-GFP (Westergard *et al*, 2016). Even low-level transmission of these species might be relevant due to their high toxicity (Mizielinska *et al*, 2014). The different results between our studies may be due to different repeat length or expression levels, as the arginine-rich

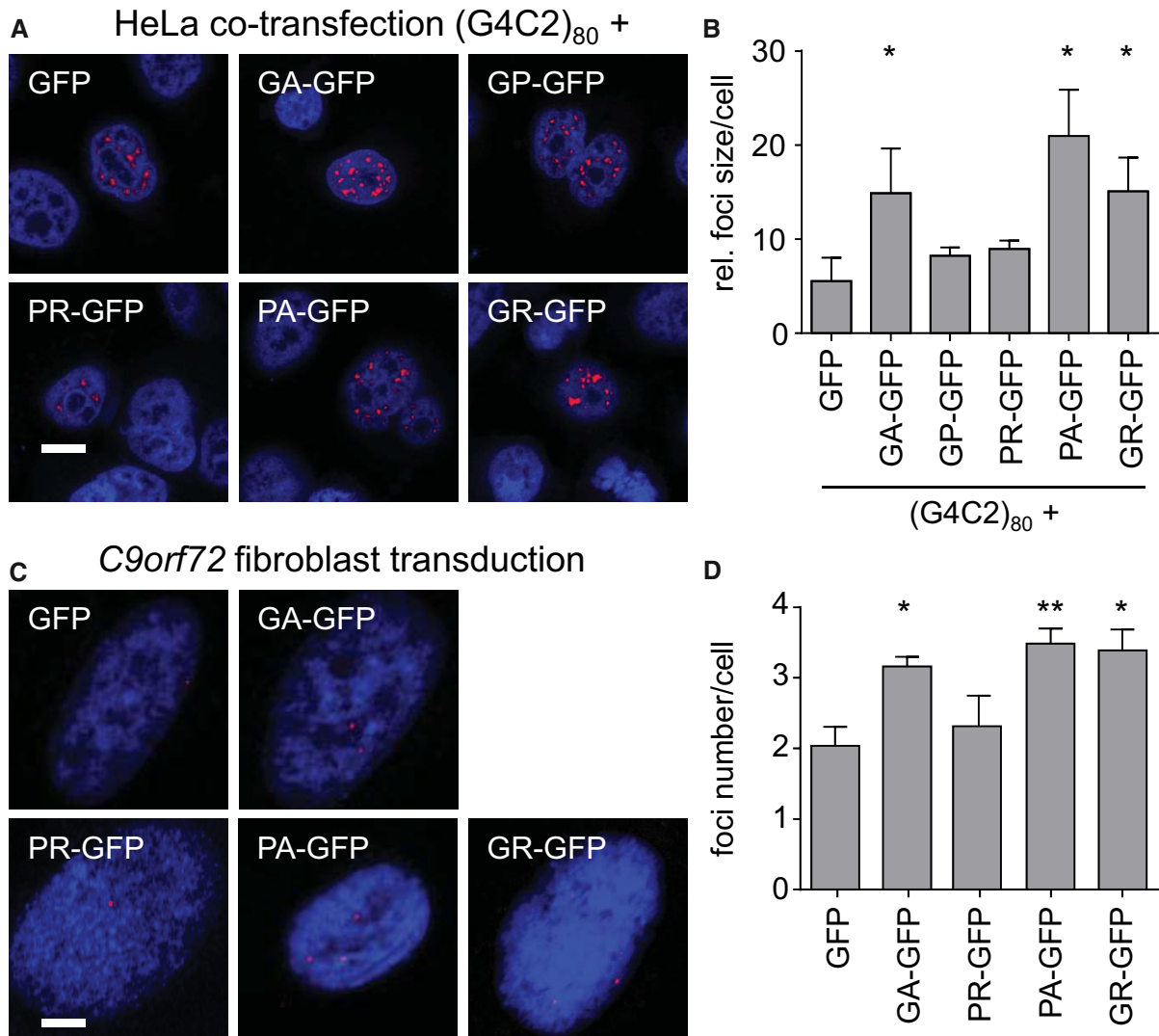


**Figure 4. DPR expression promotes formation of repeat RNA foci in HeLa cells and C9orf72 fibroblasts.**

A, B *In situ* hybridization of RNA foci (red) in HeLa cells cotransfected with (G4C2)<sub>80</sub> and GFP or DPR-GFP for 3 days. Representative images (A) and quantification (B) of foci size from three experiments (at least 30 cells per condition per experiment) are shown. DAPI labels nuclei. Scale bar 10 μm. Summary indicated the means ± SD. GFP vs. GA-GFP *P* = 0.0210; GFP vs. PA-GFP *P* = 0.0163; GFP vs. GR-GFP *P* = 0.0413; \**P* < 0.05 by one-way ANOVA with Dunnett's multiple comparisons test.

C, D *In situ* hybridization of (G4C2)<sub>n</sub> RNA foci in fibroblast of C9orf72 patients transduced with GFP or DPR-GFP lentivirus for 8–9 days. Note that we could not analyze poly-GP, because we failed to generate a codon-modified lentivirus. Representative images (C) and quantification of foci number (D) are shown. Brightness and contrast were digitally enhanced for better visibility for the presentation only. Scale bar 40 μm. Summary indicated the means ± SEM of *n* = 7 experiments for GFP, GA-GFP, PR-GFP, and PA-GFP, and *n* = 3 for GR-GFP (at least 30 cells per condition per experiment). GFP vs. GA-GFP *P* = 0.0296; GFP vs. PA-GFP *P* = 0.0041; GFP vs. GR-GFP *P* = 0.0451; \**P* < 0.05, \*\**P* < 0.01 by one-way ANOVA with Dunnett's multiple comparisons test.

DPRs show lower expression in our system (Fig 1 and May *et al*, 2014).

#### Dipeptide repeat proteins affect repeat RNA expression and/or stability

Surprisingly, poly-GA uptake did not only promote GA<sub>80</sub>-flag levels, but also increased expression of the other two RAN products poly-GP and poly-GR (Fig 3F and G). These findings complicate interpretation of the data, but two lines of evidence support seeding

of poly-GA. First, poly-GA uptake in recipient cells increased the number of GA<sub>80</sub>-flag inclusions. Second, poly-GA antibody treatment reduced GA<sub>80</sub>-flag aggregation without affecting its mRNA levels.

Moreover, treating cells with poly-GA extracts induced repeat RNA levels (Fig 3H), suggesting an effect on repeat transcription and/or translation. To exclude variable uptake, we transfected DPR expression constructs and analyzed the repeat RNA. In heterologous cells and in patient fibroblasts, poly-GA and poly-PA expression promoted RNA foci formation and poly-GA increased the levels of repeat RNA (Figs 3H and 4). Since neither of the hydrophobic DPR

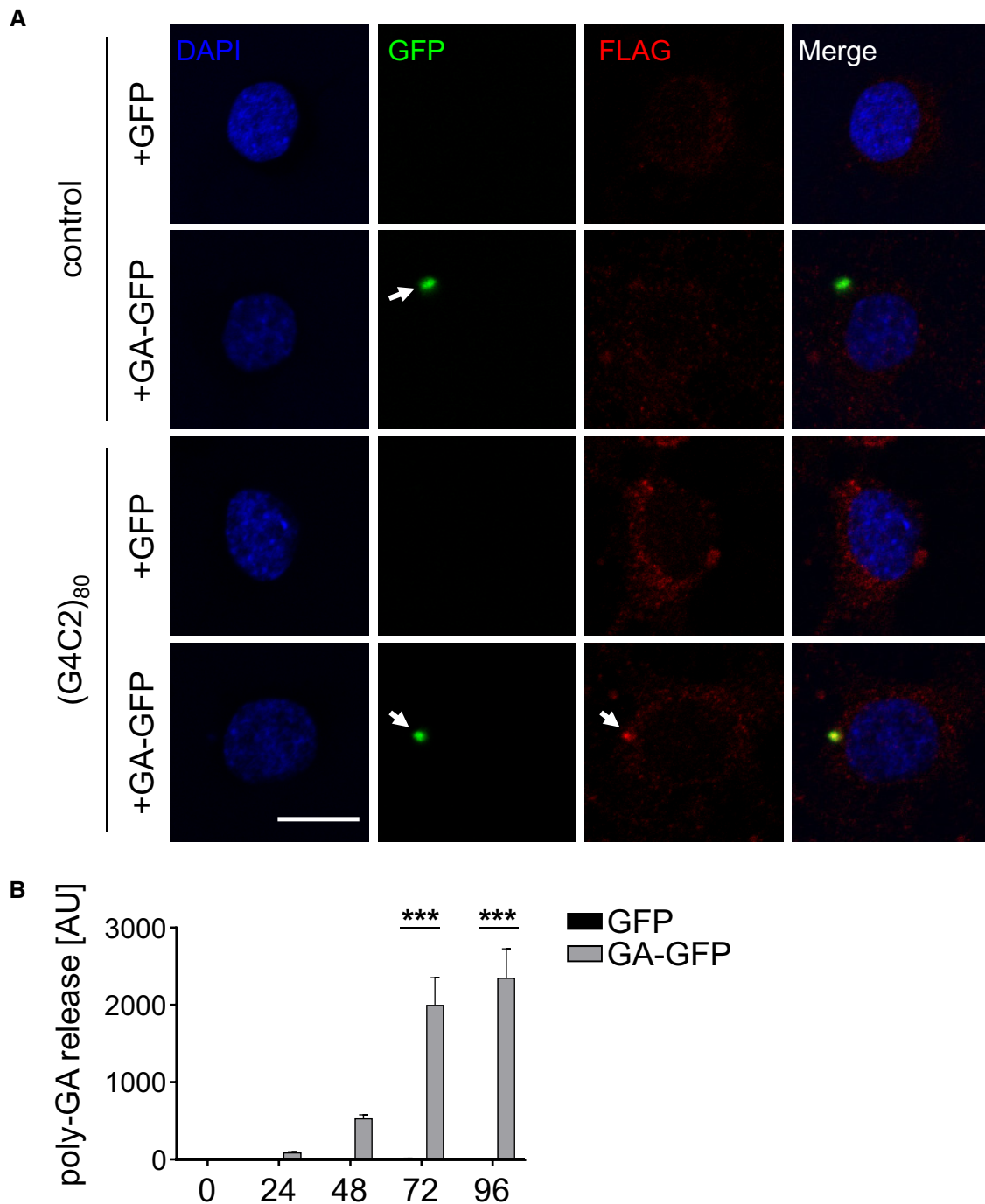


**Figure 5. Release and uptake of poly-GA by neurons.**

**A** Co-culture assay in rat primary neurons. Cortical neurons (400,000/well) on coverslips were transduced with GFP or GA<sub>175</sub>-GFP as donor. Hippocampal neurons (85,000/well) on coverslips were transduced with (G4C2)<sub>80</sub> or empty vector as receiver cells. Three days later, the washed coverslips were put into well with paraffin spacers. GFP and GA<sub>80</sub>-flag expression was analyzed 4 days later in the receiver cells by immunofluorescence. Arrows indicate co-localization of GA<sub>175</sub>-RFP with GA<sub>80</sub>-flag. Scale bar 10 μm.

**B** Cortical neurons transduced with GFP or GA<sub>175</sub>-GFP. Conditioned media were exchanged 24 h prior to transduction and collected right before and every 24 h after infection. Poly-GA levels in media were determined by immunoassay. Data are shown as mean ± SEM. Two-way ANOVA with Sidak's multiple comparisons test ( $n = 4$ ).  $t = 72$  h: GA-GFP vs. GFP  $***P < 0.0001$ ;  $t = 96$  h: GA-GFP vs. GFP  $***P < 0.0001$ .

proteins is known to bind RNA or RNA-binding proteins directly, we speculate that the DPR proteins trigger a stress response (Zhang *et al*, 2014) leading to transcriptional upregulation of repeat

transcription. Moreover, about 10% of DPR inclusions are found in the nucleus in patients, where they mainly co-localize with heterochromatin next to the nucleolus, which may support a direct effect

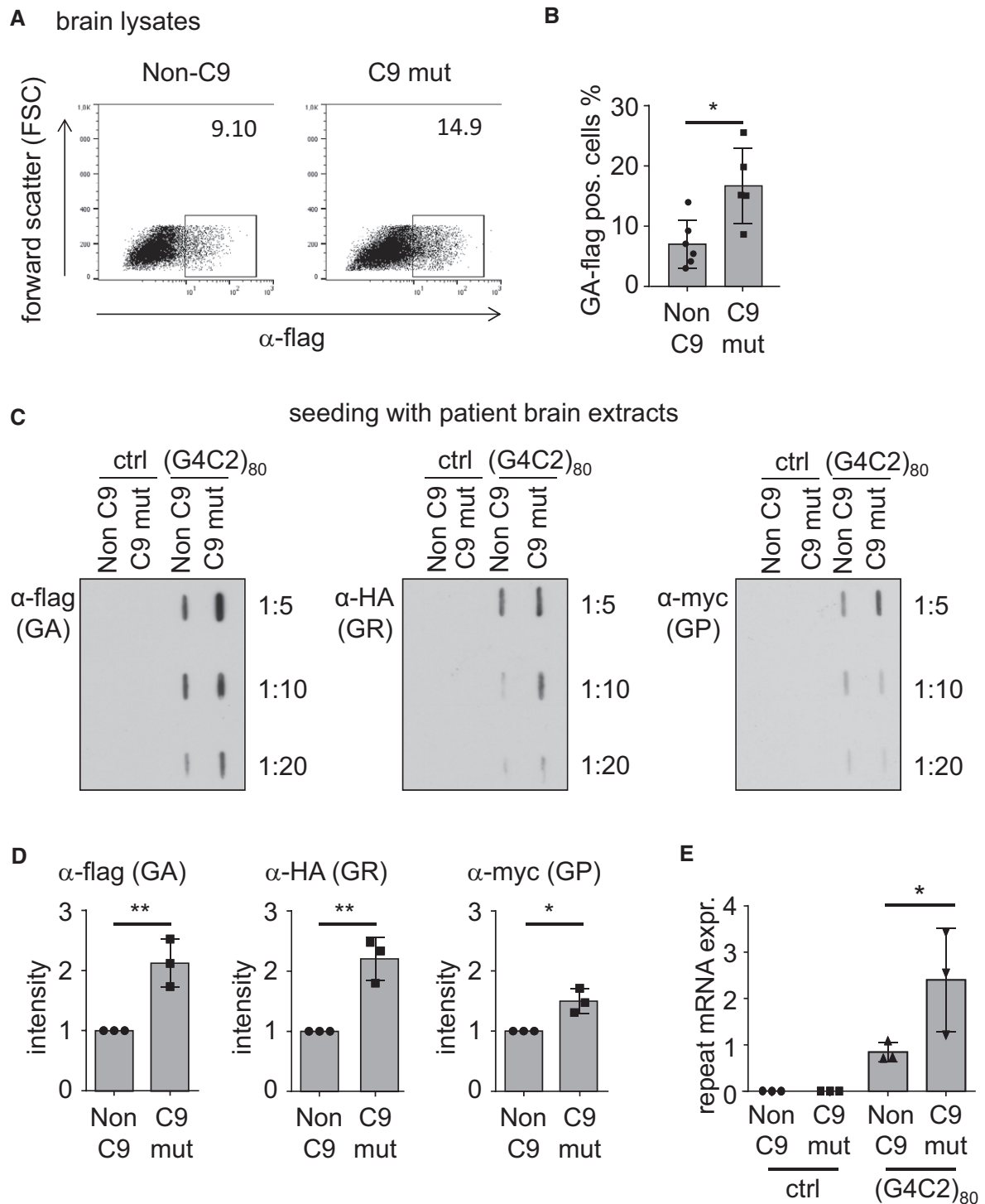


**Figure 6. Brain homogenates from *C9orf72* patients seed DPR aggregation and promote repeat RNA expression.**

Analysis of RAN translation products in HEK293 cells transfected with (G4C2)<sub>80</sub> (for 24 h) and incubated with cerebellar extracts of *C9orf72* patients and controls.

A, B Flow cytometry analysis of GA<sub>80</sub>-flag-positive cells using  $n = 5$  *C9orf72*-positive and  $n = 6$  *C9orf72*-negative cases (three healthy controls, two ALS, one FTLD)  $P = 0.0124$ ; \* $P < 0.05$  by two-tailed unpaired  $t$ -test.

C, D Filter-trap analysis of DPR products in all three reading frames using the indicated antibodies. Results from  $n = 3$  independent experiments using one patient and one control were quantified and analyzed by two-tailed unpaired  $t$ -test. Data are shown as mean  $\pm$  SD. Anti-flag (GA)  $P = 0.0079$ ; anti-HA (GR)  $P = 0.0043$ ; anti-myc (GP)  $P = 0.0128$ ; \* $P < 0.05$ , \*\* $P < 0.01$ .

E Quantitative RT-PCR shows upregulation of repeat RNA transcripts upon incubation with *C9orf72* extracts as in Fig 3H. Data are shown as mean  $\pm$  SD from  $n = 3$  patients and controls in independent experiments. Statistics were performed by one-way ANOVA with Dunnett's multiple comparisons test; (G4C2)<sub>80</sub> + non-C9 vs. (G4C2)<sub>80</sub> + C9 mut  $P = 0.0101$ ; \* $P < 0.05$ .

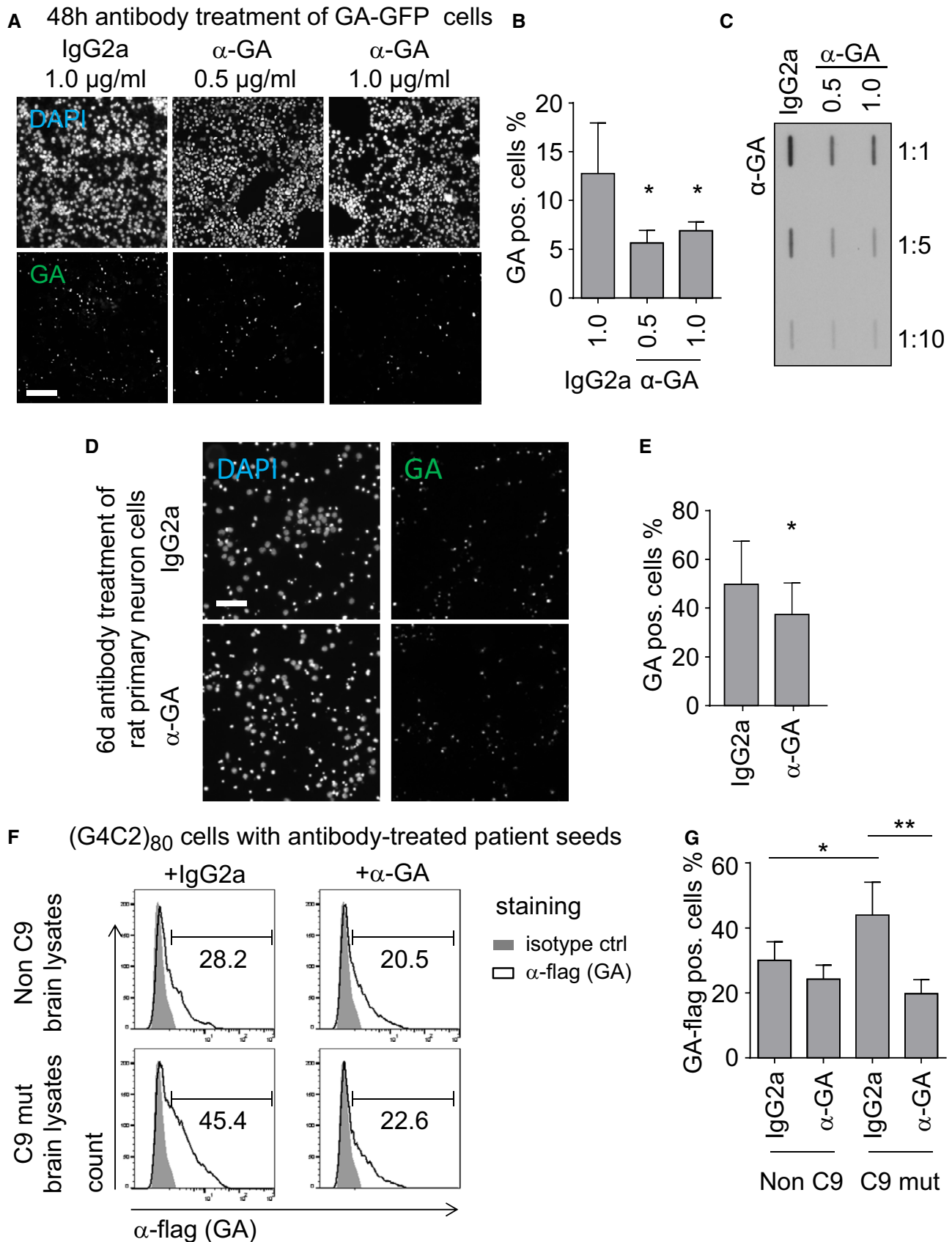


Figure 7.

**Figure 7. Anti-GA antibodies inhibit poly-GA aggregation and prevent seeding from brain tissue.**

- A, B HEK293 cells transfected with GA<sub>175</sub>-GFP were treated with anti-GA antibodies or mouse IgG2a isotype control (in the indicated concentration) for 3 days. Fluorescence microscopy image of GA-GFP aggregation (scale bar 100 μm). (B) The percentage of poly-GA-positive cells was quantified semi-automatically using BioTek Gen5 software. Data are shown as mean ± SD. IgG2a vs. anti-GA 0.5 μg/ml  $P = 0.0109$ ; IgG2a vs. anti-GA 1.0 μg/ml  $P = 0.0113$ ; \* $P < 0.05$  by one-way ANOVA with Dunnett's multiple comparisons test from three independent experiments.
- C HEK293-T-REX GA<sub>149</sub>-GFP stable cells cultured in the presence of 10 ng/ml tetracycline were treated with anti-GA antibodies or isotype control as in (A) and analyzed by filter trap. Representative filter-trap blot of three independent experiments is shown.
- D, E Rat primary neurons were transfected with GA<sub>175</sub>-GFP after 5 days *in vitro* (DIV) and treated with 1 μg/ml antibody on the following day. Neurons were analyzed after 6 days of treatment by GFP fluorescence and DAPI staining (scale bar 100 μm). The percentage of poly-GA-positive cells was quantified semi-automatically using BioTek Gen5 software. Data are shown as mean ± SD.  $P = 0.0366$ ; \* $P < 0.05$  by two-tailed unpaired *t*-test from  $n = 6$  independent experiments.
- F, G HEK293 cells transfected with (G4C2)<sub>80</sub> were treated with cerebellar extracts pre-incubated with anti-GA or isotype control. The fraction of RAN translation-derived GA<sub>80</sub>-flag was quantified by flow cytometry. Data indicated the means ± SD of  $n = 3$  patients and controls in independent experiments. Non-C9 + IgG2a vs. C9 mut + IgG2a  $P = 0.0438$ ; C9 mut + IgG2a vs. C9 mut + anti-GA  $P = 0.0013$ ; \* $P < 0.05$ , \*\* $P < 0.01$  by one-way ANOVA with Dunnett's multiple comparisons test.

on gene expression (Schludi *et al*, 2015). Surprisingly, poly-PR expression induced poly-GA by RAN translation with little effect on repeat RNA levels or foci formation (Figs 1 and 4). Poly-PR binds directly to RNA and many RNA-binding proteins (Kwon *et al*, 2014; Kanekura *et al*, 2016). Sequestration of certain RNA-binding proteins might impair the tight control of ATG-mediated translational initiation and thus promote RAN translation. Interestingly, antisense oligonucleotides consistently reduce DPR levels stronger than repeat RNA levels independently supporting a feedback mechanism (Jiang *et al*, 2016). Thus, DPR expression may trigger a vicious cycle of increasing repeat RNA and DPR expression ultimately leading to neurodegeneration.

**Poly-GA immunotherapy**

Poly-GA, the most abundant DPR protein in patients, could be at the center of *C9orf72* gain-of-function toxicity, because it forms amyloid-like fibrils capable of spreading between cells to seed further DPR aggregation and enhance RNA foci formation. Therefore, we tested whether we could reduce poly-GA aggregation using specific antibodies. Anti-GA antibodies lowered poly-GA levels in both transiently and stably transfected HEK293 cells and also in primary neurons (Fig 7). Moreover, pre-incubation with anti-GA antibodies also prevented uptake from *C9orf72* brain extracts into HEK293 cells (Fig 7).

Immunotherapy targeting extracellular Aβ aggregates has finally shown promising results in patients with Alzheimer's disease in its early stages (Sevigny *et al*, 2016). Surprisingly, anti-tau immunotherapy lowers intracellular tau aggregation and neurological deficits in mouse models (Boutajangout *et al*, 2011; Chai *et al*, 2011, 2012; Yanamandra *et al*, 2013). Even for intracellular aggregates, the antibodies are thought to act on extracellular proteins in transit between two cells. Antibody binding may induce phagocytosis through microglia via Fc receptors or inhibit neuronal uptake (Yanamandra *et al*, 2013). Given our results for cell-to-cell transmission of the different DPR species, only the hydrophobic poly-GA/GP/PA would be accessible for antibodies. Thus, anti-GA immunotherapy may be a future treatment option for *C9orf72* ALS/FTLD. Considering the long prodromal DPR accumulation accompanied by subtle brain atrophy in *C9orf72* patients (Proudfoot *et al*, 2014; Rohrer *et al*, 2015; Edbauer & Haass, 2016), mutation carriers may require very early treatment as proposed for Alzheimer's disease.

Taken together, our work shows an unexpected link between RNA and DPR toxicity and suggests a vicious cycle that may ultimately lead to neuron loss after a prodromal phase. Non-cell autonomous effects due to spreading and seeding of poly-GA, poly-GP,

and poly-PA could explain the poor correlation of DPR proteins and RNA foci with neurodegeneration in *C9orf72* patients and suggest a novel therapeutic approach through passive vaccination.

**Materials and Methods****Antibodies**

The following antibodies were used: anti-DYKDDDDK/flag (filter trap 1:1,000, FACS 1:250, Cell Signaling), anti-myc (1:1,000, clone 9E10, Santa Cruz), anti-HA (1:1,000, clone 3F10, Roche), anti-GFP (1:1,000, clone N86/8, NeuroMab), anti-GA clone 5F2 (1 μg/ml) (Mackenzie *et al*, 2013), mouse IgG2a (1 μg/ml, Sigma), and rabbit IgG (1:250, Sigma).

**Plasmids and lentivirus production**

ATG-initiated epitope-tagged synthetic expression constructs for GA<sub>175</sub>-GFP, PA<sub>175</sub>-GFP, GFP-GR<sub>149</sub>, and PR<sub>175</sub>-GFP in pEF6 or lentiviral backbone (FhSynW2) were described previously (May *et al*, 2014; Schludi *et al*, 2015). pEGFP-GP<sub>47</sub> was a kind gift from Dr. Leonard Petrucelli (Zhang *et al*, 2014) and was for some experiments subcloned into pEF6 vector. The triple-tagged (G4C2)<sub>80</sub> construct to analyze RAN translation was recently reported (Mori *et al*, 2016). Lentivirus was produced in HEK293FT cells (Life Technologies) as described previously (Fleck *et al*, 2013).

**Cell lines and cell culture**

HEK293-T-REX GA<sub>149</sub>-GFP stable cells were generated using T-REX system (Thermo Scientific) according to the manufacturer's instruction. Briefly, GA<sub>149</sub>-GFP was cloned into the pcDNA 5/FRT/TO under the control of CMV promoter and two tetracycline operator 2 (TetO2) sites and transfected in T-REX 293 cells containing the tet-repressor protein. The stable cell line was maintained in high-glucose DMEM medium supplemented with 5 μg/ml blasticidin, 10% FCS, 1% pen/strep, and 2 mM L-glutamine. Expression of GA<sub>149</sub>-GFP was induced with 10 ng/ml tetracycline. HEK293FT cells were cultured with DMEM containing 10% FCS and penicillin/streptomycin.

**Neuron culture**

Primary cortical and hippocampal cultures were prepared from E19 rats as described previously (May *et al*, 2014) and plated on

poly-D-lysine-coated coverslips. For co-culture experiments, primary neurons on coverslips with 1 to 2 mm paraffin dots glued on to them were transduced with lentivirus. After 3 days, coverslips were extensively washed and put face to face into one well for 4 days.

### Patient-derived fibroblasts

We included cell lines from three *C9orf72* ALS patients as reported previously (Japtok *et al*, 2015; Mori *et al*, 2016). All procedures were in accordance with the Helsinki convention and approved by the Ethical Committee of the University of Dresden (EK45022009; EK393122012). Patients were genotyped using EDTA blood in the clinical setting after given written consent according to German legislation independent of any scientific study by a diagnostic human genetic laboratory (CEGAT, Tübingen, Germany or Dept. Human Genetics, University of Ulm, Germany) using diagnostic standards.

### Poly-GA immunoassay

Poly-GA in neuronal media was measured by immunoassay on the Meso Scale platform (MSD) using the anti-GA clone 5F2 (Mackenzie *et al*, 2013). Streptavidin plates (MSD Gold 96-well streptavidin) were coated overnight with biotinylated 5F2 antibody (capture antibody, 1:400) in PBS. The next day, the plates were washed three times (0.05% Tween-20, PBS) and blocked for 1 h at room temperature (0.05% Tween-20, 1% BSA in PBS). Plates were incubated with pre-cleared media (5 min, 1,000 g) for 2 h at room temperature on a shaking platform. After three washes, the plates were incubated with MSD sulfo-tag-labeled 5F2 antibody (detection antibody, 1:400) for 2 h at room temperature on a shaking platform followed by three final washing steps. Upon adding 100  $\mu$ l MSD Read Buffer T, the plates were immediately measured. The electrochemical signal was detected using a Meso Scale Discovery SECTOR Imager 2400. After background correction, data are presented in arbitrary units.

### Transfection, immunofluorescence, and filter trap

HEK293FT cells and primary rat neurons were transfected using Lipofectamine 2000 (Thermo Scientific) according to the manufacturer's instructions. For immunofluorescence, cells were fixed with 4% paraformaldehyde and 4% sucrose for 10 min and stained with the indicated antibodies in GDB buffer (0.1% gelatin, 0.3% Triton X-100, 450 mM NaCl, 16 mM sodium phosphate pH 7.4). Images were taken using an LSM710 confocal laser scanning system (Carl Zeiss) with 40 $\times$  or 63 $\times$  oil immersion objectives. For filter trap, cells were lysed in Triton buffer (1% Triton X-100, 15 mM MgCl<sub>2</sub> in PBS, supplemented with 10  $\mu$ g/ml DNase and protease inhibitor) on ice. Protein concentration was determined using BCA assay (Thermo Scientific), and equal amount of protein was used. Insoluble pellets were collected by centrifugation at 13,000 rpm/17,949 g at 4°C for 30 mins and resuspended in SDS-Tris buffer (2% SDS and 100 mM Tris pH = 7) for 1 h at room temperature. Samples were diluted in SDS-Tris buffer as indicated and filtered through a cellulose acetate membrane (0.2  $\mu$ m pore).

### Preparation of cell lysates and brain extracts for seeding

Transfected HEK293FT cells or human brain tissue were homogenized in 0.1% Triton X-100 PBS buffer supplemented with

DNase, protease inhibitor, and phosphatase inhibitor cocktails, and sonicated for 2  $\times$  20 pulses with 10% amplitude (Branson Digital Sonifier, W-250 D). After brief centrifugation (1,000 g for 5 min), the protein concentration in the supernatant was determined using BCA assay (Thermo Scientific). For the seeding assay, 25  $\mu$ g of cell lysates was applied. To promote aggregate uptake of brain lysates, 25  $\mu$ g of brain lysates was mixed with 4  $\mu$ l Lipofectamine 2000 as described previously (Sanders *et al*, 2014). To block the aggregation and spreading of poly-GA, brain lysates were pre-incubated with 2  $\mu$ g anti-GA antibodies [clone 5F2 (Mackenzie *et al*, 2013)] or mouse IgG2a as control for 16 h.

### Antibody treatment

HEK293 cells transfected with GA<sub>175</sub>-GFP were treated with anti-GA antibodies or mouse IgG2a isotype control at the indicated concentration for 3 days. To assess the efficacy of anti-GA antibodies in neurons, rat primary neurons were transduced with GA<sub>175</sub>-GFP on DIV 5 and treated with anti-GA antibodies or mouse IgG2a isotype control at 1  $\mu$ g/ml for 6 days. Cells were fixed and counterstained with DAPI. Fluorescence microscopy image of GA-GFP aggregation was taken using Cytation 3 image reader (BioTek). The percentage of poly-GA-positive cells normalized to total cells was quantified semi-automatically using BioTek Gen5 software. For filter trap, HEK293-T-REX GA<sub>149</sub>-GFP stable cells cultured in the presence of 10 ng/ml tetracycline were treated with anti-GA antibodies or isotype control.

### RNA isolation and qPCR

Total RNA was prepared using the RNeasy and QIAshredder kit (Qiagen) according to the manufacturer's instructions. RNA preparations were treated with RNase-Free DNase Set (Qiagen) to minimize residual DNA contamination. 2  $\mu$ g of RNA was used for reverse transcription with M-MLV Reverse Transcriptase (Promega) using oligo-(dT)<sub>12-18</sub> primer (Invitrogen). qRT-PCR was performed using CFX384 Real-Time System (Bio-Rad) with TaqMan technology. Primers and probes to the tag region of (G4C2)<sub>80</sub> construct were designed as described previously (Mori *et al*, 2016). Signals of repeat construct-derived cDNA were normalized to *GAPDH* cDNA according to  $\Delta\Delta C_T$  method.

### Flow cytometry and fluorescence-activated cell sorting

HEK293 cells transfected with GFP or RFP were harvested and resuspended in PBS containing 1% FCS and 0.1% (w/v) NaN<sub>3</sub> (FACS-PBS). To perform intracellular staining of GA<sub>80</sub>-flag, 1–2  $\times$  10<sup>6</sup> cells/staining were fixed with 4% PFA for 10 min at 37°C, washed once with PBS, permeabilized with FACS-PBS containing 0.1% (w/v) saponin (FACS-saponin), and incubated with 4% goat serum for 10 min at 4°C to block unspecific binding sites. Cells were then incubated with saturating amount of anti-DYKDDDDK/flag antibody (1:250) or rabbit IgG (1:250) as control for 30 min at 4°C in the dark, followed by a single wash and incubation with saturating amount of secondary antibody (Alexa Fluor 647-labeled anti-rabbit IgG) for 30 min at 4°C. Cells were then washed two times with flow cytometry buffer and analyzed using

**The paper explained****Problem**

Expansion of a (G4C2) repeat in *C9orf72* causes FTL and/or ALS by a gain-of-function mechanism. Patient brains show nuclear foci of the repeat RNA and cytoplasmic aggregates of five DPR proteins that result from non-conventional translation of sense and antisense repeat transcripts in all reading frames (poly-GA, poly-GP, poly-GR, poly-PA, poly-PR). Neither nuclear foci nor DPR inclusions correlate strongly with the areas of neurodegeneration, suggesting non-cell autonomous effects.

**Results**

We show that the hydrophobic DPR proteins poly-GA/GP/PA are transmitted between cells. poly-GA uptake from cell and brain extracts boosts aggregation of all DPR products in receiving cells expressing the repeat RNA. Unexpectedly, poly-GA also promotes repeat RNA expression and foci formation, suggesting a positive feedback loop leading to a vicious cycle of DPR expression and RNA toxicity. Specific antibodies reduce poly-GA aggregation in transfected cells and prevent DPR seeding from patient brain extracts.

**Impact**

Understanding the non-cell autonomous effects of DPR proteins and the positive feedback loop triggering further repeat RNA expression is crucial to elucidate how the global *C9orf72* repeat expansion triggers highly selective neurodegeneration in ALS and FTL. Blocking this vicious cycle using anti-DPR immunotherapy may help to treat *C9orf72* patients.

MACSQuant VYB (Miltenyi). Data analysis was performed using FlowJo vX software (Treestar).

To perform fluorescence-activated cell sorting of transmitted hydrophobic DPR proteins in a co-culture assay, HEK293 cells were transfected with RFP, GFP, or DPR-GFP for 24 h and mixed in the indicated combination for additional 24 h. Double-positive cells were sorted using a FACSaria Fusion (BD Biosciences) cell sorter and plated on poly-D-lysine-coated coverslips for imaging 17 h later.

**In situ hybridization**

*In situ* hybridization was performed as described previously with minor changes (Mori *et al*, 2016). Cells were fixed with 4% paraformaldehyde, rinsed twice with SSC, and then incubated in pre-hybridization solution (40% formamide, 2× SSC, 2.5% BSA) at 65°C for 30 min. Cells were then incubated with hybridization solution (40% formamide, 2× SSC, 0.8 mg/ml tRNA (Roche), 0.8 mg/ml single-stranded salmon sperm DNA (Sigma), 0.16% BSA, 8% dextran sulfate (Sigma), 1.6 mM ribonucleoside vanadyl complex (New England Biolabs), 5 mM EDTA, 10 μg/μl 5' Cy3-labeled 2'-O-methyl-(CCCCGG)<sub>4</sub> probe [IDT probe as in (DeJesus-Hernandez *et al*, 2011)] at 65°C for HeLa cells and 60°C for primary human fibroblasts. The following day, cells were sequentially washed with 40% formamide/0.5× SSC for three times 30 min each at 65°C and then with 0.5× SSC three times 10 min each at room temperature. After a brief rinse with PBS, nuclei were counterstained with 0.5 μg/ml of DAPI for 20 min and then washed three times with PBS (3 min each). Glass coverslips were mounted and analyzed on an LSM710 confocal microscope (Carl Zeiss).

**Patient tissue**

Patient tissue was collected and provided by the Neurobiobank Munich according to the guidelines of the ethical committee at the Medical Faculty of Ludwig-Maximilians-University (LMU) Munich following the WMA Declaration of Helsinki and the Department of Health and Human Services Belmont Report.

**Expanded View** for this article is available online.

**Acknowledgements**

We thank Bettina Schmid, Benjamin Schwenk, and Sabina Tahirovic for critical comments. We thank John Hardy for providing *C9orf72* and control fibroblast cell lines. This work was supported by the NOMIS Foundation (A.H., C.H. and D.E.), Hans und Ilse Breuer Foundation (D.E.), the Munich Cluster of Systems Neurology (SyNergy) (Q.Z., M.S., C.H. and D.E.), Takeda Science Foundation (K.M.) and JSPS KAKENHI 16H06953 (K.M.) and the European Community's Health Seventh Framework Programme 617198 [DPR-MODELS] (D.E.). D.B. is supported by the Emmy Noether Programme of the German Research Foundation (DFG; BA 5132/1-1). A.H. and C.H. are supported by the Helmholtz Virtual Institute "RNA dysmetabolism in ALS and FTD (VI-510)".

**Author contributions**

QZ and DE conceived the study, analyzed data, and wrote the manuscript with input from all co-authors. QZ, CL, MM, and FS performed experiments. KM, DA, DB, MHS, JG, DF, AF, RF, SM, TA, CK, TK, AH, and CH provided crucial reagents and/or expertise.

**Conflict of interest**

CH and DE applied for a patent on DPR detection and immunotherapy.

**References**

- Ash PE, Bieniek KF, Gendron TF, Caulfield T, Lin WL, DeJesus-Hernandez M, van Blitterswijk MM, Jansen-West K, Paul JW III, Rademakers R *et al* (2013) Unconventional translation of C9ORF72 GGGGCC expansion generates insoluble polypeptides specific to c9FTD/ALS. *Neuron* 77: 639–646
- Boutajangout A, Ingadottir J, Davies P, Sigurdsson EM (2011) Passive immunization targeting pathological phospho-tau protein in a mouse model reduces functional decline and clears tau aggregates from the brain. *J Neurochem* 118: 658–667
- Braak H, Alafuzoff I, Arzberger T, Kretschmar H, Del Tredici K (2006) Staging of Alzheimer disease-associated neurofibrillary pathology using paraffin sections and immunocytochemistry. *Acta Neuropathol* 112: 389–404
- Chai X, Wu S, Murray TK, Kinley R, Cella CV, Sims H, Buckner N, Hanmer J, Davies P, O'Neill MJ *et al* (2011) Passive immunization with anti-Tau antibodies in two transgenic models: reduction of Tau pathology and delay of disease progression. *J Biol Chem* 286: 34457–34467
- Chai X, Dage JL, Citron M (2012) Constitutive secretion of tau protein by an unconventional mechanism. *Neurobiol Dis* 48: 356–366
- Chang YJ, Jeng US, Chiang YL, Hwang IS, Chen YR (2016) The glycine-alanine dipeptide repeat from C9orf72 hexanucleotide expansions forms toxic amyloids possessing cell-to-cell transmission properties. *J Biol Chem* 291: 4903–4911
- Chew J, Gendron TF, Prudencio M, Sasaguri H, Zhang YJ, Castanedes-Casey M, Lee CW, Jansen-West K, Kurti A, Murray ME *et al* (2015)

- Neurodegeneration. C9orf72 repeat expansions in mice cause TDP-43 pathology, neuronal loss, and behavioral deficits. *Science* 348: 1151–1154
- DeJesus-Hernandez M, Mackenzie IR, Boeve BF, Boxer AL, Baker M, Rutherford NJ, Nicholson AM, Finch NA, Flynn H, Adamson J et al (2011) Expanded GGGGCC hexanucleotide repeat in noncoding region of C9orf72 causes chromosome 9p-linked FTD and ALS. *Neuron* 72: 245–256
- Edbauer D, Haass C (2016) An amyloid-like cascade hypothesis for C9orf72 ALS/FTD. *Curr Opin Neurobiol* 36: 99–106
- Fleck D, van Bebber F, Colombo A, Galante C, Schwenk BM, Rabe L, Hampel H, Novak B, Kremmer E, Tahirovic S et al (2013) Dual cleavage of neuregulin 1 type III by BACE1 and ADAM17 liberates its EGF-like domain and allows paracrine signaling. *J Neurosci* 33: 7856–7869
- Gijselincx I, Van Langenhove T, van der Zee J, Slegers K, Philtjens S, Kleinberger G, Janssens J, Bettens K, Van Cauwenberghe C, Pereson S et al (2012) A C9orf72 promoter repeat expansion in a Flanders-Belgian cohort with disorders of the frontotemporal lobar degeneration-amyotrophic lateral sclerosis spectrum: a gene identification study. *Lancet Neurol* 11: 54–65
- Iba M, McBride JD, Guo JL, Zhang B, Trojanowski JQ, Lee VM (2015) Tau pathology spread in PS19 tau transgenic mice following locus coeruleus (LC) injections of synthetic tau fibrils is determined by the LC's afferent and efferent connections. *Acta Neuropathol* 130: 349–362
- Japtok J, Lojewski X, Naumann M, Klingenstein M, Reinhardt P, Sternecker J, Putz S, Demestre M, Boeckers TM, Ludolph AC et al (2015) Stepwise acquirement of hallmark neuropathology in FUS-ALS iPSC models depends on mutation type and neuronal aging. *Neurobiol Dis* 82: 420–429
- Jiang J, Zhu Q, Gendron TF, Saberi S, McAlonis-Downes M, Seelman A, Stauffer JE, Jafar-Nejad P, Drenner K, Schulte D et al (2016) Gain of toxicity from ALS/FTD-linked repeat expansions in C9orf72 is alleviated by antisense oligonucleotides targeting GGGGCC-containing RNAs. *Neuron* 90: 535–550
- Jucker M, Walker LC (2011) Pathogenic protein seeding in Alzheimer disease and other neurodegenerative disorders. *Ann Neurol* 70: 532–540
- Kanekura K, Yagi T, Cammack AJ, Mahadevan J, Kuroda M, Harms MB, Miller TM, Urano F (2016) Poly-dipeptides encoded by the C9orf72 repeats block global protein translation. *Hum Mol Genet* 25: 1803–1813
- Kwon I, Xiang S, Kato M, Wu L, Theodoropoulos P, Wang T, Kim J, Yun J, Xie Y, McKnight SL (2014) Poly-dipeptides encoded by the C9orf72 repeats bind nucleoli, impede RNA biogenesis, and kill cells. *Science* 345: 1139–1145
- Liu Y, Pattamatta A, Zu T, Reid T, Bardhi O, Borchelt DR, Yachnis AT, Ranum LP (2016) C9orf72 BAC mouse model with motor deficits and neurodegenerative features of ALS/FTD. *Neuron* 90: 521–534
- Mackenzie IR, Arzberger T, Kremmer E, Troost D, Lorenz S, Mori K, Weng SM, Haass C, Kretzschmar HA, Edbauer D et al (2013) Dipeptide repeat protein pathology in C9orf72 mutation cases: clinico-pathological correlations. *Acta Neuropathol* 126: 859–879
- May S, Hornburg D, Schludi MH, Arzberger T, Rentzsch K, Schwenk BM, Grasser FA, Mori K, Kremmer E, Banzhaf-Strathmann J et al (2014) C9orf72 FTL/ALS-associated Gly-Ala dipeptide repeat proteins cause neuronal toxicity and Unc119 sequestration. *Acta Neuropathol* 128: 485–503
- Mori K, Arzberger T, Grasser FA, Gijselincx I, May S, Rentzsch K, Weng SM, Schludi MH, van der Zee J, Cruts M et al (2013a) Bidirectional transcripts of the expanded C9orf72 hexanucleotide repeat are translated into aggregating dipeptide repeat proteins. *Acta Neuropathol* 126: 881–893
- Mori K, Lammich S, Mackenzie IR, Forne I, Zilow S, Kretzschmar H, Edbauer D, Janssens J, Kleinberger G, Cruts M et al (2013b) hnRNP A3 binds to GGGGCC repeats and is a constituent of p62-positive/TDP43-negative inclusions in the hippocampus of patients with C9orf72 mutations. *Acta Neuropathol* 125: 413–423
- Mori K, Weng SM, Arzberger T, May S, Rentzsch K, Kremmer E, Schmid B, Kretzschmar HA, Cruts M, Van Broeckhoven C et al (2013c) The C9orf72 GGGGCC repeat is translated into aggregating dipeptide-repeat proteins in FTL/ALS. *Science* 339: 1335–1338
- Mori K, Nihei Y, Arzberger T, Zhou Q, Mackenzie IR, Hermann A, Hanisch F, German Consortium for Frontotemporal Lobar D, Bavarian Brain Banking A, Kamp F, Nuscher B, Orozco D, Edbauer D, Haass C (2016) Reduced hnRNP3 increases C9orf72 repeat RNA levels and dipeptide-repeat protein deposition. *EMBO Rep* 17: 1314–1325
- Mizielinska S, Gronke S, Niccoli T, Ridler CE, Clayton EL, Devoy A, Moens T, Norona FE, Woollacott IO, Pietrzyk J et al (2014) C9orf72 repeat expansions cause neurodegeneration in *Drosophila* through arginine-rich proteins. *Science* 345: 1192–1194
- Nonaka T, Watanabe ST, Iwatsubo T, Hasegawa M (2010) Seeded aggregation and toxicity of {alpha}-synuclein and tau: cellular models of neurodegenerative diseases. *J Biol Chem* 285: 34885–34898
- Proudfoot M, Gutowski NJ, Edbauer D, Hilton DA, Stephens M, Rankin J, Mackenzie IR (2014) Early dipeptide repeat pathology in a frontotemporal dementia kindred with C9orf72 mutation and intellectual disability. *Acta Neuropathol* 127: 451–458
- Renton AE, Majounie E, Waite A, Simon-Sanchez J, Rollinson S, Gibbs JR, Schymick JC, Laaksovirta H, van Swieten JC, Myllykangas L et al (2011) A hexanucleotide repeat expansion in C9orf72 is the cause of chromosome 9p21-linked ALS-FTD. *Neuron* 72: 257–268
- Rohrer JD, Nicholas JM, Cash DM, van Swieten J, Dopfer E, Jiskoot L, van Minkelen R, Rombouts SA, Cardoso MJ, Clegg S et al (2015) Presymptomatic cognitive and neuroanatomical changes in genetic frontotemporal dementia in the Genetic Frontotemporal dementia Initiative (GENFI) study: a cross-sectional analysis. *Lancet Neurol* 14: 253–262
- Sanders DW, Kaufman SK, DeVos SL, Sharma AM, Mirbaha H, Li A, Barker SJ, Foley AC, Thorpe JR, Serpell LC et al (2014) Distinct tau prion strains propagate in cells and mice and define different tauopathies. *Neuron* 82: 1271–1288
- Schludi MH, May S, Grasser FA, Rentzsch K, Kremmer E, Kupper C, Klopstock T, German Consortium for Frontotemporal Lobar Degeneration, Alliance BBB, Arzberger T, Edbauer D (2015) Distribution of dipeptide repeat proteins in cellular models and C9orf72 mutation cases suggests link to transcriptional silencing. *Acta Neuropathol* 130: 537–555
- Sevigny J, Chiao P, Bussiere T, Weinreb PH, Williams L, Maier M, Dunstan R, Salloway S, Chen T, Ling Y et al (2016) The antibody aducanumab reduces Abeta plaques in Alzheimer's disease. *Nature* 537: 50–56
- Stohr J, Watts JC, Mensinger ZL, Oehler A, Grillo SK, DeArmond SJ, Prusiner SB, Giles K (2012) Purified and synthetic Alzheimer's amyloid beta (Abeta) prions. *Proc Natl Acad Sci USA* 109: 11025–11030
- Su Z, Zhang Y, Gendron TF, Bauer PO, Chew J, Yang WY, Fostvedt E, Jansen-West K, Belzil VV, Desaro P et al (2014) Discovery of a biomarker and lead small molecules to target r(GGGGCC)-associated defects in c9FTD/ALS. *Neuron* 83: 1043–1050
- Takeda S, Wegmann S, Cho H, DeVos SL, Commins C, Roe AD, Nicholls SB, Carlson GA, Pitstick R, Nobuhara CK et al (2015) Neuronal uptake and propagation of a rare phosphorylated high-molecular-weight tau derived from Alzheimer's disease brain. *Nat Commun* 6: 8490

- Tran H, Almeida S, Moore J, Gendron TF, Chalasani U, Lu Y, Du X, Nickerson JA, Petrucelli L, Weng Z *et al* (2015) Differential toxicity of nuclear RNA foci versus dipeptide repeat proteins in a *Drosophila* model of C9ORF72 FTD/ALS. *Neuron* 87: 1207–1214
- Westergard T, Jensen BK, Wen X, Cai J, Kropf E, Iacovitti L, Pasinelli P, Trotti D (2016) Cell-to-cell transmission of dipeptide repeat proteins linked to C9orf72-ALS/FTD. *Cell Rep* 17: 645–652
- Yanamandra K, Kfoury N, Jiang H, Mahan TE, Ma S, Maloney SE, Wozniak DF, Diamond MI, Holtzman DM (2013) Anti-tau antibodies that block tau aggregate seeding *in vitro* markedly decrease pathology and improve cognition *in vivo*. *Neuron* 80: 402–414
- Zhang YJ, Jansen-West K, Xu YF, Gendron TF, Bieniek KF, Lin WL, Sasaguri H, Caulfield T, Hubbard J, Daugherty L *et al* (2014) Aggregation-prone c9FTD/

ALS poly(GA) RAN-translated proteins cause neurotoxicity by inducing ER stress. *Acta Neuropathol* 128: 505–524

- Zu T, Gibbens B, Doty NS, Gomes-Pereira M, Huguet A, Stone MD, Margolis J, Peterson M, Markowski TW, Ingram MA *et al* (2011) Non-ATG-initiated translation directed by microsatellite expansions. *Proc Natl Acad Sci USA* 108: 260–265



**License:** This is an open access article under the terms of the Creative Commons Attribution 4.0 License, which permits use, distribution and reproduction in any medium, provided the original work is properly cited.

## Expanded View Figures

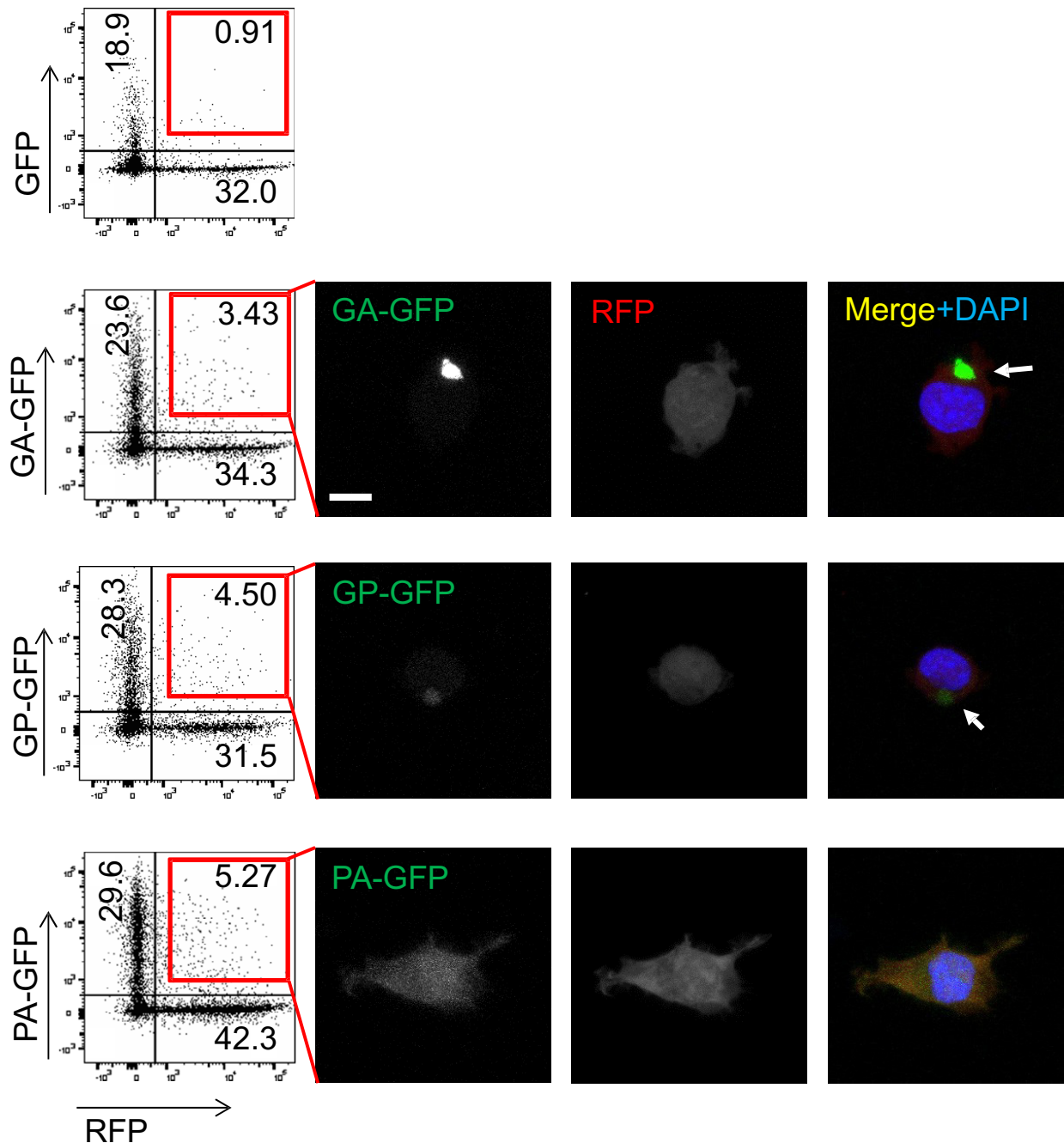


**Figure EV1. Transmission of hydrophobic DPR proteins in a co-culture assay.**

HEK293 cells were transfected with RFP, GFP, or DPR-GFP for 24 h and mixed in the indicated combination for additional 24 h as in Fig 2 before cell sorting by flow cytometry. Gating was performed on RFP-expressing cells vs. mixture of all green fluorescent cells. The fraction of double-positive cells is indicated in percent. Double-positive cells were sorted and plated on poly-D-lysine-coated coverslips and imaged 17 h later. Images show uptake of DPR-GFP into RFP-positive cells. Arrows indicate co-localization of  $GA_{175}$ -RFP aggregates with  $GA_{175}$ -GFP and  $GP_{47}$ -GFP. Scale bar 10  $\mu$ m.

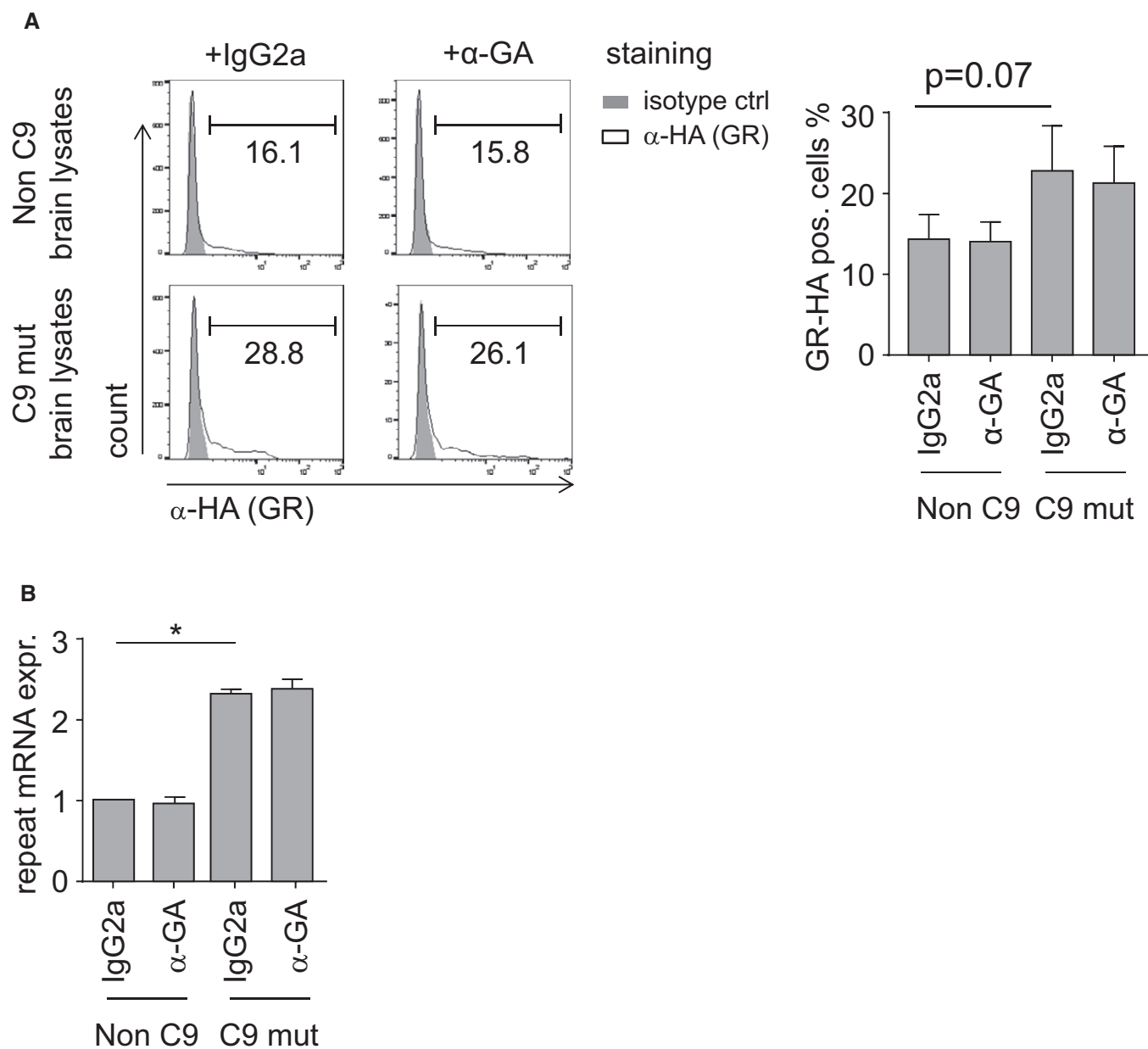


**Figure EV2. Anti-GA antibodies do not reduce expression of poly-GR and repeat RNA.**

HEK293 cells transfected with (G4C2)<sub>80</sub> were treated with cerebellar extracts pre-incubated with anti-GA or isotype control.

**A** The fraction of RAN translation-derived GR<sub>80</sub>-HA was quantified by flow cytometry. Data indicated the means  $\pm$  SD of  $n = 3$  patients and controls in independent experiments. Statistics were performed by one-way ANOVA with Dunnett's multiple comparisons test.

**B** Quantitative RT-PCR shows repeat RNA transcripts upon treatment with cerebellar extracts pre-incubated with anti-GA or isotype control. Data are shown as mean  $\pm$  SD from  $n = 3$  patients and controls in independent experiments. Statistics were performed by one-way ANOVA with Dunnett's multiple comparisons test; non-C9 + IgG2a vs. C9 mut + IgG2a  $P = 0.0168$ ;  $*P < 0.05$ .

### **Contribution to Publication IV**

As second author of this publication, I conducted experiments shown in Fig. 4C, D and Fig. 5.

## References

- Ajrout-Driss, S., Fecto, F., Ajroud, K., Lalani, I., Calvo, S.E., Mootha, V.K., Deng, H.X., Siddique, N., Tahmouh, A.J., Heiman-Patterson, T.D., *et al.* (2015). Mutation in the novel nuclear-encoded mitochondrial protein CHCHD10 in a family with autosomal dominant mitochondrial myopathy. *Neurogenetics* 16, 1-9.
- Al-Chalabi, A., Hardiman, O., Kiernan, M.C., Chio, A., Rix-Brooks, B., and van den Berg, L.H. (2016). Amyotrophic lateral sclerosis: moving towards a new classification system. *Lancet Neurol* 15, 1182-1194.
- Al-Sarraj, S., King, A., Troakes, C., Smith, B., Maekawa, S., Bodi, I., Rogelj, B., Al-Chalabi, A., Hortobagyi, T., and Shaw, C.E. (2011). p62 positive, TDP-43 negative, neuronal cytoplasmic and intranuclear inclusions in the cerebellum and hippocampus define the pathology of C9orf72-linked FTL and MND/ALS. *Acta neuropathologica* 122, 691-702.
- Alberti, S., and Hyman, A.A. (2016). Are aberrant phase transitions a driver of cellular aging? *BioEssays : news and reviews in molecular, cellular and developmental biology* 38, 959-968.
- Arai, T., Hasegawa, M., Akiyama, H., Ikeda, K., Nonaka, T., Mori, H., Mann, D., Tsuchiya, K., Yoshida, M., Hashizume, Y., *et al.* (2006). TDP-43 is a component of ubiquitin-positive tau-negative inclusions in frontotemporal lobar degeneration and amyotrophic lateral sclerosis. *Biochemical and biophysical research communications* 351, 602-611.
- Auranen, M., Ylikallio, E., Shcherbii, M., Paetau, A., Kiuru-Enari, S., Toppila, J.P., and Tynismaa, H. (2015). CHCHD10 variant p.(Gly66Val) causes axonal Charcot-Marie-Tooth disease. *Neurology Genetics* 1, e1.
- Baborie, A., Griffiths, T.D., Jaros, E., Perry, R., McKeith, I.G., Burn, D.J., Masuda-Suzukake, M., Hasegawa, M., Rollinson, S., Pickering-Brown, S., *et al.* (2015). Accumulation of dipeptide repeat proteins predates that of TDP-43 in frontotemporal lobar degeneration associated with hexanucleotide repeat expansions in C9ORF72 gene. *Neuropathology and applied neurobiology* 41, 601-612.
- Baker, M., Mackenzie, I.R., Pickering-Brown, S.M., Gass, J., Rademakers, R., Lindholm, C., Snowden, J., Adamson, J., Sadovnick, A.D., Rollinson, S., *et al.* (2006). Mutations in progranulin cause tau-negative frontotemporal dementia linked to chromosome 17. *Nature* 442, 916-919.
- Balendra, R., Moens, T.G., and Isaacs, A.M. (2017). Specific biomarkers for C9orf72 FTD/ALS could expedite the journey towards effective therapies. *EMBO molecular medicine* 9, 853-855.
- Banci, L., Bertini, I., Cefaro, C., Ciofi-Baffoni, S., Gallo, A., Martinelli, M., Sideris, D.P., Katrakili, N., and Tokatlidis, K. (2009a). MIA40 is an oxidoreductase that catalyzes oxidative protein folding in mitochondria. *Nat Struct Mol Biol* 16, 198-206.
- Banci, L., Bertini, I., Ciofi-Baffoni, S., and Tokatlidis, K. (2009b). The coiled coil-helix-coiled coil-helix proteins may be redox proteins. *FEBS letters* 583, 1699-1702.
- Bang, J., Spina, S., and Miller, B.L. (2015). Frontotemporal dementia. *Lancet* 386, 1672-1682.
- Bannwarth, S., Ait-El-Mkadem, S., Chausse, A., Genin, E.C., Lacas-Gervais, S., Fragaki, K., Berg-Alonso, L., Kageyama, Y., Serre, V., Moore, D.G., *et al.* (2014). A mitochondrial origin for frontotemporal dementia and amyotrophic lateral sclerosis through CHCHD10 involvement. *Brain* 137, 2329-2345.
- Bauerlein, F.J.B., Saha, I., Mishra, A., Kalemans, M., Martinez-Sanchez, A., Klein, R., Dudanova, I., Hipp, M.S., Hartl, F.U., Baumeister, W., *et al.* (2017). In Situ Architecture and Cellular Interactions of PolyQ Inclusions. *Cell* 171, 179-187 e110.
- Bensimon, G., Lacomblez, L., and Meininger, V. (1994). A controlled trial of riluzole in amyotrophic lateral sclerosis. ALS/Riluzole Study Group. *The New England journal of medicine* 330, 585-591.

- Berrios, G.E., and Girling, D.M. (1994). Introduction: Pick's disease and the 'frontal lobe' dementias. *History of psychiatry* 5, 539-547.
- Blauwendraat, C., Wilke, C., Simon-Sanchez, J., Jansen, I.E., Reifschneider, A., Capell, A., Haass, C., Castillo-Lizardo, M., Biskup, S., Maetzler, W., *et al.* (2018). The wide genetic landscape of clinical frontotemporal dementia: systematic combined sequencing of 121 consecutive subjects. *Genetics in medicine : official journal of the American College of Medical Genetics* 20, 240-249.
- Borrioni, B., Ferrari, F., Galimberti, D., Nacmias, B., Barone, C., Bagnoli, S., Fenoglio, C., Piaceri, I., Archetti, S., Bonvicini, C., *et al.* (2014). Heterozygous TREM2 mutations in frontotemporal dementia. *Neurobiology of aging* 35, 934 e937-910.
- Braak, H., and Braak, E. (1991). Neuropathological staging of Alzheimer-related changes. *Acta neuropathologica* 82, 239-259.
- Brettschneider, J., Arai, K., Del Tredici, K., Toledo, J.B., Robinson, J.L., Lee, E.B., Kuwabara, S., Shibuya, K., Irwin, D.J., Fang, L., *et al.* (2014). TDP-43 pathology and neuronal loss in amyotrophic lateral sclerosis spinal cord. *Acta neuropathologica* 128, 423-437.
- Brockmann, S.J., Freischmidt, A., Oeckl, P., Muller, K., Ponna, S.K., Helferich, A.M., Paone, C., Reinders, J., Kojer, K., Orth, M., *et al.* (2018). CHCHD10 mutations p.R15L and p.G66V cause motoneuron disease by haploinsufficiency. *Human molecular genetics* 27, 706-715.
- Brooks, B.R., Miller, R.G., Swash, M., Munsat, T.L., and World Federation of Neurology Research Group on Motor Neuron, D. (2000). El Escorial revisited: revised criteria for the diagnosis of amyotrophic lateral sclerosis. *Amyotroph Lateral Scler Other Motor Neuron Disord* 1, 293-299.
- Burrell, J.R., Kiernan, M.C., Vucic, S., and Hodges, J.R. (2011). Motor neuron dysfunction in frontotemporal dementia. *Brain* 134, 2582-2594.
- Burstein, S.R., Valsecchi, F., Kawamata, H., Bourens, M., Zeng, R., Zuberi, A., Milner, T.A., Cloonan, S.M., Lutz, C., Barrientos, A., *et al.* (2018). In vitro and in vivo studies of the ALS-FTLD protein CHCHD10 reveal novel mitochondrial topology and protein interactions. *Human molecular genetics* 27, 160-177.
- Byrne, S., Elamin, M., Bede, P., Shatunov, A., Walsh, C., Corr, B., Heverin, M., Jordan, N., Kenna, K., Lynch, C., *et al.* (2012). Cognitive and clinical characteristics of patients with amyotrophic lateral sclerosis carrying a C9orf72 repeat expansion: a population-based cohort study. *Lancet Neurol* 11, 232-240.
- Chacinska, A., Pfannschmidt, S., Wiedemann, N., Kozjak, V., Sanjuan Szklarz, L.K., Schulze-Specking, A., Truscott, K.N., Guiard, B., Meisinger, C., and Pfanner, N. (2004). Essential role of Mia40 in import and assembly of mitochondrial intermembrane space proteins. *The EMBO journal* 23, 3735-3746.
- Chang, Y.J., Jeng, U.S., Chiang, Y.L., Hwang, I.S., and Chen, Y.R. (2016). The Glycine-Alanine Dipeptide Repeat from C9orf72 Hexanucleotide Expansions Forms Toxic Amyloids Possessing Cell-to-Cell Transmission Properties. *J Biol Chem* 291, 4903-4911.
- Chattopadhyay, M., Durazo, A., Sohn, S.H., Strong, C.D., Gralla, E.B., Whitelegge, J.P., and Valentine, J.S. (2008). Initiation and elongation in fibrillation of ALS-linked superoxide dismutase. *Proceedings of the National Academy of Sciences of the United States of America* 105, 18663-18668.
- Chaussonot, A., Le Ber, I., Ait-El-Mkadem, S., Camuzat, A., de Septenville, A., Bannwarth, S., Genin, E.C., Serre, V., Auge, G., French research network on, F.T.D., *et al.* (2014). Screening of CHCHD10 in a French cohort confirms the involvement of this gene in frontotemporal dementia with amyotrophic lateral sclerosis patients. *Neurobiol Aging* 35, 2884 e2881-2884.
- Cheroni, C., Marino, M., Tortarolo, M., Veglianesi, P., De Biasi, S., Fontana, E., Zuccarello, L.V., Maynard, C.J., Dantuma, N.P., and Bendotti, C. (2009). Functional alterations of the ubiquitin-proteasome system in motor neurons of a mouse model of familial amyotrophic lateral sclerosis. *Human molecular genetics* 18, 82-96.

Chio, A., Borghero, G., Restagno, G., Mora, G., Drepper, C., Traynor, B.J., Sendtner, M., Brunetti, M., Ossola, I., Calvo, A., *et al.* (2012). Clinical characteristics of patients with familial amyotrophic lateral sclerosis carrying the pathogenic GGGGCC hexanucleotide repeat expansion of C9ORF72. *Brain* 135, 784-793.

Chio, A., Logroscino, G., Traynor, B.J., Collins, J., Simeone, J.C., Goldstein, L.A., and White, L.A. (2013). Global epidemiology of amyotrophic lateral sclerosis: a systematic review of the published literature. *Neuroepidemiology* 41, 118-130.

Ciechanover, A., and Kwon, Y.T. (2015). Degradation of misfolded proteins in neurodegenerative diseases: therapeutic targets and strategies. *Experimental & molecular medicine* 47, e147.

Cirulli, E.T., Lasseigne, B.N., Petrovski, S., Sapp, P.C., Dion, P.A., Leblond, C.S., Couthouis, J., Lu, Y.F., Wang, Q., Krueger, B.J., *et al.* (2015). Exome sequencing in amyotrophic lateral sclerosis identifies risk genes and pathways. *Science* 347, 1436-1441.

Ciura, S., Lattante, S., Le Ber, I., Latouche, M., Tostivint, H., Brice, A., and Kabashi, E. (2013). Loss of function of C9orf72 causes motor deficits in a zebrafish model of amyotrophic lateral sclerosis. *Ann Neurol* 74, 180-187.

Conicella, A.E., Zerze, G.H., Mittal, J., and Fawzi, N.L. (2016). ALS Mutations Disrupt Phase Separation Mediated by alpha-Helical Structure in the TDP-43 Low-Complexity C-Terminal Domain. *Structure* 24, 1537-1549.

Contreras, L., Drago, I., Zampese, E., and Pozzan, T. (2010). Mitochondria: the calcium connection. *Biochimica et biophysica acta* 1797, 607-618.

Cooper-Knock, J., Walsh, M.J., Higginbottom, A., Robin Highley, J., Dickman, M.J., Edbauer, D., Ince, P.G., Wharton, S.B., Wilson, S.A., Kirby, J., *et al.* (2014). Sequestration of multiple RNA recognition motif-containing proteins by C9orf72 repeat expansions. *Brain* 137, 2040-2051.

Courchaine, E.M., Lu, A., and Neugebauer, K.M. (2016). Droplet organelles? *The EMBO journal* 35, 1603-1612.

Cozzolino, M., Rossi, S., Mirra, A., and Carri, M.T. (2015). Mitochondrial dynamism and the pathogenesis of Amyotrophic Lateral Sclerosis. *Frontiers in cellular neuroscience* 9, 31.

Cruts, M., Gijssels, I., van der Zee, J., Engelborghs, S., Wils, H., Pirici, D., Rademakers, R., Vandenberghe, R., Dermaut, B., Martin, J.J., *et al.* (2006). Null mutations in progranulin cause ubiquitin-positive frontotemporal dementia linked to chromosome 17q21. *Nature* 442, 920-924.

Cruz, M.P. (2018). Edaravone (Radicava): A Novel Neuroprotective Agent for the Treatment of Amyotrophic Lateral Sclerosis. *P & T : a peer-reviewed journal for formulary management* 43, 25-28.

Dabir, D.V., Leverich, E.P., Kim, S.K., Tsai, F.D., Hirasawa, M., Knaff, D.B., and Koehler, C.M. (2007). A role for cytochrome c and cytochrome c peroxidase in electron shuttling from Erv1. *The EMBO journal* 26, 4801-4811.

Dai, R.M., and Li, C.C. (2001). Valosin-containing protein is a multi-ubiquitin chain-targeting factor required in ubiquitin-proteasome degradation. *Nature cell biology* 3, 740-744.

Damiano, M., Starkov, A.A., Petri, S., Kipiani, K., Kiaei, M., Mattiazzi, M., Flint Beal, M., and Manfredi, G. (2006). Neural mitochondrial Ca<sup>2+</sup> capacity impairment precedes the onset of motor symptoms in G93A Cu/Zn-superoxide dismutase mutant mice. *Journal of neurochemistry* 96, 1349-1361.

DeJesus-Hernandez, M., Mackenzie, I.R., Boeve, B.F., Boxer, A.L., Baker, M., Rutherford, N.J., Nicholson, A.M., Finch, N.A., Flynn, H., Adamson, J., *et al.* (2011). Expanded GGGGCC hexanucleotide repeat in noncoding region of C9ORF72 causes chromosome 9p-linked FTD and ALS. *Neuron* 72, 245-256.

Deng, H.X., Chen, W., Hong, S.T., Boycott, K.M., Gorrie, G.H., Siddique, N., Yang, Y., Fecto, F., Shi, Y., Zhai, H., *et al.* (2011). Mutations in UBQLN2 cause dominant X-linked juvenile and adult-onset ALS and ALS/dementia. *Nature* *477*, 211-215.

Deng, J., Yang, M., Chen, Y., Chen, X., Liu, J., Sun, S., Cheng, H., Li, Y., Bigio, E.H., Mesulam, M., *et al.* (2015). FUS Interacts with HSP60 to Promote Mitochondrial Damage. *PLoS genetics* *11*, e1005357.

Dolle, C., Flonas, I., Nido, G.S., Miletic, H., Osuagwu, N., Kristoffersen, S., Lilleng, P.K., Larsen, J.P., Tysnes, O.B., Haugarvoll, K., *et al.* (2016). Defective mitochondrial DNA homeostasis in the substantia nigra in Parkinson disease. *Nature communications* *7*, 13548.

Dols-Icardo, O., Garcia-Redondo, A., Rojas-Garcia, R., Sanchez-Valle, R., Noguera, A., Gomez-Tortosa, E., Pastor, P., Hernandez, I., Esteban-Perez, J., Suarez-Calvet, M., *et al.* (2014). Characterization of the repeat expansion size in C9orf72 in amyotrophic lateral sclerosis and frontotemporal dementia. *Human molecular genetics* *23*, 749-754.

Donnelly, C.J., Zhang, P.W., Pham, J.T., Haeusler, A.R., Mistry, N.A., Vidensky, S., Daley, E.L., Poth, E.M., Hoover, B., Fines, D.M., *et al.* (2013). RNA toxicity from the ALS/FTD C9ORF72 expansion is mitigated by antisense intervention. *Neuron* *80*, 415-428.

Driscoll, J., and Goldberg, A.L. (1989). Skeletal muscle proteasome can degrade proteins in an ATP-dependent process that does not require ubiquitin. *Proceedings of the National Academy of Sciences of the United States of America* *86*, 787-791.

Dudek, J., Rehling, P., and van der Laan, M. (2013). Mitochondrial protein import: common principles and physiological networks. *Biochimica et biophysica acta* *1833*, 274-285.

Edbauer, D., and Haass, C. (2016). An amyloid-like cascade hypothesis for C9orf72 ALS/FTD. *Current opinion in neurobiology* *36*, 99-106.

Elmore, S. (2007). Apoptosis: a review of programmed cell death. *Toxicologic pathology* *35*, 495-516.

Eytan, E., Ganoth, D., Armon, T., and Hershko, A. (1989). ATP-dependent incorporation of 20S protease into the 26S complex that degrades proteins conjugated to ubiquitin. *Proceedings of the National Academy of Sciences of the United States of America* *86*, 7751-7755.

Farg, M.A., Sundaramoorthy, V., Sultana, J.M., Yang, S., Atkinson, R.A., Levina, V., Halloran, M.A., Gleeson, P.A., Blair, I.P., Soo, K.Y., *et al.* (2014). C9ORF72, implicated in amyotrophic lateral sclerosis and frontotemporal dementia, regulates endosomal trafficking. *Human molecular genetics* *23*, 3579-3595.

Fecto, F., Yan, J., Vemula, S.P., Liu, E., Yang, Y., Chen, W., Zheng, J.G., Shi, Y., Siddique, N., Arrat, H., *et al.* (2011). SQSTM1 mutations in familial and sporadic amyotrophic lateral sclerosis. *Arch Neurol* *68*, 1440-1446.

Ferrari, R., Kapogiannis, D., Huey, E.D., and Momeni, P. (2011). FTD and ALS: a tale of two diseases. *Current Alzheimer research* *8*, 273-294.

Filimonenko, M., Stuffers, S., Raiborg, C., Yamamoto, A., Malerod, L., Fisher, E.M., Isaacs, A., Brech, A., Stenmark, H., and Simonsen, A. (2007). Functional multivesicular bodies are required for autophagic clearance of protein aggregates associated with neurodegenerative disease. *The Journal of cell biology* *179*, 485-500.

Fitzpatrick, A.W.P., Falcon, B., He, S., Murzin, A.G., Murshudov, G., Garringer, H.J., Crowther, R.A., Ghetti, B., Goedert, M., and Scheres, S.H.W. (2017). Cryo-EM structures of tau filaments from Alzheimer's disease. *Nature* *547*, 185-190.

Frazier, A.E., Dudek, J., Guiard, B., Voos, W., Li, Y., Lind, M., Meisinger, C., Geissler, A., Sickmann, A., Meyer, H.E., *et al.* (2004). Pam16 has an essential role in the mitochondrial protein import motor. *Nature structural & molecular biology* *11*, 226-233.

Gao, F., Yang, J., Wang, D., Li, C., Fu, Y., Wang, H., He, W., and Zhang, J. (2017). Mitophagy in Parkinson's Disease: Pathogenic and Therapeutic Implications. *Frontiers in neurology* 8, 527.

Gendron, T.F., Bieniek, K.F., Zhang, Y.J., Jansen-West, K., Ash, P.E., Caulfield, T., Daugherty, L., Dunmore, J.H., Castanedes-Casey, M., Chew, J., *et al.* (2013). Antisense transcripts of the expanded C9ORF72 hexanucleotide repeat form nuclear RNA foci and undergo repeat-associated non-ATG translation in c9FTD/ALS. *Acta neuropathologica* 126, 829-844.

Genin, E.C., Plutino, M., Bannwarth, S., Villa, E., Cisneros-Barroso, E., Roy, M., Ortega-Vila, B., Fragaki, K., Lespinasse, F., Pinero-Martos, E., *et al.* (2016). CHCHD10 mutations promote loss of mitochondrial cristae junctions with impaired mitochondrial genome maintenance and inhibition of apoptosis. *EMBO molecular medicine* 8, 58-72.

Gitler, A.D., and Shorter, J. (2011). RNA-binding proteins with prion-like domains in ALS and FTL-D. *Prion* 5, 179-187.

Gitler, A.D., and Tsuiji, H. (2016). There has been an awakening: Emerging mechanisms of C9orf72 mutations in FTD/ALS. *Brain research* 1647, 19-29.

Goode, A., Butler, K., Long, J., Cavey, J., Scott, D., Shaw, B., Sollenberger, J., Gell, C., Johansen, T., Oldham, N.J., *et al.* (2016). Defective recognition of LC3B by mutant SQSTM1/p62 implicates impairment of autophagy as a pathogenic mechanism in ALS-FTLD. *Autophagy* 12, 1094-1104.

Gorno-Tempini, M.L., Hillis, A.E., Weintraub, S., Kertesz, A., Mendez, M., Cappa, S.F., Ogar, J.M., Rohrer, J.D., Black, S., Boeve, B.F., *et al.* (2011). Classification of primary progressive aphasia and its variants. *Neurology* 76, 1006-1014.

Gozes, I. (2017). Specific protein biomarker patterns for Alzheimer's disease: improved diagnostics in progress. *The EPMA journal* 8, 255-259.

Grad, L.I., Guest, W.C., Yanai, A., Pokrishevsky, E., O'Neill, M.A., Gibbs, E., Semenchenko, V., Yousefi, M., Wishart, D.S., Plotkin, S.S., *et al.* (2011). Intermolecular transmission of superoxide dismutase 1 misfolding in living cells. *Proceedings of the National Academy of Sciences of the United States of America* 108, 16398-16403.

Green, K.N., Steffan, J.S., Martinez-Coria, H., Sun, X., Schreiber, S.S., Thompson, L.M., and LaFerla, F.M. (2008). Nicotinamide restores cognition in Alzheimer's disease transgenic mice via a mechanism involving sirtuin inhibition and selective reduction of Thr231-phosphotau. *The Journal of neuroscience : the official journal of the Society for Neuroscience* 28, 11500-11510.

Guerreiro, R., Bras, J., and Hardy, J. (2015). SnapShot: Genetics of ALS and FTD. *Cell* 160, 798 e791.

Guerrero-Ferreira, R., Taylor, N.M.I., Mona, D., Ringler, P., Lauer, M.E., Riek, R., Britschgi, M., and Stahlberg, H. (2018). Cryo-EM structure of alpha-synuclein fibrils. *bioRxiv.org*.

Guo, L., Kim, H.J., Wang, H., Monaghan, J., Freyermuth, F., Sung, J.C., O'Donovan, K., Fare, C.M., Diaz, Z., Singh, N., *et al.* (2018). Nuclear-Import Receptors Reverse Aberrant Phase Transitions of RNA-Binding Proteins with Prion-like Domains. *Cell* 173, 677-692 e620.

Gupta, R., Lan, M., Mojsilovic-Petrovic, J., Choi, W.H., Safren, N., Barmada, S., Lee, M.J., and Kalb, R. (2017). The Proline/Arginine Dipeptide from Hexanucleotide Repeat Expanded C9ORF72 Inhibits the Proteasome. *eNeuro* 4.

Hangen, E., Feraud, O., Lachkar, S., Mou, H., Doti, N., Fimia, G.M., Lam, N.V., Zhu, C., Godin, I., Muller, K., *et al.* (2015). Interaction between AIF and CHCHD4 Regulates Respiratory Chain Biogenesis. *Molecular cell* 58, 1001-1014.

Hara, T., Nakamura, K., Matsui, M., Yamamoto, A., Nakahara, Y., Suzuki-Migishima, R., Yokoyama, M., Mishima, K., Saito, I., Okano, H., *et al.* (2006). Suppression of basal autophagy in neural cells causes neurodegenerative disease in mice. *Nature* **441**, 885-889.

Harmey, M.A., Hallermayer, G., Korb, H., and Neupert, W. (1977). Transport of cytoplasmically synthesized proteins into the mitochondria in a cell free system from *Neurospora crassa*. *European journal of biochemistry* **81**, 533-544.

Hase, T., Riezman, H., Suda, K., and Schatz, G. (1983). Import of proteins into mitochondria: nucleotide sequence of the gene for a 70-kd protein of the yeast mitochondrial outer membrane. *The EMBO journal* **2**, 2169-2172.

Hatefi, Y. (1985). The mitochondrial electron transport and oxidative phosphorylation system. *Annual review of biochemistry* **54**, 1015-1069.

Heinemeyer, W., Fischer, M., Krimmer, T., Stachon, U., and Wolf, D.H. (1997). The active sites of the eukaryotic 20 S proteasome and their involvement in subunit precursor processing. *J Biol Chem* **272**, 25200-25209.

Hofmann, S., Rothbauer, U., Muhlenbein, N., Baiker, K., Hell, K., and Bauer, M.F. (2005). Functional and mutational characterization of human MIA40 acting during import into the mitochondrial intermembrane space. *Journal of molecular biology* **353**, 517-528.

Hogan, D.B., Jette, N., Fiest, K.M., Roberts, J.I., Pearson, D., Smith, E.E., Roach, P., Kirk, A., Pringsheim, T., and Maxwell, C.J. (2016). The Prevalence and Incidence of Frontotemporal Dementia: a Systematic Review. *Can J Neurol Sci* **43 Suppl 1**, S96-S109.

Hudson, A.J. (1981). Amyotrophic lateral sclerosis and its association with dementia, parkinsonism and other neurological disorders: a review. *Brain* **104**, 217-247.

Hutton, M., Lendon, C.L., Rizzu, P., Baker, M., Froelich, S., Houlden, H., Pickering-Brown, S., Chakraverty, S., Isaacs, A., Grover, A., *et al.* (1998). Association of missense and 5'-splice-site mutations in tau with the inherited dementia FTDP-17. *Nature* **393**, 702-705.

Jang, S.Y., Kang, H.T., and Hwang, E.S. (2012). Nicotinamide-induced mitophagy: event mediated by high NAD<sup>+</sup>/NADH ratio and SIRT1 protein activation. *J Biol Chem* **287**, 19304-19314.

Jiang, J., Zhu, Q., Gendron, T.F., Saberi, S., McAlonis-Downes, M., Seelman, A., Stauffer, J.E., Jafar-Nejad, P., Drenner, K., Schulte, D., *et al.* (2016). Gain of Toxicity from ALS/FTD-Linked Repeat Expansions in C9ORF72 Is Alleviated by Antisense Oligonucleotides Targeting GGGGCC-Containing RNAs. *Neuron* **90**, 535-550.

Jiao, B., Xiao, T., Hou, L., Gu, X., Zhou, Y., Zhou, L., Tang, B., Xu, J., and Shen, L. (2016). High prevalence of CHCHD10 mutation in patients with frontotemporal dementia from China. *Brain* **139**, e21.

Johnson, B.S., McCaffery, J.M., Lindquist, S., and Gitler, A.D. (2008). A yeast TDP-43 proteinopathy model: Exploring the molecular determinants of TDP-43 aggregation and cellular toxicity. *Proceedings of the National Academy of Sciences of the United States of America* **105**, 6439-6444.

Johnson, J.O., Glynn, S.M., Gibbs, J.R., Nalls, M.A., Sabatelli, M., Restagno, G., Drory, V.E., Chio, A., Rogaeva, E., and Traynor, B.J. (2014). Mutations in the CHCHD10 gene are a common cause of familial amyotrophic lateral sclerosis. *Brain* **137**, e311.

Jovicic, A., Mertens, J., Boeynaems, S., Bogaert, E., Chai, N., Yamada, S.B., Paul, J.W., 3rd, Sun, S., Herdy, J.R., Bieri, G., *et al.* (2015). Modifiers of C9orf72 dipeptide repeat toxicity connect nucleocytoplasmic transport defects to FTD/ALS. *Nat Neurosci* **18**, 1226-1229.

- Ju, J.S., Fuentealba, R.A., Miller, S.E., Jackson, E., Piwnica-Worms, D., Baloh, R.H., and Wehl, C.C. (2009). Valosin-containing protein (VCP) is required for autophagy and is disrupted in VCP disease. *The Journal of cell biology* 187, 875-888.
- Jucker, M., and Walker, L.C. (2011). Pathogenic protein seeding in Alzheimer disease and other neurodegenerative disorders. *Ann Neurol* 70, 532-540.
- Kabashi, E., Agar, J.N., Strong, M.J., and Durham, H.D. (2012). Impaired proteasome function in sporadic amyotrophic lateral sclerosis. *Amyotrophic lateral sclerosis : official publication of the World Federation of Neurology Research Group on Motor Neuron Diseases* 13, 367-371.
- Kanekura, K., Yagi, T., Cammack, A.J., Mahadevan, J., Kuroda, M., Harms, M.B., Miller, T.M., and Urano, F. (2016). Poly-dipeptides encoded by the C9ORF72 repeats block global protein translation. *Human molecular genetics* 25, 1803-1813.
- Kang, Y., Fielden, L.F., and Stojanovski, D. (2017). Mitochondrial protein transport in health and disease. *Seminars in cell & developmental biology*.
- Kansal, K., Mareddy, M., Sloane, K.L., Minc, A.A., Rabins, P.V., McGready, J.B., and Onyike, C.U. (2016). Survival in Frontotemporal Dementia Phenotypes: A Meta-Analysis. *Dement Geriatr Cogn Disord* 41, 109-122.
- Kawano, S., Yamano, K., Naoe, M., Momose, T., Terao, K., Nishikawa, S., Watanabe, N., and Endo, T. (2009). Structural basis of yeast Tim40/Mia40 as an oxidative translocator in the mitochondrial intermembrane space. *Proceedings of the National Academy of Sciences of the United States of America* 106, 14403-14407.
- Kerscher, O., Holder, J., Srinivasan, M., Leung, R.S., and Jensen, R.E. (1997). The Tim54p-Tim22p complex mediates insertion of proteins into the mitochondrial inner membrane. *The Journal of cell biology* 139, 1663-1675.
- Kiebler, M., Pfaller, R., Sollner, T., Griffiths, G., Horstmann, H., Pfanner, N., and Neupert, W. (1990). Identification of a mitochondrial receptor complex required for recognition and membrane insertion of precursor proteins. *Nature* 348, 610-616.
- Kiernan, M.C., Vucic, S., Cheah, B.C., Turner, M.R., Eisen, A., Hardiman, O., Burrell, J.R., and Zoing, M.C. (2011). Amyotrophic lateral sclerosis. *Lancet* 377, 942-955.
- King, O.D., Gitler, A.D., and Shorter, J. (2012). The tip of the iceberg: RNA-binding proteins with prion-like domains in neurodegenerative disease. *Brain research* 1462, 61-80.
- Ko, H.S., Uehara, T., Tsuruma, K., and Nomura, Y. (2004). Ubiquilin interacts with ubiquitylated proteins and proteasome through its ubiquitin-associated and ubiquitin-like domains. *FEBS letters* 566, 110-114.
- Komatsu, M., Waguri, S., Chiba, T., Murata, S., Iwata, J., Tanida, I., Ueno, T., Koike, M., Uchiyama, Y., Kominami, E., *et al.* (2006). Loss of autophagy in the central nervous system causes neurodegeneration in mice. *Nature* 441, 880-884.
- Koppers, M., Blokhuis, A.M., Westeneng, H.J., Terpstra, M.L., Zundel, C.A., Vieira de Sa, R., Schellevis, R.D., Waite, A.J., Blake, D.J., Veldink, J.H., *et al.* (2015). C9orf72 ablation in mice does not cause motor neuron degeneration or motor deficits. *Ann Neurol* 78, 426-438.
- Kozany, C., Mokranjac, D., Sichting, M., Neupert, W., and Hell, K. (2004). The J domain-related cochaperone Tim16 is a constituent of the mitochondrial TIM23 preprotein translocase. *Nature structural & molecular biology* 11, 234-241.
- Kozjak, V., Wiedemann, N., Milenkovic, D., Lohaus, C., Meyer, H.E., Guiard, B., Meisinger, C., and Pfanner, N. (2003). An essential role of Sam50 in the protein sorting and assembly machinery of the mitochondrial outer membrane. *J Biol Chem* 278, 48520-48523.

- Kumar, D.R., Aslinia, F., Yale, S.H., and Mazza, J.J. (2011). Jean-Martin Charcot: the father of neurology. *Clinical medicine & research* 9, 46-49.
- Kumar, V., Kashav, T., Islam, A., Ahmad, F., and Hassan, M.I. (2016). Structural insight into C9orf72 hexanucleotide repeat expansions: Towards new therapeutic targets in FTD-ALS. *Neurochemistry international* 100, 11-20.
- Kurzweily, D., Kruger, S., Biskup, S., and Heneka, M.T. (2015). A distinct clinical phenotype in a German kindred with motor neuron disease carrying a CHCHD10 mutation. *Brain* 138, e376.
- Kwiatkowski, T.J., Jr., Bosco, D.A., Leclerc, A.L., Tamrazian, E., Vanderburg, C.R., Russ, C., Davis, A., Gilchrist, J., Kasarskis, E.J., Munsat, T., *et al.* (2009). Mutations in the FUS/TLS gene on chromosome 16 cause familial amyotrophic lateral sclerosis. *Science* 323, 1205-1208.
- Kwon, I., Xiang, S., Kato, M., Wu, L., Theodoropoulos, P., Wang, T., Kim, J., Yun, J., Xie, Y., and McKnight, S.L. (2014). Poly-dipeptides encoded by the C9orf72 repeats bind nucleoli, impede RNA biogenesis, and kill cells. *Science* 345, 1139-1145.
- Lagier-Tourenne, C., Baughn, M., Rigo, F., Sun, S., Liu, P., Li, H.R., Jiang, J., Watt, A.T., Chun, S., Katz, M., *et al.* (2013). Targeted degradation of sense and antisense C9orf72 RNA foci as therapy for ALS and frontotemporal degeneration. *Proceedings of the National Academy of Sciences of the United States of America* 110, E4530-4539.
- Lee, J., Hofhaus, G., and Lisowsky, T. (2000). Erv1p from *Saccharomyces cerevisiae* is a FAD-linked sulfhydryl oxidase. *FEBS letters* 477, 62-66.
- Lee, K.H., Zhang, P., Kim, H.J., Mitrea, D.M., Sarkar, M., Freibaum, B.D., Cika, J., Coughlin, M., Messing, J., Mollie, A., *et al.* (2016). C9orf72 Dipeptide Repeats Impair the Assembly, Dynamics, and Function of Membrane-Less Organelles. *Cell* 167, 774-788 e717.
- Levine, T.P., Daniels, R.D., Gatta, A.T., Wong, L.H., and Hayes, M.J. (2013). The product of C9orf72, a gene strongly implicated in neurodegeneration, is structurally related to DENN Rab-GEFs. *Bioinformatics* 29, 499-503.
- Li, Q., Vande Velde, C., Israelson, A., Xie, J., Bailey, A.O., Dong, M.Q., Chun, S.J., Roy, T., Winer, L., Yates, J.R., *et al.* (2010). ALS-linked mutant superoxide dismutase 1 (SOD1) alters mitochondrial protein composition and decreases protein import. *Proceedings of the National Academy of Sciences of the United States of America* 107, 21146-21151.
- Ling, S.C., Polymenidou, M., and Cleveland, D.W. (2013). Converging mechanisms in ALS and FTD: disrupted RNA and protein homeostasis. *Neuron* 79, 416-438.
- Lopez-Gonzalez, R., Lu, Y., Gendron, T.F., Karydas, A., Tran, H., Yang, D., Petrucelli, L., Miller, B.L., Almeida, S., and Gao, F.B. (2016). Poly(GR) in C9ORF72-Related ALS/FTD Compromises Mitochondrial Function and Increases Oxidative Stress and DNA Damage in iPSC-Derived Motor Neurons. *Neuron* 92, 383-391.
- Lu, C.H., Macdonald-Wallis, C., Gray, E., Pearce, N., Petzold, A., Norgren, N., Giovannoni, G., Fratta, P., Sidle, K., Fish, M., *et al.* (2015). Neurofilament light chain: A prognostic biomarker in amyotrophic lateral sclerosis. *Neurology* 84, 2247-2257.
- Luk, K.C., Kehm, V., Carroll, J., Zhang, B., O'Brien, P., Trojanowski, J.Q., and Lee, V.M. (2012). Pathological alpha-synuclein transmission initiates Parkinson-like neurodegeneration in nontransgenic mice. *Science* 338, 949-953.
- Lutz, T., Neupert, W., and Herrmann, J.M. (2003). Import of small Tim proteins into the mitochondrial intermembrane space. *The EMBO journal* 22, 4400-4408.

- Mackenzie, I.R., Arzberger, T., Kremmer, E., Troost, D., Lorenzl, S., Mori, K., Weng, S.M., Haass, C., Kretzschmar, H.A., Edbauer, D., *et al.* (2013). Dipeptide repeat protein pathology in C9ORF72 mutation cases: clinico-pathological correlations. *Acta neuropathologica* 126, 859-879.
- Mackenzie, I.R., Neumann, M., Bigio, E.H., Cairns, N.J., Alafuzoff, I., Kril, J., Kovacs, G.G., Ghetti, B., Halliday, G., Holm, I.E., *et al.* (2010). Nomenclature and nosology for neuropathologic subtypes of frontotemporal lobar degeneration: an update. *Acta neuropathologica* 119, 1-4.
- MacPherson, L., and Tokatlidis, K. (2017). Protein trafficking in the mitochondrial intermembrane space: mechanisms and links to human disease. *Biochem J* 474, 2533-2545.
- Magrane, J., Cortez, C., Gan, W.B., and Manfredi, G. (2014). Abnormal mitochondrial transport and morphology are common pathological denominators in SOD1 and TDP43 ALS mouse models. *Human molecular genetics* 23, 1413-1424.
- Magrane, J., Sahawneh, M.A., Przedborski, S., Estevez, A.G., and Manfredi, G. (2012). Mitochondrial dynamics and bioenergetic dysfunction is associated with synaptic alterations in mutant SOD1 motor neurons. *The Journal of neuroscience : the official journal of the Society for Neuroscience* 32, 229-242.
- Majounie, E., Renton, A.E., Mok, K., Dopper, E.G., Waite, A., Rollinson, S., Chio, A., Restagno, G., Nicolaou, N., Simon-Sanchez, J., *et al.* (2012). Frequency of the C9orf72 hexanucleotide repeat expansion in patients with amyotrophic lateral sclerosis and frontotemporal dementia: a cross-sectional study. *Lancet Neurol* 11, 323-330.
- Malty, R.H., Jessulat, M., Jin, K., Musso, G., Vlasblom, J., Phanse, S., Zhang, Z., and Babu, M. (2015). Mitochondrial targets for pharmacological intervention in human disease. *Journal of proteome research* 14, 5-21.
- Maruyama, H., Morino, H., Ito, H., Izumi, Y., Kato, H., Watanabe, Y., Kinoshita, Y., Kamada, M., Nodera, H., Suzuki, H., *et al.* (2010). Mutations of optineurin in amyotrophic lateral sclerosis. *Nature* 465, 223-226.
- May, S., Hornburg, D., Schludi, M.H., Arzberger, T., Rentzsch, K., Schwenk, B.M., Grasser, F.A., Mori, K., Kremmer, E., Banzhaf-Strathmann, J., *et al.* (2014). C9orf72 FTL/ALS-associated Gly-Ala dipeptide repeat proteins cause neuronal toxicity and Unc119 sequestration. *Acta Neuropathol* 128, 485-503.
- Meeter, L.H., Dopper, E.G., Jiskoot, L.C., Sanchez-Valle, R., Graff, C., Benussi, L., Ghidoni, R., Pijnenburg, Y.A., Borroni, B., Galimberti, D., *et al.* (2016). Neurofilament light chain: a biomarker for genetic frontotemporal dementia. *Annals of clinical and translational neurology* 3, 623-636.
- Miller, C.M., and Harris, E.N. (2016). Antisense Oligonucleotides: Treatment Strategies and Cellular Internalization. *RNA & disease* 3.
- Miller, R.G., Mitchell, J.D., and Moore, D.H. (2012). Riluzole for amyotrophic lateral sclerosis (ALS)/motor neuron disease (MND). *The Cochrane database of systematic reviews*, CD001447.
- Mitsumoto, H., Brooks, B.R., and Silani, V. (2014). Clinical trials in amyotrophic lateral sclerosis: why so many negative trials and how can trials be improved? *Lancet Neurol* 13, 1127-1138.
- Mizielinska, S., Gronke, S., Niccoli, T., Ridler, C.E., Clayton, E.L., Devoy, A., Moens, T., Norona, F.E., Woollacott, I.O., Pietrzyk, J., *et al.* (2014). C9orf72 repeat expansions cause neurodegeneration in *Drosophila* through arginine-rich proteins. *Science* 345, 1192-1194.
- Modjtahedi, N., Tokatlidis, K., Dessen, P., and Kroemer, G. (2016). Mitochondrial Proteins Containing Coiled-Coil-Helix-Coiled-Coil-Helix (CHCH) Domains in Health and Disease. *Trends in biochemical sciences* 41, 245-260.
- Mori, K., Arzberger, T., Grasser, F.A., Gijssels, I., May, S., Rentzsch, K., Weng, S.M., Schludi, M.H., van der Zee, J., Cruys, M., *et al.* (2013a). Bidirectional transcripts of the expanded C9orf72 hexanucleotide repeat are translated into aggregating dipeptide repeat proteins. *Acta neuropathologica* 126, 881-893.

Mori, K., Lammich, S., Mackenzie, I.R., Forne, I., Zilow, S., Kretschmar, H., Edbauer, D., Janssens, J., Kleinberger, G., Cruts, M., *et al.* (2013b). hnRNP A3 binds to GGGGCC repeats and is a constituent of p62-positive/TDP43-negative inclusions in the hippocampus of patients with C9orf72 mutations. *Acta neuropathologica* 125, 413-423.

Mori, K., Weng, S.M., Arzberger, T., May, S., Rentzsch, K., Kremmer, E., Schmid, B., Kretschmar, H.A., Cruts, M., Van Broeckhoven, C., *et al.* (2013c). The C9orf72 GGGGCC repeat is translated into aggregating dipeptide-repeat proteins in FTL/ALS. *Science* 339, 1335-1338.

Morita, M., Al-Chalabi, A., Andersen, P.M., Hosler, B., Sapp, P., Englund, E., Mitchell, J.E., Habgood, J.J., de Belleruche, J., Xi, J., *et al.* (2006). A locus on chromosome 9p confers susceptibility to ALS and frontotemporal dementia. *Neurology* 66, 839-844.

Muller, J.M., Milenkovic, D., Guiard, B., Pfanner, N., and Chacinska, A. (2008). Precursor oxidation by Mia40 and Erv1 promotes vectorial transport of proteins into the mitochondrial intermembrane space. *Molecular biology of the cell* 19, 226-236.

Muller, K., Andersen, P.M., Hubers, A., Marroquin, N., Volk, A.E., Danzer, K.M., Meitinger, T., Ludolph, A.C., Strom, T.M., and Weishaupt, J.H. (2014). Two novel mutations in conserved codons indicate that CHCHD10 is a gene associated with motor neuron disease. *Brain* 137, e309.

Munch, C., O'Brien, J., and Bertolotti, A. (2011). Prion-like propagation of mutant superoxide dismutase-1 misfolding in neuronal cells. *Proceedings of the National Academy of Sciences of the United States of America* 108, 3548-3553.

Murakami, T., Qamar, S., Lin, J.Q., Schierle, G.S., Rees, E., Miyashita, A., Costa, A.R., Dodd, R.B., Chan, F.T., Michel, C.H., *et al.* (2015). ALS/FTD Mutation-Induced Phase Transition of FUS Liquid Droplets and Reversible Hydrogels into Irreversible Hydrogels Impairs RNP Granule Function. *Neuron* 88, 678-690.

Murray, D.T., Kato, M., Lin, Y., Thurber, K.R., Hung, I., McKnight, S.L., and Tycko, R. (2017). Structure of FUS Protein Fibrils and Its Relevance to Self-Assembly and Phase Separation of Low-Complexity Domains. *Cell* 171, 615-627 e616.

Neumann, M., Sampathu, D.M., Kwong, L.K., Truax, A.C., Micsenyi, M.C., Chou, T.T., Bruce, J., Schuck, T., Grossman, M., Clark, C.M., *et al.* (2006). Ubiquitinated TDP-43 in frontotemporal lobar degeneration and amyotrophic lateral sclerosis. *Science* 314, 130-133.

Ng, A.S., Rademakers, R., and Miller, B.L. (2015). Frontotemporal dementia: a bridge between dementia and neuromuscular disease. *Ann N Y Acad Sci* 1338, 71-93.

Nonaka, T., Masuda-Suzukake, M., Arai, T., Hasegawa, Y., Akatsu, H., Obi, T., Yoshida, M., Murayama, S., Mann, D.M., Akiyama, H., *et al.* (2013). Prion-like properties of pathological TDP-43 aggregates from diseased brains. *Cell Rep* 4, 124-134.

Osaka, M., Ito, D., Yagi, T., Nihei, Y., and Suzuki, N. (2015). Evidence of a link between ubiquilin 2 and optineurin in amyotrophic lateral sclerosis. *Human molecular genetics* 24, 1617-1629.

Ozel-Kizil, E., Sakarya, A., Arica, B., and Haran, S. (2013). A case of frontotemporal dementia with amyotrophic lateral sclerosis presenting with pathological gambling. *Journal of clinical neurology* 9, 133-137.

Paschen, S.A., Waizenegger, T., Stan, T., Preuss, M., Cyrklaff, M., Hell, K., Rapaport, D., and Neupert, W. (2003). Evolutionary conservation of biogenesis of beta-barrel membrane proteins. *Nature* 426, 862-866.

Pattee, G.L., Post, G.R., Gerber, R.E., and Bennett, J.P., Jr. (2003). Reduction of oxidative stress in amyotrophic lateral sclerosis following pramipexole treatment. *Amyotroph Lateral Scler Other Motor Neuron Disord* 4, 90-95.

Peleh, V., Cordat, E., and Herrmann, J.M. (2016). Mia40 is a trans-site receptor that drives protein import into the mitochondrial intermembrane space by hydrophobic substrate binding. *Elife* 5.

Penttila, S., Jokela, M., Saukkonen, A.M., Toivanen, J., Palmio, J., Lahdesmaki, J., Sandell, S., Shcherbii, M., Auranen, M., Ylikallio, E., *et al.* (2017). CHCHD10 mutations and motor neuron disease: the distribution in Finnish patients. *J Neurol Neurosurg Psychiatry* 88, 272-277.

Perrone, F., Nguyen, H.P., Van Mossevelde, S., Moisse, M., Sieben, A., Santens, P., De Bleecker, J., Vandebulcke, M., Engelborghs, S., Baets, J., *et al.* (2017). Investigating the role of ALS genes CHCHD10 and TUBA4A in Belgian FTD-ALS spectrum patients. *Neurobiol Aging* 51, 177 e179-177 e116.

Peters, O.M., Cabrera, G.T., Tran, H., Gendron, T.F., McKeon, J.E., Metterville, J., Weiss, A., Wightman, N., Salameh, J., Kim, J., *et al.* (2015). Human C9ORF72 Hexanucleotide Expansion Reproduces RNA Foci and Dipeptide Repeat Proteins but Not Neurodegeneration in BAC Transgenic Mice. *Neuron* 88, 902-909.

Poppe, L., Rue, L., Robberecht, W., and Van Den Bosch, L. (2014). Translating biological findings into new treatment strategies for amyotrophic lateral sclerosis (ALS). *Experimental neurology* 262 Pt B, 138-151.

Pottier, C., Bieniek, K.F., Finch, N., van de Vorst, M., Baker, M., Perkersen, R., Brown, P., Ravenscroft, T., van Blitterswijk, M., Nicholson, A.M., *et al.* (2015). Whole-genome sequencing reveals important role for TBK1 and OPTN mutations in frontotemporal lobar degeneration without motor neuron disease. *Acta neuropathologica* 130, 77-92.

Proudfoot, M., Gutowski, N.J., Edbauer, D., Hilton, D.A., Stephens, M., Rankin, J., and Mackenzie, I.R. (2014). Early dipeptide repeat pathology in a frontotemporal dementia kindred with C9ORF72 mutation and intellectual disability. *Acta neuropathologica* 127, 451-458.

Puigserver, P., and Spiegelman, B.M. (2003). Peroxisome proliferator-activated receptor-gamma coactivator 1 alpha (PGC-1 alpha): transcriptional coactivator and metabolic regulator. *Endocrine reviews* 24, 78-90.

Purandare, N., Somayajulu, M., Huttemann, M., Grossman, L.I., and Aras, S. (2018). The cellular stress proteins CHCHD10 and MNRR1 (CHCHD2): Partners in mitochondrial and nuclear function and dysfunction. *J Biol Chem*.

Rademakers, R., Neumann, M., and Mackenzie, I.R. (2012). Advances in understanding the molecular basis of frontotemporal dementia. *Nature reviews Neurology* 8, 423-434.

Randall, C., Mosconi, L., de Leon, M., and Glodzik, L. (2013). Cerebrospinal fluid biomarkers of Alzheimer's disease in healthy elderly. *Frontiers in bioscience* 18, 1150-1173.

Rascovsky, K., Hodges, J.R., Knopman, D., Mendez, M.F., Kramer, J.H., Neuhaus, J., van Swieten, J.C., Seelaar, H., Dopper, E.G., Onyike, C.U., *et al.* (2011). Sensitivity of revised diagnostic criteria for the behavioural variant of frontotemporal dementia. *Brain* 134, 2456-2477.

Renton, A.E., Majounie, E., Waite, A., Simon-Sanchez, J., Rollinson, S., Gibbs, J.R., Schymick, J.C., Laaksovirta, H., van Swieten, J.C., Myllykangas, L., *et al.* (2011). A hexanucleotide repeat expansion in C9ORF72 is the cause of chromosome 9p21-linked ALS-FTD. *Neuron* 72, 257-268.

Rosen, D.R., Siddique, T., Patterson, D., Figlewicz, D.A., Sapp, P., Hentati, A., Donaldson, D., Goto, J., O'Regan, J.P., Deng, H.X., *et al.* (1993). Mutations in Cu/Zn superoxide dismutase gene are associated with familial amyotrophic lateral sclerosis. *Nature* 362, 59-62.

Rosen, H.J., Gorno-Tempini, M.L., Goldman, W.P., Perry, R.J., Schuff, N., Weiner, M., Feiwell, R., Kramer, J.H., and Miller, B.L. (2002). Patterns of brain atrophy in frontotemporal dementia and semantic dementia. *Neurology* 58, 198-208.

Rowland, L.P. (2001). How amyotrophic lateral sclerosis got its name: the clinical-pathologic genius of Jean-Martin Charcot. *Arch Neurol* 58, 512-515.

Rubino, E., Rainero, I., Chio, A., Rogaeva, E., Galimberti, D., Fenoglio, P., Grinberg, Y., Isaia, G., Calvo, A., Gentile, S., *et al.* (2012). SQSTM1 mutations in frontotemporal lobar degeneration and amyotrophic lateral sclerosis. *Neurology* 79, 1556-1562.

Rubino, E., Zhang, M., Mongini, T., Boschi, S., Vercelli, L., Vacca, A., Govone, F., Gai, A., Giordana, M.T., Grinberg, M., *et al.* (2018). Mutation analysis of CHCHD2 and CHCHD10 in Italian patients with mitochondrial myopathy. *Neurobiology of aging*.

Saberi, S., Stauffer, J.E., Jiang, J., Garcia, S.D., Taylor, A.E., Schulte, D., Ohkubo, T., Schloffman, C.L., Maldonado, M., Baughn, M., *et al.* (2018). Sense-encoded poly-GR dipeptide repeat proteins correlate to neurodegeneration and uniquely co-localize with TDP-43 in dendrites of repeat-expanded C9orf72 amyotrophic lateral sclerosis. *Acta neuropathologica* 135, 459-474.

Sanders, D.W., Kaufman, S.K., DeVos, S.L., Sharma, A.M., Mirbaha, H., Li, A., Barker, S.J., Foley, A.C., Thorpe, J.R., Serpell, L.C., *et al.* (2014). Distinct tau prion strains propagate in cells and mice and define different tauopathies. *Neuron* 82, 1271-1288.

Scherling, C.S., Hall, T., Berisha, F., Klepac, K., Karydas, A., Coppola, G., Kramer, J.H., Rabinovici, G., Ahljianian, M., Miller, B.L., *et al.* (2014). Cerebrospinal fluid neurofilament concentration reflects disease severity in frontotemporal degeneration. *Ann Neurol* 75, 116-126.

Schilling, L.P., Zimmer, E.R., Shin, M., Leuzy, A., Pascoal, T.A., Benedet, A.L., Borelli, W.V., Palmi, A., Gauthier, S., and Rosa-Neto, P. (2016). Imaging Alzheimer's disease pathophysiology with PET. *Dementia & neuropsychologia* 10, 79-90.

Schludi, M.H., Becker, L., Garrett, L., Gendron, T.F., Zhou, Q., Schreiber, F., Popper, B., Dimou, L., Strom, T.M., Winkelmann, J., *et al.* (2017). Spinal poly-GA inclusions in a C9orf72 mouse model trigger motor deficits and inflammation without neuron loss. *Acta neuropathologica* 134, 241-254.

Schludi, M.H., May, S., Grasser, F.A., Rentzsch, K., Kremmer, E., Kupper, C., Klopstock, T., German Consortium for Frontotemporal Lobar, D., Bavarian Brain Banking, A., Arzberger, T., *et al.* (2015). Distribution of dipeptide repeat proteins in cellular models and C9orf72 mutation cases suggests link to transcriptional silencing. *Acta neuropathologica* 130, 537-555.

Schmidt, M., Rohou, A., Lasker, K., Yadav, J.K., Schiene-Fischer, C., Fandrich, M., and Grigorieff, N. (2015). Peptide dimer structure in an Aβ(1-42) fibril visualized with cryo-EM. *Proceedings of the National Academy of Sciences of the United States of America* 112, 11858-11863.

Scotter, E.L., Chen, H.J., and Shaw, C.E. (2015). TDP-43 Proteinopathy and ALS: Insights into Disease Mechanisms and Therapeutic Targets. *Neurotherapeutics : the journal of the American Society for Experimental NeuroTherapeutics* 12, 352-363.

Sellier, C., Campanari, M.L., Julie Corbier, C., Gaucherot, A., Kolb-Cheynel, I., Oulad-Abdelghani, M., Ruffenach, F., Page, A., Ciura, S., Kabashi, E., *et al.* (2016). Loss of C9ORF72 impairs autophagy and synergizes with polyQ Ataxin-2 to induce motor neuron dysfunction and cell death. *The EMBO journal* 35, 1276-1297.

Sevigny, J., Chiao, P., Bussiere, T., Weinreb, P.H., Williams, L., Maier, M., Dunstan, R., Salloway, S., Chen, T., Ling, Y., *et al.* (2016). The antibody aducanumab reduces Aβ plaques in Alzheimer's disease. *Nature* 537, 50-56.

Shahheydari, H., Ragagnin, A., Walker, A.K., Toth, R.P., Vidal, M., Jagaraj, C.J., Perri, E.R., Konopka, A., Sultana, J.M., and Atkin, J.D. (2017). Protein Quality Control and the Amyotrophic Lateral Sclerosis/Frontotemporal Dementia Continuum. *Frontiers in molecular neuroscience* 10, 119.

- Simone, R., Balendra, R., Moens, T.G., Preza, E., Wilson, K.M., Heslegrave, A., Woodling, N.S., Niccoli, T., Gilbert-Jaramillo, J., Abdelkarim, S., *et al.* (2018). G-quadruplex-binding small molecules ameliorate C9orf72 FTD/ALS pathology in vitro and in vivo. *EMBO molecular medicine* 10, 22-31.
- Sirrenberg, C., Bauer, M.F., Guiard, B., Neupert, W., and Brunner, M. (1996). Import of carrier proteins into the mitochondrial inner membrane mediated by Tim22. *Nature* 384, 582-585.
- Skibinski, G., Parkinson, N.J., Brown, J.M., Chakrabarti, L., Lloyd, S.L., Hummerich, H., Nielsen, J.E., Hodges, J.R., Spillantini, M.G., Thusgaard, T., *et al.* (2005). Mutations in the endosomal ESCRTIII-complex subunit CHMP2B in frontotemporal dementia. *Nat Genet* 37, 806-808.
- Smith, E.F., Shaw, P.J., and De Vos, K.J. (2017). The role of mitochondria in amyotrophic lateral sclerosis. *Neuroscience letters*.
- Snowden, J.S., Neary, D., and Mann, D.M. (2002). Frontotemporal dementia. *The British journal of psychiatry : the journal of mental science* 180, 140-143.
- Sreedharan, J., Blair, I.P., Tripathi, V.B., Hu, X., Vance, C., Rogelj, B., Ackerley, S., Durnall, J.C., Williams, K.L., Buratti, E., *et al.* (2008). TDP-43 mutations in familial and sporadic amyotrophic lateral sclerosis. *Science* 319, 1668-1672.
- Stojanovski, D., Muller, J.M., Milenkovic, D., Guiard, B., Pfanner, N., and Chacinska, A. (2008). The MIA system for protein import into the mitochondrial intermembrane space. *Biochimica et biophysica acta* 1783, 610-617.
- Straub, I.R., Janer, A., Weraarpachai, W., Zinman, L., Robertson, J., Rogaeva, E., and Shoubridge, E.A. (2018). Loss of CHCHD10-CHCHD2 complexes required for respiration underlies the pathogenicity of a CHCHD10 mutation in ALS. *Human molecular genetics* 27, 178-189.
- Strong, M.J., Lomen-Hoerth, C., Caselli, R.J., Bigio, E.H., and Yang, W. (2003). Cognitive impairment, frontotemporal dementia, and the motor neuron diseases. *Ann Neurol* 54 Suppl 5, S20-23.
- Su, Z., Zhang, Y., Gendron, T.F., Bauer, P.O., Chew, J., Yang, W.Y., Fostvedt, E., Jansen-West, K., Belzil, V.V., Desaro, P., *et al.* (2014). Discovery of a Biomarker and Lead Small Molecules to Target r(GGGGCC)-Associated Defects in c9FTD/ALS. *Neuron* 84, 239.
- Suarez-Calvet, M., Kleinberger, G., Araque Caballero, M.A., Brendel, M., Rominger, A., Alcolea, D., Fortea, J., Lleo, A., Blesa, R., Gispert, J.D., *et al.* (2016). sTREM2 cerebrospinal fluid levels are a potential biomarker for microglia activity in early-stage Alzheimer's disease and associate with neuronal injury markers. *EMBO molecular medicine* 8, 466-476.
- Sudria-Lopez, E., Koppers, M., de Wit, M., van der Meer, C., Westeneng, H.J., Zundel, C.A., Youssef, S.A., Harkema, L., de Bruin, A., Veldink, J.H., *et al.* (2016). Full ablation of C9orf72 in mice causes immune system-related pathology and neoplastic events but no motor neuron defects. *Acta neuropathologica* 132, 145-147.
- Tashiro, Y., Urushitani, M., Inoue, H., Koike, M., Uchiyama, Y., Komatsu, M., Tanaka, K., Yamazaki, M., Abe, M., Misawa, H., *et al.* (2012). Motor neuron-specific disruption of proteasomes, but not autophagy, replicates amyotrophic lateral sclerosis. *J Biol Chem* 287, 42984-42994.
- Thau, N., Knippenberg, S., Korner, S., Rath, K.J., Dengler, R., and Petri, S. (2012). Decreased mRNA expression of PGC-1alpha and PGC-1alpha-regulated factors in the SOD1G93A ALS mouse model and in human sporadic ALS. *Journal of neuropathology and experimental neurology* 71, 1064-1074.
- Tsai, R.M., and Boxer, A.L. (2016). Therapy and clinical trials in frontotemporal dementia: past, present, and future. *Journal of neurochemistry* 138 Suppl 1, 211-221.

van Blitterswijk, M., DeJesus-Hernandez, M., and Rademakers, R. (2012). How do C9ORF72 repeat expansions cause amyotrophic lateral sclerosis and frontotemporal dementia: can we learn from other noncoding repeat expansion disorders? *Current opinion in neurology* 25, 689-700.

Van Damme, P., and Robberecht, W. (2009). Recent advances in motor neuron disease. *Current opinion in neurology* 22, 486-492.

van Rheenen, W., Diekstra, F.P., van den Berg, L.H., and Veldink, J.H. (2014). Are CHCHD10 mutations indeed associated with familial amyotrophic lateral sclerosis? *Brain* 137, e313.

Vance, C., Al-Chalabi, A., Ruddy, D., Smith, B.N., Hu, X., Sreedharan, J., Siddique, T., Schelhaas, H.J., Kusters, B., Troost, D., *et al.* (2006). Familial amyotrophic lateral sclerosis with frontotemporal dementia is linked to a locus on chromosome 9p13.2-21.3. *Brain* 129, 868-876.

Vance, C., Rogelj, B., Hortobagyi, T., De Vos, K.J., Nishimura, A.L., Sreedharan, J., Hu, X., Smith, B., Ruddy, D., Wright, P., *et al.* (2009). Mutations in FUS, an RNA processing protein, cause familial amyotrophic lateral sclerosis type 6. *Science* 323, 1208-1211.

Vande Velde, C., McDonald, K.K., Boukhedimi, Y., McAlonis-Downes, M., Lobsiger, C.S., Bel Hadj, S., Zandona, A., Julien, J.P., Shah, S.B., and Cleveland, D.W. (2011). Misfolded SOD1 associated with motor neuron mitochondria alters mitochondrial shape and distribution prior to clinical onset. *PloS one* 6, e22031.

Vatsavayai, S.C., Yoon, S.J., Gardner, R.C., Gendron, T.F., Vargas, J.N., Trujillo, A., Pribadi, M., Phillips, J.J., Gaus, S.E., Hixson, J.D., *et al.* (2016). Timing and significance of pathological features in C9orf72 expansion-associated frontotemporal dementia. *Brain* 139, 3202-3216.

Vieira, R.T., Caixeta, L., Machado, S., Silva, A.C., Nardi, A.E., Arias-Carrion, O., and Carta, M.G. (2013). Epidemiology of early-onset dementia: a review of the literature. *Clin Pract Epidemiol Ment Health* 9, 88-95.

Viscomi, C., Bottani, E., Civiletto, G., Cerutti, R., Moggio, M., Fagiolari, G., Schon, E.A., Lamperti, C., and Zeviani, M. (2011). In vivo correction of COX deficiency by activation of the AMPK/PGC-1alpha axis. *Cell metabolism* 14, 80-90.

Voges, D., Zwickl, P., and Baumeister, W. (1999). The 26S proteasome: a molecular machine designed for controlled proteolysis. *Annual review of biochemistry* 68, 1015-1068.

Waite, A.J., Baumer, D., East, S., Neal, J., Morris, H.R., Ansorge, O., and Blake, D.J. (2014). Reduced C9orf72 protein levels in frontal cortex of amyotrophic lateral sclerosis and frontotemporal degeneration brain with the C9ORF72 hexanucleotide repeat expansion. *Neurobiology of aging* 35, 1779 e1775-1779 e1713.

Wan, L., and Dreyfuss, G. (2017). Splicing-Correcting Therapy for SMA. *Cell* 170, 5.

Wang, W., Li, L., Lin, W.L., Dickson, D.W., Petrucelli, L., Zhang, T., and Wang, X. (2013). The ALS disease-associated mutant TDP-43 impairs mitochondrial dynamics and function in motor neurons. *Human molecular genetics* 22, 4706-4719.

Watts, G.D., Wymer, J., Kovach, M.J., Mehta, S.G., Mumm, S., Darvish, D., Pestronk, A., Whyte, M.P., and Kimonis, V.E. (2004). Inclusion body myopathy associated with Paget disease of bone and frontotemporal dementia is caused by mutant valosin-containing protein. *Nat Genet* 36, 377-381.

Webster, C.P., Smith, E.F., Bauer, C.S., Moller, A., Hautbergue, G.M., Ferraiuolo, L., Myszczyńska, M.A., Higginbottom, A., Walsh, M.J., Whitworth, A.J., *et al.* (2016). The C9orf72 protein interacts with Rab1a and the ULK1 complex to regulate initiation of autophagy. *The EMBO journal* 35, 1656-1676.

Webster, C.P., Smith, E.F., Shaw, P.J., and De Vos, K.J. (2017). Protein Homeostasis in Amyotrophic Lateral Sclerosis: Therapeutic Opportunities? *Frontiers in molecular neuroscience* 10, 123.

- Weckbecker, D., Longen, S., Riemer, J., and Herrmann, J.M. (2012). Atp23 biogenesis reveals a chaperone-like folding activity of Mia40 in the IMS of mitochondria. *The EMBO journal* 31, 4348-4358.
- Wong, C.H., Topp, S., Gkazi, A.S., Troakes, C., Miller, J.W., de Majo, M., Kirby, J., Shaw, P.J., Morrison, K.E., de Belleruche, J., *et al.* (2015). The CHCHD10 P34S variant is not associated with ALS in a UK cohort of familial and sporadic patients. *Neurobiology of aging* 36, 2908 e2917-2908.
- Woo, J.A., Liu, T., Trotter, C., Fang, C.C., De Narvaez, E., LePochat, P., Maslar, D., Bukhari, A., Zhao, X., Deonarine, A., *et al.* (2017). Loss of function CHCHD10 mutations in cytoplasmic TDP-43 accumulation and synaptic integrity. *Nature communications* 8, 15558.
- Xiao, T., Jiao, B., Zhang, W., Pan, C., Wei, J., Liu, X., Zhou, Y., Zhou, L., Tang, B., and Shen, L. (2017). Identification of CHCHD10 Mutation in Chinese Patients with Alzheimer Disease. *Molecular neurobiology* 54, 5243-5247.
- Yamakawa, M., Ito, D., Honda, T., Kubo, K., Noda, M., Nakajima, K., and Suzuki, N. (2015). Characterization of the dipeptide repeat protein in the molecular pathogenesis of c9FTD/ALS. *Human molecular genetics* 24, 1630-1645.
- Yanamandra, K., Kfoury, N., Jiang, H., Mahan, T.E., Ma, S., Maloney, S.E., Wozniak, D.F., Diamond, M.I., and Holtzman, D.M. (2013). Anti-tau antibodies that block tau aggregate seeding in vitro markedly decrease pathology and improve cognition in vivo. *Neuron* 80, 402-414.
- Yang, M., Liang, C., Swaminathan, K., Herrlinger, S., Lai, F., Shiekhattar, R., and Chen, J.F. (2016). A C9ORF72/SMCR8-containing complex regulates ULK1 and plays a dual role in autophagy. *Sci Adv* 2, e1601167.
- Zabel, M.D., and Reid, C. (2015). A brief history of prions. *Pathogens and disease* 73, ftv087.
- Zetterberg, H., Skillback, T., Mattsson, N., Trojanowski, J.Q., Portelius, E., Shaw, L.M., Weiner, M.W., Blennow, K., and Alzheimer's Disease Neuroimaging, I. (2016). Association of Cerebrospinal Fluid Neurofilament Light Concentration With Alzheimer Disease Progression. *JAMA neurology* 73, 60-67.
- Zhang, Y.J., Gendron, T.F., Grima, J.C., Sasaguri, H., Jansen-West, K., Xu, Y.F., Katzman, R.B., Gass, J., Murray, M.E., Shinohara, M., *et al.* (2016). C9ORF72 poly(GA) aggregates sequester and impair HR23 and nucleocytoplasmic transport proteins. *Nat Neurosci* 19, 668-677.
- Zhang, Y.J., Jansen-West, K., Xu, Y.F., Gendron, T.F., Bieniek, K.F., Lin, W.L., Sasaguri, H., Caulfield, T., Hubbard, J., Daugherty, L., *et al.* (2014). Aggregation-prone c9FTD/ALS poly(GA) RAN-translated proteins cause neurotoxicity by inducing ER stress. *Acta neuropathologica* 128, 505-524.
- Zhou, Z.D., Saw, W.T., and Tan, E.K. (2017). Mitochondrial CHCHD-Containing Proteins: Physiologic Functions and Link with Neurodegenerative Diseases. *Molecular neurobiology* 54, 5534-5546.
- Zou, Z.Y., Zhou, Z.R., Che, C.H., Liu, C.Y., He, R.L., and Huang, H.P. (2017). Genetic epidemiology of amyotrophic lateral sclerosis: a systematic review and meta-analysis. *J Neurol Neurosurg Psychiatry*.
- Zu, T., Gibbens, B., Doty, N.S., Gomes-Pereira, M., Huguet, A., Stone, M.D., Margolis, J., Peterson, M., Markowski, T.W., Ingram, M.A., *et al.* (2011). Non-ATG-initiated translation directed by microsatellite expansions. *Proceedings of the National Academy of Sciences of the United States of America* 108, 260-265.
- Zubovych, I.O., Straud, S., and Roth, M.G. (2010). Mitochondrial dysfunction confers resistance to multiple drugs in *Caenorhabditis elegans*. *Molecular biology of the cell* 21, 956-969.

## Acknowledgements

Es ist geschafft! Vor fast genau 4 Jahre, am 1. Juni 2014, humpelte ich mit verletztem Fußgelenk ins Labor, um meinen ersten Tag als Doktorandin zu beginnen. Ganz nach dem Motto „der Weg ist das Ziel“ bin ich nun an diesem Ziel angelangt. Ich bin sehr glücklich und dankbar hier meine Doktorarbeit gemacht zu haben. Obwohl es nicht immer leicht war (für alle Beteiligten) und es teilweise einer Achterbahnfahrt nahe kam, hab ich es dank euch allen gemeistert! Danke für eure Unterstützung und für euren Glauben an mich:

**Eddie**, nicht nur für deine freundschaftliche und motivierende Art ein Betreuer zu sein, sondern auch für deine Neugier an (meiner) Forschung oder Sonstigem „Gibt’s was Neues? Geht da was?“, für deine tröstenden Worte und Taschentücher, wenn mein „innerer Druck“ mal wieder zu groß wurde und schließlich für all die unvergesslichen „Klopfmomente“: Ja, ich hoff da geht noch was☺!

**Prof. Dr. Christian Haass**, dass Sie mein Doktorvater und Mitglied meines Thesis Advisory Committees sind und mich mit Ihren Ideen und ihrer wissenschaftlichen Begeisterung stets inspirieren und motivieren konnten. Denn wie Nolde einst sagte "Die Klugen meistern das Leben, die Weisen durchleuchten es und schaffen neue Schwierigkeiten."

**Allen Mitgliedern meiner Prüfungskommission**, für die Zeit zum Lesen und Bewerten meiner Arbeit.

Allen Eddie-Lab-Mitglieder für das Dick und Dünn, das Hoch und Tief, das Drunter und Drüber, das ich ohne euch nicht so gut überstanden hätte. Danke für die super Stimmung (von Mariachi zu Olympischen Spielen), all eure Freundlichkeit und Hilfsbereitschaft. **Hanne**, für deine lustige Art und all die dreckigen Lachanfälle. **Meike**, für den kleinen Sonnenschein in dir, all die Neuronen und das gemeinsame Durchhalten bei den RNA-foci stainings. **Mareike**, für deine ansteckend positive Art, ich freu mich auf das kommende Mammut-Projekt mit dir. **Katie**, für deine Hilfsbereitschaft und dass du immer ein Lachen übrig hast, sogar für meine richtig schlechten Witze. **Qihui**, für deine bayerische Liebe und die Zusammenarbeit im Labor. **Niko**, neuer Sitznachbar, dass du mein Chaos so gut erträgst. **Daniel**, du Cloning-Machine, für meine Karies und meine baldigen Schwimmreifen. **Henni**, dass ein paar meiner Projekte in so gute Hände geraten sind. Tief durchatmen, alles wird gut Prinzessin Lillifee. **Bahram**, du Rodelprofi, für den Spaß im Labor und bei Outdoor-Aktivitäten. Ich freu mich auf die nächste Schlauchbootsfahrt.

Meinen ehemaligen Kollegen, **Stephie**, für die herzliche Starthilfe hier im Labor und dass wir immer noch so gut befreundet sind. **Benni**, für die Super Post Doc Tipps und für die Songauskopplung der Trambauer Brothers. **Kristin**, für deinen ewigen Segen auf meine Klonierungen. **Denise**, für deine motivierende Art, **Franzi**, für deine „soften“ Mischungen „Hopfa und Moiz, God dahoids!“

**Linnea, Johanna und Michaela**, dass ihr so super Praktikantinnen wart. Es war mir eine große Freude und eine super Erfahrung euch zu betreuen und mit euch gemeinsam zu arbeiten. Ohne euch wären all meine Publikationen nicht so schnell möglich gewesen!

Allen, die mich unterstützt haben diese Doktorarbeit innerhalb kürzester Zeit zu schreiben, um das knappe Zeitfenster für das Wrap-Up Post Doc Programm von IMPRS einhalten zu können. Ein großes Dankeschön geht hierbei an **Eddie, Stephie, Linnea, Martin, Hanne, Mareike, Henni** und **Katie** für das Speed-Korrekturlesen meiner Arbeit!

**Hans-Joerg, Ingrid, Maxi, Amy und Victoria**, vom IMPRS Coordination Office, für eure tolle Unterstützung während meiner Doktorandenzeit. Es war ein sehr großes Privileg für mich ein Mitglied des IMPRS-Graduierten Programms des Max-Planck Instituts zu sein.

Den weiteren Mitgliedern meines Thesis Advisory Committees, **Dr. Irina Dudanova** und **Prof. Dr. Daniel Wilson**, für die jährlichen TAC-Meetings, euren wissenschaftlichen Input und die Hilfe nie meinen Focus zu verlieren.

Unseren Kooperationspartnern vom MPI, **Dr. Ruben Fernandez-Busnandiego, Dr. Qiang Guo, Dr. Mark S. Hipp** für die sehr angenehme und spannende Arbeit am Cell-Paper. Sowas erlebt man nicht alle Tage!

**Johannes Trambauer**, für die gemeinsamen Erlebnisse im und außerhalb vom Lab, auch wenn du mich hin und wieder gerne mit dem Zug wegschicken oder selbst die Sbahn zur Flucht aufsuchen wolltest, **Franziska Eck**, für deine leckeren Rezepte, den gelegentlichen Ratsch und die netten Abende mit dir. **Alice Suelzen**, für die gemeinsamen Fahrten in die Arbeit und für die Organisation des Haass Lab Cultural Program. **Anna Daria**, für die vielen Joggingrunden nach der Arbeit.

Allen Freunden aus der **Oberpfalz**, der **Uni-**, **Felsennelkenanger-** und **Rechts der Isar-Crew** und **Paulina** (alias Timon), für die Zeitgestaltung außerhalb vom Lab und dass wir uns schon so lange kennen.

**Martin Haribert** (mit **Lisl**), du Optimist, für deine nicht endend wollenden positiven Worte, deine Hilfe während meiner Revision und dein Verständnis, auch wenn es nichts zu verstehen gibt. Ich bin froh, dass es dich gibt und dir der Leberkässemel-Entzug noch nicht geschadet hat ☺.

Zu guter Letzt, meiner liebe Familie, für eure großen, offenen Ohren, eure lieben Motivationen und euren unendlichen Glauben an mich. „Ohne eich war des alls ned so gschmeidig gwen“!